AFRL-AFOSR-UK-TR-2012-0030

Novel laser-based technique for measurements of primary atomization characteristics of liquid jets

Dr. Yannis Hardalupas

Imperial College of Science, Technology, and Medicine
Exhibition Road
London, United Kingdom SW7 2BX

EOARD Grant 09-3036

Report Date: August 2012

Final Report from 20 July 2009 to 19 July 2012

Air Force Research Laboratory
Air Force Office of Scientific Research
European Office of Aerospace Research and Development
Unit 4515 Box 14, APO AE 09421

REPORT DOCUMENTATION PAGE

Form Approved OMB No. 0704-0188

1. REPORT DATE *(DD-MM-YYYY)*	2. REPORT TYPE	3. DATES COVERED *(From – To)*
22 August 2012	Final Report	20 July 2009 – 19 July 2012

4. TITLE AND SUBTITLE

Novel laser-based technique for measurements of primary atomization characteristics of liquid jets

5a. CONTRACT NUMBER

FA8655-09-1-3036

5b. GRANT NUMBER

Grant 09-3036

5c. PROGRAM ELEMENT NUMBER

61102F

6. AUTHOR(S)

Dr. Yannis Hardalupas

5d. PROJECT NUMBER

5d. TASK NUMBER

5e. WORK UNIT NUMBER

7. PERFORMING ORGANIZATION NAME(S) AND ADDRESS(ES)

Imperial College of Science, Technology, and Medicine
Exhibition Road
London, United Kingdom SW7 2BX

8. PERFORMING ORGANIZATION REPORT NUMBER

N/A

9. SPONSORING/MONITORING AGENCY NAME(S) AND ADDRESS(ES)

EOARD
Unit 4515 BOX 14
APO AE 09421

10. SPONSOR/MONITOR'S ACRONYM(S)

AFRL/AFOSR/RSW (EOARD)

11. SPONSOR/MONITOR'S REPORT NUMBER(S)

AFRL-AFOSR-UK-TR-2012-0030

12. DISTRIBUTION/AVAILABILITY STATEMENT

Approved for public release; distribution is unlimited.

13. SUPPLEMENTARY NOTES

14. ABSTRACT

The purpose of the research documented herein is to provide guidelines for the application of a novel optical technique, developed uniquely at Imperial College, London, UK, for measurements of primary atomization characteristics of liquid jets in different atomiser geometries. The novel technique measures the 'optical connectivity' of a liquid jet leaving an atomiser by doping the liquid with a fluorescent dye (or using the natural fluorescence of the liquid) and illuminating the liquid body through the injector nozzle by a laser beam at a suitable wavelength. The liquid jet acts as an optical guide, which is interrupted when it breaks up, and, therefore, detection of the spatial, instantaneous fluorescent intensity distribution determines the distribution of the volume of liquid upstream of the breakup position, together with instantaneous intact length of the liquid jet. In addition, the surface wave instabilities along the air-liquid interface and the three dimensional structure of the liquid jet can be identified. The special feature of the novel technique is that the laser light is 'piped' through the liquid nozzle, which provides its unique advantage over other techniques, since it eliminates the interaction of the laser light with the dense droplet field surrounding the liquid core that limits other techniques.

This report is comprised of 6 progress reports for each 6 month period of this effort.

15. SUBJECT TERMS

EOARD, Propulsion, Fuels, Combustion

16. SECURITY CLASSIFICATION OF:			17. LIMITATION OF ABSTRACT	18, NUMBER OF PAGES	19a. NAME OF RESPONSIBLE PERSON
a. REPORT	b. ABSTRACT	c. THIS PAGE			Gregg Abate
UNCLAS	UNCLAS	UNCLAS	SAR	189	**19b. TELEPHONE NUMBER** *(Include area code)* +44 (0)1895 616021

Final Report

Novel laser-based technique for measurements of primary atomization characteristics of liquid jets

Professor Yannis Hardalupas

Imperial College of Science, Technology and Medicine

Grant: FA8655-09-1-3036

20 July 2009 – 19 July 2012

This final report is a compilation of progress reports over the life of the grant. Those reports and their page numbers in this report are:

PROGRESS REPORT

AWARD N°: FA8655-09-1-3036 1

TITLE: Novel laser-based technique for measurements of primary atomisation characteristics of liquid jets

INVESTIGATOR: Professor Y. Hardalupas

ORGANISATION: Imperial College of Science, Technology and Medicine

REPORTING PERIOD: From: 20 July 2009 To: 20 January 2010

PROJECT START DATE: 20 July 2009

DATE OF ISSUE OF THIS REPORT: 19 January 2010

ADMINISTRATIVE OFFICE: European Office of Aerospace Research and Development (EOARD)

GOVERNMENT PROGRAM MANAGER: Dr. Surya Surampudi

Table of Contents

List of Figures

Figure 8: Effect of the refractive index of the liquid on the fluorescent intensity along the length of the liquid column. No significant change is observed for refractive indices between 1.33 and 1.50. (Example for L/D=0.25, G/D=0.05, γ=0.001m^{-1}, ω=20°)

Figure 9: Effect of laser beam divergence at the exit of the liquid nozzle on the fluorescent intensity along the length of the liquid column. Lower divergence results in higher fluorescent intensity. (Example for L/D=2.0, G/D=0.25, γ=0.0002m^{-1}, n_1=1.33)

Figure 10: Effect of laser beam profile at the exit of the liquid nozzle on the fluorescent intensity along the length of the liquid column. There is little variation of the fluorescent intensity regardless of the laser beam profile. (Example for L/D=1.0, G/D=0.10, γ=0.02m^{-1}, n_1=1.33, ω=20°)

Figure 11: Electrical connectivity technique. a) Recorded signal as a function of time and b) probability density function of measured signal for different axial locations of the probe.

Figure 12: Measured breakup length with the optical connectivity (OC), the electrical connectivity (EC) and high speed photography (HS) techniques. Flows 1 and 2 according to Table 2.

List of Tables

Summary

During the first stages of atomization in an air-blast atomizer, the liquid stream is destabilized under the influence of a coaxial stream of air, until its continuity is broken. A novel technique [Charalampous *et al.* 2007 (1)] has been proposed to measure the length of the continuous liquid jet, based on the internal illumination of the liquid jet through the spray nozzle. The liquid jet acts as a light guide, which propagates along the length of the jet, in the same way as light travels along the length of an optical fiber. The light excites a fluorescent dye that is dissolved in the liquid jet, making the volume of the liquid jet luminous. Then, the connectivity of the liquid jet is linked to the optical connectivity of the fluorescent jet. However, since the surface of the liquid jet is not smooth, as that of an optical fiber, due to the development of waves on the jet surface, there are losses of light intensity due to refraction through the jet surface and absorption by the fluorescence dye, as it propagates along the liquid jet. The current project evaluates the optical connectivity technique numerically and experimentally. First, numerical simulations of the light propagation within liquid columns of various geometries are presented. The effects of the morphological characteristics of the interfacial waves on the gas-liquid interface (wavelength and amplitude) and the type of perturbation (sinus or varicose) as well as the absorption of laser light within the liquid jet and the characteristics of the laser beam (divergence and intensity profile) were considered. Next, a comparison of the continuous length of the liquid jet of an airblast atomizer is presented as measured with the optical connectivity technique and an electrical connectivity technique. In the latter approach, the continuity of the jet is determined by the electrical conductivity between the spray nozzle and a probe placed in the electrically charged liquid downstream of the liquid nozzle exit. The comparison shows that the optical connectivity technique performs better than the electrical connectivity technique in measuring the mean breakup length of the liquid jet.

Introduction

During the first stages of atomization of a liquid jet, the jet is progressively destabilized under the influence of the forces that result from the interaction of the liquid stream with the surrounding air (2; 3). During this process the jet geometry changes as liquid is removed from its surface and waves develop on the surface until their amplitude becomes large enough to lead to breakup of the liquid jet. The distance from the nozzle exit to the point downstream the nozzle, where the liquid jet breaks up defines what is known as the “primary atomization region”. The determination of the extent of this region is important for the performance of atomizers and evaluation of the numerical modeling of the atomization process.

A number of techniques have been proposed for the measurement of the length of the continuous jet. These include photography (4; 5), electrical conductivity (6-9), X-ray absorption (10-12) and ballistic imaging (13-15). A recently proposed method is the optical connectivity technique (1). It has been shown that in dense sprays it can provide a good measurement of the breakup length of sprays in conditions where the continuous length of the jet would be difficult to determine with photography as the atomization products that surround the jet could hinder the view to the continuous jet.

However, the optical connectivity technique is not without limitations. As the technique is based on the propagation of light within an atomizing liquid jet, there will unavoidably be some scattering losses at the interface that will reduce the intensity of the propagating light. Therefore, for long liquid jets, the technique will not be possible to operate due to complete attenuation of the propagating light along the liquid. Here, we develop a numerical model of the liquid jet to determine how the laser light that is seeded at the base of the jet propagates along the length of the jet and what are the effects of its geometry on the losses of the intensity of the laser light. In addition we use the electrical conductivity technique (6-8) to make comparisons of the measured lengths of the continuous jet. In the electrical connectivity technique, the continuity of the jet is determined by the electrical conductivity between the spray nozzle and a probe placed in the electrically charged liquid downstream of the liquid nozzle exit. This is equivalent to the optical connectivity approach.

The next section of this report describes the operation of the optical connectivity technique and presents the geometrical optics approach that was developed to evaluate numerically the influence of various parameters on the accuracy of measurements of the length of the continuous liquid jet and describes the electrical connectivity technique and the airblast atomizer used for the measurements. The next section presents the results. The numerical results, based on the geometrical optics approach, are reported and quantify the performance of the optical connectivity technique and provide guidelines for optimization. The experimental results describe the data processing approach for the electrical connectivity technique and the comparison of measurements of the length of the continuous liquid jet with the electrical and optical connectivity techniques follow. The paper ends with a summary of the main findings.

Methods, Assumptions and Procedure

(a) Optical Connectivity Technique

An optical connectivity technique has been developed for the measurement of the continuous length of sprays. The technique works by introducing a laser beam within the flow of the liquid upstream of the nozzle that exits with the liquid through the nozzle in the direction parallel to the nozzle axis. In this way the laser beam is largely contained within the liquid jet by reflecting on the liquid interface propagating downstream and illuminating the liquid jet volume. A ray of laser light is guided along the length of the liquid jet by reflecting on the gas-liquid interface at the jet surface. As long as the angle of incidence between the surface of the jet and the laser light rays is greater then the angle of total internal reflection, the rays are completely reflected back inside the liquid without intensity losses from refraction. This principle is similar to the way that a laser beam propagates within an optical fiber. However, if the angle of incidence of a laser light ray on the liquid jet interface becomes smaller than that for total internal reflection then there will be some intensity losses due to refraction.

The laser beam continues to propagate downstream the jet until it meets the breaking point of liquid jet, where it can no longer be contained within the jet and is diffused randomly in different directions. The introduction of a fluorescing dye into the liquid makes part of the laser beam to be absorbed along the length of the liquid jet, and subsequently be re-emitted as fluorescence. In this way the atomizing jet becomes luminous and can be imaged (**Figure 13**).

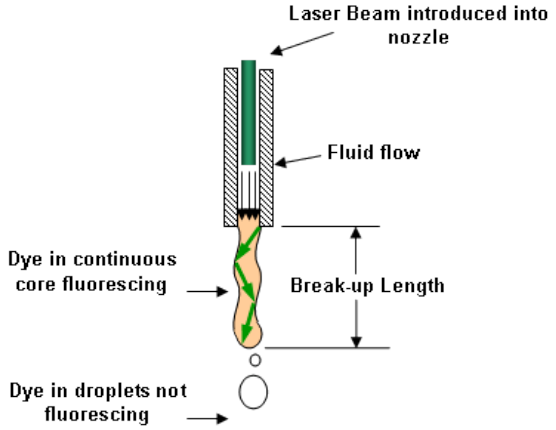

Figure 13: Principle of the optical connectivity technique

Depending on the roughness of the surface of the liquid jet, the amount of energy losses of the laser beam along the length of the jet changes. For a relatively smooth jet surface, the fluorescent intensity from the liquid jet is relatively uniform along its length (**Figure 14a**) and there is little decrease within the imaged region. The locations of the arrows indicate local maxima of intensity, which occur due to the local liquid jet surface structure, but these have no influence on the uniformity of the intensity along the liquid jet. However, if the surface of the jet is wavy, the image of the fluorescent intensity clearly shows that the intensity decreases along the length of the jet (**Figure 14b**). This is caused by the increased amount of energy losses on the gas liquid interface in the latter case. Therefore, there are limits on the length of the continuous jet that can be visualized with the fluorescence technique, which depend on the geometry of the liquid jet and the fluorescent dye concentration. Therefore, there is a need to evaluate the dependence of the propagating laser light intensity along the liquid jet on the

various parameters of the liquid jet. This will be performed with a geometrical optics calculation approach, as described in the following section.

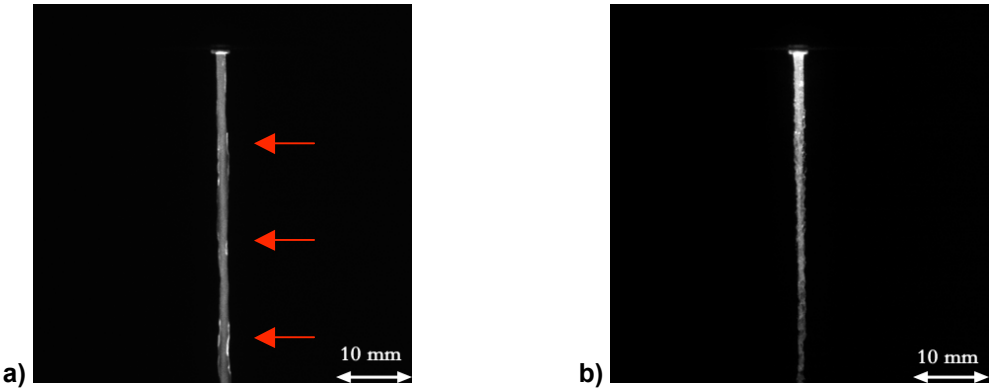

Figure 14: Fluorescent intensity image using illumination from within the nozzle of a straight jet a) with smooth surface and b) wavy surface. The image of the jet in the first case shows that along the jet length the fluorescent intensity is relatively uniform, while the decrease of the fluorescent intensity along the jet length is notable in the second case. The nozzle exit is at the top of the image.

(b) Geometrical Optics Simulations

For the evaluation of the effect of the shape of the jet geometry on the propagation of light within a column of liquid, the propagation of laser light rays is calculated using geometrical optics. This simulation has the benefit of enabling the evaluation of the effect of all operating parameters, which is difficult to achieve experimentally.

The liquid jet for this investigation is considered as a two-dimensional liquid column. The central axis of the liquid column extends along the x-axis of a Cartesian coordinate system. The interface of the jet is described by the sinusoidal wave function along the x-axis:

$$y = G\sin\left(\frac{2\pi x}{L} + \phi\right) + y_0 \qquad (1)$$

where G is the amplitude of the wave on the interface and L is the wavelength of the wave on the surface of the interface. ϕ is the phase of the wave on the surface of the interface and sinusoidal disturbances are present along the liquid column when the phases of the top and bottom interfaces are matched or varicose disturbances appear when the phases of the waves between the top and bottom surfaces are shifted by π.

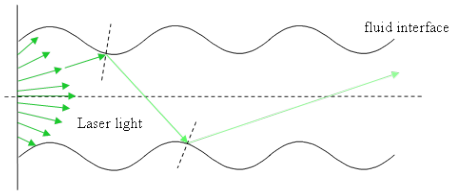

Figure 15: Basic geometry of the considered liquid jet and diverging rays at the base of the liquid column.

For the geometrical optics calculations, a monochromatic laser beam that propagates inside the liquid column is considered. The laser beam is simulated by a large number of rays that start at

the base of the liquid column at uniformly spaced intervals and propagate downstream the nozzle exit. The ray that begins on the axis of the column is aligned parallel to the axis. However, in order to consider the influence of the divergence (ω) of the laser beam, the angle between the rays at the column base and the axis is progressively changed as the distance between the axis and the starting point of the rays along the *y*-axis increases.

The calculation of the path of the rays when they are incident to the surface of the liquid column is estimated by:

$$R = V - 2(V \cdot N)N \tag{2}$$

where *V* is the incident ray vector, *N* is the vector normal to the jet surface at intersection point (between the wave and the incident ray) and *R* is the vector of the reflected ray.

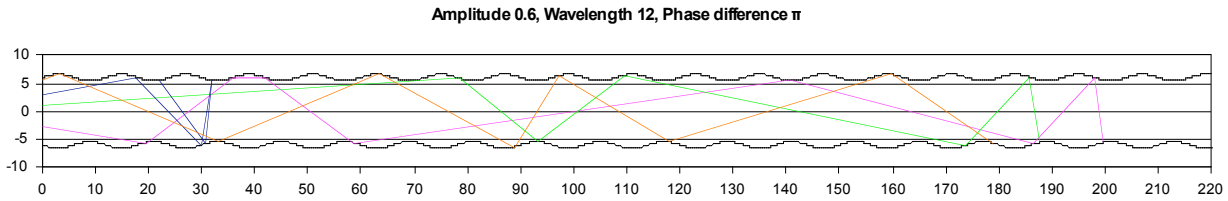

Figure 16: Example of propagation of light rays within a liquid column as determined by geometrical optics calculations. The vertical axis shows the width of the liquid column around the center and the horizontal axis shows the length along the direction of motion of the liquid column.

As the rays propagate along the liquid column, the initial intensity of each beam I_0 is reduced due to refraction of the light at the liquid interface, which is lost, and absorption from the dye present in the liquid, which is re-emitted as fluorescence.

Considering the angle of incidence between the rays and the local interfacial surface of the liquid, the critical angle for total internal reflection is given by the relationship:

$$\theta_{crit} = \sin^{-1}\left(\frac{n_2}{n_1}\right) \tag{3}$$

where n_1, n_2 the refractive indices of the liquid and the gas phases. However, when the angle of incidence between a ray and the air-liquid interface is smaller that the angle of incidence for total internal reflection, there are losses of the intensity of the ray. The fraction of the intensity of incident light that is reflected from the interface is given by the reflection coefficient *R*, and the fraction refracted by the transmission coefficient *T*. The Fresnel equations are used to calculate *R* and *T*. The calculations of *R* and *T* depend on polarization of the incident ray. If the light is polarized with the electric field of the light perpendicular to the plane of **Figures 3** or **4** (s-polarized), the reflection coefficient is:

$$R_s = \left[\frac{\sin(\theta_1 - \theta_2)}{\sin(\theta_1 + \theta_2)}\right]^2 \tag{4}$$

If the incident light is polarized in the plane of the **Figures 3** or **4** (p-polarized), the reflection coefficient *R* is:

$$R_p = \left[\frac{\tan(\theta_2 - \theta_1)}{\tan(\theta_1 + \theta_2)}\right]^2 \tag{5}$$

The Beer-Lambert law estimates the reduction of the intensity of the rays due to the absorption caused by the fluorescent dye present in the liquid through which the ray is traveling:

$$I = I_0 e^{-\gamma z} \tag{6}$$

where γ is the absorption coefficient, *z* the path length traveled by the ray, I_0 is the initial intensity of the ray and *I* the intensity of the ray after it has traveled a distance *z* in the absorbing medium.

The total reduction of the initial intensity I_0 of the laser beam that travels along a path of length *z* in an absorbing medium until it reaches the interface is given by the formula:

$$I = \left(\frac{\left[\frac{\sin(\theta_1 - \theta_2)}{\sin(\theta_1 + \theta_2)}\right]^2 + \left[\frac{\tan(\theta_2 - \theta_1)}{\tan(\theta_1 + \theta_2)}\right]^2}{2} \right) I_0 \cdot (e^{-\gamma z}) \tag{7}$$

While the refracted part of the laser light intensity is lost, the absorbed light intensity along the ray path is subsequently re-emitted as fluorescence. By summation of the losses of the laser light intensity of each ray due to absorption at each distance downstream of the nozzle exit, the profile of the fluorescent intensity with distance from the nozzle exit is determined. In this way, the limitations of the visualization of the fluorescent liquid jet can be determined. The parameters that influence the loss of light intensity are morphological (wavelength, *L*, amplitude, *G*, and phase, ϕ of the waves on the surface of the liquid column), physical (absorption of light within the liquid, γ, and refractive index of liquid, n_1) and optical (divergence of rays of laser light, ω). The wavelength and the amplitude of the waves on the liquid surface were normalized by the diameter of the liquid jet at the nozzle exit *D*.

Table 3. Range of considered parameters for geometrical optics calculations

G/*D*	0.03 - 0.25
L/*D*	0.25 - 4.00
ϕ	0, π
γ	0.00008 m^{-1} - 0.1m^{-1}
n_1	1.33, 1.40, 1.50
ω	5°, 10°, 20°

A summary of the range of parameters that are examined in this investigation is presented in **Table 3**. However, a limited number of combinations of these parameters were considered due to processing power requirements.

(c) Electrical Connectivity technique

In the electrical conductivity technique (6-9), an electrical potential is applied between the nozzle and a probe placed within the liquid jet downstream of the liquid nozzle exit (**Figure**). When there is a continuous stream of conducting liquid, such as tap water, an electrical current will run through the liquid between the nozzle and the probe. The detection of electrical connection between the nozzle and the probe indicates that the continuous length of liquid jet is at least as long as the distance between the two. The electrical connectivity technique was implemented in the air-blast atomizer of (4). A solid-state battery supplied constant voltage up to 10V (adjustable by 0.1mV increments) between the liquid nozzle and the probe. The probe was a straight stainless steel rod of 1mm diameter aligned normal to the central axis of the liquid nozzle. A resistance of 1MΩwas connected in series between the voltage source and the nozzle, and a 12-bit A/D card connected to a PC digitized the time dependent voltage drop across the liquid jet. The electrical conductivity technique has the potential of measuring the continuous lengths of liquid jets without limitations on their length. However, it has been reported that the electrical conductivity technique tends to overestimate the breakup length (6). Here we conduct a comparison of the two techniques in conditions that have a short breakup length.

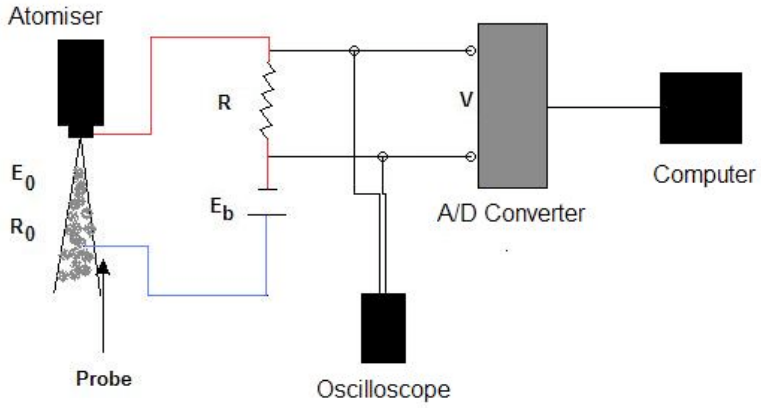

Figure 5: Schematic of the implementation of the electrical conductivity technique on a spray

(d) Coaxial Airblast Atomiser

The experimental investigation was performed on the coaxial air-blast atomizer configuration, described in detail in (4). In this investigation the atomizer was placed vertically and the spray exhausted downwards. The internal diameter of the liquid nozzle was *D*=2.3mm and the internal diameter of the coaxial air nozzle was 22.95mm.

The configuration of the original atomizer was modified as shown in **Figure 6**. A hollow tube open at the top end and fitted with a quartz window at the lower end was inserted within the central tube of the atomizing liquid, up to the conical contraction of the liquid nozzle. This addition acts as a light guide, which allows a laser pulse to propagate through the central tube

without interacting with the liquid for the full length of the central tube. Upstream of the liquid nozzle exit, the laser beam exits through the light guide tube window, propagates through the liquid flow and exits through the nozzle in the same direction as the flow of the atomized liquid. In this way, the intact liquid jet acts as an optical fiber, which allows the propagation of the laser light till the location of the break up. In this approach the laser beam is delivered within the continuous section of the liquid jet without the attenuation caused by approaches that introduce the laser beam through the surrounding spray and ensures that low light intensity is present beyond the surface of the liquid jet.

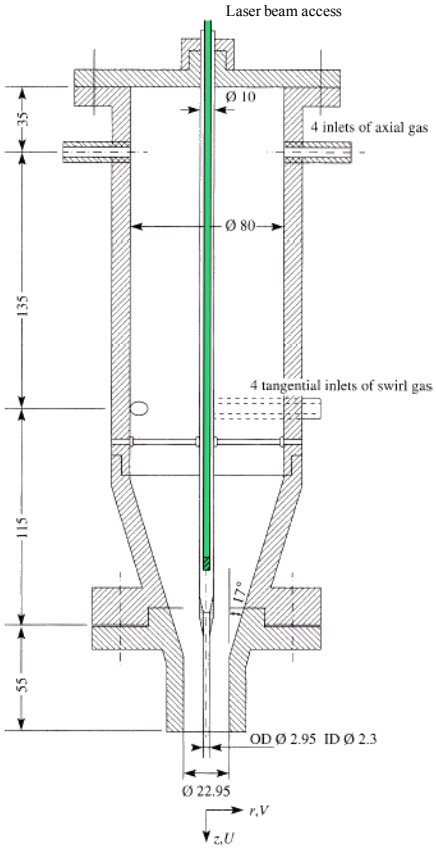

Figure 6: Geometry of coaxial airblast atomizer. The addition of the laser light-guide tube within the liquid jet is shown in green.

The introduction of the laser beam through the liquid jet nozzle is combined with the addition of the fluorescing Rhodamine WT dye within the liquid. This addition leads to the emission of fluorescent light from the liquid along the path of the laser beam. Two reasons make the addition of the dye advantageous. The first is that as the laser beam propagates through the liquid core it interacts with the surface of the liquid jet and some light may be scattered, leading to difficulties in detecting the interface of the liquid jet. The addition of laser dye means that the fluorescing light from the liquid jet can be detected at a longer wavelength than that of the incoming laser beam and avoid background noise on images due to the scattered light. The second reason is that the fluorescing light tracks the volume of the liquid and, therefore, is emitted from everywhere within the liquid jet, as opposed to scattered light which is associated with the surface of the liquid jet. The concentration of the fluorescing dye was adjusted to ensure that the absorption of the incident light remained low enough to allow laser light to

propagate through the liquid for around 150 mm, which was longer than the break-up length for all examined cases.

Measurements were obtained with the electrical connectivity technique for the operating conditions of the airblast atomizer summarized in **Table 2**. Measurements of the breakup length were obtained previously on the same airblast atomizer with the optical connectivity technique (1) and with high speed film photography (4) and are used here for comparison.

Table 2. Range of considered atomiser conditions

Water flowrate (l/min)	Air flowrate (l/min)
FLOWS 1	
0.5	500
0.5	750
0.5	1000
0.5	1250
0.5	1500
0.5	1750
0.5	500
FLOWS 2	
1.0	750
1.0	1000
1.0	1250
1.0	1500
1.0	1750

Results and discussion

(a) Geometrical Optics Calculations

The influence of the morphological characteristics of the liquid column on the decay of the fluorescent intensity along its length is examined first. The effect of the amplitude of the waves on the surface of the liquid column on the decay of the fluorescent light intensity along the length of the column is shown in **Figure** . It is generally observed that there is a larger decrease in the fluorescent intensity with axial distance from the nozzle exit as the amplitude of the surface waves increases. This can be explained from **Figure** , where the paths of the same ray are traced within liquid columns with surface waves of small and large amplitudes, and can be attributed to two factors. One is that when the amplitude of the waves is small, the rays hit the inner surface of the liquid jet at angles greater than the angle for total internal reflection of Equation (3). In this way, the intensity losses due to refraction of laser light outside the liquid remain minimal and most of the losses of the laser light are due to absorption by the fluorescent dye within the liquid. In contrast, when the amplitude of the surface waves is large, the losses due to refraction are greater and the fluorescent intensity of the liquid jet decreases faster with axial distance. In addition to the losses due to refraction, another issue with large amplitude surface waves is that more rays tend to be reflected backwards (towards the nozzle exit) when they impinge against troughs of large amplitude. This causes lower penetration of the laser

beam along the liquid column and, as a result, the fluorescent intensity along the liquid column decreases.

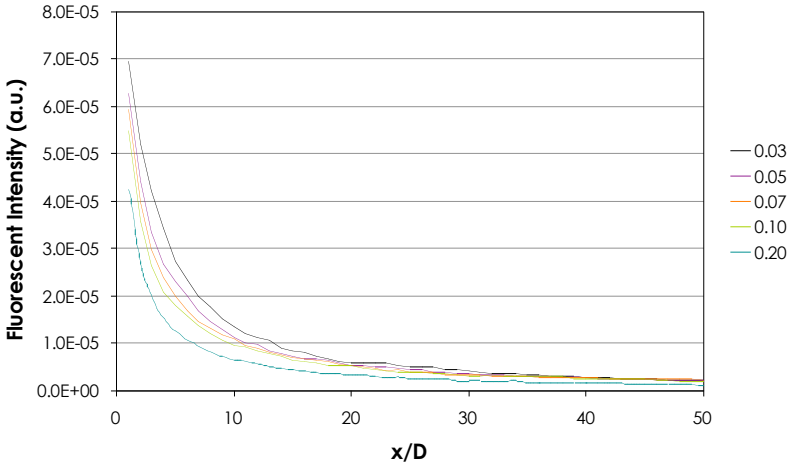

Figure 7: Effect of the amplitude of the surface waves of the liquid column on the fluorescent intensity along the length of the column. Smaller amplitudes result in higher fluorescent intensity. (Example for L/D=0.25, γ=0.00008m^{-1}, n_1=1.33, ω=20°)

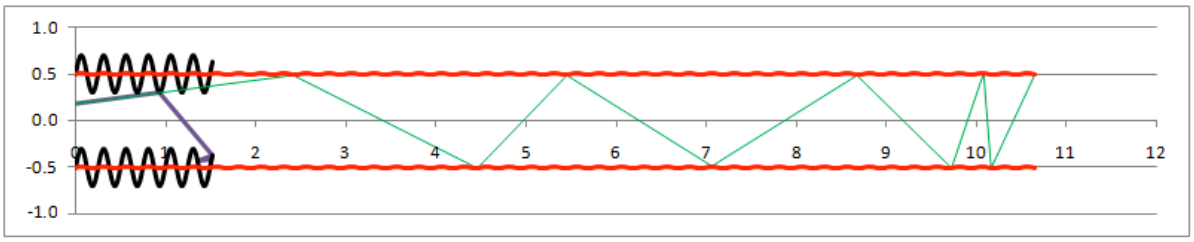

Figure 8: Paths of the same ray inside liquid columns with large and small amplitude of surface waves, which have the same wavelength.

The wavelength of the surface waves was also found to influence the fluorescent intensity of the liquid jet significantly. As demonstrated in **Figure** , when the wavelength of the surface waves decreases, the fluorescent light intensity along the liquid length reduces. The effect is more profound as the wavelength of the surface wave decreases to about the dimension of the liquid nozzle exit D. For even smaller wavelengths, the changes in the fluorescent intensity are small. The effect can be explained as before by considering the angle of incidence of the rays of the laser beam and the internal surface of the liquid jet, which is demonstrated in **Figure** where the path of the same ray is shown within a liquid jet of long and short wavelength. When the wavelength is large, the rays impinge on the surface at large angles and total internal reflection occurs. In addition, the reflected light is mostly in the forward direction and therefore propagates further along the liquid column. For the longest wavelength considered, the fluorescent intensity profile has some variations, which can be attributed to the morphology of the column, since they appear at distances of about half a wavelength. As the unevenness of the profile is minor there are no issues with the visualization of the continuous liquid column. For shorter wavelengths, the probability of refraction of rays outside the liquid jet and losses of the laser beam intensity is increased as the angle of incidence becomes routinely high. Nevertheless, when the wavelength of the surface waves decreases to about the size of the liquid nozzle, no reduction is demonstrated on the profile of the fluorescent intensity with further reduction of the surface wavelength. The reason for this is not yet clear.

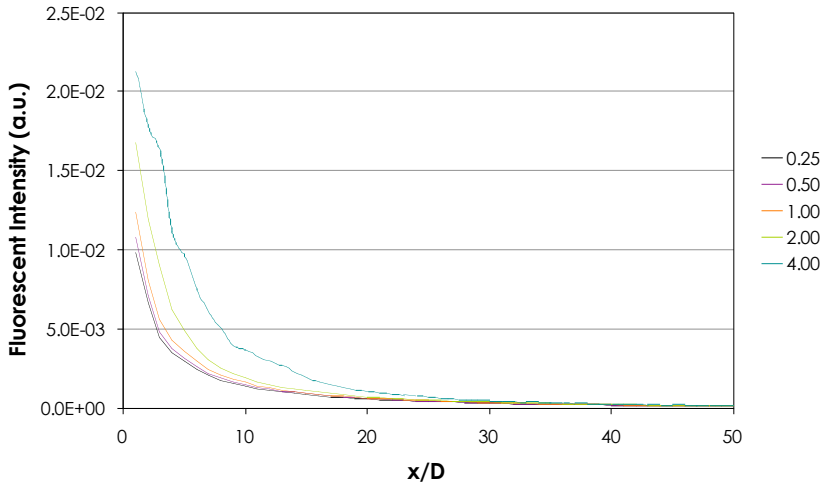

Figure 9: Effect of the wavelength of the surface waves of the liquid column on the fluorescent intensity along the length of the column. Longer wavelengths result in higher fluorescent intensity. (Example for G/D=0.20, γ=0.02m^{-1}, n_1=1.33, ω=20°)

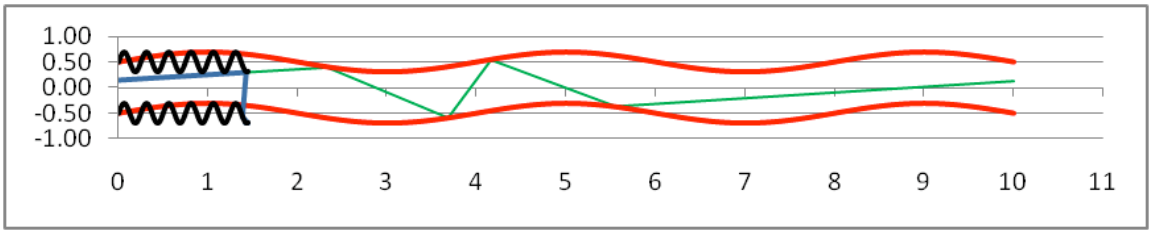

Figure 10: Paths of the same ray inside liquid columns with large and small wavelengths and same amplitude.

The last morphological consideration is the phase between the two surface waves. When the two waves are in phase, the result is a sinusoidal overall profile of the liquid column, as shown in **Figure** a. However, when the two waves have a phase difference of 180°, then the profile of the liquid column is varicose, as shown in **Figure** b.

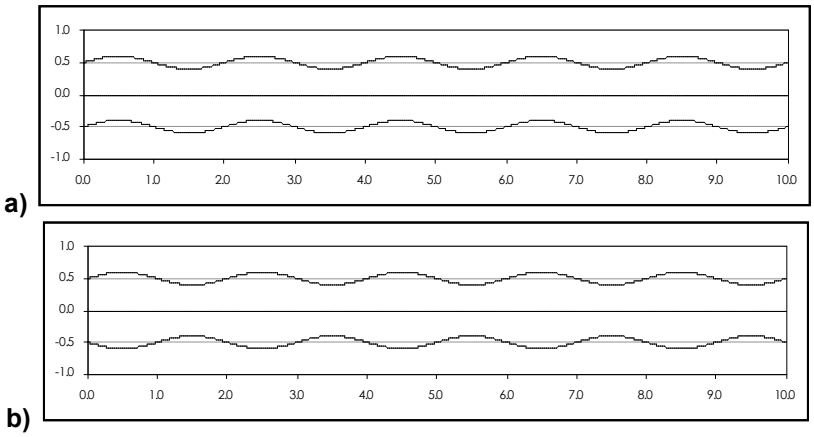

Figure 11: Sinusoidal and varicose profiles of the liquid column for a) ϕ=0° b) ϕ=π phase difference between the waves on the liquid interfaces of the column.

Despite the different morphology of the sinusoidal and varicose behaviour of the liquid columns, the profiles of the fluorescent intensity do not diverge much, as demonstrated in **Figure 17**. The likely explanation is that morphologically it is mostly the amplitude and wavelength of the surface waves that are significant, as they determine the angle of incidence of the laser light on the inner surface of the liquid interface and, in turn, whether total internal reflection without intensity losses or reflection with intensity losses due to refraction will occur. The phase relation between the two interfaces does not considerably affect the angle of incidence and, therefore, the fluorescent intensity remains largely unaffected.

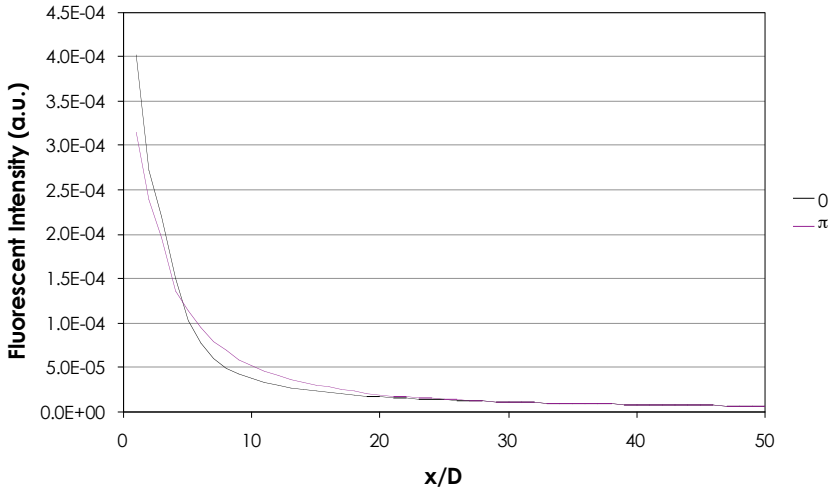

Figure 17: Effect of the phase between the surface waves of the liquid column on the fluorescent intensity along the length of the column. a) ϕ=0° (sinusoidal jet), b) ϕ=π (varicose jet). (Example for L/D=2.0, G/D=0.25, γ=0.0004m^{-1}, n_1=1.40, ω=20°)

Further to the reduction of the fluorescent intensity along the length of the liquid column due to morphological parameters of the liquid column, the intensity of the laser rays is also reduced due to the absorption of the laser intensity by the fluorescing dye. In contrast to the losses of light due to refraction at the liquid interface, where the refracted light is lost and does not contribute to the fluorescent intensity of the liquid column, the laser energy lost due to absorption by the laser dye is converted to fluorescent light. Increase of the absorption within the liquid always leads to increase of the fluorescent intensity and therefore improves the visualization of the continuous liquid column. The fluorescent intensity at the base of the liquid column was found to scale linearly with the absorption coefficient (i.e. the dye concentration). Therefore, doubling the dye concentration in the liquid leads to a twofold increase of the fluorescent intensity. However, when the dye concentration is increased, due to the increased absorption of the laser light intensity, the fluorescent intensity downstream will decrease. For example, in **Figure 18**, the fluorescent intensity for γ=0.1m^{-1} is much higher close to the nozzle exit than for the other examined cases but, at about 15D downstream the nozzle, it decreases below the fluorescent intensity of a liquid column with γ=0.04m^{-1}. While an exact estimate of the "correct" dye concentration within the liquid cannot be obtained, an indicative rule is that the inverse of the absorption coefficient, which is known as the optical depth, should be well above the length of the liquid column that is to be visualized.

The refractive index of the liquid determines the angle of total reflection. From Equation (3) for the refractive indices of n_1=1.33, n_1=1.40 and n_1=1.50, the angle of total internal reflection becomes θ_{crit}=48.7°, θ_{crit}=45.6°, and θ_{crit}=41.8° respectively. This range of refractive indices

includes most liquids that might be encountered in atomization processes. Despite the change of the critical angle, the change of the fluorescent intensity profile is generally marginal, as shown in **Figure 19**. While this is contrary to what was expected, it is likely that the number of rays affected by a change in the angle of total internal reflection by about 7° is not sufficient to change significantly the overall fluorescent intensity.

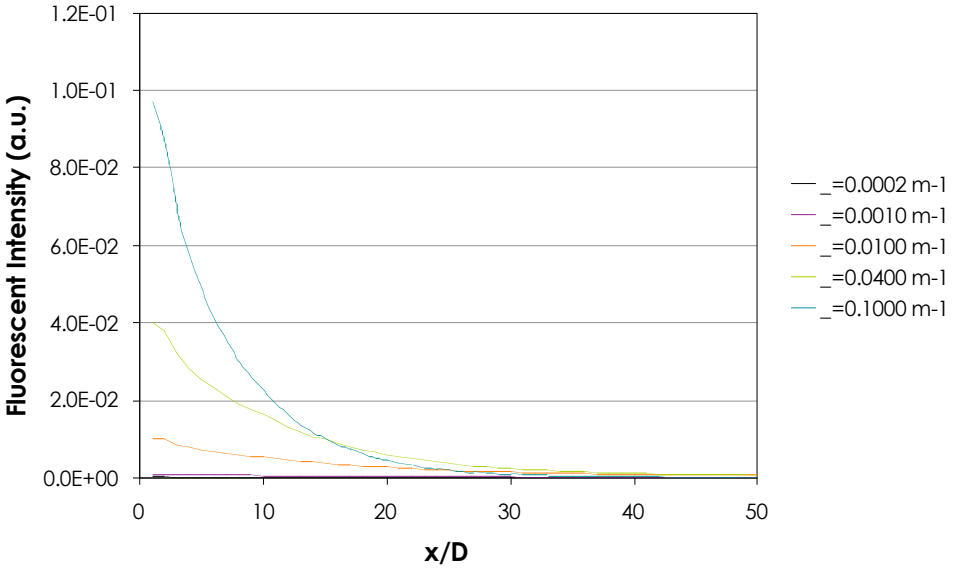

Figure 18: Effect of absorption coefficient of the liquid on the fluorescent intensity along the length of the liquid column. Greater absorption coefficient results in higher fluorescent intensity along the length of the liquid column. (Example for L/D=2.0, G/D=0.1, n_1=1.40, ω=5°)

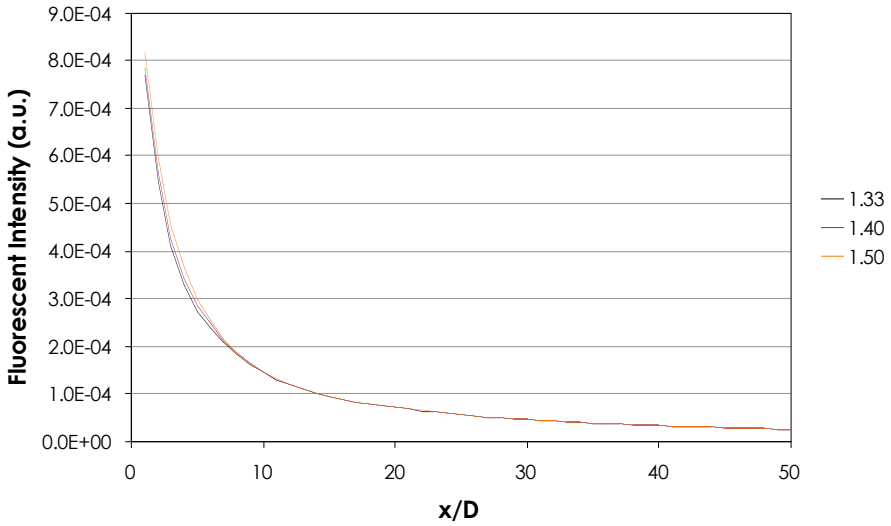

Figure 19: Effect of the refractive index of the liquid on the fluorescent intensity along the length of the liquid column. No significant change is observed for refractive indices between 1.33 and 1.50. (Example for L/D=0.25, G/D=0.05, γ=0.001m^{-1}, ω=20°)

The characteristics of the laser beam at the base of the liquid nozzle were also examined. First the divergence of the laser beam is considered. It was found that as the divergence of the beam

increases the fluorescent intensity along the length of the liquid column drops (**Figure 20**). This is due to the rays of the laser light pointing progressively outwards from the liquid column axis, increasing the probability that the angle of incidence on the liquid-gas interface will be below the critical angle for total internal reflection and, therefore, losses due to refraction are more likely. Since the divergence of the laser beam can be controlled by the optical treatment of the laser beam, it is recommended that the beam is as collimated as possible when it exits the liquid nozzle.

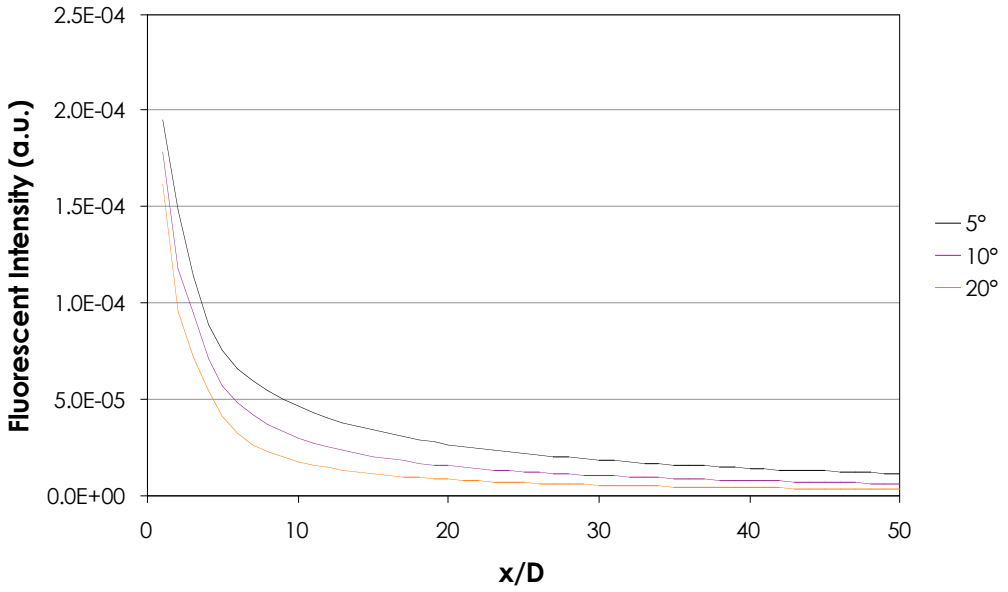

Figure 20: Effect of laser beam divergence at the exit of the liquid nozzle on the fluorescent intensity along the length of the liquid column. Lower divergence results in higher fluorescent intensity. (Example for L/D=2.0, G/D=0.25, γ=0.0002m^{-1}, n_1=1.33)

Finally, the profile of the intensity of the laser beam was considered. A top hat intensity profile is uncommon, while a Gaussian intensity profile is more realistic for a laser beam. The integral of the intensity within the base of the nozzle exit was retained equal among the cases considered to make sure that the illumination of the liquid column was the same for all cases. However, despite the change in the distribution of the laser intensity as it enters the liquid, there was negligible change in the overall fluorescent intensity profile (**Figure 21**). This is advantageous for the optical connectivity technique as the shaping of the intensity profile of a laser beam is not trivial to control.

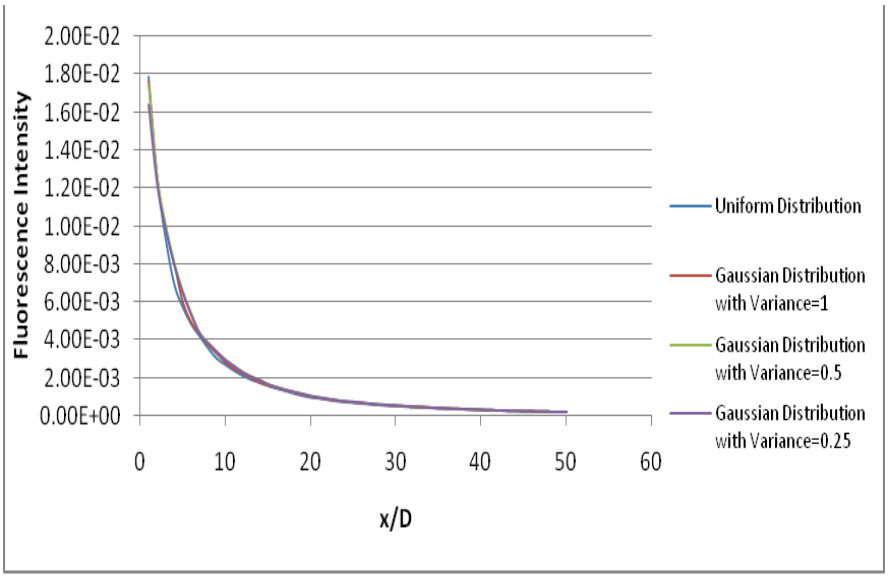

Figure 21: Effect of laser beam profile at the exit of the liquid nozzle on the fluorescent intensity along the length of the liquid column. There is little variation of the fluorescent intensity regardless of the laser beam profile. (Example for L/D=1.0, G/D=0.10, γ=0.02m^{-1}, n_1=1.33, ω=20°)

(b) Comparison between Optical and Electrical Connectivity Techniques

In the previous section, it was shown that the intensity of the fluorescent light along a liquid column depends on many parameters for the optical connectivity technique. In all cases, the intensity of the fluorescent light does not propagate indefinitely within the liquid column, but decreases progressively along the length of the column. It is possible that, when the continuous length of the liquid column is long, the fluorescent intensity might become too low to be detected along the full length of the continuous liquid column. This has been demonstrated experimentally (1). For this reason, the optical connectivity technique was recommended for cases of good atomization, which lead to short breakup lengths. We provide here a comparison between the optical and electrical connectivity techniques, which may assist the evaluation of the optical connectivity technique.

The interpretation of the signal from the electrical connectivity technique (example shown in **Figure 22**a) was not straightforward, since it was not clear when the liquid jet was connected or disconnected. When the probe was very close to the nozzle, the measured values of the voltage drop had a high mean value and narrow spread (**Figure 22**b). For long distances downstream from the nozzle, the measured values of voltage were close to 0 and values had a narrow spread. In intermediate distances from the nozzle exit, the range of measured voltages was wide and could obtain large values of voltage (over 5V). The atomization process lowers the measured voltage in comparison to the voltage measured for an undisturbed liquid column due to the increase of the electrical resistance of the liquid column. In addition, as the probe was traversed away from the nozzle, the probability density function changed shape and its skewness changed from positive to negative. Measurements that have probability density function with positive skewness occur at distances close to the liquid nozzle, where the liquid jet is atomizing and its cross section decreases along its length. Measurements with probability density functions with negative skewness represent liquid jets that have either had the majority of their mass removed or are completely discontinuous. Since, for this investigation, we are only interested in the mean breakup length of the liquid jet, it was decided that the criterion to determine the breakup length was based on the distance from the nozzle where the skewness

of the probability density function of the measured voltages was zero. This was selected because of the expectation that the liquid jet will be continuous for only half of the measurements at the mean breakup position.

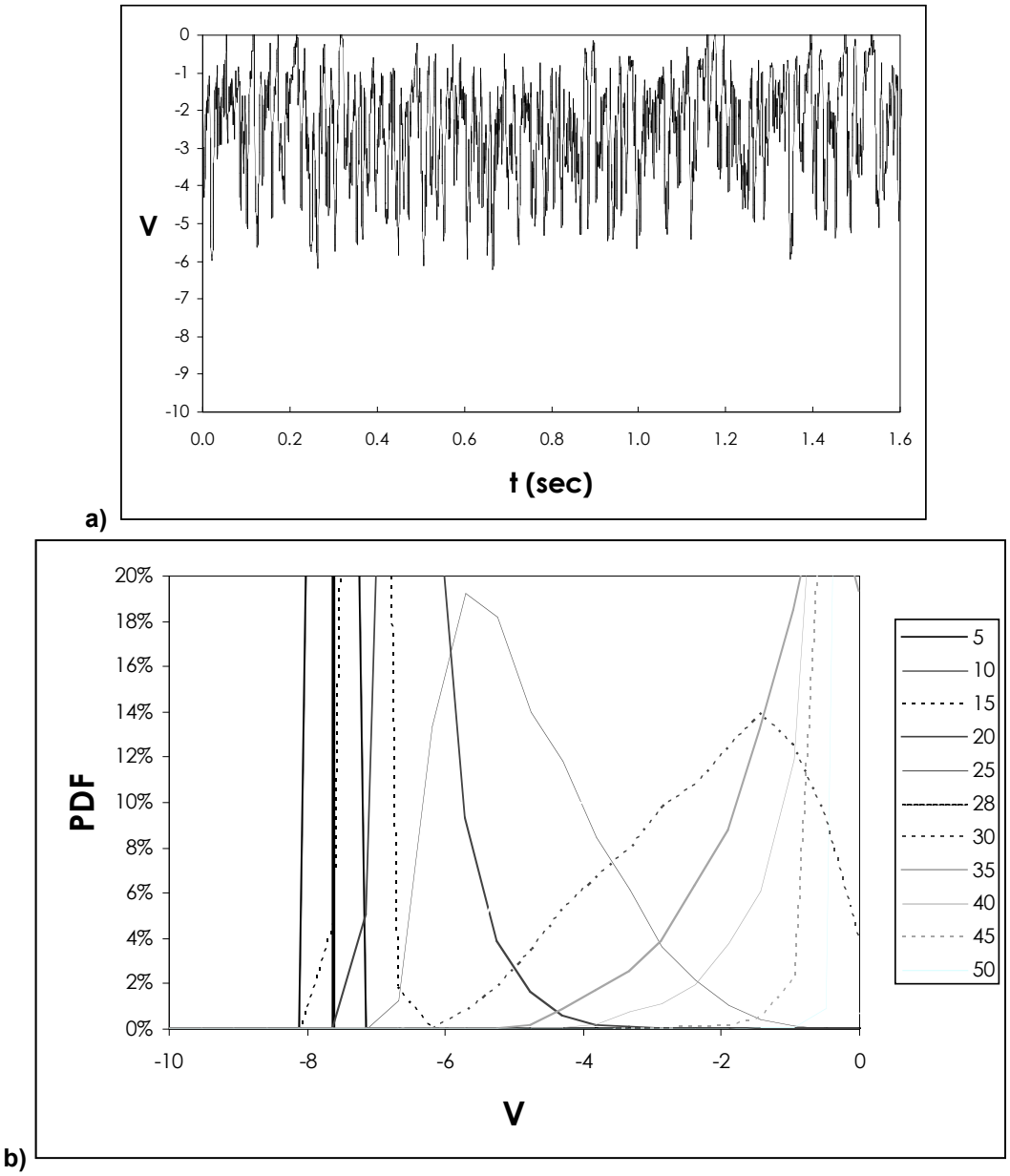

Figure 22: Electrical connectivity technique. a) Recorded signal as a function of time and b) probability density function of measured signal for different axial locations of the probe

A comparison of the average breakup length measured by time resolved electrical connectivity, optical connectivity and high-speed photography techniques is presented in **Figure 23** as a function of the gas to liquid momentum ratio MR, defined as:

$$MR = \frac{\rho_G U_G^2 (D_G^2 - D^2)}{\rho_L U_L^2 D_L^2} \tag{3}$$

The implementation of the optical connectivity technique in the airblast atomizer is described in detail in (16, 17).

In all cases the measured breakup length by the electrical conductivity technique is larger than the breakup length measured with the optical connectivity technique. For flows indicated as type 1 (Table 2) in **Figure 18**, for which the breakup length is shorter, there is better agreement between the two techniques. The electrical conductivity technique measures longer breakup lengths by about 2*D*, but the observed trends are similar. However, for flows indicated as type 2 (Table 2) in **Figure 18**, there is a larger difference in the measured values of the breakup length with the electrical conductivity technique showing longer breakup lengths by over 10*D* in some cases. This demonstrates a deviation of the results between the two techniques. While the breakup length for type 2 flows is increased and laser beam intensity losses along the length of the continuous liquid jet are more significant, comparison with the time resolved photographic measurements of (4) show that there is better agreement with the optical connectivity technique than with the electrical conductivity technique. The reason why the electrical conductivity technique measures greater values of breakup length is unclear. The possibility of charge transfer without contact between the liquid nozzle and the probe by a continuous liquid jet has been suggested (6). Corona discharge is unlikely to cause current through the gas between the liquid nozzle and the probe, because it requires very high potential between the two as explained by Yule and Salters (8), which is not the case here. However, charge might still be transferred between the nozzle and the probe by a different mechanism. Kelvin through his water dropper experiment (18) demonstrated that even a very low potential is sufficient to electrically charge water droplets and these droplets can transfer their charge between the liquid nozzle and a vessel below. While the current that can be transferred through this mechanism is not known, such possibility does exist and may explain the increased breakup length measured by the electrical connectivity technique.

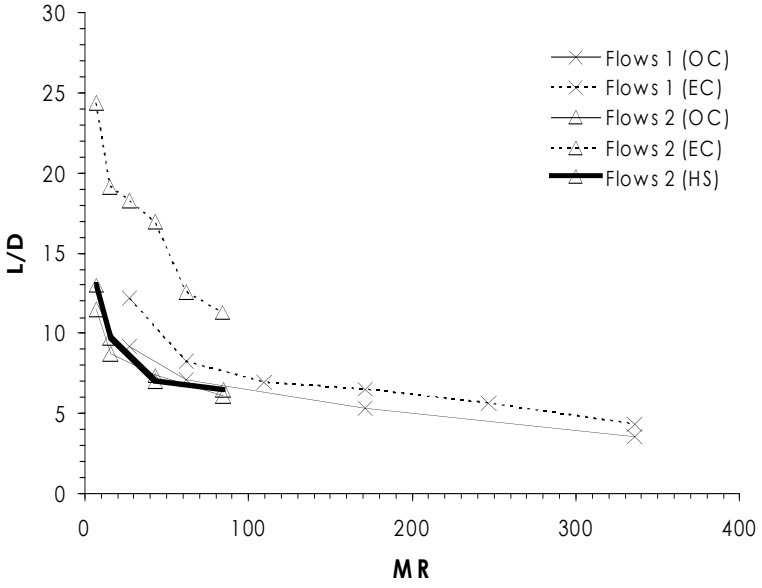

Figure 23: Measured breakup length with the optical connectivity (OC), the electrical connectivity (EC) and high speed photography (HS) techniques. Flows 1 and 2 according to Table 2.

Conclusions

The optical connectivity technique was examined numerically by geometrical optics simulations of the propagation of light within the liquid jet and by comparison with the electrical conductivity technique.

The simulations showed the following:

(a) From the morphological characteristics of the liquid jet, shorter wavelengths and greater amplitudes of the interfacial waves on the liquid interface result to lower fluorescent intensity along the liquid jet.

(b) The type of perturbation (sinus or varicose) of the liquid column did not appear to influence the profile of the fluorescent intensity considerably.

(c) The dye concentration of the liquid was found to influence significantly the ability to visualize the continuous liquid length. The fluorescent intensity at the exit of the liquid nozzle scales linearly with the dye concentration. However, increasing the dye concentration decreases the fluorescent intensity faster with distance from the nozzle exit. It is recommended that the optical depth of the liquid is adjusted to be well over the continuous length of the liquid jet that is visualized.

(d) The refractive index of the liquid does not affect the fluorescent intensity of the liquid jet significantly.

(e) When considering the characteristics of the laser beam, higher divergence of the beam at the nozzle exit causes higher losses of intensity due to refraction through the liquid interface. Collimation of the beam is recommended.

(f) The laser beam intensity profile was not found to have a significant effect on the fluorescent intensity profile along the liquid jet.

The optical connectivity technique was also compared experimentally with the electrical conductivity technique. It was found that for flows with shorter breakup lengths, the difference between the measured mean breakup length with the two techniques was less than two liquid nozzle diameters, while the electrical connectivity always indicated longer breakup lengths. For flows with longer breakup length, the discrepancies between the two measurement techniques increased to over 10 liquid nozzle diameters. High-speed photographic measurements showed breakup length values closer to those measured with the optical conductivity technique, which gives more confidence in the accuracy of the optical connectivity approach.

References

1. Charalampous, G., Hardalupas, Y., and Taylor, A.M.K.P., "A novel technique for measurements of the intact liquid jet core in a coaxial airblast atomizer," *45th AIAA Aerospace Sciences Meeting and Exhibit, AIAA 2007-1337*, Reno, USA 2007.

2. Lefebvre, A.H., *Atomization and sprays*, Hemisphere Publishing Corporation 1989.

3. Lasheras, J.C. and Hopfinger, E.J., "Liquid jet instability and atomization in a coaxial gas stream," *Annual Review of Fluid Mechanics*, Vol. 32, 2000, pp. 275-308.

4. Engelbert, C., Hardalupas, Y., and Whitelaw, J.H., "Breakup Phenomena in Coaxial Airblast Atomizers," *Proceedings of the Royal Society of London Series A-Mathematical and Physical Sciences*, Vol. 451, No. 1941, 1995, pp. 189-229.

5. Varga, C.M., Lasheras, J.C., and Hopfinger, E.J., "Initial breakup of a small-diameter liquid jet by a high-speed gas stream," *Journal of Fluid Mechanics*, Vol. 497, 2003, pp. 405-434.

6. Chehroudi B., Chen S.H., and Bracco F.V., "On the intact core of full-cone sprays," *SAE Technical Papers 850126*, 1985.

7. Hiroyasu H., Arai M., and Shimizu M., Break-up length of a liquid jet and internal flow in a nozzle. ICLASS-91. 1991.

8. Yule, A.J. and Salters, D.G., "A Conductivity Probe Technique for Investigating the Breakup of Diesel Sprays," *Atomization and Sprays*, Vol. 4, No. 1, 1994, pp. 41-63.

9. Hiroyasu H., Shimizu M., and Arai M., "The breakup of high speed jet in a high pressure gaseous atmosphere," *ICLASS-82*, 1982.

10. Cai, W.Y., Powell, C.F., Yue, Y., Narayanan, S., Wang, J., Tate, M.W., Renzi, M.J., Ercan, A., Fontes, E., and Gruner, S.M., "Quantitative analysis of highly transient fuel sprays by time-resolved x-radiography," *Applied Physics Letters*, Vol. 83, No. 8, 2003, pp. 1671-1673.

11. Renzi, M. J., Tate, M.W., Ercan, A., Gruner, S.M., Fontes, E., Powell, C.F., MacPhee, A.G., Narayanan, S., Wang, J., Yue, Y., and Cuenca, R., "Pixel array detectors for time resolved radiography (invited)," *Review of Scientific Instruments*, Vol. 73, No. 3, 2002, pp. 1621-1624.

12. Yue, Y., Powell, C.F., Poola, R., Wang, J., and Schaller, J.K., "Quantitative measurements of diesel fuel spray characteristics in the near-nozzle region using X-ray absorption," *Atomization and Sprays*, Vol. 11, No. 4, 2001, pp. 471-490.

13. Linne, M., Paciaroni, M., Hall, T., and Parker, T., "Ballistic imaging of the near field in a diesel spray," *Experiments in Fluids*, Vol. 40, No. 6, 2006, pp. 836-846.

14. Linne, M.A., Paciaroni, M., Gord, J.R., and Meyer, T.R., "Ballistic imaging of the liquid core for a steady jet in crossflow," *Applied Optics*, Vol. 44, No. 31, 2005, pp. 6627-6634.

15. Paciaroni, M., Linne, M., Hall, T., Delplanque, J.P., and Parker, T., "Single-shot two-dimensional ballistic imaging of the liquid core in an atomizing spray," *Atomization and Sprays*, Vol. 16, No. 1, 2006, pp. 51-69.

16. Charalampous, G., Hardalupas, Y., and Taylor, A.M.K.P., "Novel Technique for Measurements of Continuous Liquid Jet Core in an Atomizer," *AIAA Journal*, Vol. 47, No. 11, 2009, pp. 2605-2615.

17. Charalampous, G., Hardalupas, Y., and Taylor, A.M.K.P., “3-Dimensional structure of the intact liquid jet core during coaxial air-blast atomisation”. *Intern. Journal of Spray and Combustion Dynamics (IJSCD)*, Vol. 1, 2009, pp. 389-415.

18. Thomson W., "On a self-acting apparatus for multiplying and maintaining electric charges, with applications to illustrate the voltaic theory," *Proceedings of the Royal Society of London*, Vol. 16, 1867, pp. 67-72.

List of Symbols, Abbreviations and Acronyms

D	=	inner diameter of the liquid jet nozzle
D_L	=	outer diameter of the liquid jet nozzle
D_G	=	Inner diameter of the gaseous jet nozzle
G	=	Amplitude of feature on jet surface
L	=	Wavelength of feature on jet surface
MR	=	Gas-to-liquid Momentum ratio
n_1	=	Index of refraction of liquid
n_2	=	Index of refraction of gas
U_G	=	Average gaseous velocity at the annulus
U_L	=	Average liquid velocity at the nozzle exit
γ	=	Absorption coefficient
ν_L	=	Kinematic viscosity of the liquid
ϕ	=	Phase of sinus surface wave
ω	=	Laser beam divergence
σ	=	Surface tension

PROGRESS REPORT

AWARD N°: FA8655-09-1-3036 1

TITLE: Novel laser-based technique for measurements of primary atomisation characteristics of liquid jets

INVESTIGATOR: Professor Y. Hardalupas

ORGANISATION: Imperial College of Science, Technology and Medicine

REPORTING PERIOD: From: 20 July 2009 To: 19 July 2010

PROJECT START DATE: 20 July 2009

DATE OF ISSUE OF THIS REPORT: 3 August 2010

ADMINISTRATIVE OFFICE: European Office of Aerospace Research and Development (EOARD)

GOVERNMENT PROGRAM MANAGER: Dr. Brad Thompson

Table of Contents

List of Figures

Figure 14: Effect of the refractive index of the liquid on the fluorescent intensity along the length of the liquid column. No significant change is observed for refractive indices between 1.33 and 1.50. (Example for L/D=0.25, G/D=0.05, γ=0.001m^{-1}, ω=20°)

Figure 15: Effect of laser beam divergence at the exit of the liquid nozzle on the fluorescent intensity along the length of the liquid column. Lower divergence results in higher fluorescent intensity. (Example for L/D=2.0, G/D=0.25, γ=0.0002m^{-1}, n_1=1.33)

Figure 16: Effect of laser beam profile at the exit of the liquid nozzle on the fluorescent intensity along the length of the liquid column. There is little variation of the fluorescent intensity regardless of the laser beam profile. (Example for L/D=1.0, G/D=0.10, γ=0.02m^{-1}, n_1=1.33, ω=20°)

Figure 17: Time resolved imaging reveals the location of jet breaking point, which could be missed by single frame photography. The horizontal dark line is the electrical conductivity probe. The arrows indicate the location that liquid jet breakup may have been initiated on each single image. (example shown for a liquid flow rate of 0.5l/min and air flow rates of 1250l/min)

Figure 18: Interaction between the liquid jet and the probe a) obstructed atomisation b) unobstructed atomisation. (Example shown for a liquid flow rate of 0.5l/min and air flow rates of 1000l/min). The horizontal dark line is the electrical conductivity probe.

Figure 19: Diagrams illustrating the average values against the distance between the probe and the nozzle for the different flow conditions. Location of estimated breaking point shown as a red dot.

Figure 20: Sequence of temporally resolved photographic images (for a liquid flow rate of 0.5l/min and air flow rates of 1250l/min) overlapped by the measured voltage between the nozzle and the probe (red line).

Figure 21: Example of photography (left) and optical connectivity (right). The optical connectivity technique is less influenced by the presence of the product of atomisation around the spray. (Example shown for a liquid flow rate of 0.5l/min and air flow rates of 1250l/min).

Figure 22: Comparison of the breakup length measurements obtained by the three experimental techniques. Each technique is indicated as HS: High-speed photography, EC: Electrical Connectivity, OC: Optical Connectivity.

List of Tables

Summary

During the first stages of atomization in an air-blast atomizer, the liquid stream is destabilized under the influence of a coaxial stream of air, until its continuity is broken. A novel technique [Charalampous *et al.* 2007 (1)] has been proposed to measure the length of the continuous liquid jet, based on the internal illumination of the liquid jet through the spray nozzle. The liquid jet acts as a light guide, which propagates along the length of the jet, in the same way as light travels along the length of an optical fiber. The laser light excites a fluorescent dye that is dissolved in the liquid jet, making the volume of the liquid jet luminous. Then, the connectivity of the liquid jet is linked to the optical connectivity of the fluorescent jet. However, since the surface of the liquid jet is not smooth, as that of an optical fiber, due to the development of waves on the jet surface, there are losses of light intensity due to refraction through the jet surface and absorption by the fluorescence dye, as it propagates along the liquid jet. The current project evaluates the optical connectivity technique numerically and experimentally. First, numerical simulations of the light propagation within liquid columns of various geometries are presented. The effects of the morphological characteristics of the interfacial waves on the gas-liquid interface (wavelength and amplitude) and the type of perturbation (sinus or varicose) as well as the absorption of laser light within the liquid jet and the characteristics of the laser beam (divergence and intensity profile) were considered. Next, a comparison is presented between measurements of the break-up length of liquid jet in an airblast atomiser obtained with three different techniques. The first technique is high-speed shadowgraphy, where the breakup process of a liquid jet is recorded with high temporal resolution, so that potential difficulties in identifying the breakup length due to obstruction of the liquid jet core by the surrounding dense spray are eased in comparison to single frame photography. The second technique is the electrical conductivity method, where the continuity of an electrically conducting atomising jet is measured by the presence of an electrical connection between the spray nozzle and a probe placed within the liquid jet downstream of the nozzle exit. The third is the optical connectivity method, which is based on laser illumination of an atomising liquid jet, doped with a fluorescing dye, from within the nozzle. The breakup length measurements with all three techniques are compared and the advantages and limitations of each method and the extent of their applicability are discussed. The comparison shows that the optical connectivity technique performs better than the other techniques in measuring the mean breakup length of the liquid jet.

Introduction

During the first stages of atomization of a liquid jet, the jet is progressively destabilized under the influence of the forces that result from the interaction of the liquid stream with the surrounding air (2, 3). During this process the jet geometry changes as liquid is removed from its surface and waves develop on the surface until their amplitude becomes large enough to lead to breakup of the liquid jet. The distance from the nozzle exit to the point downstream the nozzle, where the liquid jet breaks up defines what is known as the “primary atomization region”. The length of the continuous core of the liquid jet, known as the “breakup length”, determines the extent of the primary atomization region and the performance of atomizing nozzles.

A number of techniques have been proposed for the measurement of the length of the continuous jet. These include photography (4, 5), electrical conductivity (6-9), X-ray absorption (10-12) and ballistic imaging (13-15). A recently proposed method is the optical connectivity technique (1). It has been shown that in dense sprays it can provide good measurement of the breakup length of liquid jet at conditions where the continuous length of the jet would be difficult to determine with photography as the atomization products that surround the jet could hinder the view to the continuous jet.

In the current report, three techniques will be used, namely the high-speed shadowgraphy, electrical connectivity and the optical connectivity.

Photography (usually shadowgraphy) is the most commonly used method, as it is straightforward to apply and places only moderate demands on equipment. In this method, the atomizing jet is imaged directly by a camera. A light source is necessary to illuminate the liquid jet and is usually placed behind the jet propagating directly into the camera lens. In this way, the shadow of the jet is imaged and its contour is well defined in the acquired images. The break-up length is estimated from the geometry of the recorded contour. While this method is easy to implement, when atomization becomes more intense, the droplets around the jet core might obstruct parts of the jet and the break-up length could be measured longer than it is.

The electrical conductivity technique is based on the conduction of electricity along the length of the continuous liquid jet downstream the nozzle. A potential is applied between the spray nozzle and a probe downstream. If there is continuity of the liquid phase between the nozzle and the probe, a closed electrical circuit will ensue. The probe can be moved across different positions to determine the continuity of the liquid jet as a function of downstream distance. If the detected potential is low it is verified that there is electrical connectivity up to a specific point indicating continuity of the liquid jet core. On the contrary, the discontinuity of the liquid jet can be located where the conductivity is negligible. In earlier work, many researchers developed a conductivity probe technique to enable the investigation of the breakup zone in a variety of applications. Yule and Salters (8) investigated the breakup zone of a transient diesel spray as a function of time and position employing a wire probe. Hiroyasu et al (7, 9) studied the breakup length of a high-speed liquid jet by measuring an electrical resistance between the nozzle and a fine wire screen detector located in a spray jet. Chehroudi et al (6) tried to determine the shape and length of the intact liquid core by applying a voltage between the nozzle unit and fine needles, rods and screens. The results show that current is carried not only by intact liquid cores but also by atomized unconnected sprays.

The novel optical connectivity of a liquid jet (16, 17) relies on illuminating a liquid jet from within the nozzle by a laser beam, which propagates downstream, while reflecting at the gas-liquid interface. Due to the higher index of refraction of the liquid jet to that of the surrounding gas, a

laser light ray that interacts with the gas-liquid interface at a sufficiently large incident angle undergoes total internal reflection. As a consequence, the laser beam is reflected completely back into the liquid stream and propagates downstream for a long distance in the same way that light propagates along optical fibers. Collandon (18) demonstrated this phenomenon as early as 1842. The addition of a fluorescent dye, such a Rhodamine WT in the liquid jet, causes some of the intensity of the laser beam to be absorbed and re-emitted at a longer wavelength as fluorescence. This causes the volume of the continuous jet to become luminous which allows the evaluation of the break-up length. Beyond the point of liquid discontinuity, the laser beam is diffused and its intensity is significantly reduced. The optical connectivity technique is not without limitations. As the technique is based on the propagation of light within an atomizing liquid jet, there will unavoidably be some scattering losses at the interface that will reduce the intensity of the propagating light. Therefore, for long liquid jets, the technique will not be possible to operate due to complete attenuation of the propagating light along the liquid. Here, we develop a numerical model of the liquid jet to determine how the laser light that is seeded at the base of the jet propagates along the length of the jet and what are the effects of its geometry on the losses of the intensity of the laser light.

In addition we use the electrical conductivity technique (6-8) and high speed shadowgraphy to make comparisons of the measured lengths of the continuous jet. In the electrical connectivity technique, the continuity of the jet is determined by the electrical conductivity between the spray nozzle and a probe placed in the electrically charged liquid downstream of the liquid nozzle exit. This is equivalent to the optical connectivity approach.

The next section of this report describes the operation of the optical connectivity technique and presents the geometrical optics approach that was developed to evaluate numerically the influence of various parameters on the accuracy of measurements of the length of the continuous liquid jet and describes the electrical connectivity technique and the airblast atomizer used for the measurements. This section also describes the setup of the photography (shadowgraphy) measurements and the electrical connectivity and describes the coaxial airblast atomizer used for the current experiments. The next section presents the results. The numerical results, based on the geometrical optics approach, are reported and quantify the performance of the optical connectivity technique and provide guidelines for optimization. The experimental results describe the data processing approach for the electrical connectivity technique and the comparison of measurements of the length of the continuous liquid jet with the high speed shadowgraphy, electrical and optical connectivity techniques follow. The paper ends with a summary of the main findings.

Methods, Assumptions and Procedure

(a) Optical Connectivity Technique

An optical connectivity technique has been developed for the measurement of the continuous length of sprays. The technique works by introducing a laser beam within the flow of the liquid upstream of the nozzle that exits with the liquid through the nozzle in the direction parallel to the nozzle axis. In this way the laser beam is largely contained within the liquid jet by reflecting on the liquid interface propagating downstream and illuminating the liquid jet volume. A ray of laser light is guided along the length of the liquid jet by reflecting on the gas-liquid interface at the jet surface. As long as the angle of incidence between the surface of the jet and the laser light rays is greater then the angle of total internal reflection, the rays are completely reflected back inside

the liquid without intensity losses from refraction. This principle is similar to the way that a laser beam propagates within an optical fiber. However, if the angle of incidence of a laser light ray on the liquid jet interface becomes smaller than that for total internal reflection then there will be some intensity losses due to refraction.

The laser beam continues to propagate downstream the jet until it meets the breaking point of liquid jet, where it can no longer be contained within the jet and is diffused randomly in different directions. The introduction of a fluorescing dye into the liquid makes part of the laser beam to be absorbed along the length of the liquid jet, and subsequently be re-emitted as fluorescence. In this way the atomizing jet becomes luminous and can be imaged (**Figure 1**).

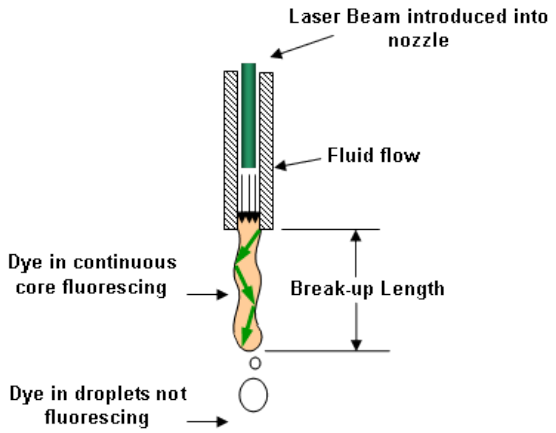

Figure 6: Principle of the optical connectivity technique

Depending on the roughness of the surface of the liquid jet, the amount of energy losses of the laser beam along the length of the jet changes. For a relatively smooth jet surface, the fluorescent intensity from the liquid jet is relatively uniform along its length (**Figure 2a**) and there is little decrease within the imaged region. The locations of the arrows indicate local maxima of intensity, which occur due to the local liquid jet surface structure, but these have no influence on the uniformity of the intensity along the liquid jet. However, if the surface of the jet is wavy, the image of the fluorescent intensity clearly shows that the intensity decreases along the length of the jet (**Figure 2b**). This is caused by the increased amount of light intensity losses at the gas liquid interface in the latter case. Therefore, there are limits on the length of the continuous jet that can be visualized with the fluorescence technique, which depend on the geometry of the liquid jet and the fluorescent dye concentration. Therefore, there is a need to evaluate the dependence of the propagating laser light intensity along the liquid jet on the various parameters of the liquid jet. This will be performed with a geometrical optics calculation approach, as described in the following section.

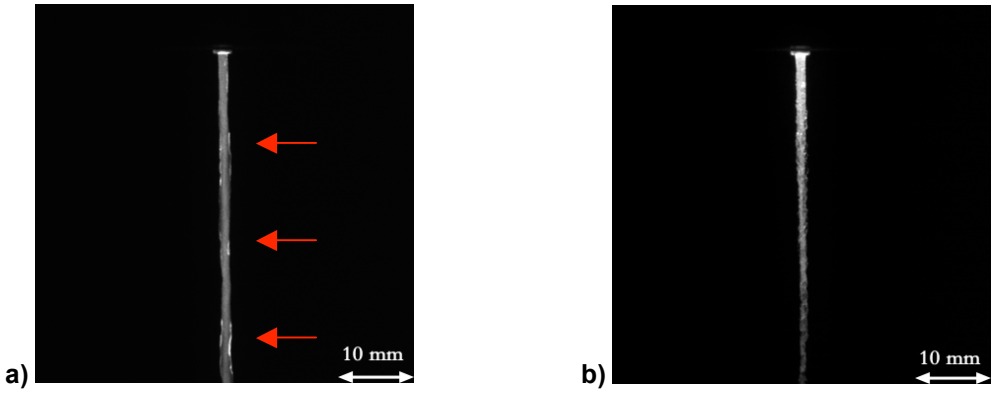

Figure 2: Fluorescent intensity image using illumination from within the nozzle of a straight jet a) with smooth surface and b) wavy surface. The image of the jet in the first case shows that along the jet length the fluorescent intensity is relatively uniform, while the decrease of the fluorescent intensity along the jet length is notable in the second case. The nozzle exit is at the top of the image.

(b) Geometrical Optics Simulations

For the evaluation of the effect of the shape of the jet geometry on the propagation of light within a column of liquid, the propagation of laser light rays is calculated using geometrical optics. This simulation has the benefit of enabling the evaluation of the effect of all operating parameters, which is difficult to achieve experimentally.

The liquid jet for this investigation is considered as a two-dimensional liquid column. The central axis of the liquid column extends along the x-axis of a Cartesian coordinate system. The interface of the jet is described by the sinusoidal wave function along the x-axis:

$$y = G\sin\left(\frac{2\pi x}{L} + \phi\right) + y_0 \qquad (1)$$

where G is the amplitude of the wave on the interface and L is the wavelength of the wave on the surface of the interface. ϕ is the phase of the wave on the surface of the interface and sinusoidal disturbances are present along the liquid column when the phases of the top and bottom interfaces are matched or varicose disturbances appear when the phases of the waves between the top and bottom surfaces are shifted by π.

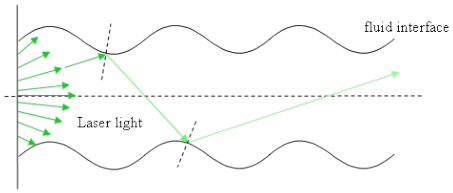

Figure 3: Basic geometry of the considered liquid jet and diverging rays at the base of the liquid column.

For the geometrical optics calculations, a monochromatic laser beam that propagates inside the liquid column is considered (**Figure 3**). The laser beam is simulated by a large number of rays that start at the base of the liquid column at uniformly spaced intervals and propagate downstream the nozzle exit. The ray that begins on the axis of the column is aligned parallel to

the axis. However, in order to consider the influence of the divergence (ω) of the laser beam, the angle between the rays at the column base and the axis is progressively changed as the distance between the axis and the starting point of the rays along the *y*-axis increases.

The calculation of the path of the rays when they are incident to the surface of the liquid column is estimated by:

$$R = V - 2(V \cdot N)N \tag{2}$$

where *V* is the incident ray vector, *N* is the vector normal to the jet surface at intersection point (between the wave and the incident ray) and *R* is the vector of the reflected ray.

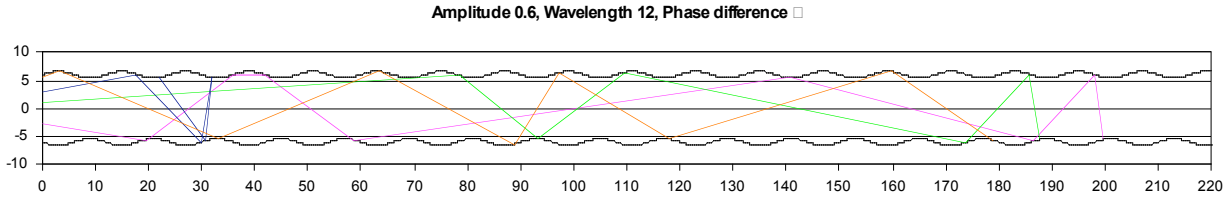

Figure 4: Example of propagation of light rays within a liquid column as determined by geometrical optics calculations. The vertical axis shows the width of the liquid column around the center and the horizontal axis shows the length along the direction of motion of the liquid column.

As the rays propagate along the liquid column (**Figure 4**), the initial intensity of each beam I_0 is reduced due to refraction of the light at the liquid interface, which is lost, and absorption from the dye present in the liquid, which is re-emitted as fluorescence.

Considering the angle of incidence between the rays and the local interfacial surface of the liquid, the critical angle for total internal reflection is given by the relationship:

$$\theta_{crit} = \sin^{-1}\left(\frac{n_2}{n_1}\right) \tag{3}$$

where n_1, n_2 the refractive indices of the liquid and the gas phases. However, when the angle of incidence between a ray and the air-liquid interface is smaller that the angle of incidence for total internal reflection, there are losses of the intensity of the ray. The fraction of the intensity of incident light that is reflected from the interface is given by the reflection coefficient *R*, and the fraction refracted by the transmission coefficient *T*. The Fresnel equations are used to calculate *R* and *T*. The calculations of *R* and *T* depend on polarization of the incident ray. If the light is polarized with the electric field of the light perpendicular to the plane of **Figures 3** or **4** (s-polarized), the reflection coefficient is:

$$R_s = \left[\frac{\sin(\theta_1 - \theta_2)}{\sin(\theta_1 + \theta_2)}\right]^2 \tag{4}$$

If the incident light is polarized in the plane of the **Figures 3** or **4** (p-polarized), the reflection coefficient *R* is:

$$R_p = \left[\frac{\tan(\theta_2 - \theta_1)}{\tan(\theta_1 + \theta_2)}\right]^2 \tag{5}$$

The Beer-Lambert law estimates the reduction of the intensity of the rays due to the absorption caused by the fluorescent dye present in the liquid through which the ray is traveling:

$$I = I_0 e^{-\gamma z} \tag{6}$$

where γ is the absorption coefficient, z the path length traveled by the ray, I_0 is the initial intensity of the ray and I the intensity of the ray after it has traveled a distance z in the absorbing medium.

The total reduction of the initial intensity I_0 of the laser beam that travels along a path of length z in an absorbing medium until it reaches the interface is given by the formula:

$$I = \left(\frac{\left[\frac{\sin(\theta_1 - \theta_2)}{\sin(\theta_1 + \theta_2)}\right]^2 + \left[\frac{\tan(\theta_2 - \theta_1)}{\tan(\theta_1 + \theta_2)}\right]^2}{2} \right) I_0 \cdot (e^{-\gamma z}) \tag{7}$$

While the refracted part of the laser light intensity is lost, the absorbed light intensity along the ray path is subsequently re-emitted as fluorescence. By summation of the losses of the laser light intensity of each ray due to absorption at each distance downstream of the nozzle exit, the profile of the fluorescent intensity with distance from the nozzle exit is determined. In this way, the limitations of the visualization of the fluorescent liquid jet can be determined. The parameters that influence the loss of light intensity are morphological (wavelength, *L*, amplitude, *G*, and phase, ϕ, of the waves on the surface of the liquid column), physical (absorption of light within the liquid, γ, and refractive index of liquid, n_1) and optical (divergence of rays of laser light, ω). The wavelength and the amplitude of the waves on the liquid surface were normalized by the diameter of the liquid jet at the nozzle exit *D*.

Table 1. Range of considered parameters for geometrical optics calculations

G/*D*	0.03 - 0.25
L/*D*	0.25 - 4.00
ϕ	0, π
γ	0.00008 m^{-1} - 0.1m^{-1}
n_1	1.33, 1.40, 1.50
ω	5°, 10°, 20°

A summary of the range of parameters that are examined in this investigation is presented in **Table** . However, a limited number of combinations of these parameters were considered due to processing power requirements.

(c) Electrical Connectivity technique

In the electrical conductivity technique (6-9), an electrical potential is applied between the nozzle and a probe placed within the liquid jet downstream of the liquid nozzle exit (**Figure 5**). When there is a continuous stream of conducting liquid, such as tap water, an electrical current will run through the liquid between the nozzle and the probe. The detection of electrical connection between the nozzle and the probe indicates that the continuous length of liquid jet is at least as long as the distance between the two. The electrical connectivity technique was implemented in the air-blast atomizer of (4).

For the electrical connectivity technique a circuit was designed around the liquid jet as illustrated in **Figure 5**. A constant voltage of 10V (adjustable by 0.1mV increments) from a stabilised battery supply was applied between the liquid nozzle of the atomizer and a stainless needle probe, 1.1mm in diameter. The probe crossed the centreline of the liquid nozzle at a normal angle to the axis of the atomiser. The distance between the needle probe and the nozzle was adjusted by a vertical traverse. The distance from the nozzle exit was considered in steps of 1mm. A 1 MΩ resistance was connected between the positive pole of a power supply and the probe to regulate the current in the circuit. The negative pole of the supplier was wired straight to the nozzle of the atomizer. In order to minimize electrical noise, the circuit was grounded. The potential between the nozzle and the probe was recorded by a 12-bit National Instruments PCI-6023E analogue to digital converter. Low voltages indicate low resistance between the nozzle and the probe demonstrating electrical connectivity and therefore continuity of the liquid jet, while high voltages indicate high resistance between the probe and the nozzle and therefore marginal or no continuity of the liquid jet. The acquisition rate of the potential between the probe and the nozzle of the A/D converter was synchronised to the 20kHz frame rate of the high-speed camera to obtain simultaneous measurements with both measurement techniques.

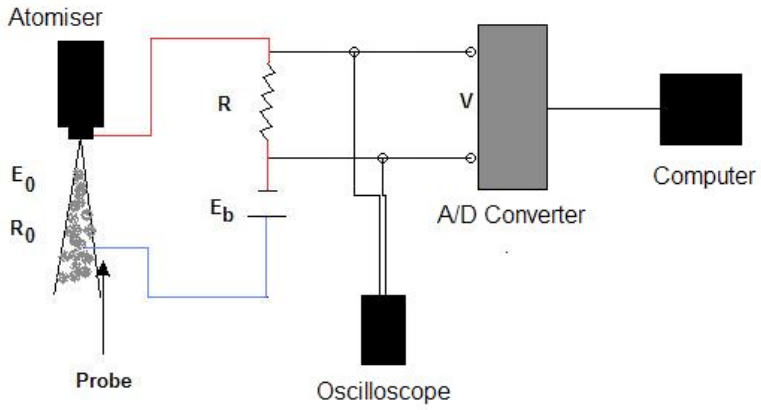

Figure 5: Schematic of the implementation of the electrical conductivity technique on a spray

(d) High speed photography (shadowgraphy)

For the photographic imaging a Photron Fastcam-APX RS camera fitted with a 105mm lens was used. The camera was operated at 20000 frames/sec in order to obtain a temporally resolved sequence of images for each flow condition. The temporally resolved photographic record, makes the determination of the break-up point less ambiguous in cases where the full length of the atomizing jet is not clearly visible when the products of atomization obstruct optical access to the liquid jet as the breaking point can be traced upstream for the sequence of frames. The

source of illumination was a 100W lamp that was placed behind the liquid jet so that the imaging of the shadow of the liquid jet was in the forward scattering direction. The instantaneous shadow of the liquid jet and droplets was recorded by the camera and subsequently processed.

(e) Coaxial Airblast Atomiser

The experimental investigation was performed on the coaxial air-blast atomizer configuration, described in detail in (4). In this investigation the atomizer was placed vertically and the spray exhausted downwards. The internal diameter of the liquid nozzle was *D*=2.3mm and the internal diameter of the coaxial air nozzle was 22.95mm.

The configuration of the original atomizer was modified as shown in **Figure 6**. A hollow tube open at the top end and fitted with a quartz window at the lower end was inserted within the central tube of the atomizing liquid, up to the conical contraction of the liquid nozzle. This addition acts as a light guide, which allows a laser pulse to propagate through the central tube without interacting with the liquid for the full length of the central tube. Upstream of the liquid nozzle exit, the laser beam exits through the light guide tube window, propagates through the liquid flow and exits through the nozzle in the same direction as the flow of the atomized liquid. In this way, the intact liquid jet acts as an optical fiber, which allows the propagation of the laser light till the location of the break up. In this approach the laser beam is delivered within the continuous section of the liquid jet without the attenuation caused by approaches that introduce the laser beam through the surrounding spray and ensures that low light intensity is present beyond the surface of the liquid jet.

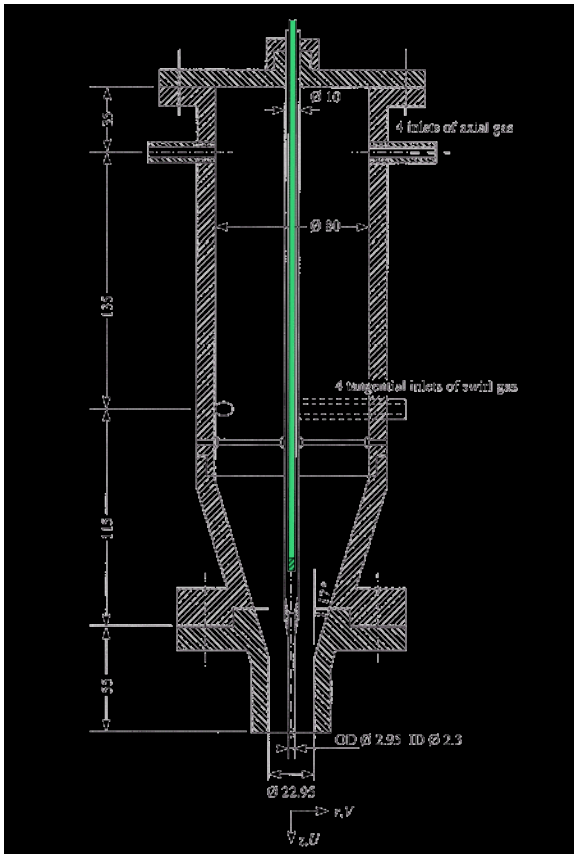

Figure 6: Geometry of coaxial airblast atomizer. The addition of the laser light-guide tube within the liquid jet is shown in green.

The introduction of the laser beam through the liquid jet nozzle is combined with the addition of the fluorescing Rhodamine WT dye within the liquid. This addition leads to the emission of fluorescent light from the liquid along the path of the laser beam. Two reasons make the addition of the dye advantageous. The first is that as the laser beam propagates through the liquid core it interacts with the surface of the liquid jet and some light may be scattered, leading to difficulties in detecting the interface of the liquid jet. The addition of laser dye means that the fluorescing light from the liquid jet can be detected at a longer wavelength than that of the incoming laser beam and avoid background noise on images due to the scattered light. The second reason is that the fluorescing light tracks the volume of the liquid and, therefore, is emitted from everywhere within the liquid jet, as opposed to scattered light which is associated with the surface of the liquid jet. The concentration of the fluorescing dye was adjusted to ensure that the absorption of the incident light remained low enough to allow laser light to propagate through the liquid for around 150 mm, which was longer than the break-up length for all examined cases.

The measurements of the breakup length with the optical connectivity technique were obtained by steering a Nd:YAG laser, operating at 532nm, into the light guide tube by a system of mirrors and lenses so that it entered in a direction parallel to the tube axis to minimise reflections on the internal surfaces of the tube. The laser beam exited just before the contraction of the liquid jet nozzle, in a direction parallel to the nozzle axis so that it propagates in the direction of the liquid stream. The atomizing liquid was doped with Rhodamine WT dye, which is excited by light at 532nm and fluoresces strongly with a peak at 587nm. As a consequence, the liquid jet became luminous along the length of propagation of the beam. For the imaging of the fluorescent jet an Andor ICCD camera with a resolution of 1024x1024 pixels was used. A long pass optical filter that absorbs the laser wavelength at 532nm and transmits the longer wavelengths of the fluorescent light was placed in front of the camera lens to suppress scattered light. The optical connectivity measurements were not temporarily resolved and were obtained independently of the high-speed measurements.

Measurements with optical connectivity, electrical conductivity and high-speed photography were obtained for a liquid flow rate of 0.5l/min and air flow rates of 500, 750, 1000, 1250, 1500 and 1750 l/min. For the optical connectivity technique, the gas flow rates were 500, 750, 1250 and 1750 l/min. The initial operating conditions of the atomiser were expressed in terms of non-dimensional parameters, namely Reynolds number, Re, Weber number, We, and gas-to-liquid momentum ratio, MR, which are defined below:

$$\mathrm{Re} = \frac{\rho_L U_L D_L}{\mu} \tag{8}$$

$$We = \frac{\rho_L \left(U_L - U_G\right)^2 D_L}{\sigma} \tag{9}$$

$$MR = \frac{\rho_G U_G^2 (D_G^2 - D_O^2)}{\rho_G U_L^2 D_L^2} \tag{10}$$

where ρ_L is the liquid density, ρ_G is the gas density, D_L is the internal diameter of the liquid nozzle, D_G is the internal diameter of the gas nozzle exit, U_L is the cross section average velocity at the liquid nozzle exit, U_G is the cross section average velocity at the gas nozzle exit,

μ is the liquid dynamic viscosity and σ is the surface tension of the liquid The resulting liquid Reynolds number was 5442 while the Weber number ranged between 80-1041 and the momentum flow ratio between 27-335.

Results and discussion

This section presents first the results of the laser light propagation through a liquid jet with wavy surface using the geometrical optics approach described in the previous section. Then, results from measurements with the electrical connectivity, high-speed photography and optical connectivity techniques are presented. A comparison between the breakup length measurements with the three techniques is presented and discussed.

(a) Geometrical Optics Calculations

The influence of the morphological characteristics of the liquid column on the decay of the fluorescent intensity along its length is examined first. The effect of the amplitude of the waves on the surface of the liquid column on the decay of the fluorescent light intensity along the length of the column is shown in **Figure 7**. It is generally observed that there is a larger decrease in the fluorescent intensity with axial distance from the nozzle exit as the amplitude of the surface waves increases. This can be explained from **Figure 8**, where the paths of the same ray are traced within liquid columns with surface waves of small and large amplitudes, and can be attributed to two factors. One is that when the amplitude of the waves is small, the rays hit the inner surface of the liquid jet at angles greater than the angle for total internal reflection of Equation (3). In this way, the intensity losses due to refraction of laser light outside the liquid remain minimal and most of the losses of the laser light are due to absorption by the fluorescent dye within the liquid. In contrast, when the amplitude of the surface waves is large, the losses due to refraction are greater and the fluorescent intensity of the liquid jet decreases faster with axial distance. In addition to the losses due to refraction, another issue with large amplitude surface waves is that more rays tend to be reflected backwards (towards the nozzle exit) when they impinge against troughs of large amplitude. This causes lower penetration of the laser beam along the liquid column and, as a result, the fluorescent intensity along the liquid column decreases.

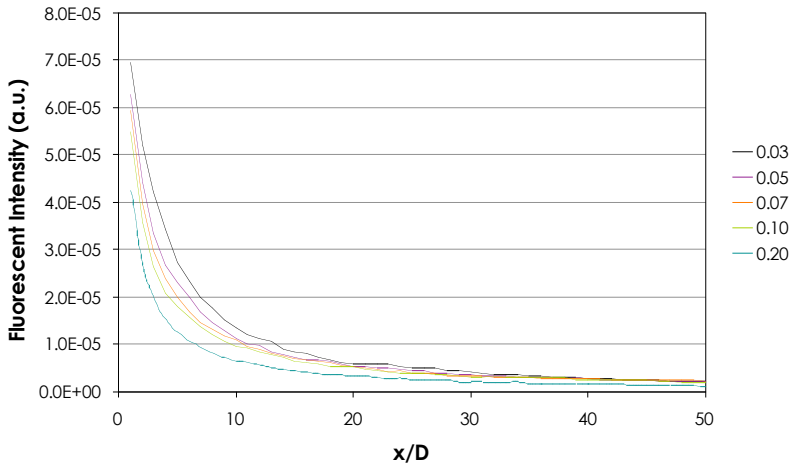

Figure 7: Effect of the amplitude of the surface waves of the liquid column on the fluorescent intensity along the length of the column. Smaller amplitudes result in higher fluorescent intensity. (Example for L/D=0.25, γ=0.00008m^{-1}, n_1=1.33, ω=20°)

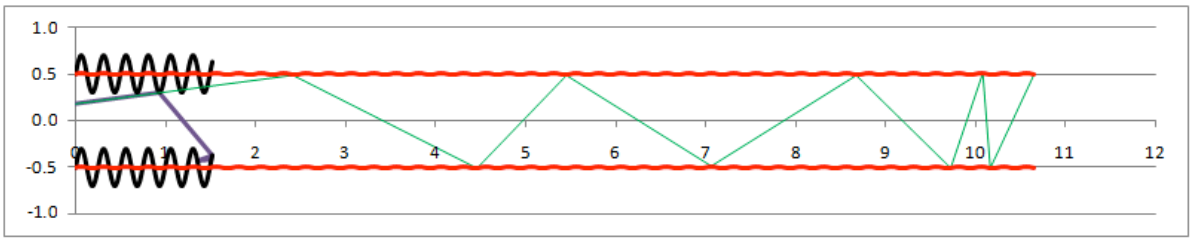

Figure 8: Paths of the same ray inside liquid columns with large and small amplitude of surface waves, which have the same wavelength.

The wavelength of the surface waves was also found to influence the fluorescent intensity of the liquid jet significantly. As demonstrated in **Figure 9**, when the wavelength of the surface waves decreases, the fluorescent light intensity along the liquid length reduces. The effect is more profound as the wavelength of the surface wave decreases to about the dimension of the liquid nozzle exit *D*. For even smaller wavelengths, the changes in the fluorescent intensity are small. The effect can be explained as before by considering the angle of incidence of the rays of the laser beam and the internal surface of the liquid jet, which is demonstrated in **Figure 10**, where the path of the same ray is shown within a liquid jet with surface waves of long and short wavelength. When the wavelength is large, the rays impinge on the surface at large angles and total internal reflection occurs. In addition, the reflected light is mostly in the forward direction and therefore propagates further along the liquid column. For the longest wavelength considered, the fluorescent intensity profile has some variations, which can be attributed to the morphology of the column, since they appear at distances of about half a wavelength. As the unevenness of the profile is minor there are no issues with the visualization of the continuous liquid column. For shorter wavelengths, the probability of refraction of rays outside the liquid jet and losses of the laser beam intensity is increased as the angle of incidence becomes routinely high. Nevertheless, when the wavelength of the surface waves decreases to about the size of the liquid nozzle, no reduction is demonstrated on the profile of the fluorescent intensity with further reduction of the surface wavelength. The reason for this is not yet clear.

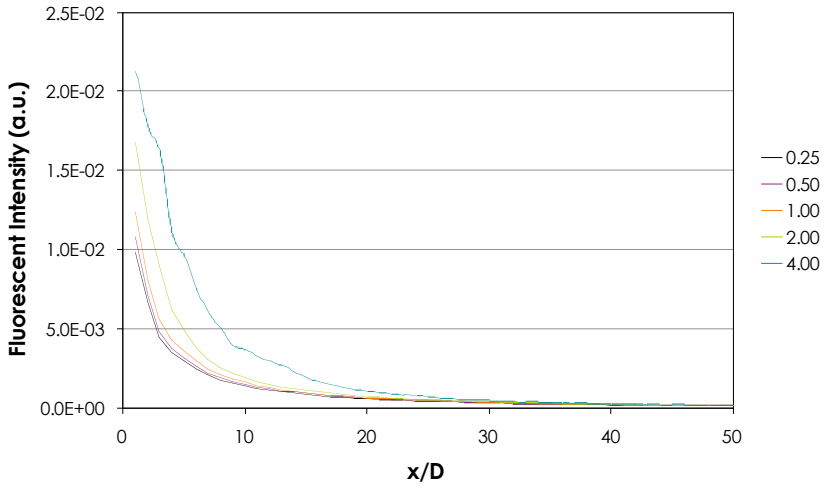

Figure 9: Effect of the wavelength of the surface waves of the liquid column on the fluorescent intensity along the length of the column. Longer wavelengths result in higher fluorescent intensity. (Example for G/D=0.20, γ=0.02m^{-1}, n_1=1.33, ω=20°)

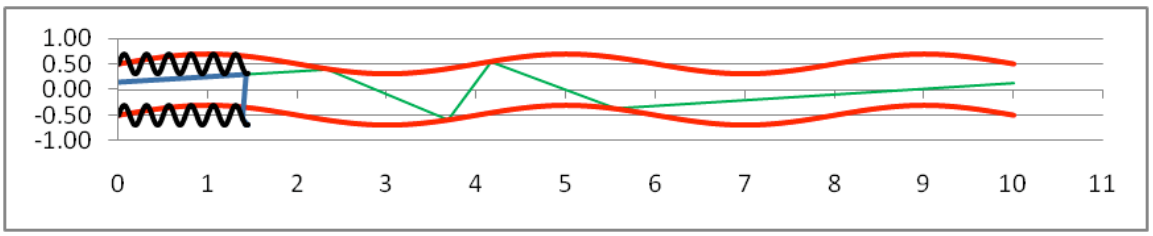

Figure 10: Paths of the same ray inside liquid columns with large and small wavelengths and same amplitude.

The last morphological consideration is the phase between the two surface waves. When the two waves are in phase, the result is a sinusoidal overall profile of the liquid column, as shown in **Figure 11a**. However, when the two waves have a phase difference of 180°, then the profile of the liquid column is varicose, as shown in **Figure 11b**.

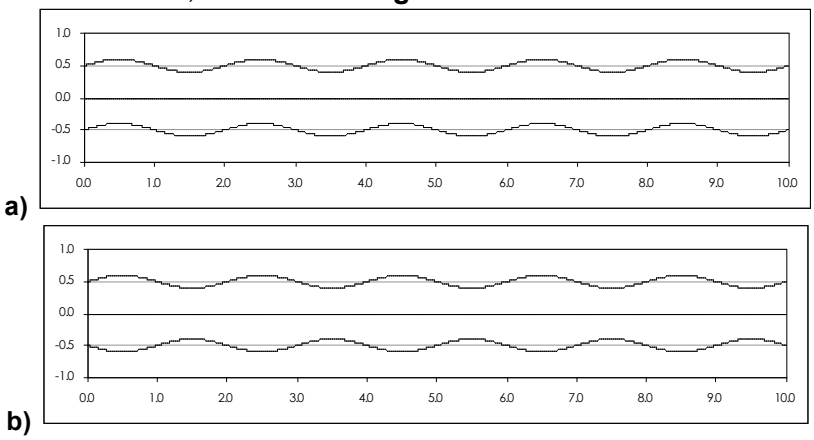

Figure 11: Sinusoidal and varicose profiles of the liquid column for a) ϕ=0° b) ϕ=π phase difference between the waves on the liquid interfaces of the column.

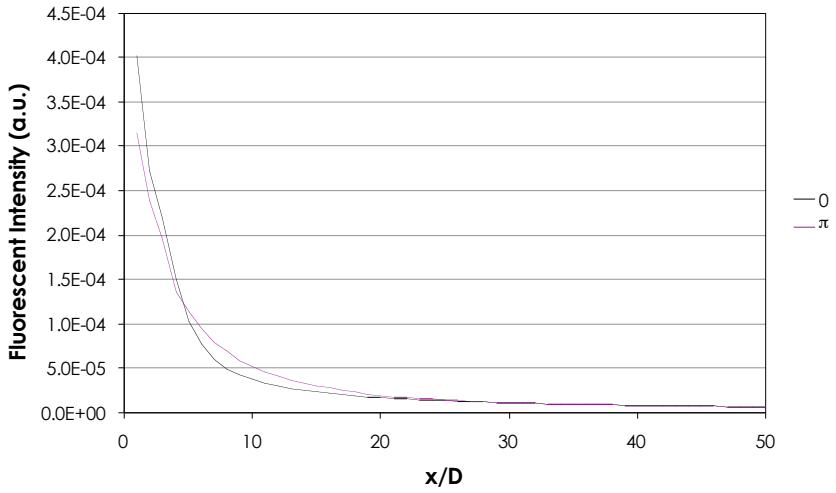

Figure 7: Effect of the phase between the surface waves of the liquid column on the fluorescent intensity along the length of the column. a) ϕ=0° (sinusoidal jet), b) ϕ=π (varicose jet). (Example for L/D=2.0, G/D=0.25, γ=0.0004m^{-1}, n_1=1.40, ω=20°)

Despite the different morphology of the sinusoidal and varicose behaviour of the liquid columns, the profiles of the fluorescent intensity do not diverge much, as demonstrated in **Figure 7**. The

likely explanation is that morphologically it is mostly the amplitude and wavelength of the surface waves that are significant, as they determine the angle of incidence of the laser light on the inner surface of the liquid interface and, in turn, whether total internal reflection without intensity losses or reflection with intensity losses due to refraction will occur. The phase relation between the two interfaces does not considerably affect the angle of incidence and, therefore, the fluorescent intensity remains largely unaffected.

Further to the reduction of the fluorescent intensity along the length of the liquid column due to morphological parameters of the liquid column, the intensity of the laser rays is also reduced due to the absorption of the laser intensity by the fluorescing dye. In contrast to the losses of light due to refraction at the liquid interface, where the refracted light is lost and does not contribute to the fluorescent intensity of the liquid column, the laser energy lost due to absorption by the laser dye is converted to fluorescent light. Increase of the absorption within the liquid always leads to increase of the fluorescent intensity and therefore improves the visualization of the continuous liquid column. The fluorescent intensity at the base of the liquid column was found to scale linearly with the absorption coefficient (i.e. the dye concentration). Therefore, doubling the dye concentration in the liquid leads to a twofold increase of the fluorescent intensity. However, when the dye concentration is increased, due to the increased absorption of the laser light intensity, the fluorescent intensity downstream of the nozzle exit will decrease faster than for low dye concentrations. For example, in **Figure 8**, the fluorescent intensity for γ=0.1m^{-1} is much higher close to the nozzle exit than for the other examined cases but, at about 15*D* downstream the nozzle, it decreases below the fluorescent intensity of a liquid column with γ=0.04m^{-1}. While an exact estimate of the "correct" dye concentration within the liquid cannot be obtained, an indicative rule is that the inverse of the absorption coefficient, which is known as the optical depth, should be well above the length of the liquid column that is to be visualized.

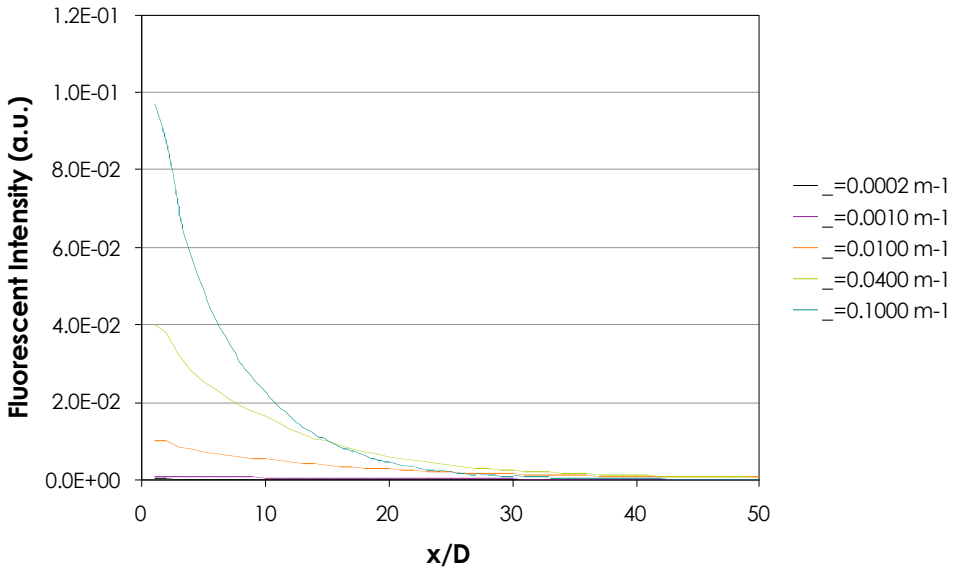

Figure 8: Effect of absorption coefficient of the liquid on the fluorescent intensity along the length of the liquid column. Greater absorption coefficient results in higher fluorescent intensity along the length of the liquid column. (Example for *L*/*D*=2.0, *G*/*D*=0.1, n_1=1.40, ω=5°)

The refractive index of the liquid determines the angle of total reflection. From Equation (3) for the refractive indices of n_1=1.33, n_1=1.40 and n_1=1.50, the angle of total internal reflection becomes θ_{crit}=48.7°, θ_{crit}=45.6°, and θ_{crit}=41.8° respectively. This range of refractive indices includes most liquids that might be encountered in atomization processes. Despite the change of the critical angle, the change of the fluorescent intensity profile is generally marginal, as shown in **Figure 9**. While this is contrary to what was expected, it is likely that the number of rays affected by a change in the angle of total internal reflection by about 7° is not sufficient to change significantly the overall fluorescent intensity.

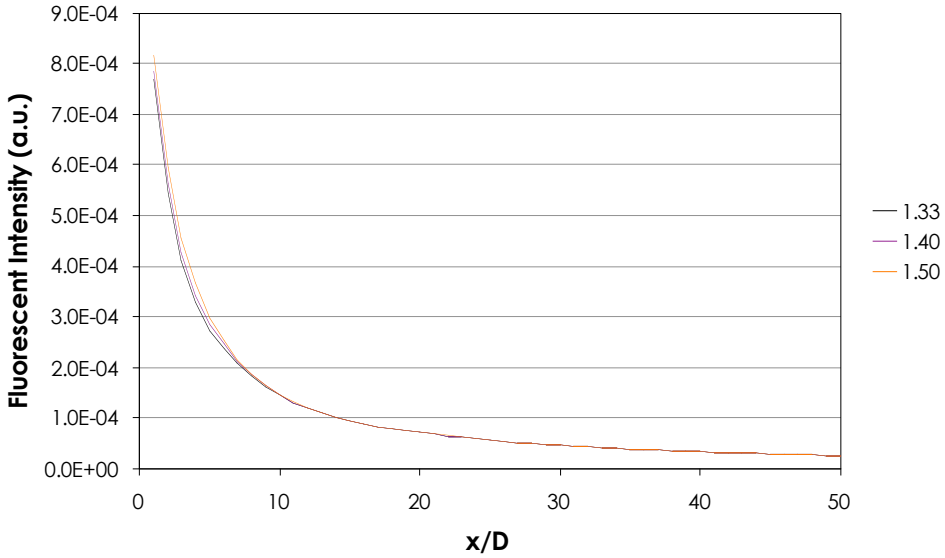

Figure 9: Effect of the refractive index of the liquid on the fluorescent intensity along the length of the liquid column. No significant change is observed for refractive indices between 1.33 and 1.50. (Example for L/D=0.25, G/D=0.05, γ=0.001m^{-1}, ω=20°)

The characteristics of the laser beam at the base of the liquid nozzle were also examined. First the divergence of the laser beam is considered. It was found that as the divergence of the beam increases the fluorescent intensity along the length of the liquid column drops (**Figure**). This is due to the rays of the laser light pointing progressively outwards from the liquid column axis, increasing the probability that the angle of incidence on the liquid-gas interface will be below the critical angle for total internal reflection and, therefore, losses due to refraction are more likely. Since the divergence of the laser beam can be controlled by the optical treatment of the laser beam, it is recommended that the beam is as collimated as possible when it exits the liquid nozzle.

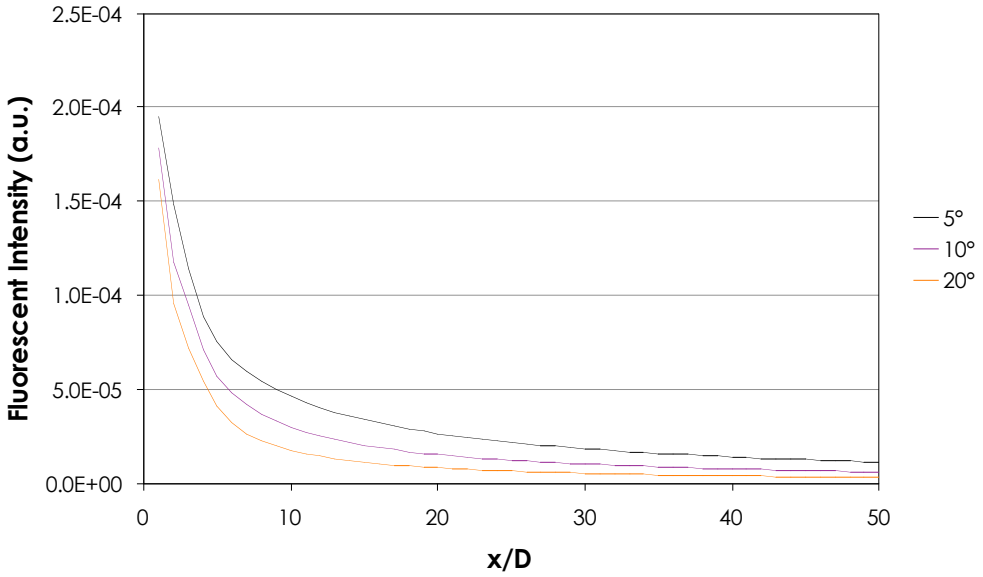

Figure 15: Effect of laser beam divergence at the exit of the liquid nozzle on the fluorescent intensity along the length of the liquid column. Lower divergence results in higher fluorescent intensity. (Example for L/D=2.0, G/D=0.25, γ=0.0002m^{-1}, n_1=1.33)

Finally, the profile of the intensity of the laser beam was considered. A top hat intensity profile is uncommon, while a Gaussian intensity profile is more realistic for a laser beam. The integral of the intensity within the base of the nozzle exit was retained equal among the cases considered to make sure that the illumination of the liquid column was the same for all cases. However, despite the change in the distribution of the laser intensity as it enters the liquid, there was negligible change in the overall fluorescent intensity profile (
Figure). This is advantageous for the optical connectivity technique as the shaping of the intensity profile of a laser beam is not trivial to control.

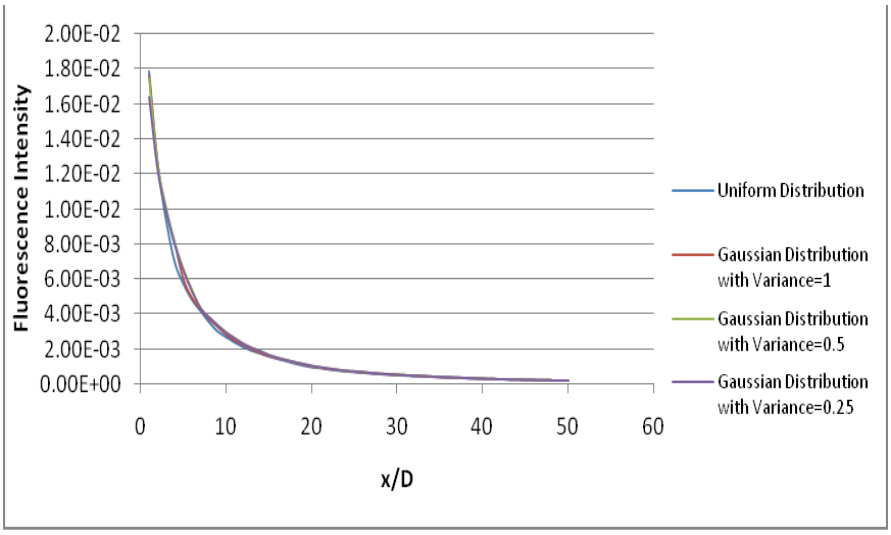

Figure 16: Effect of laser beam profile at the exit of the liquid nozzle on the fluorescent intensity along the length of the liquid column. There is little variation of the fluorescent intensity regardless of the laser beam profile. (Example for L/D=1.0, G/D=0.10, γ=0.02m^{-1}, n_1=1.33, ω=20°)

In summary, the geometrical optics calculations showed that the intensity of the fluorescent light along a liquid column depends on many parameters for the optical connectivity technique. In all cases, the intensity of the fluorescent light does not propagate indefinitely within the liquid column, but decreases progressively along the length of the column. It is possible that, when the continuous length of the liquid column is long, the fluorescent intensity might become too low to be detected along the full length of the continuous liquid column. This has been demonstrated experimentally (1). For this reason, the optical connectivity technique was recommended for cases of good atomization, which lead to short breakup lengths. However, a comparison between the optical and electrical connectivity techniques and high-speed photography is provided below, which may assist the evaluation of the optical connectivity technique.

(b) Comparison between Optical and Electrical Connectivity Techniques

This section starts with the breakup length measurements obtained from high-speed photography. The results from the electrical conductivity technique follow and the voltage drop between the nozzle and the needle are presented. The approach that is used to identify the breakup point of the liquid jet with these two techniques is discussed. The optical connectivity (16) measurements together with some imaging examples are presented next. The section ends with a comparison between breakup length measurements obtained with all three techniques.

The photographic images are considered first. The images of **Figure 17** demonstrate that the exact location of the liquid jet breakup point is not easily determined from single images, especially for conditions where the ligaments and the droplets that surround the liquid jet are dense and can prevent a clear observation of the breakup region. However, from the temporally resolved sequence of images, when studied frame by frame, the breakup location can be determined with higher confidence. When a frame with a discontinued liquid column was observed in the sequence, the corresponding point was chosen as the breakup point. This procedure is illustrated in **Figure 17**, where the first frame shows an apparently continuous jet but within the next few frames it is revealed that the breaking point was actually hidden upstream.

The presence of the electrical connectivity probe (thick horizontal line on images of **Figures 17 and 18**), can be observed in the images, was an issue as it might interfere with the flow of the liquid jet in some occasions, especially when the needle position was close to the nozzle exit (**Figure 18**, left). In this case, the liquid jet core was considered that it was still continuous when a continuous liquid column was connecting the nozzle with the electrical conductivity probe. The first image, for which the liquid column was not perfectly continuous, was considered as a candidate breakup position. When the needle was further downstream the nozzle exit, the liquid flow was not obstructed significantly (**Figure 18**, right).

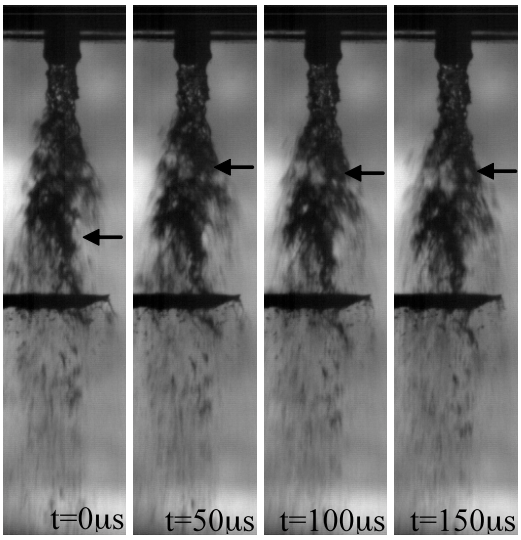

Figure 10: Time resolved imaging reveals the location of jet breaking point, which could be missed by single frame photography. The horizontal dark line is the electrical conductivity probe. The arrows indicate the location that liquid jet breakup may have been initiated on each single image. (Example shown for a liquid flow rate of 0.5l/min and air flow rates of 1250l/min)

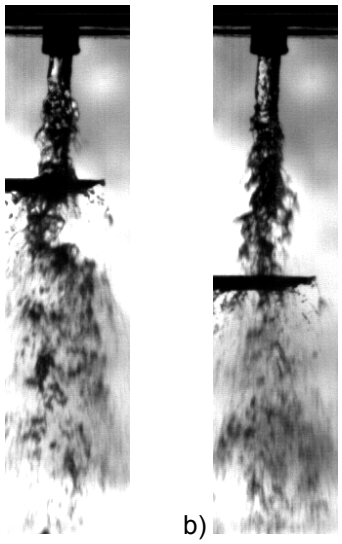

Figure 11: Interaction between the liquid jet and the probe a) obstructed atomisation b) unobstructed atomisation. (Example shown for a liquid flow rate of 0.5l/min and air flow rates of 1000l/min). The horizontal dark line is the electrical conductivity probe.

In the electrical conductivity technique, the probe traversed along the central axis of the liquid nozzle from a distance of 1mm from the nozzle exit downstream in increments of 1mm. For each position of the probe, the time dependent voltage drop between the nozzle and the probe was recorded and processed to calculate the statistical quantities of the mean, the standard deviation, the median value, the skewness and the kurtosis. However, only the mean voltage value is presented here.

The average values of the voltage drop between the nozzle and the probe increase when the needle is moved further away from the nozzle exit and finally reaches the maximum value of 10

Volts. This is equivalent to no conductivity signal from the spray, and indicates that the needle is at a location that the liquid jet is not continuous. The value of 10 Volts is predetermined by adjusting the power supply of the electrical conductivity technique to indicate no conductivity between the nozzle and the needle.

The results of the average values of the voltage drop between the nozzle and the probe are presented in **Figure 19**. These indicate that at a specific distance downstream from the liquid nozzle, the voltage drop between the nozzle and the probe begins to rise rapidly. When the mean voltage measured between the nozzle and the probe is increasing gradually (at values between 2 V and around 4 V), the liquid jet column is continuous. When the measured voltages across the nozzle and the probe start to increase, the local probability of the liquid jet being discontinuous at that location increases. The estimation of the breakup length for each operating condition using the conductivity technique was determined by the change in the slope of the average voltage signal across the nozzle and the probe. When the slope begins to increase rapidly this was determined to be the location of the breakup point and this is indicated by the red dot on the graphs of **Figure 19**.

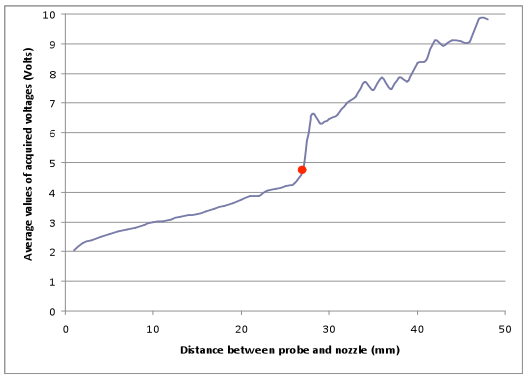

a) Water flowrate: 0.5 l/min, air flowrate 500 l/min

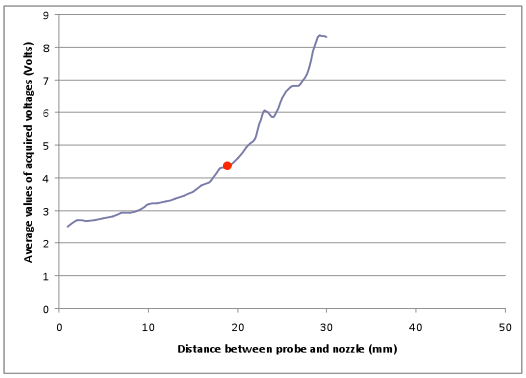

b) Water flowrate: 0.5 l/min, air flowrate 750 l/min

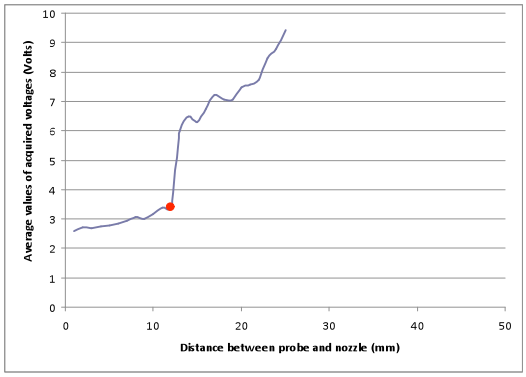

c) Water flowrate: 0.5 l/min, air flowrate 1000 l/min

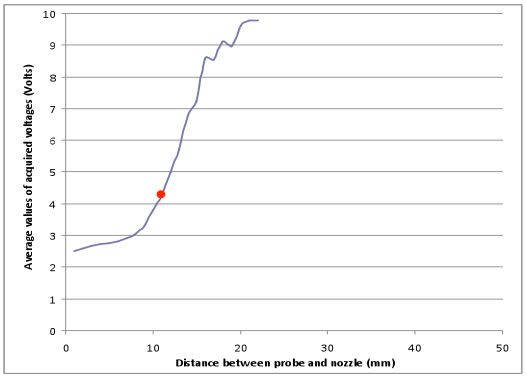

d) Water flowrate: 0.5 l/min, air flowrate 1250 l/min

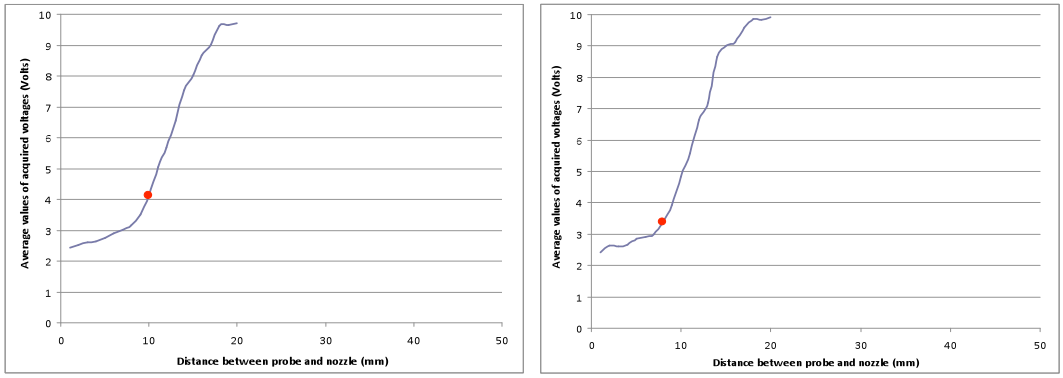

e) Water flowrate: 0.5 l/min, air flowrate 1500 l/min f) Water flowrate: 0.5 l/min, air flowrate 1750 l/min

Figure 12: Diagrams illustrating the average values against the distance between the probe and the nozzle for the different flow conditions. Location of estimated breaking point shown as a red dot.

The comparison of the measured voltages across the nozzle and the probe in relation to matching images of the liquid jet showed that there is correspondence between the apparent contact of the liquid jet on the electrical probe and the voltage drop between the probe and the nozzle. This can be illustrated in the example of **Figure 20**, which shows a sequence of images of the atomising jet along with the measured voltage drop across the jet nozzle and the probe. The progressively decreasing area of contact between the water jet and the needle probe between the acquired images 312 to 320 shows an increasing trend in the measured voltages between the nozzle and the probe while in frames 321 to 322 the increasing contact between the jet and the probe decreases the value of the measured voltage. The peak value of the voltage drop in this example is located at image 320 where the apparent contact between the jet and the probe is very small. Despite the small amount of contact the measured voltage drop in this case is only around 6V. This indicates that the resistance of the water jet is low resulting in good electrical conductivity even for small contact between the probe and the jet such as what would be caused by detaching ligaments from the main jet.

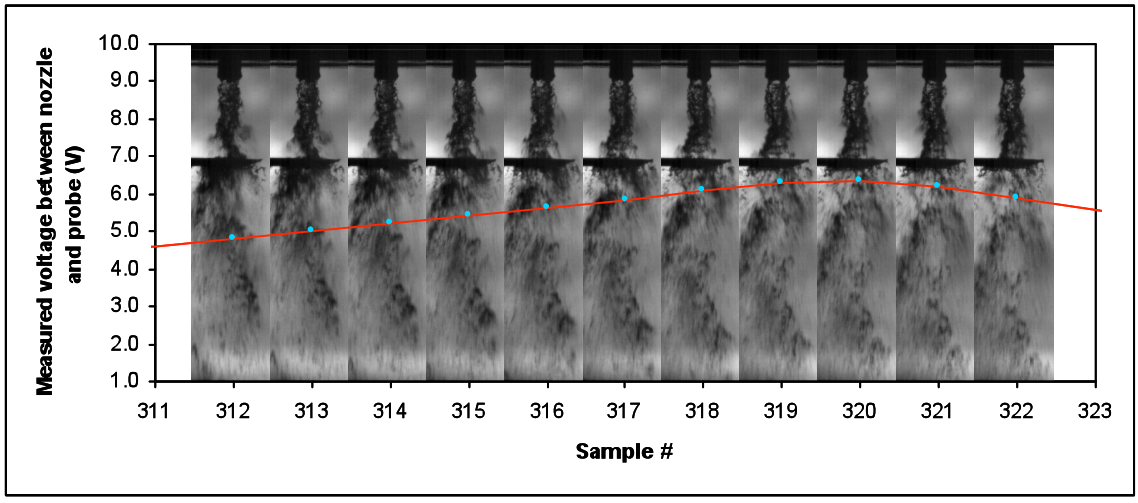

Figure 13: Sequence of temporally resolved photographic images (for a liquid flow rate of 0.5l/min and air flow rates of 1250l/min) overlapped by the measured voltage between the nozzle and the probe (red line).

Figure 21 shows an example of the instantaneous shape of the liquid jet obtained using shadowgraphy and optical connectivity techniques, which have been measured simultaneously. In the former, all of the liquid phase in the line of sight between the light source and the imaging camera is visualised without distinction between the central jet and the detached liquid structures. The latter is less influenced by the products of atomisation that surround the liquid jet, since the laser beam that travels along the liquid jet is making the liquid jet fluoresce and does not illuminate the surrounding area significantly so the fluorescent intensity of the surrounding liquid phase is very low. It is clear that single shadowgraphic images cannot easily provide information on the break-up length of the liquid jet. The optical connectivity technique shows that the liquid jet has broken earlier than the shadowgraphic image suggest.

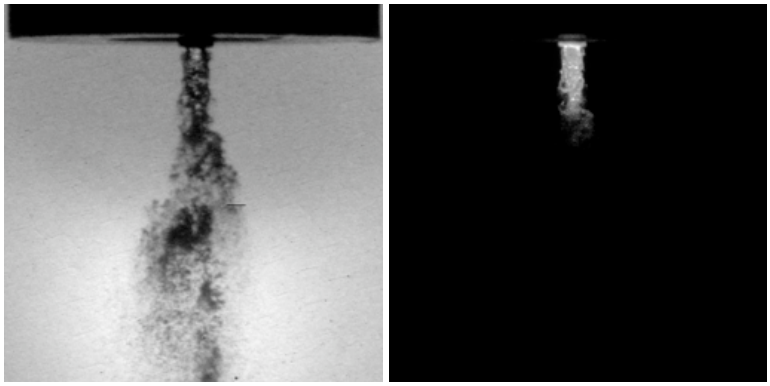

Figure 14: Example of photography (left) and optical connectivity (right). The optical connectivity technique is less influenced by the presence of the product of atomisation around the spray. (example shown for a liquid flow rate of 0.5l/min and air flow rates of 1250l/min).

The comparison of the measurements of the average breakup length L, normalised by the liquid jet diameter D_L, obtained with all three techniques is presented in **Figure 22** as a function of the gas to liquid momentum ratio MR.

Figure 22 shows that there is generally good agreement between the measurements of breakup length with the considered techniques. High-speed photography and electrical conductivity techniques show better agreement between them while the optical connectivity technique measures somewhat different breakup lengths for low MR. This is expected since the high-speed photography and the electrical conductivity measurements were conducted simultaneously while the optical connectivity technique measurements were obtained at a different time. As discussed earlier, some uncertainty remains in the evaluation of the breakup length due to influence of the judgement of the user on image processing. There is an advantage of high-speed photography over single frame photography due to the ability to observe the history of any event along the liquid jet and decide accordingly, even when the observation of the liquid core is restricted by the products of atomisation. Single frame photography can result to an overestimation of the breakup length as demonstrated in Figure 10. In the first frame, the jet appears to be continuous. However, after 50μs, it is revealed that there is a discontinuity upstream of the location of the needle, which is more clearly seen at the subsequent frames, when the liquid is divided in two distinct lumps, one that is attached to the nozzle and one that is detached from the main jet. The availability of the temporal sequence of images of the liquid jet assists the decision that the liquid jet became discontinuous at the image of time 50μs of Figure 10.

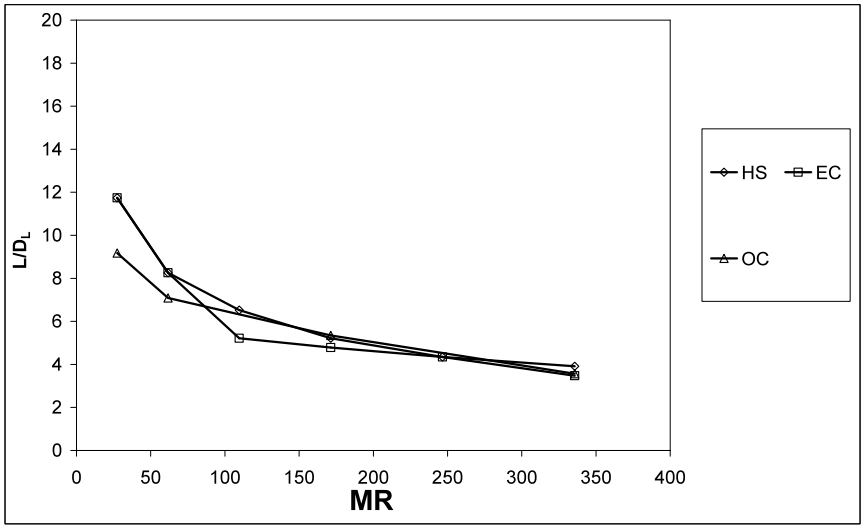

Figure 15: Comparison of the breakup length measurements obtained by the three experimental techniques. Each technique is indicated as HS: High speed photography, EC: Electrical Connectivity, OC: Optical Connectivity.

In the measurements of the breakup length with the electrical conductivity technique, as the liquid jet breaks up, there is not always a complete separation between the sprayed liquid and the detached lumps of liquid, which was shown earlier to be able to conduct electricity without causing great increases in the measured voltage drop between the nozzle and the probe. This is demonstrated in Figure 13, where the presence of a number of ligaments does allow electrical current to flow through the liquid jet although the contact with the probe is small. The presence of interconnecting ligaments between the main lumps of liquid of the atomised spray has been considered in the past by Yule and Salters [4] in relation to the electrical conductivity technique. They also proposed that the spray does not breakup in a single column but in a number of interconnecting masses. There are differences between the diesel injector considered by Yule and Salters [4] and the airblast atomiser considered here. The products of atomisation in the former were decelerated by the quiescent air environment leading to a denser spray than in the airblast atomiser used here in which liquid mass is transported by the high speed coaxial air flow downstream. However, the premise of a connection between the central liquid jet and detached masses of liquid is present in the airblast atomiser.

Finally, considering the optical connectivity technique, the measured breakup length is in most cases shorter than the other two techniques. Nevertheless, the observed differences in **Figure 22** are small. It was explained in Charalampous et al. (16) that the optical connectivity technique is based on the propagation of a laser beam within the length of a liquid jet in the same way that light propagates in optical fibers. Close to the breaking point the beam cannot propagate within the ligaments that connect the detaching masses of liquid and diffuses. As a result the breakup length measured by the optical connectivity technique will be weighted towards the beginning of the breaking point while the other two techniques will predict a somewhat longer breakup length as they are more likely to detect the breakup point at a later stage than the optical connectivity technique.

Conclusions

The optical connectivity technique for measurement of breakup length of liquid jets was examined numerically, by geometrical optics simulations of the propagation of light within a liquid jet, and experimentally, by comparison of measurements with electrical conductivity and high-speed shadowgraphy techniques.

The simulations showed the following:

(a) From the morphological characteristics of the liquid jet, shorter wavelengths and greater amplitudes of the interfacial waves on the liquid interface result to lower fluorescent intensity along the liquid jet.

(b) The type of perturbation (sinus or varicose) of the liquid column did not appear to influence the profile of the fluorescent intensity along the distance from the nozzle exit of the liquid jet considerably.

(c) The dye concentration of the liquid was found to influence significantly the ability to visualize the continuous liquid length. The fluorescent intensity at the exit of the liquid nozzle scales linearly with the dye concentration. However, increasing the dye concentration decreases the fluorescent intensity faster with distance from the nozzle exit. It is recommended that the optical depth of the liquid be adjusted to be well over the continuous length of the liquid jet that is visualized.

(d) The refractive index of the liquid does not affect the fluorescent intensity emitted from the liquid jet significantly.

(e) When considering the characteristics of the laser beam, higher divergence of the laser beam at the nozzle exit causes higher losses of light intensity due to refraction through the liquid interface. Collimation of the beam is recommended.

(f) The laser beam intensity profile was not found to have a significant effect on the fluorescent intensity profile along the liquid jet.

The comparison between the electrical conductivity, optical connectivity and high-speed shadowgraphy measurements of the time-averaged breakup length of an airblast atomiser spray was presented. The findings are as follows:

(i) In the case of shadowgraphy, the presence of detached liquid in the line of sight between the jet and the camera can obstruct optical access to the central jet. By high speed shadowgraphy the temporal evolution of the liquid jet can reveal in greater detail the breakup process and remove some of the uncertainty in the interpretation of the recorded images.

(ii) In the electrical conductivity technique, it was shown that the presence of ligaments that interconnect the detached liquid masses is sufficient to allow the conduction of electricity, which could predispose the interpretation of the measured signal to longer breakup lengths.

(iii) In the optical connectivity technique, the measured breakup length is somewhat shorter than the other techniques. This is due to the difficulty of the light to propagate within the narrow ligaments that connect separated masses of liquid close to the breaking point. As a result the optical connectivity technique is inclined to detect the beginning of the breaking point while shadowgraphy and electrical conductivity technique are more likely to detect longer lengths because they include in the measured length the finer liquid features that arise from the central jet.

(iv) In general, high-speed shadowgraphy measured breakup length values closer to those measured with the optical conductivity technique, which gives more confidence in the accuracy of the optical connectivity approach.

References

1. Charalampous, G., Hardalupas, Y. and Taylor, A.M.K.P., "A novel technique for measurements of the intact liquid jet core in a coaxial airblast atomizer". Presented at *45th AIAA Aerospace Sciences Meeting and Exhibit,* Reno, USA, 2007, *paper no. AIAA 2007-1337*.

2. Lefebvre, A.H., *Atomization and sprays*, Hemisphere Publishing Corporation 1989.

3. Lasheras, J.C. and Hopfinger, E.J., "Liquid jet instability and atomization in a coaxial gas stream". *Annual Review of Fluid Mechanics*, Vol. 32, 2000, pp. 275-308.

4. Engelbert, C., Hardalupas, Y. and Whitelaw, J.H., "Breakup Phenomena in Coaxial Airblast Atomizers". *Proceedings of the Royal Society of London Series A-Mathematical and Physical Sciences*, Vol. 451, No. 1941, 1995, pp. 189-229.

5. Varga, C.M., Lasheras, J.C. and Hopfinger, E.J., "Initial breakup of a small-diameter liquid jet by a high-speed gas stream". *Journal of Fluid Mechanics*, Vol. 497, 2003, pp. 405-434.

6. Chehroudi B., Chen S.H. and Bracco F.V., "On the intact core of full-cone sprays". *SAE Technical Papers 850126*, 1985.

7. Hiroyasu H., Arai M. and Shimizu M., "Break-up length of a liquid jet and internal flow in a nozzle". ICLASS-91. 1991.

8. Yule, A.J. and Salters, D.G., "A Conductivity Probe Technique for Investigating the Breakup of Diesel Sprays". *Atomization and Sprays*, Vol. 4, No. 1, 1994, pp. 41-63.

9. Hiroyasu H., Shimizu M. and Arai M., "The breakup of high speed jet in a high pressure gaseous atmosphere". *ICLASS-82*, 1982.

10. Cai, W.Y., Powell, C.F., Yue, Y., Narayanan, S., Wang, J., Tate, M.W., Renzi, M.J., Ercan, A., Fontes, E. and Gruner, S.M., "Quantitative analysis of highly transient fuel sprays by time-resolved x-radiography". *Applied Physics Letters*, Vol. 83, No. 8, 2003, pp. 1671-1673.

11. Renzi, M. J., Tate, M.W., Ercan, A., Gruner, S.M., Fontes, E., Powell, C.F., MacPhee, A.G., Narayanan, S., Wang, J., Yue, Y. and Cuenca, R., "Pixel array detectors for time resolved radiography (invited)". *Review of Scientific Instruments*, Vol. 73, No. 3, 2002, pp. 1621-1624.

12. Yue, Y., Powell, C.F., Poola, R., Wang, J. and Schaller, J.K., "Quantitative measurements of diesel fuel spray characteristics in the near-nozzle region using X-ray absorption". *Atomization and Sprays*, Vol. 11, No. 4, 2001, pp. 471-490.

13. Linne, M., Paciaroni, M., Hall, T. and Parker, T., "Ballistic imaging of the near field in a diesel spray". *Experiments in Fluids*, Vol. 40, No. 6, 2006, pp. 836-846.

14. Linne, M.A., Paciaroni, M., Gord, J.R. and Meyer, T.R., "Ballistic imaging of the liquid core for a steady jet in crossflow". *Applied Optics*, Vol. 44, No. 31, 2005, pp. 6627-6634.

15. Paciaroni, M., Linne, M., Hall, T., Delplanque, J.P. and Parker, T., "Single-shot two-dimensional ballistic imaging of the liquid core in an atomizing spray". *Atomization and Sprays*, Vol. 16, No. 1, 2006, pp. 51-69.

16. Charalampous, G., Hardalupas, Y. and Taylor, A.M.K.P., "Novel Technique for Measurements of Continuous Liquid Jet Core in an Atomizer". *AIAA Journal*, Vol. 47, No. 11, 2009, pp. 2605-2615.

17. Charalampous, G., Hardalupas, Y. and Taylor, A.M.K.P., "3-Dimensional structure of the intact liquid jet core during coaxial air-blast atomisation". *Intern. Journal of Spray and Combustion Dynamics (IJSCD)*, Vol. 1, 2009, pp. 389-415.

18. Colladon, D. "On the reflections of a ray of light inside a parabolic liquid stream". *Comptes Rendus*, Vol. 15, 1842, pp. 800-802.

19. Thomson W., "On a self-acting apparatus for multiplying and maintaining electric charges, with applications to illustrate the voltaic theory". *Proceedings of the Royal Society of London*, Vol. 16, 1867, pp. 67-72.

List of Symbols, Abbreviations and Acronyms

D_L = inner diameter of the liquid jet nozzle
D_0 = outer diameter of the liquid jet nozzle
D_G = Inner diameter of the gaseous jet nozzle
G = Amplitude of feature on jet surface
L = Wavelength of feature on jet surface
MR = Gas-to-liquid Momentum ratio
Re = Reynolds number of liquid jet
We = Weber number of liquid jet
n_1 = Index of refraction of liquid
n_2 = Index of refraction of gas
U_G = Average gaseous velocity at the annulus
U_L = Average liquid velocity at the nozzle exit
γ = Absorption coefficient
μ = Kinematic viscosity of the liquid
ρ_G or ρ_L = Density of gas or liquid
ϕ = Phase of sinus surface wave
ω = Laser beam divergence
σ = Surface tension

PROGRESS REPORT

AWARD N°: FA8655-09-1-3036 1

TITLE: Novel laser-based technique for measurements of primary atomisation characteristics of liquid jets

INVESTIGATOR: Professor Y. Hardalupas

ORGANISATION: Imperial College of Science, Technology and Medicine

REPORTING PERIOD: From: 20 July 2010 To: 19 January 2011

PROJECT START DATE: 20 July 2009

DATE OF ISSUE OF THIS REPORT: 28 January 2011

ADMINISTRATIVE OFFICE: European Office of Aerospace Research and Development (EOARD)

GOVERNMENT PROGRAM MANAGER: Dr. Gregg Abate

Table of Contents

List of Figures

Figure 10: The atomizer design of a liquid jet exposed to a crossflow of air, which can have a swirling velocity component.

Figure 11: The inner tube of the atomizer, which supplies the liquid to the rounded edged nozzle with diameter of 1mm.

Figure 12: The quartz tube, which extends the length of the nozzle downstream of the liquid jet injection location, to maintain the confinement of the air stream and avoid its expansion.

Summary

During the first stages of atomization in an airblast atomizer, the liquid stream is destabilized under the influence of a coaxial stream of air, until its continuity is broken. A novel technique [Charalampous *et al.* 2007 (1)] has been proposed to measure the length of the continuous liquid jet, based on the internal illumination of the liquid jet through the spray nozzle. The liquid jet acts as a light guide, which allows light to propagate along the length of the jet in the same way as light travels along an optical fiber. The laser light excites a fluorescent dye that is dissolved in the liquid jet, making the volume of the liquid jet luminous. Then, the connectivity of the liquid jet is linked to the optical connectivity of the fluorescent jet. However, since the surface of the liquid jet is not smooth, as that of an optical fiber, due to the development of waves on the jet surface, there are losses of light intensity due to refraction through the jet surface and absorption by the fluorescence dye, as it propagates along the liquid jet. Therefore, the applicability of the technique requires evaluation in different types of liquid jets.

During the current reporting period of the project, the emphasis has been to consider the applicability of the optical connectivity technique in liquid jets exposed to a cross stream of air. There are two contributions.

First, the previously developed numerical approach to evaluate the light propagation within liquid columns of various geometries was extended to allow the effect of the inclination of the liquid column to be included in the computer program. This development was completed and initial results of the effect of liquid column inclination are presented.

Second, an axisymmetric facility that allows the injection of a liquid jet in a cross flow of air was designed. The facility is unique, because it allows swirling air flow to interact with the injected liquid jet. No measurements are available of the behaviour of liquid jets exposed to a swirling air cross-stream. The facility provides appropriate optical access to the liquid jet in order to illuminate it with laser light through its injection nozzle and allow measurements of the liquid jet development and breakup using the optical connectivity technique.

It should also be noted that Reference (20) [Charalampous G., Hadjiyiannis C., Hardalupas Y. and Taylor A.M.K.P. (2010) “Measurement of continuous liquid jet length in atomizers with optical connectivity, electrical conductivity and high-speed photography techniques”. In “Proceedings of 23rd Annual Conference on Liquid Atomization and Spray Systems, ILASS – Europe 2010”, paper 152, Brno, Czech Republic, 6-8 September 2010] was presented at the ILASS conference during this reporting period. A journal publication associated with this work is prepared for submission.

Introduction

During the first stages of atomization of a liquid jet, the jet is progressively destabilized under the influence of the forces that result from the interaction of the liquid stream with the surrounding air (2, 3). During this process the jet geometry changes as liquid is removed from its surface and waves develop on the surface until their amplitude becomes large enough to lead to breakup of the liquid jet. The distance from the nozzle exit to the point downstream the nozzle, where the liquid jet breaks up defines what is known as the “primary atomization region”. The length of the continuous core of the liquid jet, known as the “breakup length”, determines the extent of the primary atomization region and the performance of atomizing nozzles.

A number of techniques have been proposed for the measurement of the length of the continuous jet. These include photography (4, 5), electrical conductivity (6-9), X-ray absorption (10-12) and ballistic imaging (13-15). A recently proposed method is the optical connectivity technique (1). It has been shown that in dense sprays it can provide good measurement of the breakup length of liquid jet at conditions where the continuous length of the jet would be difficult to determine with photography as the atomization products that surround the jet could hinder the view to the continuous jet.

Photography (usually shadowgraphy) is the most commonly used method, as it is straightforward to apply and places only moderate demands on equipment. In this method, the atomizing jet is imaged directly by a camera. A light source is necessary to illuminate the liquid jet and is usually placed behind the jet propagating directly into the camera lens. In this way, the shadow of the jet is imaged and its contour is well defined in the acquired images. The break-up length is estimated from the geometry of the recorded contour. While this method is easy to implement, when atomization becomes more intense, the droplets around the jet core might obstruct parts of the jet and the break-up length could be measured longer than it is.

The electrical conductivity technique is based on the conduction of electricity along the length of the continuous liquid jet downstream the nozzle. A potential is applied between the spray nozzle and a probe downstream. If there is continuity of the liquid phase between the nozzle and the probe, a closed electrical circuit will ensue. The probe can be moved across different positions to determine the continuity of the liquid jet as a function of downstream distance. If the detected potential is low it is verified that there is electrical connectivity up to a specific point indicating continuity of the liquid jet core. On the contrary, the discontinuity of the liquid jet can be located where the conductivity is negligible. In earlier work, many researchers developed a conductivity probe technique to enable the investigation of the breakup zone in a variety of applications. Yule and Salters (8) investigated the breakup zone of a transient diesel spray as a function of time and position employing a wire probe. Hiroyasu et al (7, 9) studied the breakup length of a high-speed liquid jet by measuring an electrical resistance between the nozzle and a fine wire screen detector located in a spray jet. Chehroudi et al (6) tried to determine the shape and length of the intact liquid core by applying a voltage between the nozzle unit and fine needles, rods and screens. The results show that current is carried not only by intact liquid cores but also by atomized unconnected sprays.

The novel optical connectivity of a liquid jet (16, 17) relies on illuminating a liquid jet from within the nozzle by a laser beam, which propagates downstream, while reflecting at the gas-liquid interface. Due to the higher index of refraction of the liquid jet to that of the surrounding gas, a laser light ray that interacts with the gas-liquid interface at a sufficiently large incident angle undergoes total internal reflection. As a consequence, the laser beam is reflected completely back into the liquid stream and propagates downstream for a long distance in the same way that

light propagates along optical fibers. Collandon (18) demonstrated this phenomenon as early as 1842. The addition of a fluorescent dye, such a Rhodamine WT in the liquid jet, causes some of the intensity of the laser beam to be absorbed and re-emitted at a longer wavelength as fluorescence. This causes the volume of the continuous jet to become luminous which allows the evaluation of the break-up length. Beyond the point of liquid discontinuity, the laser beam is diffused and its intensity is significantly reduced. The optical connectivity technique is not without limitations. As the technique is based on the propagation of light within an atomizing liquid jet, there will unavoidably be some scattering losses at the interface that will reduce the intensity of the propagating light. Therefore, for long liquid jets, the technique will not be possible to operate due to complete attenuation of the propagating light along the liquid. Here, we develop a numerical model of the liquid jet to determine how the laser light that is seeded at the base of the jet propagates along the length of the jet and what are the effects of its geometry on the losses of the intensity of the laser light.

During the previous reporting period, measurements of break-up length of a liquid jet in an airblast coaxial atomizer from the optical connectivity technique, the electrical connectivity and high speed photography were compared and advantages and limitations of the optical connectivity technique were identified (19, 20). In the current reporting period, the emphasis is directed towards the applicability of the optical connectivity technique in liquid jets exposed to a cross stream of air.

The next section of this report describes the operation of the optical connectivity technique and presents the geometrical optics approach that was developed to evaluate numerically the influence of various parameters on the accuracy of measurements of the length of the continuous liquid jet. This approach was extended to include the effect of the liquid column inclination relative to the initial direction of injection, which coincides with the direction of the initial propagation of the laser light.

The third section presents and discusses the results. Preliminary numerical results of the operation of the optical connectivity technique for inclined liquid columns, based on the developed geometrical optics approach, are reported. The second part of this section presents the design of an atomizer that allows the study of a liquid jet exposed to a cross-stream of air. This describes a unique facility that will allow the air flow to acquire variable levels of swirl and, as a consequence, study the primary breakup of a liquid jet in a cross-stream of swirling air flow. This section provides an initial literature review, which verifies the lack of studies of liquid jets exposed in swirling cross flow of air, presents the design criteria and associated estimates and describes the final design. The report ends with a summary of the main achievements and future plans.

Methods, Assumptions and Procedure

(a) Optical Connectivity Technique

An optical connectivity technique has been developed for the measurement of the continuous length of sprays. The technique works by introducing a laser beam within the flow of the liquid upstream of the nozzle that exits with the liquid through the nozzle in the direction parallel to the nozzle axis. In this way the laser beam is largely contained within the liquid jet by reflecting on the liquid interface propagating downstream and illuminating the liquid jet volume. A ray of laser light is guided along the length of the liquid jet by reflecting on the gas-liquid interface at the jet

surface. As long as the angle of incidence between the surface of the jet and the laser light rays is greater then the angle of total internal reflection, the rays are completely reflected back inside the liquid without intensity losses from refraction. This principle is similar to the way that a laser beam propagates within an optical fiber. However, if the angle of incidence of a laser light ray on the liquid jet interface becomes smaller than that for total internal reflection then there will be some intensity losses due to refraction.

The laser beam continues to propagate downstream the jet until it meets the breaking point of liquid jet, where it can no longer be contained within the jet and is diffused randomly in different directions. The introduction of a fluorescing dye into the liquid makes part of the laser beam to be absorbed along the length of the liquid jet, and subsequently be re-emitted as fluorescence. In this way the atomizing jet becomes luminous and can be imaged (**Figure 1**).

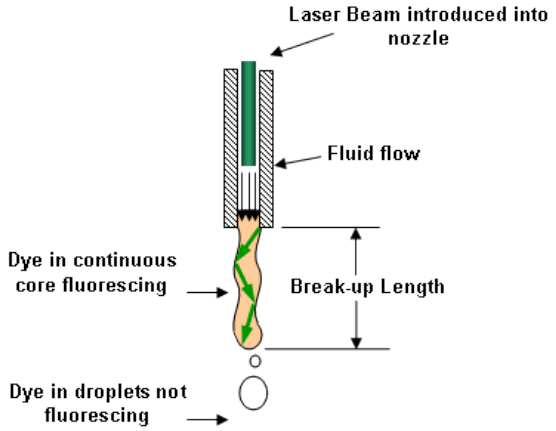

Figure 1: Principle of the optical connectivity technique

An example of the instantaneous image of a highly magnified liquid jet, illuminated by a laser beam according to the principle of the optical connectivity technique, is presented in **Figure 2**. The ability to detect the instabilities along the surface of the interface of liquid jet can be identified.

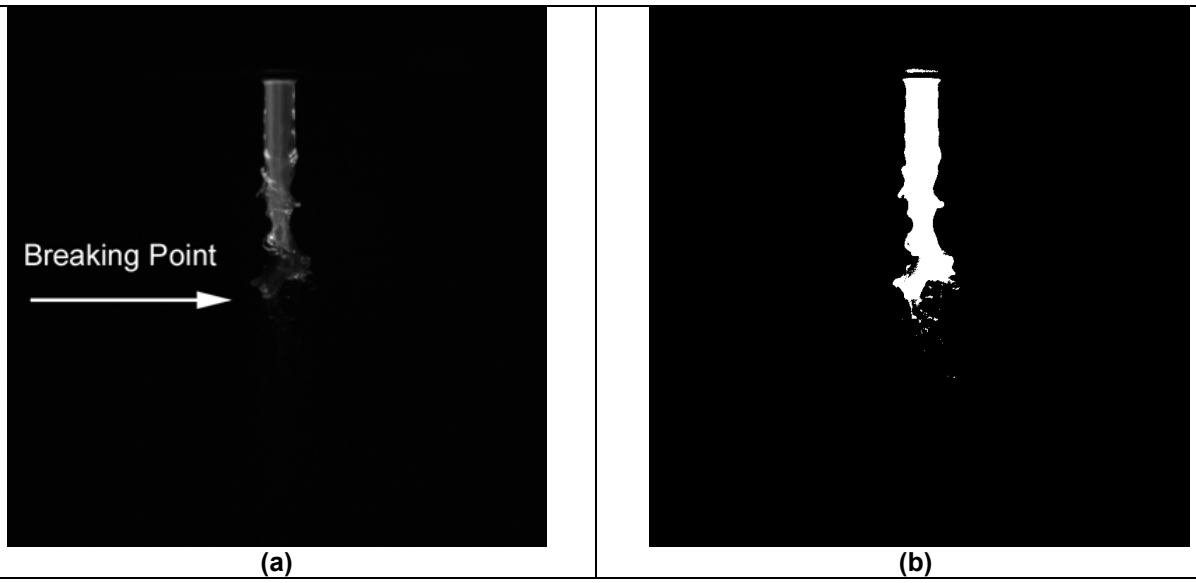

Figure 2: (a) Example instantaneous image of a liquid jet obtained from the optical connectivity technique. (b) The image of (a) after image processing, which indicates the intact length of the liquid jet and the instabilities along the surface of the liquid jet.

(b) Geometrical Optics Simulations

For the evaluation of the effect of the shape of the jet geometry on the propagation of light within a column of liquid, the propagation of laser light rays is calculated using geometrical optics. This simulation has the benefit of enabling the evaluation of the effect of all operating parameters, which is difficult to achieve experimentally.

The liquid jet for this investigation is considered as a two-dimensional liquid column. The central axis of the liquid column extends along the x-axis of a Cartesian coordinate system. The interface of the jet is described by the sinusoidal wave function along the x-axis:

$$y = G\sin\left(\frac{2\pi x}{L} + \phi\right) + y_0 \qquad (1)$$

where *G* is the amplitude of the wave on the interface and *L* is the wavelength of the wave on the surface of the interface. ϕ is the phase of the wave on the surface of the interface and sinusoidal disturbances are present along the liquid column when the phases of the top and bottom interfaces are matched or varicose disturbances appear when the phases of the waves between the top and bottom surfaces are shifted by π.

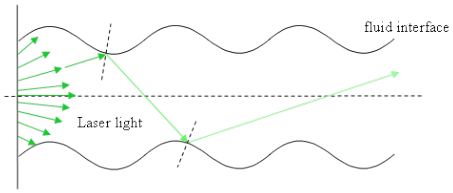

Figure 3: Basic geometry of the considered liquid jet and diverging rays at the base of the liquid column.

For the geometrical optics calculations, a monochromatic laser beam that propagates inside the liquid column is considered (**Figure 3**). The laser beam is simulated by a large number of rays that start at the base of the liquid column at uniformly spaced intervals and propagate downstream the nozzle exit. The ray that begins on the axis of the column is aligned parallel to the axis. However, in order to consider the influence of the divergence (ω) of the laser beam, the angle between the rays at the column base and the axis is progressively changed as the distance between the axis and the starting point of the rays along the *y*-axis increases.

The calculation of the path of the rays when they are incident to the surface of the liquid column is estimated by:

$$R = V - 2(V \cdot N)N \qquad (2)$$

where *V* is the incident ray vector, *N* is the vector normal to the jet surface at intersection point (between the wave and the incident ray) and *R* is the vector of the reflected ray.

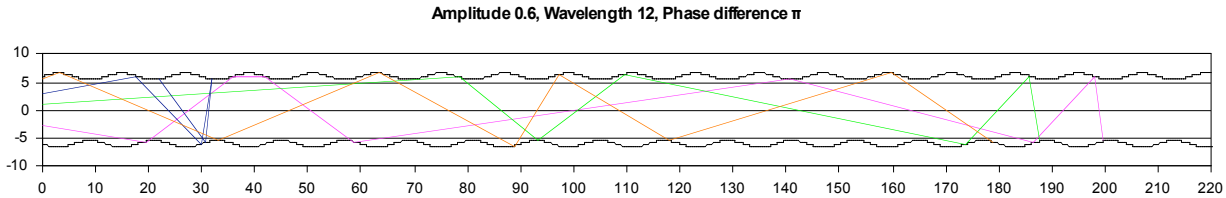

Figure 4: Example of propagation of light rays within a liquid column as determined by geometrical optics calculations. The vertical axis shows the width of the liquid column around the center and the horizontal axis shows the length along the direction of motion of the liquid column.

As the rays propagate along the liquid column (**Figure 4**), the initial intensity of each beam I_0 is reduced due to refraction of the light at the liquid interface, which is lost, and absorption from the dye present in the liquid, which is re-emitted as fluorescence.

Considering the angle of incidence between the rays and the local interfacial surface of the liquid, the critical angle for total internal reflection is given by the relationship:

$$\theta_{crit} = \sin^{-1}\left(\frac{n_2}{n_1}\right) \tag{3}$$

where n_1, n_2 the refractive indices of the liquid and the gas phases. However, when the angle of incidence between a ray and the air-liquid interface is smaller that the angle of incidence for total internal reflection, there are losses of the intensity of the ray. The fraction of the intensity of incident light that is reflected from the interface is given by the reflection coefficient *R*, and the fraction refracted by the transmission coefficient *T*. The Fresnel equations are used to calculate *R* and *T*. The calculations of *R* and *T* depend on polarization of the incident ray. If the light is polarized with the electric field of the light perpendicular to the plane of **Figures 3** or **4** (s-polarized), the reflection coefficient is:

$$R_s = \left[\frac{\sin(\theta_1 - \theta_2)}{\sin(\theta_1 + \theta_2)}\right]^2 \tag{4}$$

If the incident light is polarized in the plane of the **Figures 3** or **4** (p-polarized), the reflection coefficient *R* is:

$$R_p = \left[\frac{\tan(\theta_2 - \theta_1)}{\tan(\theta_1 + \theta_2)}\right]^2 \tag{5}$$

The Beer-Lambert law estimates the reduction of the intensity of the rays due to the absorption caused by the fluorescent dye present in the liquid through which the ray is traveling:

$$I = I_0 e^{-\gamma z} \tag{6}$$

where γ is the absorption coefficient, *z* the path length traveled by the ray, I_0 is the initial intensity of the ray and *I* the intensity of the ray after it has traveled a distance *z* in the absorbing medium.

The total reduction of the initial intensity I_0 of the laser beam that travels along a path of length *z* in an absorbing medium until it reaches the interface is given by the formula:

$$I = \left(\frac{\left[\frac{\sin(\theta_1 - \theta_2)}{\sin(\theta_1 + \theta_2)}\right]^2 + \left[\frac{\tan(\theta_2 - \theta_1)}{\tan(\theta_1 + \theta_2)}\right]^2}{2} \right) I_0 \cdot (e^{-\gamma z}) \quad (7)$$

While the refracted part of the laser light intensity is lost, the absorbed light intensity along the ray path is subsequently re-emitted as fluorescence. By summation of the losses of the laser light intensity of each ray due to absorption at each distance downstream of the nozzle exit, the profile of the fluorescent intensity with distance from the nozzle exit is determined. In this way, the limitations of the visualization of the fluorescent liquid jet can be determined. The parameters that influence the loss of light intensity are morphological (wavelength, *L*, amplitude, *G*, and phase, ϕ of the waves on the surface of the liquid column), physical (absorption of light within the liquid, γ, and refractive index of liquid, n_1) and optical (divergence of rays of laser light, ω). The wavelength and the amplitude of the waves on the liquid surface were normalized by the width of the liquid column at the nozzle exit *D*.

The emphasis is on the behavior of the optical connectivity technique for an inclined liquid jet, as develops when a liquid jet is exposed to a cross-stream of air. The software was modified to include the option to vary the inclination angle of the liquid jet, while the options to vary all the other parameters, i.e. the frequency and amplitude of the surface waves along the interface, the refractive index of the liquid, the absorption coefficient of the fluorescing dye and the characteristics of the laser light, remained available. Example results are presented in the results section below with the full parametric study to follow during the next reporting period.

Results and discussion

This section presents preliminary results of the laser light propagation through a liquid jet with wavy surface using the geometrical optics approach described in the previous section. The extension of the developed numerical approach to inclined liquid columns is demonstrated. Then, a brief review of the available literature on liquid jets exposed to cross-steams of air is provided, which demonstrates that there are no available experiments with liquid jets injected in swirling air cross-streams. This verifies the need for such a study, since the interaction of liquid jets with swirling air streams is common to wide range of gas turbine combustor injectors. Therefore, the design of such an experimental facility is presented.

(a) Geometrical Optics Calculations

The propagation of laser light rays in an inclined liquid column with a wavy surface is demonstrated at **Figure 5**. As the rays propagate along the liquid column, the initial intensity of each beam I_0 is reduced due to refraction of the light at the liquid interface, which is lost, and absorption from the dye present in the liquid, which is re-emitted as fluorescence. The intensity losses at the liquid interface occur when the rays hit the inner surface of the liquid at angles greater than the angle for total internal reflection of Equation (3).

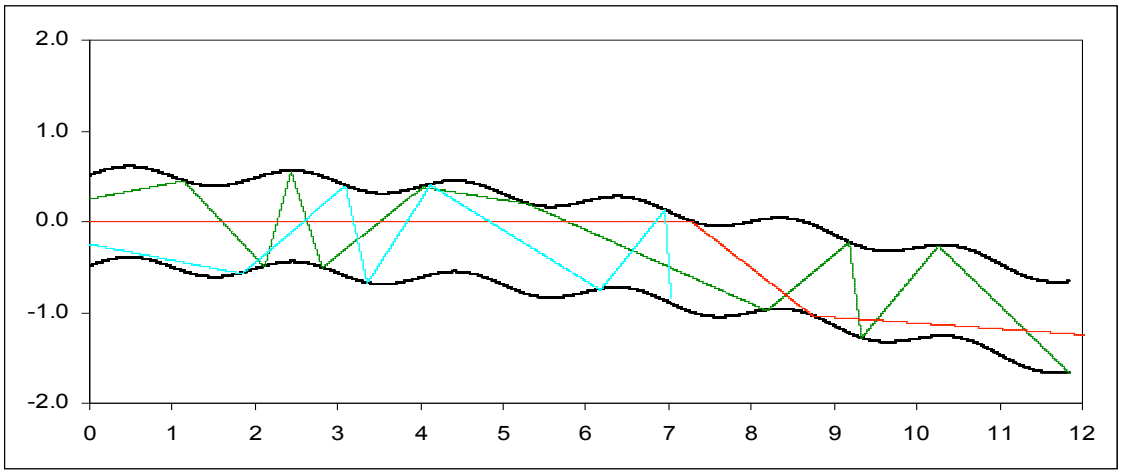

Figure 5: Example of propagation of light rays within an inclined liquid column as determined by geometrical optics calculations. The vertical axis shows the width of the liquid column around the axis normalized by the width of the column. The horizontal axis shows the distance along the direction of motion of the liquid column, normalized by the width of the liquid column (Example for γ=0.00008m^{-1}, n_1=1.33, ω=20°).

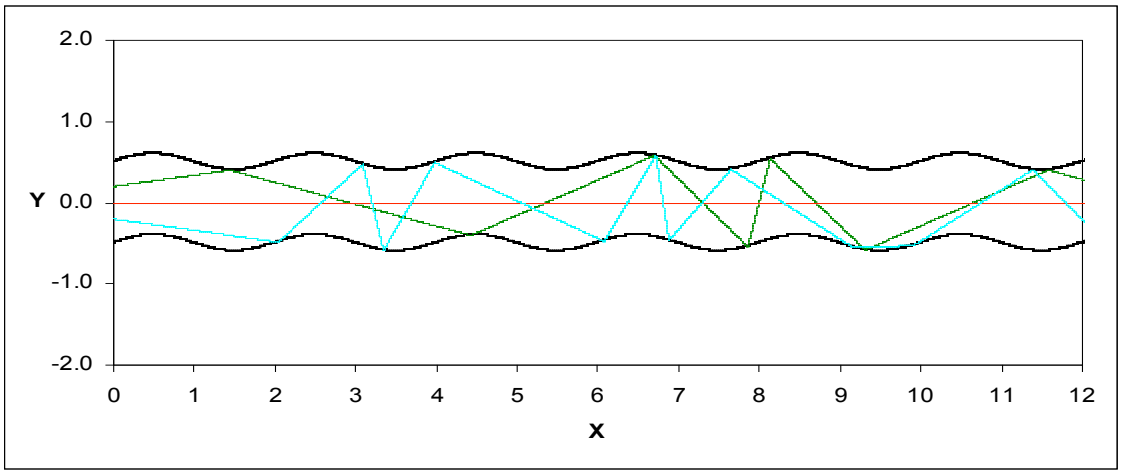

Figure 6: Example of propagation of light rays within a straight liquid column, as determined by geometrical optics calculations. The liquid column is the same as that of Figure 5, but without inclination. The vertical axis shows the width of the liquid column around the axis normalized by the width of the column. The horizontal axis shows the distance along the direction of motion of the liquid column, normalized by the width of the liquid column (Example for γ=0.00008m^{-1}, n_1=1.33, ω=20°).

Figure 6 shows the propagation of the laser light rays within a liquid column without inclination. The amplitude and frequency of the surface wave and the width of the liquid column are the same as those of the inclined column of Figure 5. An observation of the propagation of the rays indicates that all the rays interact with the liquid jet interface closer to the nozzle exit of the inclined liquid column. An example of this is the 'red' ray of **Figures 5** and **6**, which is

propagating along the centre of the liquid column. This ray is continuing along a straight line in the straight liquid column and does not interact with the liquid surface, as expected. The same ray is internally reflected on the inclined liquid jet interface. Therefore, it is expected that the intensity losses of laser light due to refraction at the liquid interface will be higher for the inclined liquid column. However, this may be reduced since the majority of losses of the laser light are due to absorption by the fluorescent dye within the liquid.

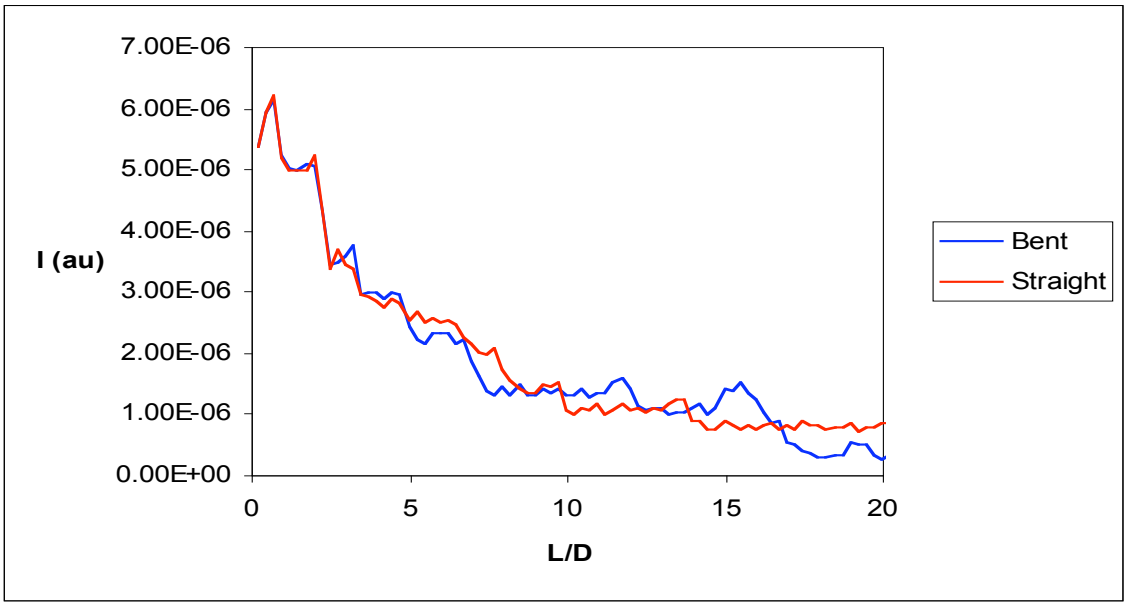

Figure 7: Effect of the inclination of the liquid column on the fluorescent intensity as a function of the distance from the nozzle exit. The wavelength and amplitude of the surface wave on the liquid column are the same for the two cases (Example for γ=0.00008m^{-1}, n_1=1.33, ω=20°).

Figure 7 shows the comparison of the laser light intensity propagating in the liquid column as a function of distance from nozzle axis for the straight and the inclined liquid column. The fluorescent intensity emitted from the liquid column is similar for the two cases up to around 15 times the liquid column width. After this distance, the fluorescent intensity tends to be lower in the inclined liquid column. This is in agreement with the earlier discussion.

In summary, the geometrical optics calculations showed that the intensity of the fluorescent light along a liquid column depends on many parameters for the optical connectivity technique. In all cases, the intensity of the fluorescent light does not propagate indefinitely within the liquid column, but decreases progressively along the length of the column. It is possible that, when the continuous length of the liquid column is long, the fluorescent intensity might become too low to be detected along the full length of the continuous liquid column. This has been demonstrated experimentally (1). For this reason, the optical connectivity technique was recommended for cases of good atomization, which lead to short breakup lengths. However, a comparison between the straight and inclined liquid columns suggests that the fluorescent intensity is reduced faster for the inclined column.

(b) Design of experimental facility of liquid jet in a cross stream of swirling air flow

This section starts with a summary of the literature, continues with an evaluation of the design criteria and ends with the reporting of the design of the experimental facility.

Literature review

The atomization of liquid jets in a crossflow air stream is relevant to most gas turbine combustors and combustors for hypersonic vehicles. The atomization of a liquid jet in a cross-stream of air is characterized by two main regions:
(a) Primary breakup of liquid jet. In this region, the liquid jet penetrates into the air cross-stream and becomes inclined in the direction of the air flow, while its shape changes. During this process, ligaments are formed from the liquid jet surface, which eventually become droplets.
(b) The spray region. In this region, some surviving ligaments break up further and form stable droplets, which, together with the other existing droplets from the upstream region, determine the downstream spray characteristics.

In all the available studies, which are reviewed below, a planar air flow geometry has been used. As a consequence, the air stream is mainly flowing in one direction and it is not possible to introduce additional velocity components to the air stream. However, in atomizers of gas turbine combustors, the liquid jet is injected in an axisymmetric flow of air, which tends to have a swirling component. Therefore, the emphasis here is to design an injector of a liquid jet in a cross stream of air, which can also have variable levels of swirl component, and provide appropriate optical access for studies of the liquid jets. However, information available from the literature must be considered in order to identify the dimensions of the new atomizer design.

Some earlier studies, which also provide a review, are those of Less and Schertz (21) and Wu *et al.* (22). These studies establish that the momentum flux ratio of the liquid jet to the air cross-flow of Equ. (8) is a relevant parameter that characterizes the behaviour of the liquid jet.

$$MFR = \frac{\rho_L U_L^2}{\rho_G U_G^2} \tag{8}$$

Increase of MFR leads to increase of jet penetration, which delays the breakup of the liquid column into large fragments and enhances the stripping-off of fine droplets from the liquid jet surface. However, both breakup mechanism of the liquid jet are present at variable degree at the same time depending on the value of the MFR. Some additional relevant parameters for the characterization of the behaviour of the liquid jet are:

Weber number, based on the gas velocity $$We_G = \frac{\rho_G U_G^2 D_L}{\sigma} \tag{9}$$

Weber number, based on the liquid velocity $$We_L = \frac{\rho_L U_L^2 D_L}{\sigma} \tag{10}$$

Reynolds number of liquid jet $$\mathrm{Re}_L = \frac{U_L D_L}{\nu_L} \tag{11}$$

All these parameters will be used in the atomizer design analysis below.

The available studies in the literature and thir main findings are summarized below. Low-speed

wind tunnel experiments were conducted by Aavani *et al.* (23) to examine the effect of jet exit behaviour on the near-field characteristics of jets in cross-flow. Ghosh and Hunt (24) focused on the interaction between an external air cross-flow and the spray jet. Arienti and Soteriou (25) analysed the mechanism of primary break of the liquid jet in a cross flow using proper orthogonal decomposition to identify the liquid flow structures that are responsible for the breakup. Studies of bag-type breakup of non-turbulent liquid jets in a crossflow were carried out by Ng *et al.* (26) and results showed that the waves on the surface of the liquid column within the bag breakup regime could be explained from Rayleigh – Taylor instability. Rachner *et al.* (27) modeled the penetration and atomization of a plain jet of kerosene fuel in air crossflow and could identify the two main breakup mechanisms, which are known as the surface breakup and the liquid column breakup. Sedarsky *et al.* (28) used Particle Image Velocimetry, high-speed shadowgraphy and ballistic imaging to observe the breakup of a liquid jet in a crossflow of air under a variety of conditions. The experimental configuration consisted of four interchangeable nozzle tips of different exit diameter. Bai *et al.* (29) presented an experimental study on turbulent mixing of spray droplets for different injection angles. The optimum mixing effect can be achieved for an angle of 60° and the most stable of the flow field structure and the greatest sustained distance of the counter rotating-vortex pair can be found when the angle is 90°. A numerical study to model the liquid jet breakup in high speed crossflow was attempted by Balasubramanyam and Chen (30) using an improved drag coefficient correlation, which would capture the spray phenomenon more accurately specifically for application to high speed flow. Phase Doppler Anemometry measurements of the two-phase flow structure and droplet dispersion were performed by Fan *et al.* (31) and confirmed the complex interaction between the liquid jet and crossflow and suggested that the flow field depends primarily on the jet-to-crossflow velocity ratio. Hale *et al.* (32) investigated surface heat transfer in a row of short length nozzles of jets in crossflow and found that horseshoe vortices are weak structures that dissipate as their legs wrap around the jet. The turbulence characteristics of a jet in crossflow were examined by Barata *et al.* (33) using Laser Doppler Anemometry. Their aim was to investigate the effect of the velocity ratio between the jet and the crossflow. The conclusion of Hale *et al.* (32) that the flow appears as a vortex wrapped around the jet with its size increasing with the velocity ratio was established by the measurements of (33). Shedd *et al.* (34) used high-speed digital imaging to visualize the formation of the liquid film formed on the surface of a channel due to the injection of a liquid jet in crossflow and it was observed that film thickness increased with increasing momentum flux ratio.

The spray structure in near-injector region of an aerated liquid jet in subsonic crossflow was investigated by Lee *et al.* (35). Six holograms were recorded and the droplet velocities in the streamwise and the crossflow direction could be measured by observing the displacements of the center of each droplet between the double pulses. Osta *et al.* (36) examined the effect of nozzle length/diameter ratio on the breakup using nozzles with different length-to-diameter ratios. The liquid jets were observed using single- and double-pulsed shadowgraphy and holography. The main conclusion was that the breakup length decreases with increasing length-to-diameter ratio. Kihm *et al.* (37) visualized both under expanded sonic gas jets from a converging nozzle (SN-type) and over expanded supersonic gas jets from a converging-diverging nozzle (CD-type). They found out that the SN-type develops wider spray, which lowers the probability of droplet coalescence and generates finer sprays. Lee *et al.* (38) used pulsed shadowgraph and holography for turbulent round liquid jets injected normal to air crossflow in a shock tube. They used two different nozzles with different injector passages and smooth rounded entrances with length-to-diameter ratios larger than 100 to ensure fully developed turbulent pipe flow at the jet exit for large Re. Sallam *et al.* (39) investigated the breakup at the surface of turbulent round liquid jets in still gases using single- and double- pulse shadowgraphy and holography for nozzle with smooth rounded entrances with langth-to-diameter ratio larger

than 100 to ensure fully developed turbulent pipe flow at the jet exit for large Reynolds numbers. Three modes of liquid column breakup were observed: (a) a weakly turbulent Rayleigh-like breakup mode at small jet exit We and Re, (b) a turbulent breakup mode at moderate jet exit We and Re and (c) an aerodynamic bag/shear breakup mode at large jet exit We. Finally, Sallam *et al.* (40), for nonturbulent liquid jets, used shadowgraphy to demonstrate three regimes of primary breakup: bag breakup, multimode (or bag/shear) breakup and shear breakup. It is worth noting that round supercavitating nozzles were used that had sharp edged inlets and exits, with length-to-diameter ratios smaller than 3. This arrangement yields uniform nonturbulent round liquid jets in opposition to findings of Reference (39). Finally, several studies were performed of liquid jets injected in supersonic cross-streams of air (41-46). Although effects of the supersonic streams are present, the overall structure and development of the liquid jets remain qualitatively the same.

The above review confirms that all the studies of liquid jets injected in cross-stream of air have been performed in geometries that could not consider a swirling component of air stream velocity. As a consequence, an experimental facility was designed which allows the study of liquid jets exposed to a swirling air stream. This is relevant to prefilming atomizers that are used in gas turbine combustors.

Considerations for atomizer design

The new atomizer should inject a liquid jet in an air cross-stream, which could have a swirling velocity component. Also, this atomizer should have the capability to operate without swirling air stream and at conditions already studied in planar geometries of jets in crossflows. The first step was to review the literature and determine which factors are important and can influence the operation of the atomizer, which was performed above and established the relevant non-dimensional quantities.

The next step was to perform some calculations and find out how the atomizer will behave for different air flow conditions without swirl. An important aspect of the design was to establish the trajectory of the liquid jet in a cross-stream of air, since this will determine the width of the air stream of the atomizer. This is a requirement in order to avoid the impingement of the liquid jet on the external wall of the air stream. We used the empirical correlation reported by Lee *et al.* (38) to establish the trajectory of the liquid jet. In addition, the momentum flux ratio, the gas crossflow and the liquid Weber numbers and the liquid jet Reynolds number were calculated for different dimensions and flow conditions of the atomizer. These factors decide the atomization characteristics, the structure of the spray and the distance from the injection location, where the breakup of the liquid core occurs.

Therefore, **Figures 8 and 9** present the predictions of the trajectory of the liquid jet based on the correlation of Lee *et al.* (38). The vertical axis is the cross-stream distance and the horizontal is the streamwise distance, presented in dimensional form with units of mm. These calculations were performed for two liquid jet exit diameters, namely 0.5mm (**Figure 8(a), (b)** and **(c)**) and 1mm (**Figure 9(a), (b)** and **(c)**) and for different liquid flowrates and cross-stream air velocities. Underneath each figure, a small table is presented, which includes the corresponding momentum flux ratio, the gas crossflow and liquid Weber numbers and the liquid jet Reynolds number for all the examined conditions. These parameters were defined in Equations (8), (9), (10) and (11).

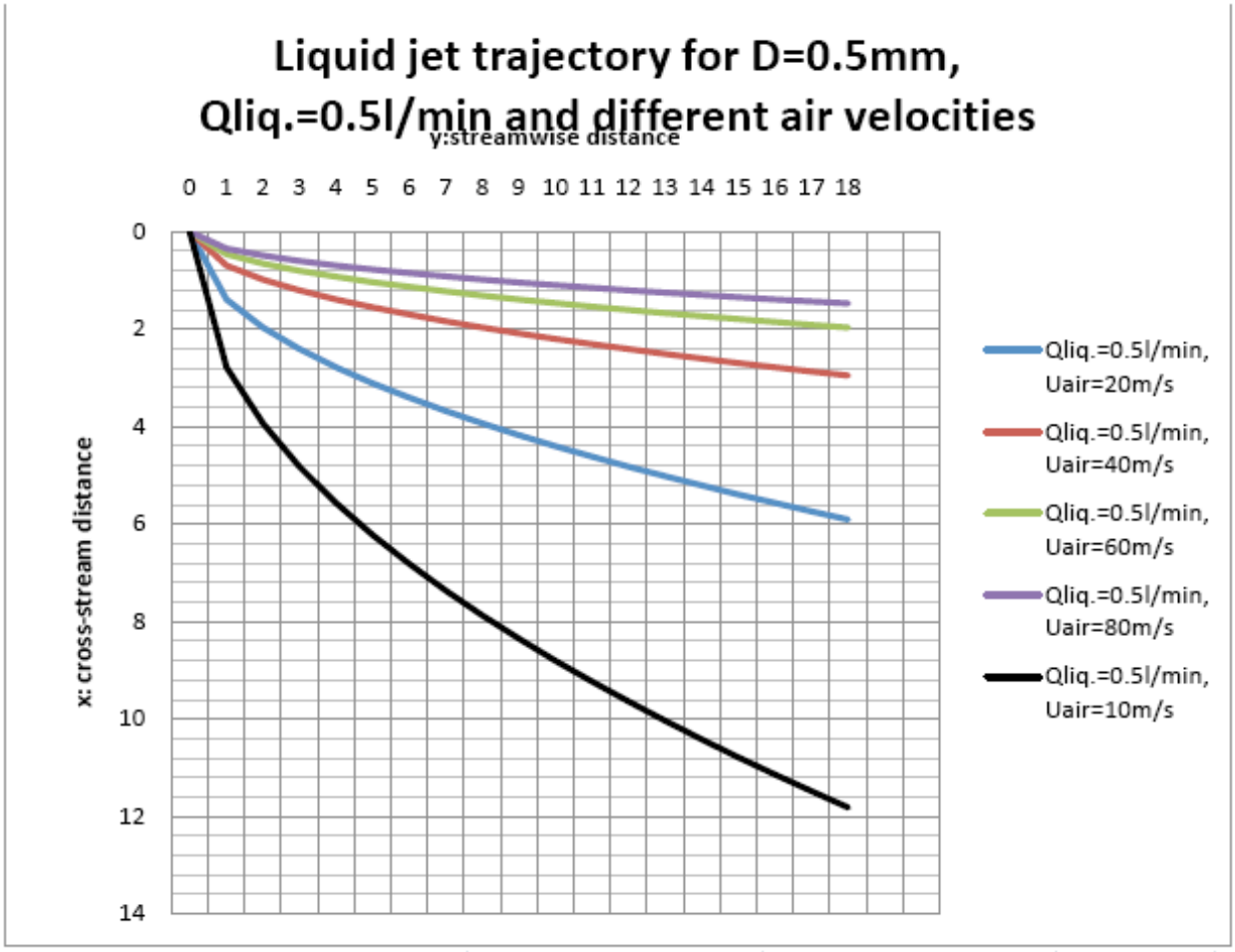

	Crossflow We	Liquid We	Momentum ratios	Jet Re
	8.276566757	122579.3066	14810.40512	18928.07002
	33.10626703	122579.3066	3702.601279	18928.07002
	132.4250681	122579.3066	925.6503197	18928.07002
	297.9564033	122579.3066	411.4001421	18928.07002
	529.7002725	122579.3066	231.4125799	18928.07002

Figure 8(a): Liquid jet trajectory for diameter of liquid jet exit D=0.5mm, liquid flow rate of 0.5l/min and different air velocities

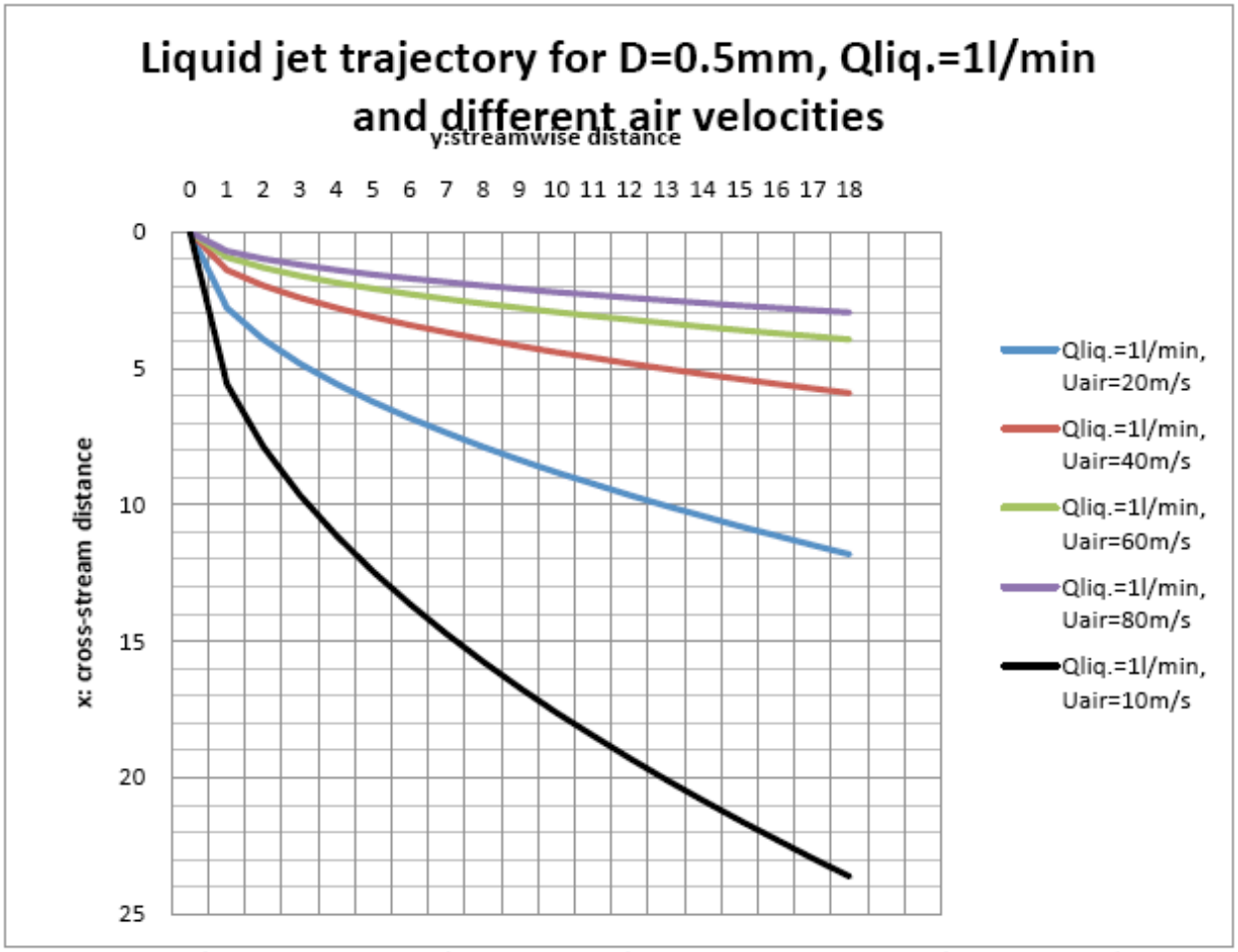

	Crossflow We	Liquid We	Momentum ratios	Jet Re
	8.276566757	490317.2266	59241.62046	37856.14004
	33.10626703	490317.2266	14810.40512	37856.14004
	132.4250681	490317.2266	3702.601279	37856.14004
	297.9564033	490317.2266	1645.600568	37856.14004
	529.7002725	490317.2266	925.6503197	37856.14004

Figure 8(b): Liquid jet trajectory for diameter of liquid jet exit D=0.5mm, liquid flow rate of 1 l/min and different air velocities

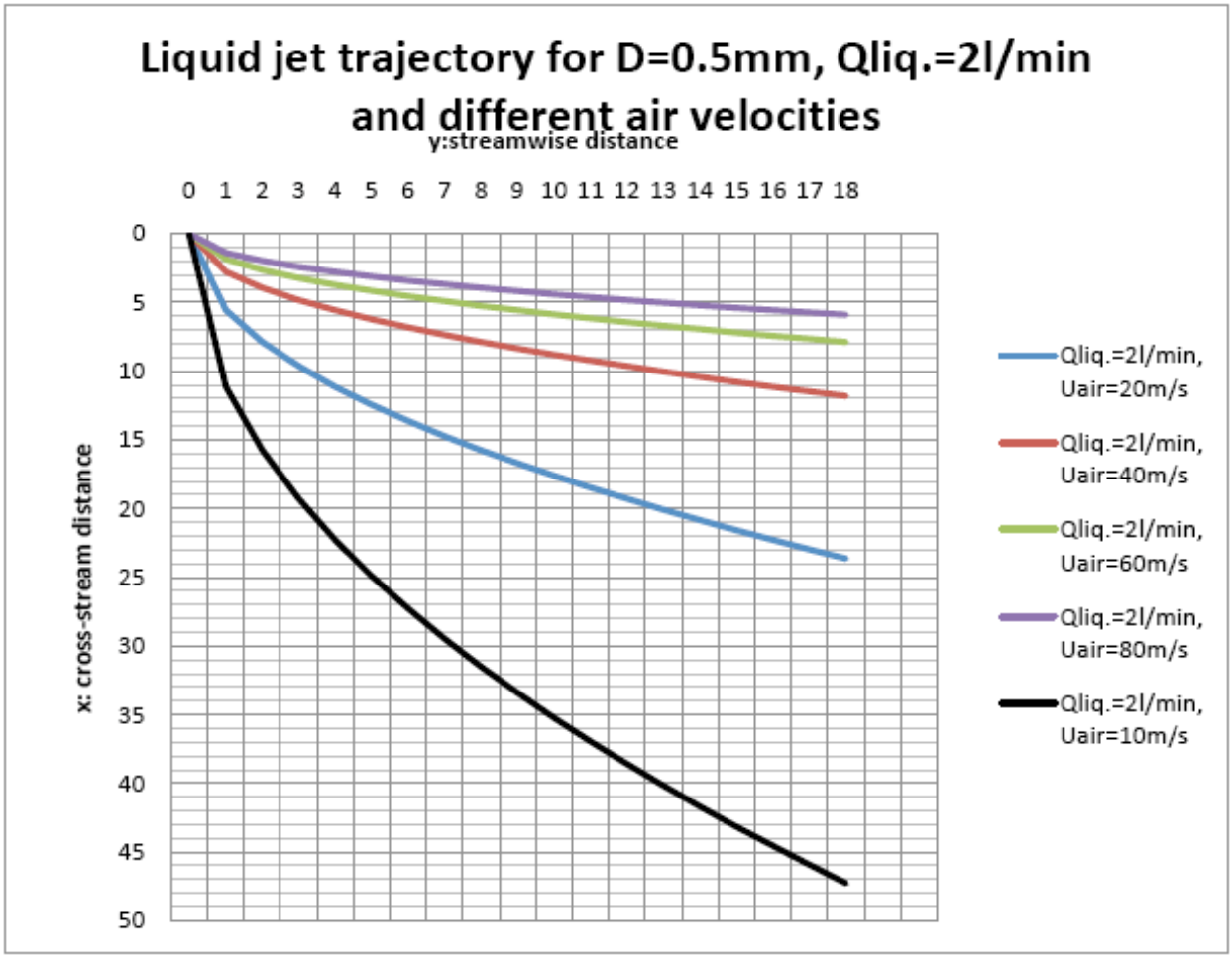

	Crossflow We	Liquid We	Momentum ratios	Jet Re
	8.276566757	1961268.906	236966.4818	75712.28007
	33.10626703	1961268.906	59241.62046	75712.28007
	132.4250681	1961268.906	14810.40512	75712.28007
	297.9564033	1961268.906	6582.402273	75712.28007
	529.7002725	1961268.906	3702.601279	75712.28007

Figure 8(c): Liquid jet trajectory for diameter of liquid jet exit D=0.5mm, liquid flow rate of 2 l/min and different air velocities

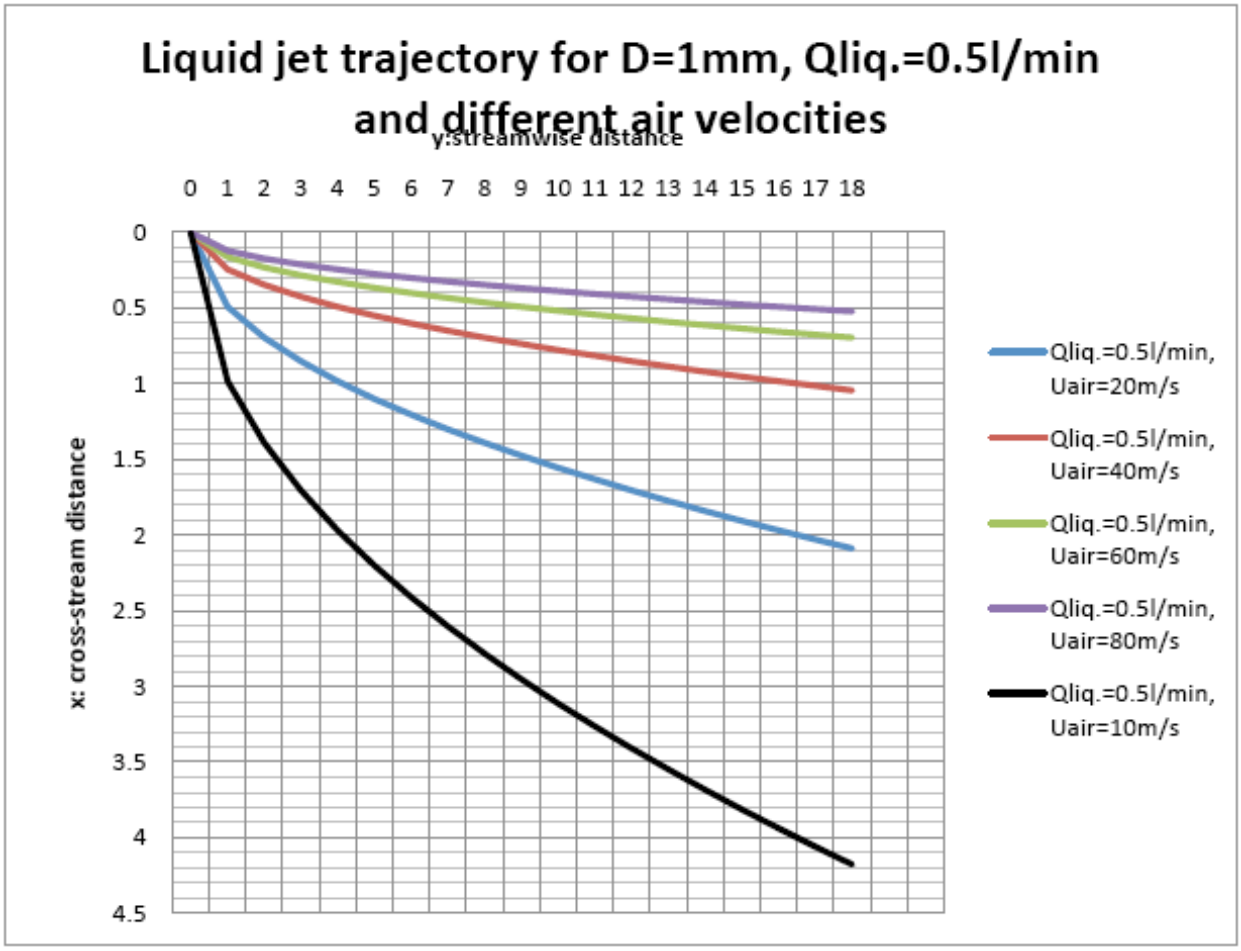

	Crossflow We	Liquid We	Momentum ratios	Jet Re
	16.55313351	15322.41333	925.6503197	9464.035009
	66.21253406	15322.41333	231.4125799	9464.035009
	264.8501362	15322.41333	57.85314498	9464.035009
	595.9128065	15322.41333	25.71250888	9464.035009
	1059.400545	15322.41333	14.46328625	9464.035009

Figure 9(a): Liquid jet trajectory for diameter of liquid jet exit D=1mm, liquid flow rate of 0.5 l/min and different air velocities

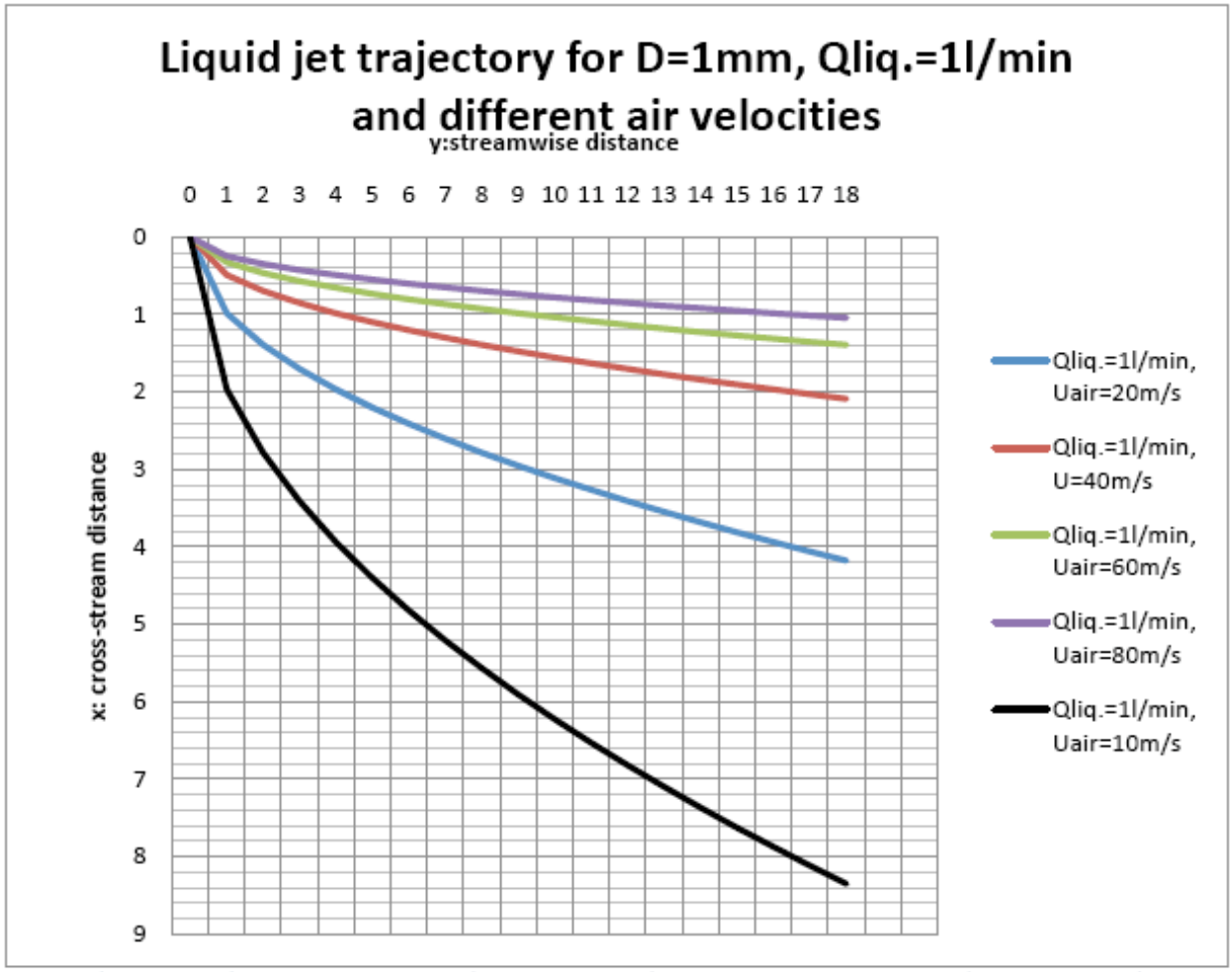

	Crossflow We	Liquid We	Momentum ratios	Jet Re
	16.55313351	61289.65332	3702.601279	18928.07002
	66.21253406	61289.65332	925.6503197	18928.07002
	264.8501362	61289.65332	231.4125799	18928.07002
	595.9128065	61289.65332	102.8500355	18928.07002
	1059.400545	61289.65332	57.85314498	18928.07002

Figure 9(b): Liquid jet trajectory for diameter of liquid jet exit D=1mm, liquid flow rate of 1 l/min and different air velocities

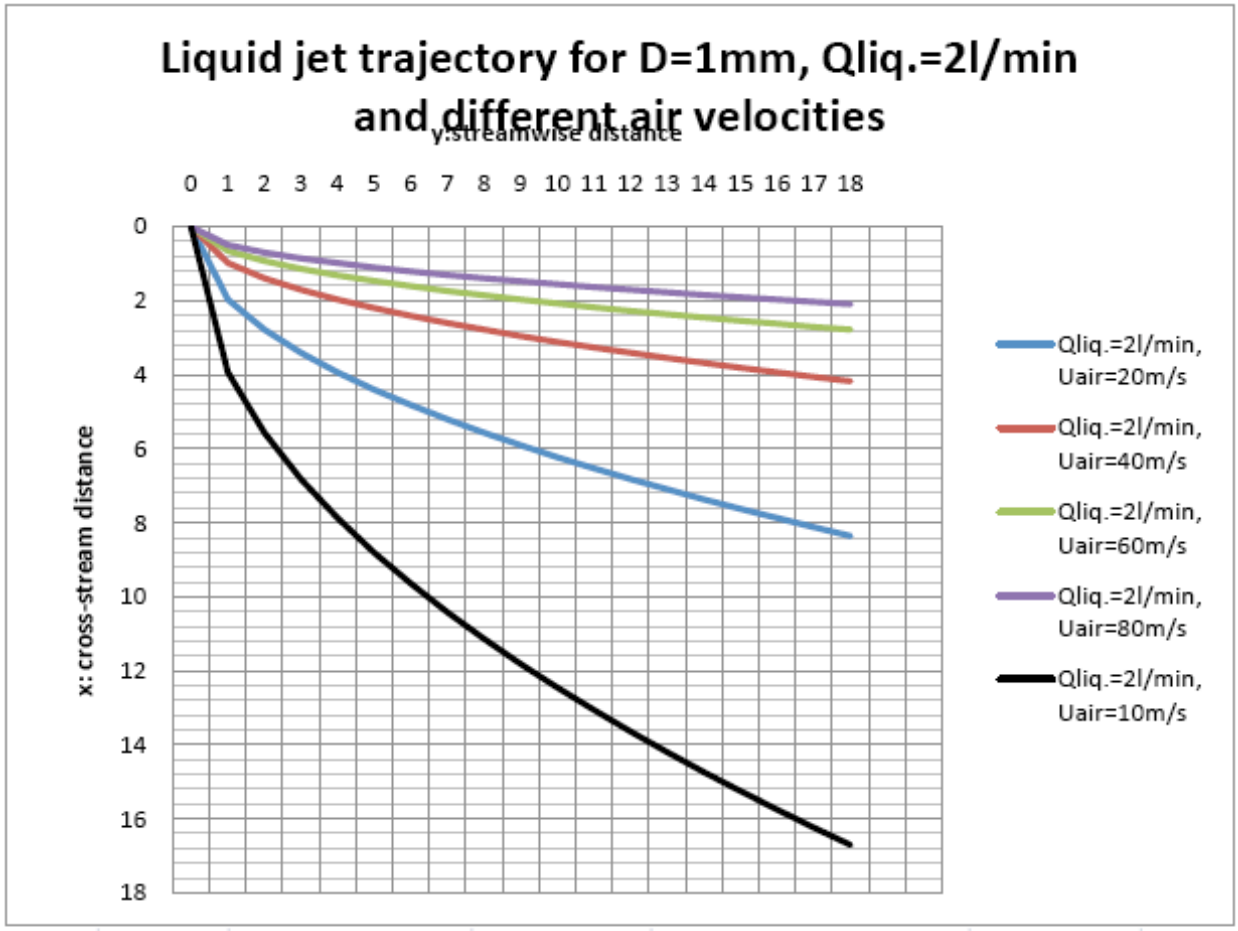

	Crossflow We	Liquid We	Momentum ratios	Jet Re
	16.55313351	245158.6133	14810.40512	37856.14004
	66.21253406	245158.6133	3702.601279	37856.14004
	264.8501362	245158.6133	925.6503197	37856.14004
	595.9128065	245158.6133	411.4001421	37856.14004
	1059.400545	245158.6133	231.4125799	37856.14004

Figure 9(c): Liquid jet trajectory for diameter of liquid jet exit D=1mm, liquid flow rate of 2 l/min and different air velocities

Atomiser Design

Figure 10 presents the atomizer design. The air stream has to be axisymmetric, and not planar as found in the literature, in order to be able to introduce swirl and control the relative magnitude of axial and swirling component of air velocity. The swirling air flow component will be generated through the introduction of the air flow in the upstream pipe through tangential air inlets.

The above analysis provided estimates of the effects of the dimensions of the liquid jet exit and flow conditions on the diameter of the crossflow air stream. The most suitable liquid jet exit diameter is 1mm, according to the calculations presented above, because the diameter of the air stream can remain smaller for a wider range of flow conditions without the trajectory of the liquid jet hitting at the outer wall of the airstream. The selected width of the air stream is 15mm.

However, the section of the atomizer exit can be exchanged by connecting a new converging section at the flange shown in **Figure 10**. This flexibility is important in order to allow for differences of the behaviour of the liquid jet from what is expected in the literature, especially when swirl is introduced to the air stream.

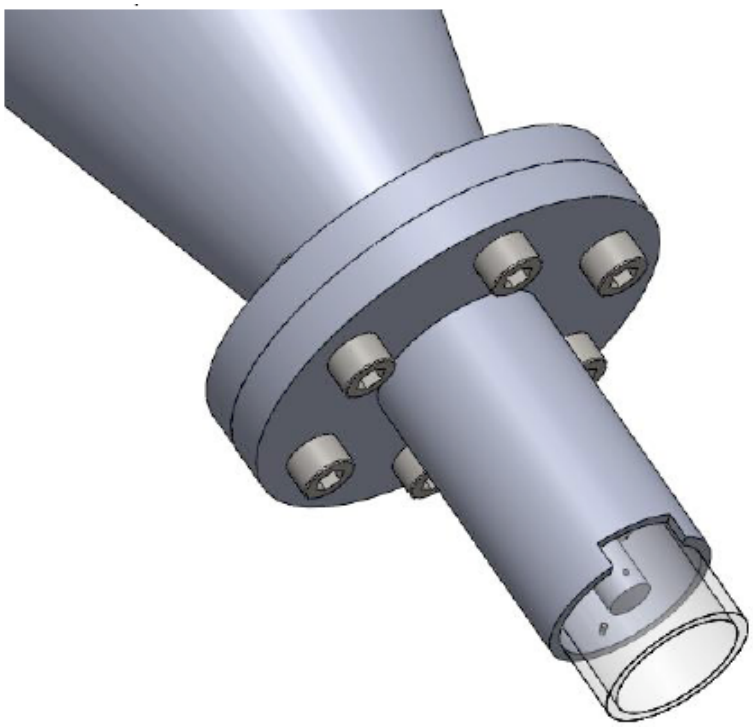

Figure 10: The atomizer design of a liquid jet exposed to a crossflow of air, which can have a swirling velocity component.

An important detail is shown in **Figure 10**. One hole is present at the outer wall of the air stream and at the opposite side of the liquid jet injection nozzle. A second hole, that cannot be observed at the current view of Figure 10, exists on the surface of the liquid tube and at the opposite side of the injection nozzle. These two holes have the same diameter as the injection nozzle (1 mm) and are required in order to allow the laser beam to be introduced in the liquid jet. This is an important requirement for the application of the optical connectivity technique to the measurement of the intact length of the liquid jet. These two holes are covered by appropriate quartz windows. **Figure 11** shows a close up of the liquid jet nozzle exit on the liquid supply tube, which will have rounded edges in order to avoid liquid cavitation due to flow separation through the injection nozzle.

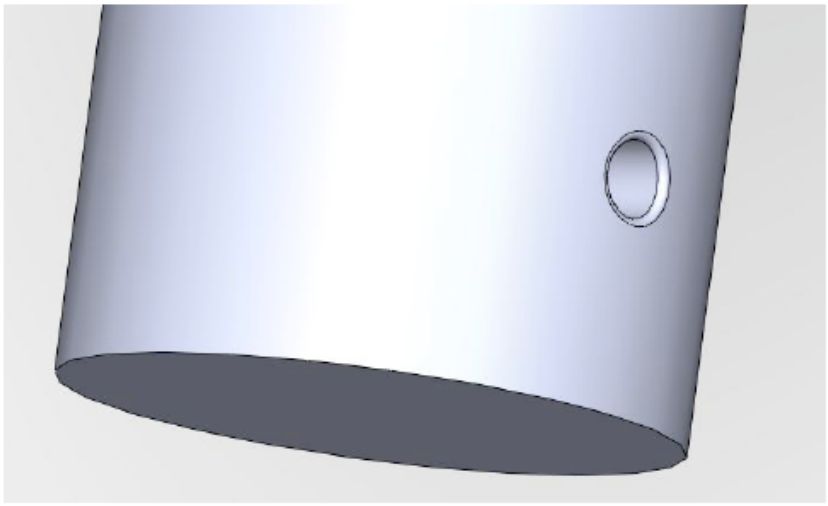

Figure 11: The inner tube of the atomizer, which supplies the liquid to the rounded edged nozzle with diameter of 1mm.

In **Figure 12** the quartz tube that is added at the nozzle exit is presented. The quartz tube, which is 15mm long, is added to confine the air flow and ensure that the flow remains the same while it interacts with the liquid jet. The length of this tube was selected on the basis of the expected longest breakup length for the selected flow conditions of **Figures 8 and 9**. The breakup of the liquid column should be completed inside the quartz tube before the air stream begins to expand. However, this estimate is based on liquid jets exposed to non-swirling air streams. It is clear that the results will change when swirl is introduced but the expectation is that the selected distance will be adequate for liquid jets in swirling air cross stream.

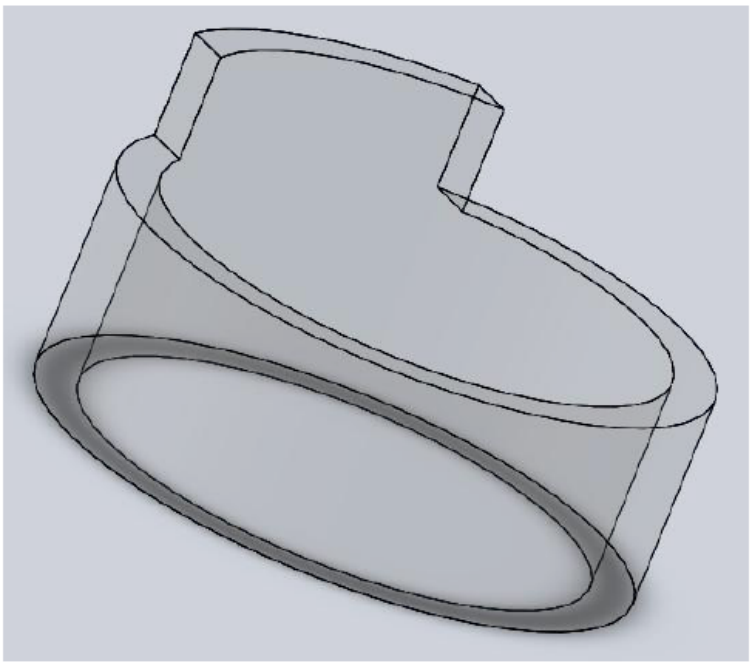

Figure 12: The quartz tube, which extends the length of the nozzle downstream of the liquid jet injection location, to maintain the confinement of the air stream and avoid its expansion.

Summary and future work

The assessment of the optical connectivity technique for measurement of breakup length of different types of liquid jets has continued by considering the effect of inclined liquid jets that occur when they are exposed to a cross-stream of air. Two contributions were made during the current reporting period. The first is on the numerical evaluation of the technique for measurements in inclined liquid jets. The second contribution is on the design of an atomizer, which can allow liquid jets to be exposed to cross-steams of swirling or non-swirling air flows.

The numerical evaluation of the technique achieved the following:

(a) The computer program, based on geometrical optics theory for the propagation of the laser light in a liquid jet, was modified to allow the consideration of inclined liquid columns.
(b) Initial results have been obtained, which demonstrate qualitative differences between straight and inclined liquid jets.
(c) An initial comparison between inclined and straight jets suggests that the emitted fluorescent intensity is reduced faster with distance along the jet due to the increased interaction between the laser light and the surface of the liquid jet in the inclined case. However, theeffect appears to be smaller than expected because the reduction fo the laser light is affected more by the absorption by the fluorescent dye.

An atomizer design for injection of a liquid jet in a cross-stream of air, which can be swirling of non-swirling, was achieved as follows:

(i) An extensive literature review was performed of atomization studies of liquid jets in a cross-stream of air, which established that no information is available on the breakup of liquid jets that are exposed to a swirling air stream.
(ii) The design parameters were established and calculations were performed using available correlations from the literature for liquid jets in non-swirling air cross-streams in order to establish the trajectory of the liquid jet for different liquid jet diameters, liquid and gas flowrates. In this way, the dimensions of the liquid jet nozzle and the width of the air stream were determined.
(iii) An axisymmetric design of the atomizer was established, which allows the introduction of variable level of swirl in the cross-stream, which interacts with the liquid jet. The atomizer has appropriate optical access in order to introduce the laser light within the liquid jet through the injection nozzle. Also, appropriate optical access is provided in order to observe the development and breakup of the liquid jet. The design is flexible so that the dimensions of the air stream can be varied, as required.

The plans for the next reporting period include:

(i) Full parametric study of the operation of the optical connectivity technique in inclined liquid jets and comparison with the operation for straight liquid jets.
(ii) Time dependent measurements of the breakup of the liquid jet in a coaxial airblast atomizer with the optical connectivity technique, which will allow appropriate data processing to determine the characteristics of the surface waves and the dominating liquid flow structures, influencing the atomization process.
(iii) The manufacturing of the atomizer of a liquid jet in a swirling air stream.

In this way, the third year of the project will be able to focus more on the characteristics of the atomization of a liquid jet in a cross-stream of air with and without swirl.

References

1. Charalampous G., Hardalupas Y. and Taylor A.M.K.P., "A novel technique for measurements of the intact liquid jet core in a coaxial airblast atomizer". Presented at *45th AIAA Aerospace Sciences Meeting and Exhibit,* Reno, USA, 2007, *paper no. AIAA 2007-1337*.

2. Lefebvre A.H., *Atomization and sprays*, Hemisphere Publishing Corporation 1989.

3. Lasheras J.C. and Hopfinger E.J., "Liquid jet instability and atomization in a coaxial gas stream". *Annual Review of Fluid Mechanics*, Vol. 32, 2000, pp. 275-308.

4. Engelbert C., Hardalupas Y. and Whitelaw J.H., "Breakup Phenomena in Coaxial Airblast Atomizers". *Proceedings of the Royal Society of London Series A-Mathematical and Physical Sciences*, Vol. 451, No. 1941, 1995, pp. 189-229.

5. Varga C.M., Lasheras J.C. and Hopfinger E.J., "Initial breakup of a small-diameter liquid jet by a high-speed gas stream". *Journal of Fluid Mechanics*, Vol. 497, 2003, pp. 405-434.

6. Chehroudi B., Chen S.H. and Bracco F.V., "On the intact core of full-cone sprays". *SAE Technical Papers 850126*, 1985.

7. Hiroyasu H., Arai M. and Shimizu M., "Break-up length of a liquid jet and internal flow in a nozzle". ICLASS-91. 1991.

8. Yule A.J. and Salters D.G., "A Conductivity Probe Technique for Investigating the Breakup of Diesel Sprays". *Atomization and Sprays*, Vol. 4, No. 1, 1994, pp. 41-63.

9. Hiroyasu H., Shimizu M. and Arai M., "The breakup of high speed jet in a high pressure gaseous atmosphere". *ICLASS-82*, 1982.

10. Cai W.Y., Powell C.F., Yue Y., Narayanan S., Wang J., Tate M.W., Renzi M.J., Ercan A., Fontes E. and Gruner S.M., "Quantitative analysis of highly transient fuel sprays by time-resolved x-radiography". *Applied Physics Letters*, Vol. 83, No. 8, 2003, pp. 1671-1673.

11. Renzi M.J., Tate M.W., Ercan A., Gruner S.M., Fontes E., Powell C.F., MacPhee A.G., Narayanan S., Wang J., Yue Y. and Cuenca R., "Pixel array detectors for time resolved radiography (invited)". *Review of Scientific Instruments*, Vol. 73, No. 3, 2002, pp. 1621-1624.

12. Yue Y., Powell C.F., Poola R., Wang J. and Schaller J.K., "Quantitative measurements of diesel fuel spray characteristics in the near-nozzle region using X-ray absorption". *Atomization and Sprays*, Vol. 11, No. 4, 2001, pp. 471-490.

13. Linne M., Paciaroni M., Hall T. and Parker T., "Ballistic imaging of the near field in a diesel spray". *Experiments in Fluids*, Vol. 40, No. 6, 2006, pp. 836-846.

14. Linne M.A., Paciaroni M., Gord J.R. and Meyer T.R., "Ballistic imaging of the liquid core for a steady jet in crossflow". *Applied Optics*, Vol. 44, No. 31, 2005, pp. 6627-6634.

15. Paciaroni M., Linne M., Hall T., Delplanque J.P. and Parker T., "Single-shot two-dimensional ballistic imaging of the liquid core in an atomizing spray". *Atomization and Sprays*, Vol. 16, No. 1, 2006, pp. 51-69.

16. Charalampous G., Hardalupas Y. and Taylor A.M.K.P., "Novel Technique for Measurements of Continuous Liquid Jet Core in an Atomizer". *AIAA Journal*, Vol. 47, No. 11, 2009, pp. 2605-2615.

17. Charalampous G., Hardalupas Y. and Taylor A.M.K.P., "3-Dimensional structure of the intact liquid jet core during coaxial air-blast atomisation". *Intern. Journal of Spray and Combustion Dynamics (IJSCD)*, Vol. 1, 2009, pp. 389-415.

18. Colladon D. "On the reflections of a ray of light inside a parabolic liquid stream". *Comptes Rendus*, Vol. 15, 1842, pp. 800-802.

19. Charalampous G, Hardalupas Y, Taylor A.M.K.P. (2010) "Numerical and experimental evaluation of the optical connectivity technique for measurement of liquid breakup length in atomizers". Presented at 48th Aerospace Sciences Meeting & Exhibit, AIAA paper 2010-0200, AIAA, Washington, 2010.

20. Charalampous G., Hadjiyiannis C., Hardalupas Y. and Taylor A.M.K.P. (2010) "Measurement of continuous liquid jet length in atomizers with optical connectivity, electrical conductivity and high-speed photography techniques". In "Proceedings of 23rd Annual Conference on Liquid Atomization and Spray Systems, ILASS – Europe 2010", paper 152, Brno, Czech Republic, 6-8 September 2010.

21. Less D.M. and Schertz J.A., "Transient behavior of liquid jets injected normal to a high-velocity gas stream", AIAA J., Vol. 24, 1986, pp. 1979-1985.

22. Wu P.K., Kirkendall K.A., Fuller R.P. and Nejad A.S., "Breakup processes of liquid jets in subsonic crossflows", J. Propul. Power, Vol. 13, 1997, pp. 64-73,.

23. Aavani, K., Taeibi-Rahni, M., Soltani, M. R., Experiments in near-field of turbulent jets into a crossflow, Scientia Iranica, Vol. 13, No. 2, pp. 134-151.

24. Ghosh, S., and Hunt, J. C. R., Spray jets in a cross-flow, J. Fluid Mech., 1998, vol. 365, pp. 109-136.

25. Arienti M. and Soteriou M.C., "Time-resolved proper orthogonal decomposition of liquid jet dynamics", Physics Of Fluids, Vol. 21, 2009, 112104.

26. Ng C.-L., Sankarakrishnan R. and Sallam K.A., "Bag breakup of nonturbulent liquid jets in crossflow", Int. J. Multiphase Flow, Vol. 34, 2008, 241.

27. Rachner, M., Becker, J., Hassa, C., Doerr, T., Modelling of the atomization of a plain liquid fuel jet in crossflow at gas turbine conditions, Aerospace Science and Technology, Vol. 6, 2002, pp. 495-506.

28. Sedarsky, D., Paciaroni, M., Berrocal, E., Petterson, P., Zelina, J., Gord, J., Linne, M., "Model validation image data for breakup of a liquid jet in crossflow: part I", Experiments in Fluids, Vol. 49, 2010, pp. 391-408.

29. Bai, B. F., Zhang, H. B., Liu, L., Sun, H. J., "Experimental study on turbulent mixing of spray droplets in crossflow", Experimental Thermal and Fluid Science, Vol. 33, 2009, pp. 1012-1020.

30. Balasubramanyam, M. S. and Chen, C. P., "Modeling liquid jet breakup in high speed cross-flow with finite-conductivity evaporation", International Journal of Heat and Mass Transfer, Vol. 51, 2008, pp. 3896-3905.

31. Fan, J. Y., Xu, S. L. and Wang, D. Z., "PDA measurements of two-phase flow structure and particle dispersion for a particle-laden jet in crossflow", Journal of Hydrodynamics, Vol. 22, No. 1, 2010, pp. 9-18.

32. Hale, C. A., Plesniak, M. W. and Ramadhyani, S., "Structural features and surface heat transfer associated with a row of short-hole jets in crossflow", International Journal of Heat and Fluid Flow, Vol. 21, 2000, pp. 542-553.

33. Barata, J. M. M., Durao, D. F. G., Heitor, M. V. and McGuirk, J. J., "The turbulence characteristics of a single impinging jet through a crossflow", Experimental Thermal and Fluid Science, Vol. 5, 1992, pp. 487-498.

34. Shedd, T. A., Corn, M. L., Cohen, J. M., Arienti, M. and Soteriou, M. C., "Liquid film formation by an impinging jet in a high-velocity air stream", 47th AIAA Aerospace Sciences Meeting Including the New Horizons Forum and Aerospace Exposition, AIAA 2009-0998, 2009.

35. Lee, J., Sallam, K. A., Lin, K.-C. and Carter, C. D., "Spray structure in near-injector region of aerated jet in subsonic crossflow", 46th AIAA Aerospace Sciences Meeting and Exhibit, AIAA 2008-1043, 2008.

36. Osta, A. and Sallam, K. A., "Effect of nozzle length/diameter ratio on the breakup of liquid jets in crossflow", 46th AIAA Aerospace Sciences Meeting and Exhibit AIAA 2008-1040, 2008.

37. Kihm, K. D., Kim, T. K. and Son, S. Y., "Visualization of high-speed gas jets and their airblast sprays of cross-injected liquid", Experiments in Fluids Vol. 27, 1999, pp. 102-106.

38. Lee, K., Aalburg, C., Diez, F. J. and Faeth, G. M., Sallam, K. A., "Primary breakup of turbulent round liquid jets in uniform crossflows", AIAA Journal, Vol. 45, No. 8, 2007.

39. Sallam, K. A., Dai, Z. and Faeth, G. M., "Liquid breakup at the surface of turbulent round liquid jets in still gases", International Journal of Multiphase Flow, Vol. 28, 2002, pp. 427-449.

40. Sallam, K. A., Aalburg, C. and Faeth, G. M., Breakup of round nonturbulent liquid jets in gaseous crossflows, 41st Aerospace Sciences Meeting and Exhibit, AIAA 2003-1326, 2003.

41. Geary E.L. and Margettes M.J., “Penetration of a High Velocity Gas Stream by a Water Jet”, *Journal of Spacecraft*, Vol. 6, No. 1, 1969, pp. 79-81.

42. Reichenbach P.R. and Horn K.P., “Investigation of Injectant Properties in Jet Penetration in a Supersonic Stream”, *AIAA Journal*, Vol. 9, No. 3, 1971, pp. 469-471.

43. Kush E.A. and Schetz J.A., “Liquid Jet Injection into a Supersonic Flow”, *AIAA Journal*, Vol. 11, No. 9, 1979, pp. 1223-1224.

44. Schetz J.A., Kush E.A. and Joshi P.B., “Wave Phenomena in Liquid Jet Breakup in a Supersonic Crossflow,” *AIAA Journal*, Vol. 15, 1979, pp. 774-778.

45. Nejad A.S. and Schetz J.A., “Effects of Properties and Location in the Plume on Droplet Diameter for Injection in a Supersonic Stream”, *AIAA Journal*, Vol. 21, No. 7, 1983, pp. 956-961.

46. Nejad A.S. and Schetz J.A., “Effects of Viscosity and Surface Tension on a Jet Plume in Supersonic Cross-Flow”, *AIAA Journal*, Vol. 22, No. 4, 1984, pp. 458-459.

List of Symbols, Abbreviations and Acronyms

D_L = inner diameter of the liquid jet nozzle
G = Amplitude of feature on jet surface
L = Wavelength of feature on jet surface
MFR = Liquid-to-Gas Momentum Flux ratio
Re_L = Reynolds number of liquid jet
We_L = Weber number based on liquid jet velocity
We_G = Weber number based on gas velocity
n_1 = Index of refraction of liquid
n_2 = Index of refraction of gas
U_G = Average gaseous velocity of the cross stream
U_L = Average liquid velocity at the nozzle exit
γ = Absorption coefficient
μ = Kinematic viscosity of the liquid
ν_L = Dynamic Viscosity of the liquid
ρ_G or ρ_L = Density of gas or liquid
ϕ = Phase of sinus surface wave
ω = Laser beam divergence
σ = Surface tension

PROGRESS REPORT

AWARD N°: FA8655-09-1-3036 1

TITLE: Novel laser-based technique for measurements of primary atomization characteristics of liquid jets

INVESTIGATOR: Professor Y. Hardalupas

ORGANISATION: Imperial College of Science, Technology and Medicine

REPORTING PERIOD: From: 20 July 2010 To: 19 July 2011

PROJECT START DATE: 20 July 2009

DATE OF ISSUE OF THIS REPORT: 20 July 2011

ADMINISTRATIVE OFFICE: European Office of Aerospace Research and Development (EOARD)

GOVERNMENT PROGRAM MANAGER: Dr. Gregg Abate

Table of Contents

List of Figures

the axis normalized by the width of the column. The horizontal axis shows the distance along the direction of motion of the liquid column, normalized by the width of the liquid column (Example for γ=0.00008m^{-1}, n_1=1.33, ω=20°).

Figure 17. Example of propagation of light rays within a straight liquid column, as determined by geometrical optics calculations. The liquid column is the same as that of Figure 16, but without inclination. The vertical axis shows the width of the liquid column around the axis normalized by the width of the column. The horizontal axis shows the distance along the direction of motion of the liquid column, normalized by the width of the liquid column (Example for γ=0.00008m^{-1}, n_1=1.33, ω=20°).

Figure 18. Fluorescent intensity profiles with distance from the liquid column base for amplitude of surface wave of G/D=0.1, wavelength of L/D=0.5 and no laser beam divergence.

Figure 19. Fluorescent intensity profiles with distance from the liquid column base for amplitude of surface wave of G/D=0.1, wavelength of L/D=0.5 and 10° laser beam divergence.

Figure 20. Fluorescent intensity profiles with distance from the liquid column base for amplitude of surface wave of G/D=0.1, wavelength of L/D=1.0 and no laser beam divergence.

Figure 21. Fluorescent intensity profiles with distance from the liquid column base for amplitude of surface wave of G/D=0.1, wavelength of L/D=1.0 and 10° laser beam divergence.

Figure 22. Fluorescent intensity profiles with distance from the liquid column base for amplitude of surface wave of G/D=0.1, wavelength of L/D=2.0 and no laser beam divergence.

Figure 23. Fluorescent intensity profiles with distance from the liquid column base for amplitude of surface wave of G/D=0.1, wavelength of L/D=2.0 and 10° laser beam divergence.

Figure 24(a). Liquid jet trajectory for diameter of liquid jet exit D=0.5mm, liquid flow rate of 0.5l/min and different air velocities.

Figure 24(b). Liquid jet trajectory for diameter of liquid jet exit D=0.5mm, liquid flow rate of 1 l/min and different air velocities.

Figure 24(c). Liquid jet trajectory for diameter of liquid jet exit D=0.5mm, liquid flow rate of 2 l/min and different air velocities.

Figure 25(a). Liquid jet trajectory for diameter of liquid jet exit D=1mm, liquid flow rate of 0.5 l/min and different air velocities.

Figure 25(b). Liquid jet trajectory for diameter of liquid jet exit D=1mm, liquid flow rate of 1 l/min and different air velocities.

Figure 25(c). Liquid jet trajectory for diameter of liquid jet exit D=1mm, liquid flow rate of 2 l/min and different air velocities.

Figure 26. The atomizer design of a liquid jet exposed to a crossflow of air, which can have a swirling velocity component.

Figure 27. The inner tube of the atomizer, which supplies the liquid to the round-edged nozzle with diameter of 1mm.

Figure 28. The quartz tube extends the length of the nozzle downstream of the liquid jet injection location in order to maintain the confinement of the air stream and avoid its expansion.

Summary

During the first stages of atomization of an airblast atomizer, the liquid stream is destabilized under the influence of a stream of air, until its continuity is broken. The geometry of the injector affects the way that the liquid jet breaks up and understanding the physics of the primary atomization process is important for the control of the spatial and temporal spray characteristics downstream of the nozzle. A novel technique (Charalampous *et al.* 2007 [1]) has been proposed to measure the length of the continuous liquid jet, quantify the spatial and temporal characteristics of the instabilities along the liquid-gas interface and examine the way that the liquid breaks up to form droplets. This technique relies on the optical connectivity of a liquid jet when it is internally illuminated through the spray nozzle. The liquid jet acts as a light guide, which allows light to propagate along the length of the jet in the same way as light travels along an optical fiber. The laser light excites a fluorescent dye that is dissolved in the liquid jet, making the volume of the liquid jet luminous. Then, the connectivity of the liquid jet is linked to the optical connectivity of the fluorescent jet. However, since the optical characteristics of the liquid jet are not the same as those of an optical fiber, there are losses of light intensity due to refraction through the liquid-gas interface and absorption by the fluorescence dye, as it propagates along the liquid jet. Therefore, the applicability of the technique requires evaluation in different geometries of liquid jets.

During the current reporting period, representing the second year of the project, two areas were addressed:

(a) Application of high-speed, time-dependent optical connectivity technique on a liquid jet breaking up in a coaxial atomizer, in order to measure the spatial and temporal characteristics of the liquid-gas interface and the time-dependent breakup length.

(b) Evaluation of the applicability of the optical connectivity technique in liquid jets exposed to a cross stream of air. A theoretical and experimental approach was followed.
The theoretical approach made use of the developed numerical approach in the first year of the project to evaluate the light propagation within liquid columns of various geometries. The computational approach was extended to include the effect of the inclination of the liquid column. This development was completed and the computer program was used to evaluate the effect of liquid column inclination.
The experimental approach was based on designed and manufacturing an axisymmetric facility that allows the injection of a liquid jet in a cross flow of air. This experimental facility is unique, because it allows swirling air flow to interact with the injected liquid jet. No measurements have been reported in the literature of the behaviour of liquid jets exposed to a swirling air cross-stream. The facility provides appropriate optical access to the liquid jet in order to illuminate it with laser light through its injection nozzle and allow measurements of the liquid jet development and breakup using the optical connectivity technique.

1. Introduction

During the first stages of atomization of a liquid jet, the jet is progressively destabilized under the influence of the forces that result from the interaction of the liquid stream with the surrounding air (2, 3). During this process the jet geometry changes as liquid is removed from its surface and waves develop on the surface until their amplitude becomes large enough to lead to breakup of the liquid jet. The distance from the nozzle exit to the point downstream the nozzle, where the liquid jet breaks up defines what is known as the “primary atomization region”. The length of the continuous core of the liquid jet, known as the “breakup length”, determines the extent of the primary atomization region and the performance of atomizing nozzles.

A number of techniques have been proposed for the measurement of the length of the continuous jet. These include photography [4, 5], electrical conductivity [6-9], X-ray absorption [10-12] and ballistic imaging [13-15]. A recently proposed method is the optical connectivity technique [1]. It has been shown that, in dense sprays, the optical connectivity technique can measure the breakup length of the liquid jet at conditions where the continuous length of the jet is difficult to measure with photography, as the atomization products that surround the jet hinder the view to the continuous jet.

Photography (usually shadowgraphy) is the most commonly used method, as it is straightforward to apply and places only moderate demands on equipment. In this method, the atomizing jet is imaged directly by a camera. A light source illuminates the liquid jet and is usually placed on the opposite side of the camera to allow the light to propagate through the liquid jet. In this way, the shadow of the jet is imaged and its contour is well defined in the acquired images. The break-up length is estimated from the geometry of the recorded contour. While this method is easy to implement, when atomization becomes more intense, the droplets around the jet core might obstruct parts of the jet and the break-up length may be measured longer than its real value.

The electrical conductivity technique is based on the conduction of electricity along the length of a continuous liquid jet downstream the nozzle exit. A potential is applied between the atomizer nozzle and a probe downstream. If there is continuity of the liquid phase between the nozzle and the probe, a closed electrical circuit will ensue. The probe can be moved across different positions to determine the continuity of the liquid jet as a function of downstream distance. If the detected potential is low it is verified that there is electrical connectivity up to a specific point indicating continuity of the liquid jet core. On the contrary, the discontinuity of the liquid jet can be located where the conductivity is negligible. In earlier work, many researchers developed a conductivity probe technique to enable the investigation of the breakup zone in a variety of applications. Yule and Salters [8] investigated the breakup zone of a transient diesel spray as a function of time and position employing a wire probe. Hiroyasu et al [7, 9] studied the breakup length of a high-speed liquid jet by measuring an electrical resistance between the nozzle and a fine wire screen detector located in a spray jet. Chehroudi et al. [6] tried to determine the shape and length of the intact liquid core by applying a voltage between the nozzle unit and fine needles, rods and screens. The results show that current is carried not only by intact liquid cores but also by atomized unconnected sprays.

The novel optical connectivity technique [16, 17] relies on illuminating a liquid jet from within the nozzle by a laser beam, which propagates downstream, while reflecting at the gas-liquid interface. Due to the higher index of refraction of the liquid jet to that of the surrounding gas, a laser light ray that interacts with the gas-liquid interface at a sufficiently large incident angle undergoes total internal reflection. As a consequence, the laser beam is reflected completely

back into the liquid stream and propagates downstream for a long distance in the same way that light propagates along optical fibers. Collandon [18] demonstrated this phenomenon as early as 1842. The addition of a fluorescent dye, such a Rhodamine WT in the liquid jet, causes some of the intensity of the laser beam to be absorbed and re-emitted at a longer wavelength as fluorescence. This causes the volume of the continuous jet to become luminous, which allows the evaluation of the break-up length. Beyond the point of liquid discontinuity, the laser beam is diffused and its intensity is significantly reduced. The optical connectivity technique is not without limitations. As the technique is based on the propagation of light within an atomizing liquid jet, there will unavoidably be some scattering losses at the gas-liquid interface that will reduce the intensity of the propagating light. Therefore, for long liquid jets, the technique will not be possible to operate due to complete attenuation of the propagating light along the liquid before the break up point. Therefore, a numerical model of light propagation along a liquid jet was developed to determine how the laser light that is seeded at the base of the jet propagates along its length and what are the effects of its geometry on the losses of the intensity of the laser light.

During the first year of the project, measurements of break-up length of a liquid jet in an airblast coaxial atomizer were obtained with the optical connectivity technique, the electrical connectivity and high-speed photography. The results from the three measurement techniques were compared and advantages and limitations of the optical connectivity technique were identified [19, 20]. In the current reporting period, the emphasis was directed in two directions: (a) the development of time-dependent optical connectivity technique and its application to the measurement of the temporal and spatial characteristics of the gas-liquid interface and the breakup length of a liquid jet in a coaxial airblast atomizer; (b) the applicability of the optical connectivity technique in liquid jets exposed to a cross stream flow of gas.

The next section of this report describes the experimental and numerical tools. This includes the description of: (a) the development of the optical connectivity technique for time-dependent measurements and associated data processing approaches in order to evaluate the temporal and spatial characteristics of instabilities of the liquid-gas interface of an atomizing liquid jet; (b) the geometrical optics approach, developed to evaluate numerically light propagation through a liquid column, that was extended to include the effect of the liquid column inclination relative to the initial direction of injection, which coincides with the direction of the initial propagation of the laser light. This theoretical approach evaluated the influence of various parameters on the accuracy of measurements of the length of the continuous liquid jet with the optical connectivity technique.

The third section presents and discusses the results. The following subsections exist. (a) Time-dependent measurements of the liquid jet characteristics during primary breakup in a coaxial atomizer. This includes the findings from Proper Orthogonal Decomposition (POD) analysis of the temporal and spatial characteristics of the liquid-gas interface of the liquid jet. (b) Numerical analysis, based on the developed geometrical optics approach, of the operation of the optical connectivity technique for inclined liquid columns. (c) The design of an atomizer that allows the study of a liquid jet exposed to a cross-stream of air. This describes a unique facility that allows the air flow to acquire variable levels of swirl and, as a consequence, study the primary breakup of a liquid jet in a cross-stream of swirling air flow. This section provides an initial literature review, which verifies the lack of studies of liquid jets exposed to swirling cross flow of air, presents the design criteria and associated estimates and describes the final design.

The report ends with a summary of the main achievements.

2. Methods, Assumptions and Procedure

2.1 Principle of Optical Connectivity Technique

An optical connectivity technique has been developed for the measurement of the continuous length of liquid jets during the atomization process in atomizers. The technique works by introducing a laser beam within the flow of the liquid upstream of the nozzle that exits with the liquid through the nozzle in the direction parallel to the nozzle axis. In this way the laser beam is largely contained within the liquid jet by reflecting on the liquid interface propagating downstream and illuminating the liquid jet volume. A ray of laser light is guided along the length of the liquid jet by reflecting on the gas-liquid interface at the jet surface. As long as the angle of incidence between the surface of the jet and the laser light rays is greater then the angle of total internal reflection, the rays are completely reflected back inside the liquid without intensity losses from refraction. This principle is similar to the way that a laser beam propagates within an optical fiber. However, if the angle of incidence of a laser light ray on the liquid jet interface becomes smaller than that for total internal reflection then there will be some intensity losses due to refraction.

The laser beam continues to propagate downstream the jet until it meets the breaking point of liquid jet, where it can no longer be contained within the jet and is diffused randomly in different directions. The introduction of a fluorescing dye into the liquid makes part of the laser beam to be absorbed along the length of the liquid jet, and subsequently be re-emitted as fluorescence. In this way the atomizing jet becomes luminous and can be imaged (**Figure 1**).

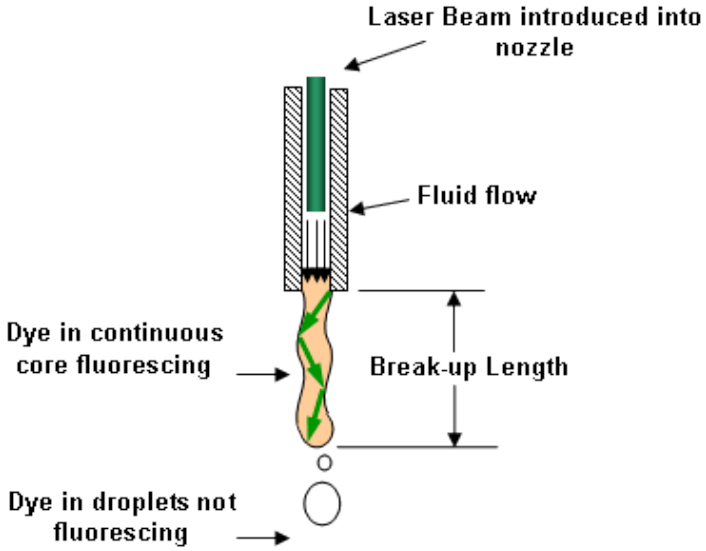

Figure 1. Principle of the optical connectivity technique

An example of the instantaneous image of a highly magnified liquid jet, illuminated by a laser beam according to the principle of the optical connectivity technique, is presented in **Figure 2**. The ability to detect the instabilities along the surface of the interface of liquid jet can be identified.

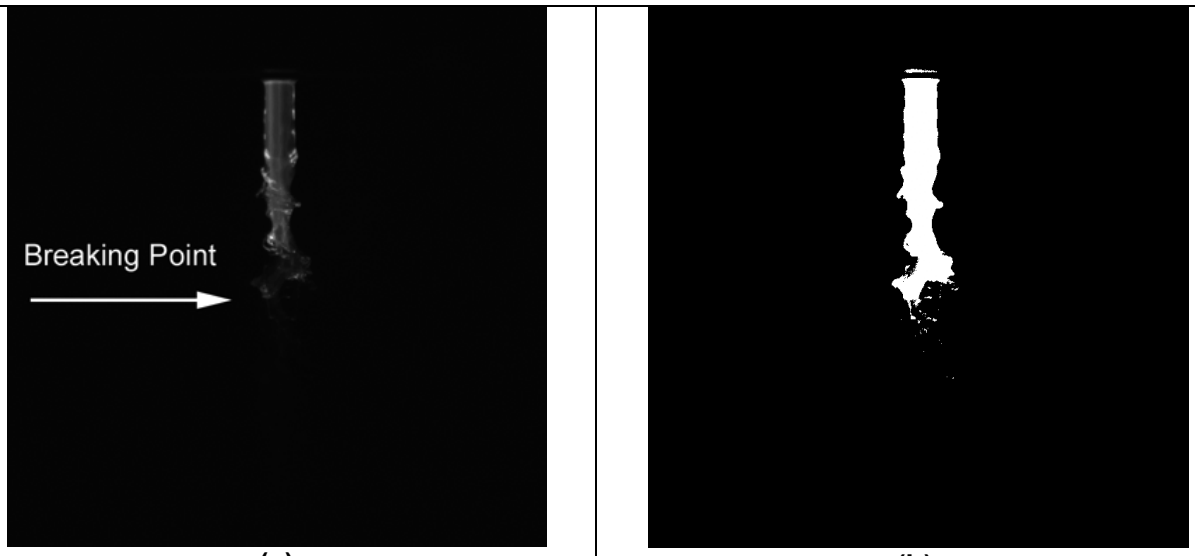

Figure 2. (a) Example instantaneous image of a liquid jet obtained from the optical connectivity technique. (b) The image of (a) after image processing, which indicates the intact length of the liquid jet and the instabilities along the gas-liquid interface of the liquid jet.

2.2 Coaxial airblast atomizer and optical instrumentation

2.2.1 Coaxial airblast atomizer

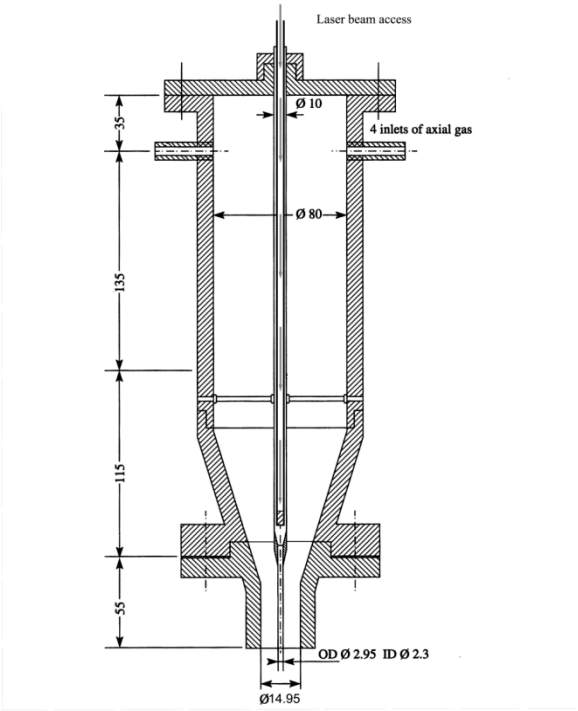

Figure 3. Geometry of coaxial airblast atomizer.

An air-blast atomizer, shown schematically in **Figure 3**, was used to atomize the liquid in this investigation. A detailed description of the atomizer is provided in [4] and only the basic features are described here. The two working fluids are water and air. The liquid nozzle, which is placed along the axis of the atomizer, has internal diameter of 2.3 mm and external diameter of 2.95 mm and the gas nozzle, which surrounds the liquid nozzle, has internal diameter of 14.95 mm. The atomizer was set up vertically and exhausted downwards. The configuration of the atomizer and the air and water supplies, is illustrated in **Figure 4**. Water is delivered from the water tank (A) to pump (B). The flow rate was controlled by adjusting valves (C), (D) and (L). The water flow rate was measured by rotameter (E) on a scale of 0-2 l/min with a 0.1 l/min resolution. The atomized liquid was collected in tank (I) and then was returned to the main tank (A) using a water pump (J). The air flow rate was adjusted from vane (F) and the flowrate was measured by rotameter (G) on a scale of 0-2000 l/min with a resolution of 50 l/min. Air flow rate measurements were corrected for atmospheric temperature and pressure conditions.

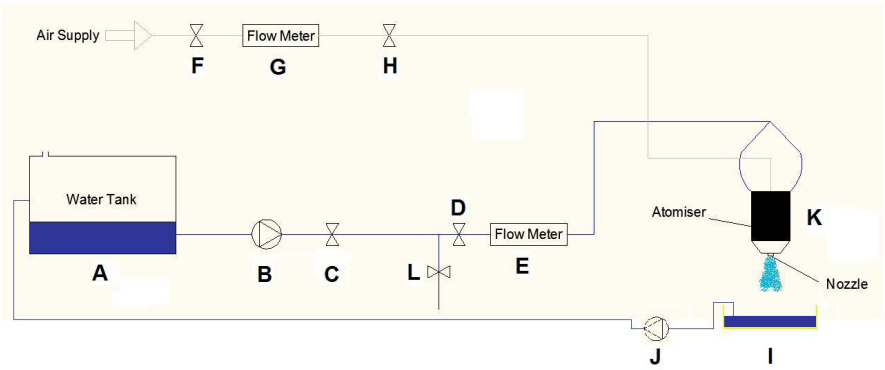

Figure 4. Air and water supply circuit to the coaxial airblast atomizer

Time resolved shadowgraphic photography and fluorescence imaging, based on the optical connectivity technique, were obtained for the flow conditions described in Table 1.

Case	Liquid flow rate (l/min)	Air flow rate (l/min)	Re	We	MR
1	0.1	250	1080	21	171
2	0.1	300	1080	30	246
3	0.1	350	1080	42	335
4	0.1	400	1080	55	438
5	0.1	450	1080	69	554
6	0.1	500	1080	86	685

Table 1. Operating conditions of coaxial airblast atomizer for high-speed photographic and optical connectivity imaging

The initial operating conditions of the atomizer were expressed in terms of non-dimensional parameters, namely Reynolds number, Re, Weber number, We, and momentum ratio, MR, which are defined below:

$$\mathrm{Re} = \frac{\rho_L U_L D_L}{\mu} \qquad (1)$$

$$We = \frac{\rho_G \left(U_L - U_G\right)^2 D_L}{\sigma} \tag{2}$$

$$MR = \frac{\rho_G U_G^2 (D_G^2 - D_L^2)}{\rho_L U_L^2 D_L^2} \tag{3}$$

where ρ_L is the liquid density, ρ_G is the gas density, D_L is the internal diameter of the liquid nozzle, D_G is the internal diameter of the gas nozzle exit, U_L is the cross section average velocity at the liquid nozzle exit, U_G is the cross section average velocity at the gas nozzle exit, μ is the liquid dynamic viscosity and σ is the surface tension of the liquid.

For the flow conditions of Table 1, assuming a gas boundary layer thickness around the liquid jet of about the size of the liquid nozzle, the theoretical wavelength due to Kelvin Helmholtz instability [21] is of the order of 60 mm and the maximum frequency of the order of 550Hz. Both can be well resolved by the spatial and temporal resolution of the high speed camera.

2.2.2 Time-resolved measurements with high-speed shadowgraphy and optical connectivity techniques

Time resolved shadowgraphic photography and fluorescence imaging, based on the optical connectivity technique, of the primary atomization region of the liquid jet were obtained in the near nozzle region of the coaxial airblast atomizer.

A Photron Fastcan-APX RS camera fitted with a 105mm lens was used to acquire the high-speed images for both techniques. For the optical connectivity measurements, a Schott OG550 long pass filter was used to suppress the scattered light intensity and capture the luminous liquid column. The high-speed camera was operated at 3000 frames/sec in order to obtain a temporarily resolved sequence of images for different operating conditions.

For the optical connectivity technique, the second harmonic of a Nd:YLF laser (Quantronix Darwin Duo) was used to excite the fluorescence of Rhodamine WT by guiding the laser beam with a system of lenses through the liquid jet nozzle. Laser pulses with a rate of 3000 Hz were generated in order to illuminate the liquid jet.

For the time resolved shadowgraphic photography a 100W lamp was used as source of illumination. It was placed behind the liquid jet so that the imaging of the shadow of the liquid jet was in the forward scattering direction.

For each operating condition of the coaxial atomizer and for each technique, 1024 images were acquired. Due to the dynamic nature of atomization, there is high variability in the timescales and the lengthscales of the morphology of the liquid jet in the acquired images from photographic and optical connectivity techniques. A useful tool for the analysis of the spray images from both techniques is Proper Orthogonal Decomposition (POD). This method reduces the description of the acquired images to contributions from individual Proper Orthogonal Modes (POM) from which only the most energetic are usually sufficient to describe the jet dynamics.

This technique has been applied in the analysis and modelling of turbulent flows [22], to ensembles of velocity fields in internal combustion engine, where the POD modes give some indication of the swirl and make it possible to describe the evolution of spatial complexity of the flow [23], and in cross-flow atomization to provide an analysis of liquid jet dynamics and to identify the jet deformation [24]. Finally, POD finds applications in computational processing, some numerical examples can be found in [25]. As a consequence, POD analysis was developed and the acquired images were processed and identified the contributions of different modes to the overall structure of the liquid jet. The findings from the shadowgraphic photography and the optical connectivity fluorescence images were compared.

2.3 Geometrical Optics for light propagation in liquid columns

For the evaluation of the effect of the shape of the jet geometry on the propagation of light within a column of liquid, the propagation of laser light rays is calculated using geometrical optics. This simulation has the benefit of enabling the evaluation of the effect of all operating parameters, which is difficult to achieve experimentally.

The liquid jet for this investigation is considered as a two-dimensional liquid column. The central axis of the liquid column extends along the x-axis of a Cartesian coordinate system. The interface of the jet is described by the sinusoidal wave function along the x-axis:

$$y = G\sin\left(\frac{2\pi x}{L} + \phi\right) + y_0 \qquad (4)$$

where G is the amplitude of the wave on the interface and L is the wavelength of the wave on the surface of the interface. ϕ is the phase of the wave on the surface of the interface and sinusoidal disturbances are present along the liquid column when the phases of the top and bottom interfaces are matched or varicose disturbances appear when the phases of the waves between the top and bottom surfaces are shifted by π.

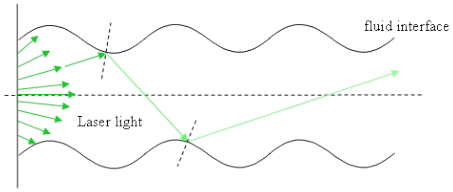

Figure 5. Geometry of the considered liquid column with surface waves and diverging laser beam rays at the base of the liquid column.

For the geometrical optics calculations, a monochromatic laser beam that propagates inside the liquid column is considered (**Figure 5**). The laser beam is simulated by a large number of rays that start at the base of the liquid column at uniformly spaced intervals and propagate downstream the nozzle exit. The ray that begins on the axis of the column is aligned parallel to the axis. However, in order to consider the influence of the divergence (ω) of the laser beam, the angle between the rays at the column base and the axis is progressively changed as the distance between the axis and the starting point of the rays along the *y*-axis increases.

The calculation of the path of the rays when they are incident to the surface of the liquid column is estimated by:

$$R = V - 2(V \cdot N)N \tag{5}$$

where V is the incident ray vector, N is the vector normal to the jet surface at intersection point (between the wave and the incident ray) and R is the vector of the reflected ray.

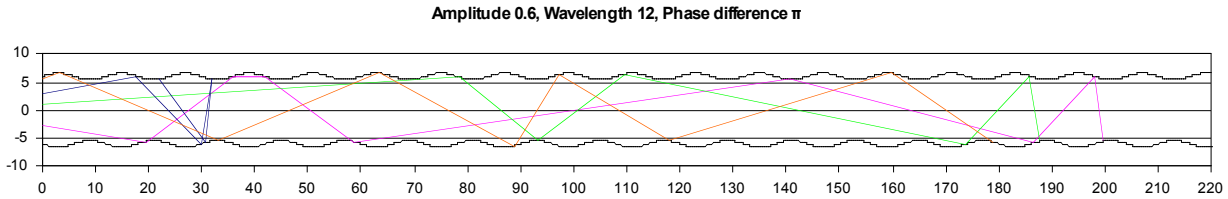

Figure 6. Example of propagation of laser light rays within a liquid column, as determined by geometrical optics calculations. The vertical axis shows the width of the liquid column around the center and the horizontal axis shows the length along the direction of motion of the liquid column.

As the rays propagate along the liquid column (**Figure 6**), the initial intensity of each beam I_0 is reduced due to refraction of the light at the liquid interface, which is lost, and absorption from the dye present in the liquid, which is re-emitted as fluorescence.

Considering the angle of incidence between the rays and the local interfacial surface of the liquid, the critical angle for total internal reflection is given by the relationship:

$$\theta_{crit} = \sin^{-1}\left(\frac{n_2}{n_1}\right) \tag{6}$$

where n_1, n_2 the refractive indices of the liquid and the gas phases. However, when the angle of incidence between a ray and the air-liquid interface is smaller that the angle of incidence for total internal reflection, there are losses of the intensity of the ray. The fraction of the intensity of incident light that is reflected from the interface is given by the reflection coefficient R, and the fraction refracted by the transmission coefficient T. The Fresnel equations are used to calculate R and T. The calculations of R and T depend on polarization of the incident ray. If the light is polarized with the electric field of the light perpendicular to the plane of **Figures 5** or **6** (s-polarized), the reflection coefficient is:

$$R_s = \left[\frac{\sin(\theta_1 - \theta_2)}{\sin(\theta_1 + \theta_2)}\right]^2 \tag{7}$$

If the incident light is polarized in the plane of the **Figures 5** or **6** (p-polarized), the reflection coefficient R is:

$$R_p = \left[\frac{\tan(\theta_2 - \theta_1)}{\tan(\theta_1 + \theta_2)}\right]^2 \tag{8}$$

The Beer-Lambert law estimates the reduction of the intensity of the rays due to the absorption caused by the fluorescent dye present in the liquid through which the ray is traveling:

$$I = I_0 e^{-\gamma z} \tag{9}$$

where γ is the absorption coefficient, z the path length traveled by the ray, I_0 is the initial intensity of the ray and I the intensity of the ray after it has traveled a distance z in the absorbing medium.

The total reduction of the initial intensity I_0 of the laser beam that travels along a path of length z in an absorbing medium until it reaches the interface is given by the formula:

$$I = \left(\frac{\left[\frac{\sin(\theta_1 - \theta_2)}{\sin(\theta_1 + \theta_2)}\right]^2 + \left[\frac{\tan(\theta_2 - \theta_1)}{\tan(\theta_1 + \theta_2)}\right]^2}{2} \right) I_0 \cdot (e^{-\gamma z}) \tag{10}$$

While the refracted part of the laser light intensity is lost, the absorbed light intensity along the ray path is subsequently re-emitted as fluorescence. By summation of the losses of the laser light intensity of each ray due to absorption at each distance downstream of the nozzle exit, the profile of the fluorescent intensity with distance from the nozzle exit is determined. In this way, the limitations of the visualization of the fluorescent liquid jet can be determined. The parameters that influence the loss of light intensity are morphological (wavelength, L, amplitude, G, and phase, ϕ, of the waves on the surface of the liquid column), physical (absorption of light within the liquid, γ, and refractive index of liquid, n_1) and optical (divergence of rays of laser light, ω). The wavelength and the amplitude of the waves superimposed on the liquid surface were normalized by the width of the liquid column at the nozzle exit D.

The emphasis is on the behavior of the optical connectivity technique for an inclined liquid jet, as develops when a liquid jet is exposed to a cross-stream of air. The previously developed software was modified to include the option to vary the inclination angle of the liquid jet, while the options to vary all the other parameters, i.e. the frequency and amplitude of the surface waves along the interface, the refractive index of the liquid, the absorption coefficient of the fluorescing dye and the characteristics of the laser light, remained available. The following text describes the way that the inclined liquid jet was introduced in the analysis and the range of parameters that have been considered in the parametric study that is presented in the results section below.

The jet is described as a two-dimensional geometry in the XY plane of **Figure 7** with X aligned with the central jet axis. Two sinus waveforms with wavelength L and amplitude G as in Equation (11) are used to describe the top and bottom jet boundaries. The two sinus waveforms are displaced by a fixed offset of 0.5 and -0.5 for the top and bottom boundaries respectively so that the base of the liquid jet is of unity size, representing the liquid jet diameter. The inclined trajectory of the liquid jet is represented as a parabolic profile. The rate of inclination is controlled by the value of parameter α of Equation (11). A straight jet is obtained for α=0, while the jet becomes increasingly more inclined for increasingly large values of parameter α.

$$Y = G \cdot \sin\left(\frac{2\pi X}{L}\right) + a \cdot \left(\frac{X}{50}\right)^2 + offset \qquad (11)$$

The geometries considered here are presented in graphical form in Figure through Figure .

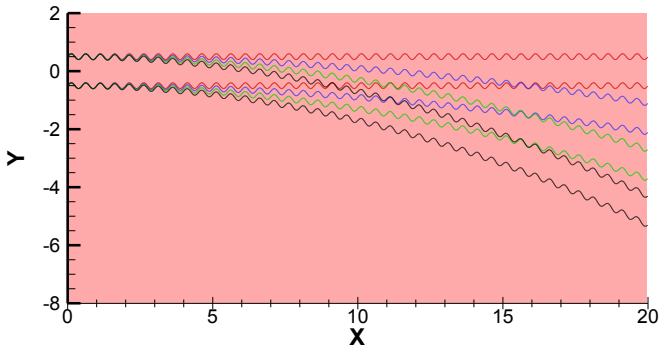

Figure 7. Geometry of inclined simulated liquid columns for wavelength of sinusoidal disturbances of L/D=0.5 and rate of inclination of 0, 10, 20 and 30

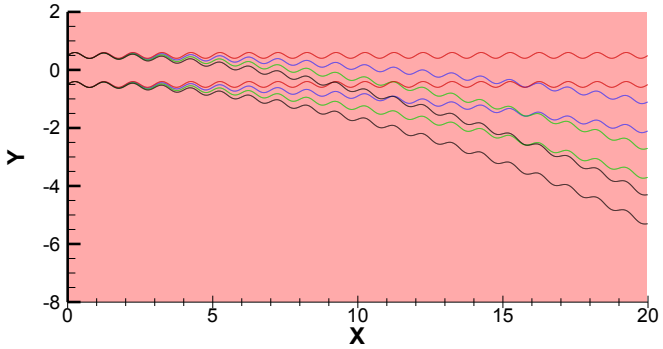

Figure 8. Geometry of inclined simulated liquid columns for wavelength of sinusoidal disturbances of L/D=1.0 and rate of inclination of 0, 10, 20 and 30

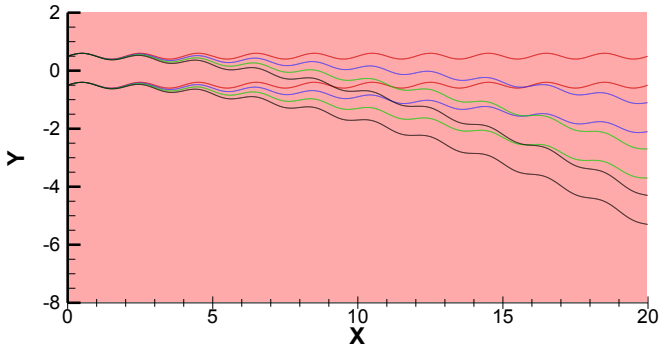

Figure 9. Geometry of inclined simulated liquid columns for wavelength of sinusoidal disturbances of L/D=2.0 and rate of inclination of 0, 10, 20 and 30.

The laser beam is described by an array of equally spaced rays that are emitted from the base of the jet in the positive X direction. Two cases of ray directionality are considered. In the first, all the rays are parallel to the X axis as shown in **Figure a**. In the latter only the central ray is parallel to the X-axis while divergence increases along the Y-axis with maximum divergence at the jet boundaries as shown in as shown in **Figure b**. The summary of the geometrical characteristics of liquid jet geometry and beam divergence considered here is presented in **Table**

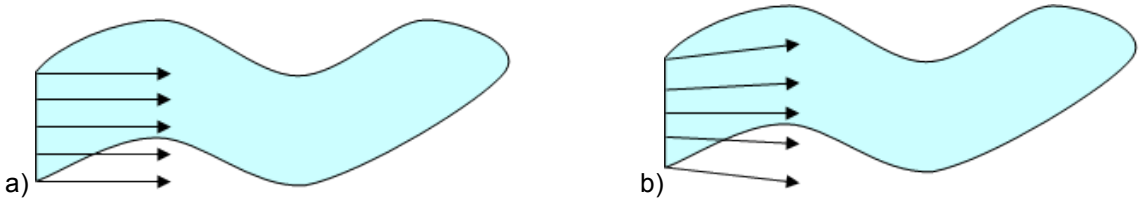

Figure 10. Initial laser beam direction: a) parallel rays b) diverging rays

L/D	G/D	Liquid column Inclination rate	Max divergence
-	-	-	degrees
0.5	0.1	0 10 20 30	0 10
1.0	0.1	0 10 20 30	0 10
2.0	0.1	0 10 20 30	0 10

Table 2. Geometrical characteristics of liquid column with surface disturbances with amplitude G and wavelength L and laser beam divergence. D is the column width at the base.

3. Results and discussion

This section presents the results in three sub-sections. (a) Time-resolved measurements of optical connectivity and shadowgraphy of the primary breakup region of a liquid jet in a coaxial airblast atomizer. The emphasis of the results is on Proper Orthogonal Decomposition (POD) analysis of the intensity fluctuations on the images. (b) Light scattering calculations of laser light propagation through a liquid jet with wavy surface using the geometrical optics approach described in the previous section. (c) Design of an experimental facility to inject a liquid jet in cross flow of swirling air stream. A brief review of the available literature on liquid jets exposed to cross-steams gas flows is provided, which demonstrates that there are no available experiments with liquid jets injected in swirling air cross-streams. This verifies the need for such a study, since the interaction of liquid jets with swirling air streams is common to a wide range of gas turbine combustor injectors.

3.1 Time-resolved measurements of liquid jet primary breakup of coaxial airblast atomizer

The previous section described the coaxial airblast atomizer, the optical techniques and the optical arrangements that were used to apply time-resolved optical connectivity and shadowgraphy to measure the primary breakup of a liquid jet in a coaxial airblast atomizer. Table 1 provides the operating conditions of the atomizer that have been studied. For each experimental condition and for each technique N=1024 images were acquired. The imaging results are presented below in terms of findings following a Proper Orthogonal Decomposition analysis.

Figure 11 shows two example images: the first one is acquired with shadowgraphy and the second with optical connectivity. In the shadowgraphic image, **Figure 11a**, the detached droplets and ligaments downstream of the continuous jet, are imaged along with the atomizing liquid jet, while in the optical connectivity image, **Figure b**, only the liquid jet core is visualised. As a result, the POD processing of the photographic images will produce modes that describe the development of the primary and secondary atomization zones, while optical connectivity will reflect the development of the continuous liquid jet.

a)  b) 

Figure 11. Example images from (a) shadowgraphic imaging and (b) optical connectivity imaging for operating conditions of Case 6 of Table 1.

Considering that the sample size is much smaller than the number of pixels that are contained in each of the acquired images, the number of modes, ε_i, that are obtained from the POD processing of the images, are 1024. For each measurement, the POD modes are sorted hierarchically, according to their eigenvalue. In this way, the first mode of each measurement captures the greatest amount of pixel intensity fluctuations, with succeeding modes containing progressively less information of pixel intensity fluctuations. If most of the pixel intensity fluctuations are captured in the first few modes, it is possible to deconstruct the atomization process to an overlap of a limited number of geometrical characteristics that develop on the liquid jet stream and downstream. When this is not the case, then the process is too complex and cannot be described in simple terms.

The quality of the description of the atomization process by the first i modes is quantifiable by the ratio of the sum of the eigenvalues λ of each mode, up to mode i, over the sum of all the eigenvalues

$$\varepsilon_i = \frac{\sum_{n=1}^{i} \lambda_n}{\sum_{n=1}^{N} \lambda_n} \qquad (12)$$

In **Figure 12**, ε_i of Equation (12) is plotted against the eigenmode number for all flow conditions and for both measurement techniques. There are two main observables. The first is that in all flow conditions and for both measurement techniques, a significant number of modes are required to describe the atomization process with accuracy. While about 30%-60% of the pixel intensity fluctuations are captured in the 10 first POD modes that are associated with larger scale features, the minimum number of modes for all investigated flow conditions required to capture 80% of the pixel intensity fluctuations is 53. This number is clearly too high for the breakdown of the description of atomization to a few energetic modes. In addition, the number of modes required to attain the same degree of completeness of description of atomization differs significantly between shadowgraphic and optical connectivity imaging. The optical connectivity method requires by far fewer modes. For example in case 5 of Table 1, in order to describe 80% of the pixel intensity fluctuations, 55 modes are needed for the images of the optical connectivity method and 116 modes are needed for the images of the shadowgraphic method. Since the shadowgraphic images, which contain information of the dispersion of the spray droplets and ligaments downstream of the liquid jet, describe a more complex phenomenon, more POD modes are needed for a good description. On the other hand, while the optical connectivity technique does not capture information of the relation between the primary and secondary atomization regions, it is likely that the separation of the two can isolate as much as possible the features that evolve on the jet core.

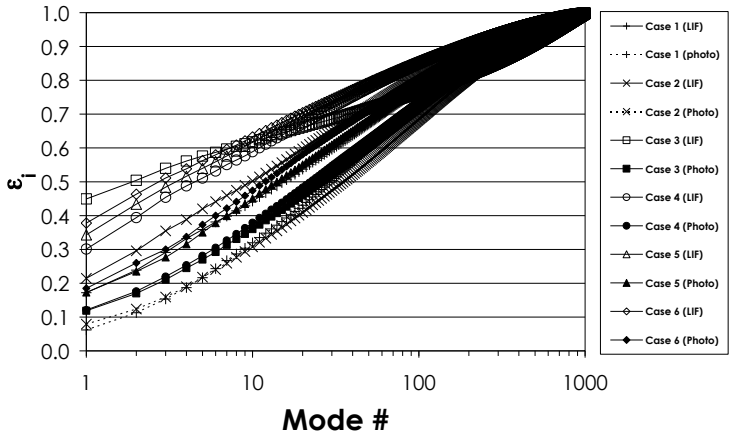

Figure 12. Cumulative contribution of the first POD modes normalised by the total pixel intensity fluctuations. Optical connectivity requires fewer modes than shadowgraphic imaging.

By examining the contours of the POD modes, many geometrical features of the atomization process are identifiable. The features concentrate mostly in the area of liquid breakup for the optical connectivity technique and around the breakup location and downstream region for the shadowgraphic technique due to the greater amount of pixel intensity variations in these regions. For both measurement techniques the first modes, which are the most energetic, are dominated by spatially wide features, as, for example, shown in **Figure a**. With increasing mode

number the captured features contain less information and become finer, as for example **Figure b**, although they do not become completely random.

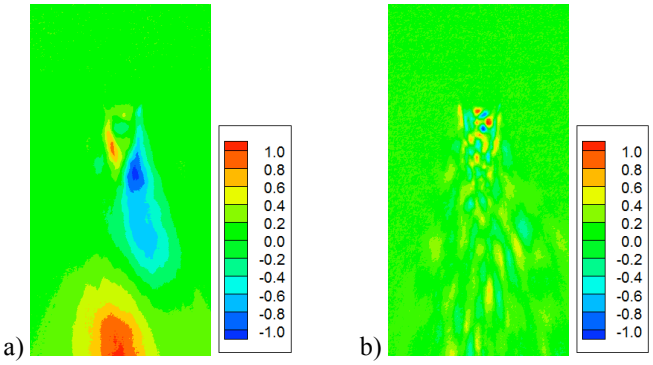

Figure 13. Normalised contours of POD analysis a) mode 2 and b) mode 100 for high-speed imaging and for the flow conditions of Case 6 of Table 1, showing the transition from broad scale to fine scale features. Red and blue colours represent respectively, positive and negative intensity deviations from the mean image.

The spatial distribution of positive and negative (red and blue colours respectively) lobes indicates that the most energetic modes can be classified in two categories; those that are symmetric around the jet axis and those that are anti-symmetric around the jet axis. The first indicate longitudinally developing features around the jet, such as Kelvin Helmholtz instabilities, while the latter indicate oscillatory behaviour, such as flapping.

The anti-symmetric modes appear to be more clearly captured by shadowgraphy. For example, **Figure 14** shows the contours of the first five POD modes for flow condition Case 1 of Table 1; mode 2 clearly shows the flapping motion of the liquid jet close to breakup, while modes 3 and 4 show the oscillation of the straight portion of the liquid jet around its centreline. The flapping motion of the liquid jet close to the breakup point is also captured well from the shadowgraphic imaging for other flow conditions, as for example modes 2-5 of **Figure 15** for flow condition Case 6 of Table 1. It is possible that the inclination of the POD processing of the shadowgraphic images to capture modes that are related to flapping as the most energetic, is due to the imaging of the dispersed droplets downstream the breakup region, which follow the flapping motion of the liquid core. The POD processing of the optical connectivity fluorescent intensity images shows that the flapping motion of the liquid jet is captured well in mode 2 for all the considered flow conditions, as evidenced in **Figure 14** and **Figure 15** by the comparison of the shape of the contours of POD mode 2 for the two methods. However axi-symmetric modes are captured earlier with optical connectivity than shadowgraphy, as for example in modes 3 and 5, which suggest that when the primary atomization region is examined without the presence of dispersed droplets, these modes are equally important.

While POD processing of the obtained images from both techniques identifies a multitude of modes, as shown in **Figure 12**, the overall contribution of the individual modes to the total image intensity fluctuations is small. For example, even the flapping mode 2 of **Figure 14**, while clearly distinguishable and with clear physical significance to the atomization process, accounts only for about 6% of the total amount of image intensity variability for both imaging techniques. As the number of modes that are needed to describe the atomization process is large and their spatial characteristics span from the size of the liquid jet length to the resolution of the imaging system, at this stage no clear interpretation of their significance can be deduced. Further investigation is required to examine the combined contribution of the POD modes to the atomization process.

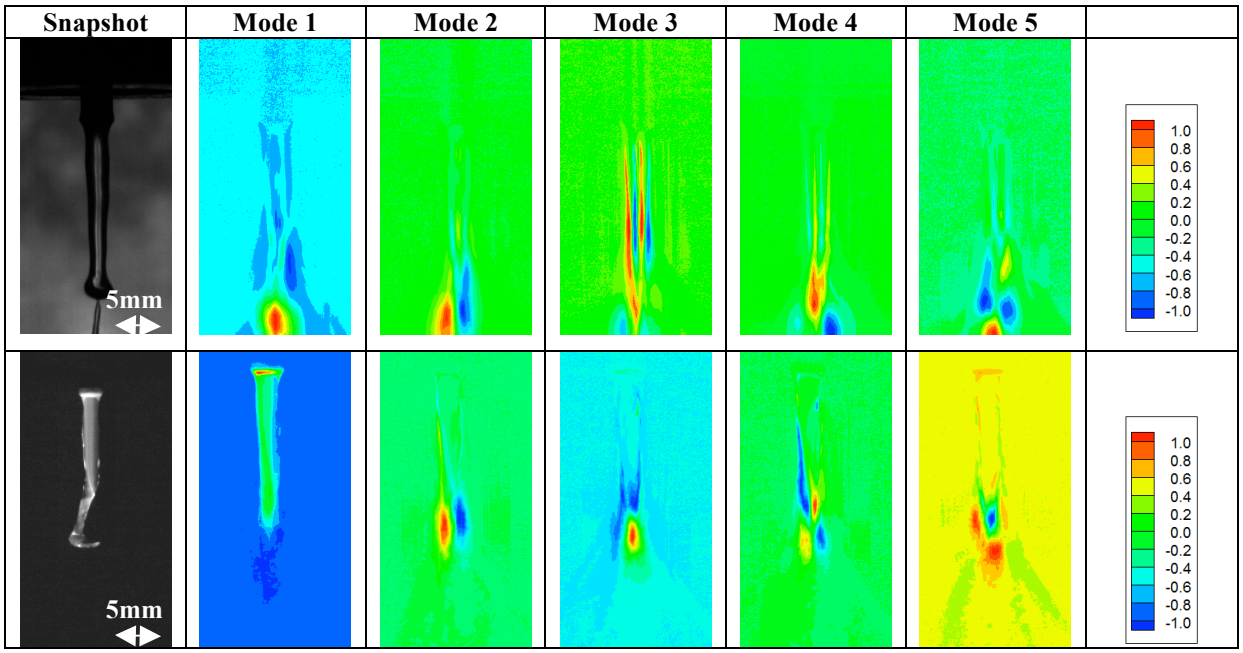

Figure 14. Normalised contours of the first 5 POD modes from high-speed shadowgraphy and optical connectivity imaging for the flow conditions of Case 1 of Table 1.

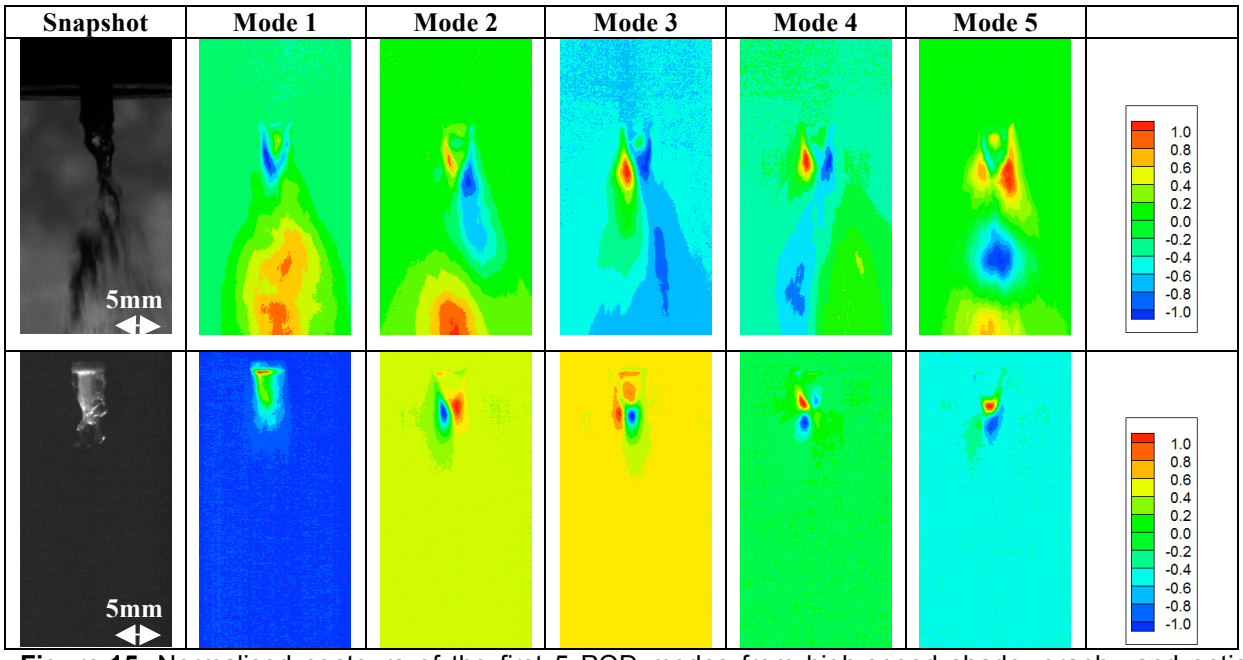

Figure 15. Normalised contours of the first 5 POD modes from high-speed shadowgraphy and optical connectivity imaging for the flow conditions of Case 6 of Table 1.

In summary, the processing of the acquired images using POD analysis revealed a multiplicity of modes with spatial characteristics that range in scale of the liquid jet length down to the resolution of the imaging system. The photographic approach considers the full spray structure,

including the continuous liquid jet core and the products of atomization, while the optical connectivity method probed only the continuous liquid jet core. Modes with broad spatial features were found to contain more information on the variation of the intensity of the imaged jet than the modes that capture finer features. While many modes are clearly identifiable, in none of the investigated flow conditions did they account for a portion of the intensity variability of the images that would imply dominance of a single or combination of a few modes. However, the first 10 POD modes contributed between 30 and 60% of the total intensity fluctuations identified on the images. This suggests that for the flow conditions examined, the atomization process is complex and cannot be described as a simple process, but needs to be examined as a complex combination of overlapping effects. Further investigation is required to examine the combined effect of the individual modes to the atomization process.

3.2 Theoretical study of light propagation in inclined liquid jets

This study is evaluating the application of the optical connectivity technique in inclined liquid jets, as occurring when liquid jets are exposed in a cross-flow of air. The geometrical optics approach that was explained in Section 2 was applied to a variety of liquid columns over a range of conditions indicated by Table 2. D is the width of the liquid column at the base and the refractive index of the liquid is 1.33 (water) for all examined cases.

The propagation of laser light rays in an inclined liquid column with a wavy surface is demonstrated at **Figure 16**. As the rays propagate along the liquid column, the initial intensity of each beam I_0 is reduced due to refraction of the light at the liquid interface, which is lost to the surroundings, and absorption from the dye present in the liquid, which is re-emitted as fluorescence. The intensity losses at the liquid interface occur when the rays impinge the inner surface of the liquid at angles greater than the angle for total internal reflection of Equation (6).

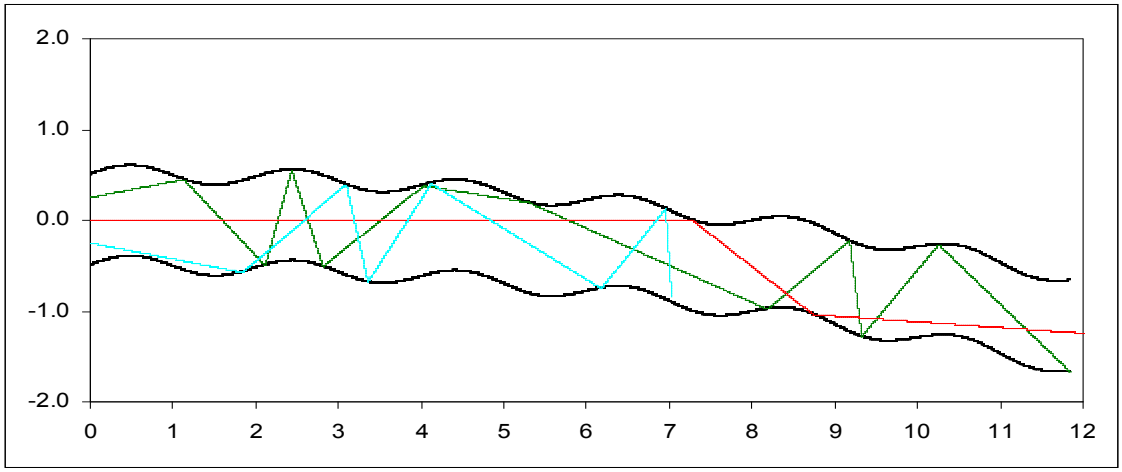

Figure 16. Example of propagation of light rays within an inclined liquid column as determined by geometrical optics calculations. The vertical axis shows the width of the liquid column around the axis normalized by the width of the column. The horizontal axis shows the distance along the direction of motion of the liquid column, normalized by the width of the liquid column (Example for γ=0.00008m^{-1}, n_1=1.33, ω=20°).

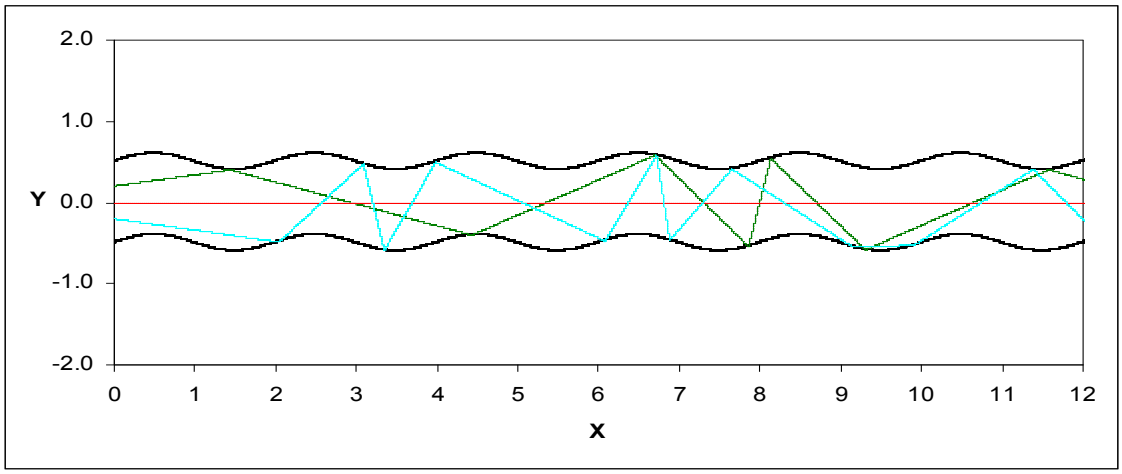

Figure 17. Example of propagation of light rays within a straight liquid column, as determined by geometrical optics calculations. The liquid column is the same as that of Figure 16, but without inclination. The vertical axis shows the width of the liquid column around the axis normalized by the width of the column. The horizontal axis shows the distance along the direction of motion of the liquid column, normalized by the width of the liquid column (Example for γ=0.00008m^{-1}, n_1=1.33, ω=20°).

Figure 17 shows the propagation of the laser light rays within a liquid column without inclination. The amplitude and frequency of the surface wave and the width of the liquid column are the same as those of the inclined column of **Figure 16**. An observation of the propagation of the rays indicates that all the rays interact with the liquid jet interface closer to the nozzle exit of the inclined liquid column. An example of this is the 'red' ray of **Figures 16** and **17**, which is propagating along the centre of the liquid column. This ray is continuing along a straight line in the straight liquid column and does not interact with the liquid surface, as expected. The same ray is internally reflected on the inclined liquid jet interface. Therefore, it is expected that the intensity losses of laser light due to refraction at the liquid interface will be higher for the inclined liquid column. However, this may be reduced since the majority of losses of the laser light are due to absorption by the fluorescent dye within the liquid. Results from the parameter range of Table 2 are presented below.

The fluorescent intensity profiles along the X-axis are presented for all the combinations of geometrical conditions considered here in **Figure 18** through **Figure 23.** In each figure, groups of fluorescent intensity profiles for the liquid columns with the same geometrical characteristics apart of the degree of inclination are presented. In this way, it is easy to isolate the effect of jet inclination on the fluorescent intensity along the liquid axis. In **Figure** , the effects for liquid columns with fine surface features (wavelength L/D=0.5 and amplitude G/D=0.1) are demonstrated. In this case, there is no beam divergence. For the straight column, the fluorescent intensity profile is flat, which demonstrates that there are no losses along the column length except very close to the base where some of the peripheral rays hit the troughs of surface waves at angles below the critical angle for total internal reflection. The observations change when the column becomes inclined and more rays hit the surface at high angles resulting in refractive losses of the ray intensity, which, in turn, result to losses in the intensity of fluorescence, which maintains a high intensity for a good length along the column (5-15 column base widths depending on case) until there is a sharp decrease. The column length, where the fluorescent intensity remains high, decreases for increasingly inclined liquid columns.

When divergence of the rays is introduced, there is a drastic change in the evolution of the fluorescent profiles, which collapse to a single trend regardless of the amount of inclination, as seen in **Figure 19**. The drop of the fluorescent intensity at a certain distance from the nozzle is not observed here but instead an exponential decrease is seen. This can be explained by considering the angle of incidence on the jet surface. In the case of the parallel rays when the jet becomes inclined, the angle of incidence of the rays on the jet surface is similar for most of the rays. As such, when the first of the rays hit the surface at an angle greater than that of total internal reflection and there are refractive losses of intensity, most of the other rays hit the surface at a similar angle within a short distance. As a result, the fluorescent intensity decreases sharply within a narrow column length. In contrast, when the rays are divergent, the increased randomness of the angle at which rays interact with the surface results to some of them being refracted at a short distance from the nozzle, but there are enough of them reflecting back into the column to propagate along its length. Consequently, the decrease of the fluorescent intensity follows an exponential decay and the fluorescent intensity after 10 column base widths is maintained to 20% of the intensity at the base of the column.

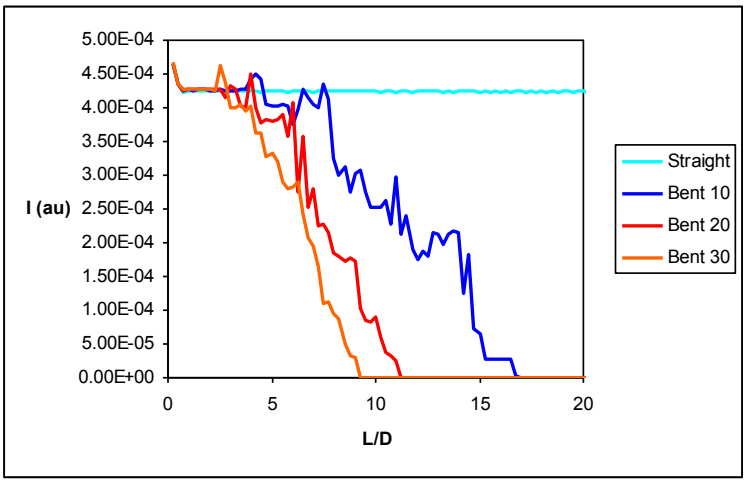

Figure 18. Fluorescent intensity profiles with distance from the liquid column base for amplitude of surface wave of G/D=0.1, wavelength of L/D=0.5 and no laser beam divergence.

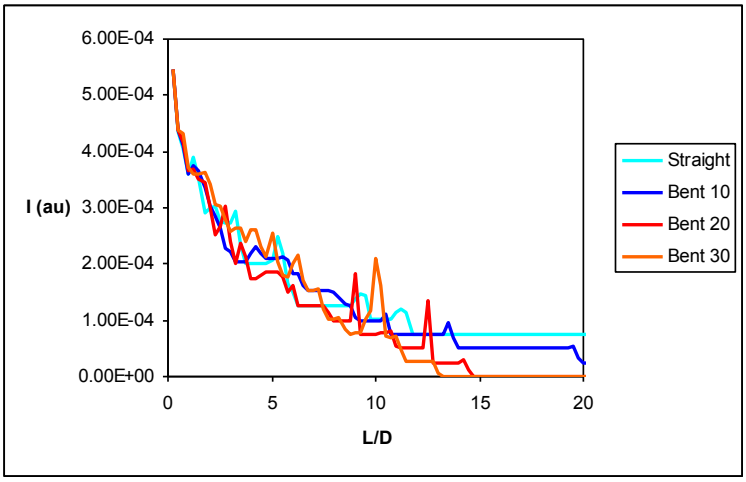

Figure 19. Fluorescent intensity profiles with distance from the liquid column base for amplitude of surface wave of G/D=0.1, wavelength of L/D=0.5 and 10° laser beam divergence.

When the features of the surface waves are less intense (wavelength L/D=1.0, amplitude G/D=0.1) and the jet surface becomes smoother, there is a small increase in the length for which the fluorescent intensity is high. However, the change is minor and generally the fluorescent intensity profiles of both the non-divergent beam profiles of **Figure** and the divergent beam of **Figure** evolve in the same fashion as the profiles of **Figure** and **Figure** respectively.

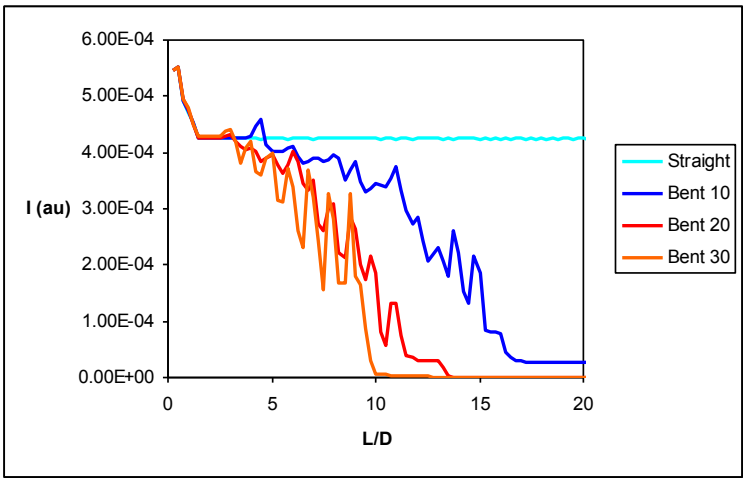

Figure 20. Fluorescent intensity profiles with distance from the liquid column base for amplitude of surface wave of G/D=0.1, wavelength of L/D=1.0 and no laser beam divergence.

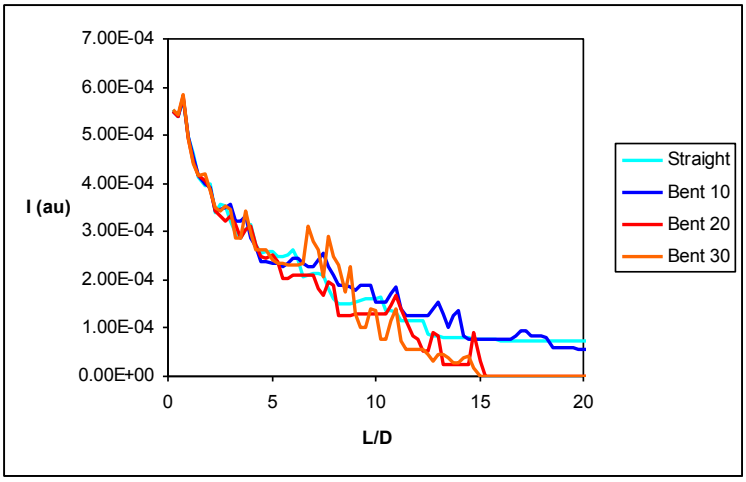

Figure 21. Fluorescent intensity profiles with distance from the liquid column base for amplitude of surface wave of G/D=0.1, wavelength of L/D=1.0 and 10° laser beam divergence.

Finally, the fluorescent intensity profiles of the smoother columns (G/D=0.1, L/D=2.0) are presented in **Figure** for the case of the non-diverging beam and in **Figure** for the diverging beam. In Figure 22, it is seen that the expectedly flat fluorescent intensity profile for the straight column shows a step decrease at a certain distance. This is because some of the rays that were reflected close to the base of the column are not interacting with the column surface at a high angle and are consequently refracted outside the column resulting to a step change in the fluorescent intensity profile for that case. The evolution of the rest of the fluorescent intensity profiles is as it would be expected from the previously discussed cases with an extension of the

region of high intensity. For the case of the most inclined liquid column, a high peak of the fluorescent intensity can be clearly observed at a distance of about 15 column base widths. This is a problem generated by the resolution of the grid that is used for the numerical simulation. Due to the finite resolution of the grid that was used to calculate the ray path, one of the beams was trapped in this region oscillating between the top and bottom boundaries for a great number of times. Consequently, the fluorescent intensity of this part of the column is artificially high while the rest of the column length is unaffected. In the case of the divergent beam, there is an extension of the length of the column where the fluorescent intensity drops to around 20% of the intensity at the column base, which is now found at around 10 base column diameters. The smoothing of the column surface has a positive effect on the propagation of the laser beam within the column as more beams get reflected back into the column when they reach the surface.

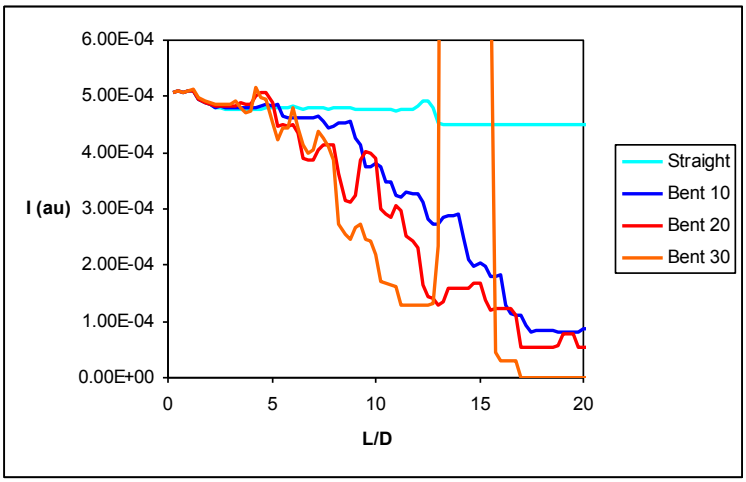

Figure 22. Fluorescent intensity profiles with distance from the liquid column base for amplitude of surface wave of G/D=0.1, wavelength of L/D=2.0 and no laser beam divergence.

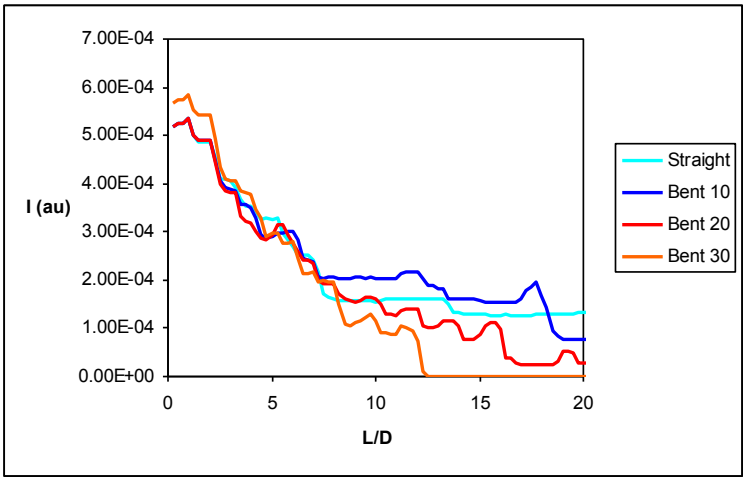

Figure 23. Fluorescent intensity profiles with distance from the liquid column base for amplitude of surface wave of G/D=0.1, wavelength of L/D=2.0 and 10° laser beam divergence.

In summary, the geometrical optics calculations for the optical connectivity technique showed that the intensity of the fluorescent intensity along the length of the liquid column is reduced

progressively and the rate of the reduction depends on amplitude and wavelength of surface wave. It is possible that, when the continuous length of the liquid column is long, the fluorescent intensity might become too low to be detected along the full length of the continuous liquid column. This has been demonstrated experimentally [1]. A comparison between straight and inclined liquid columns suggested that the fluorescent intensity is reduced faster for the inclined column, although there are cases where this observation may not occur depending on the smoothness of the surface waves. In general, it is recommended to use the optical connectivity technique for cases of good atomization, which lead to short breakup lengths.

3.3 Design of experimental facility for the study of a liquid jet in a cross stream of swirling air flow

This section describes the design of an experimental facility for the study of liquid jets exposed to swirling air flow streams. A summary of the literature is presented first to establish that there is no available study for such geometry, which is important to many aero engine and gas turbine applications. An evaluation of the design criteria follows and the section ends with the reporting of the design of the experimental facility.

3.3.1 Literature review

The atomization of liquid jets in a crossflow air stream is relevant to many aero engines, gas turbine combustors and combustors for hypersonic vehicles. The atomization of a liquid jet in a cross-stream of air is characterized by two main regions:

(i) Primary breakup of liquid jet.
In this region, the liquid jet penetrates into the air cross stream and becomes inclined in the direction of the air flow, while its shape changes. During this process, ligaments are formed from the liquid jet surface, which eventually become droplets.

(ii) The spray region.
In this region, some surviving ligaments break up further and form stable droplets, which, together with the other existing droplets from the upstream region, determine the downstream spray characteristics.

In all the available studies, which are reviewed below, a planar air flow geometry has been used. As a consequence, the air stream is mainly flowing in one direction and it is not possible to introduce additional velocity components to the air stream. However, in atomizers of aero-engines and gas turbine combustors, the liquid jet is injected in an axisymmetric annular flow of air, which tends to have a swirling component. Therefore, the emphasis here is to design an injector of a liquid jet in a cross stream of air, which can also have variable levels of swirling component, and provides appropriate optical access for studies of the development of the liquid jet. However, information available from the literature must be considered in order to obtain some guidelines for the dimensions of the new atomizer design.

Some earlier studies, which also provide a review, are those of Less and Schertz [26] and Wu *et al.* [27]. These studies establish that the momentum flux ratio of the liquid jet to the air cross-flow of Equ. (13) is a relevant parameter that characterizes the behaviour of the liquid jet.

$$MFR = \frac{\rho_L U_L^2}{\rho_G U_G^2} \tag{13}$$

Increase of MFR leads to increase of jet penetration, which delays the breakup of the liquid column into large fragments and enhances the stripping-off of fine droplets from the liquid jet surface. However, both breakup mechanism of the liquid jet are present at variable degree at the same time depending on the value of the MFR. Some additional relevant parameters for the characterization of the behaviour of the liquid jet are:

Weber number, based on the gas velocity $$We_G = \frac{\rho_G U_G^2 D_L}{\sigma} \tag{14}$$

Weber number, based on the liquid velocity $$We_L = \frac{\rho_L U_L^2 D_L}{\sigma} \tag{15}$$

Reynolds number of liquid jet $$\mathrm{Re}_L = \frac{U_L D_L}{\nu_L} \tag{16}$$

All these parameters will be used in the atomizer design analysis below.

The available studies in the literature and their main findings are summarized below. Low-speed wind tunnel experiments were conducted by Aavani *et al.* [28] to examine the effect of jet exit behaviour on the near-field characteristics of jets in cross-flow. Ghosh and Hunt [29] focused on the interaction between an external air cross-flow and the spray jet. Arienti and Soteriou [30] analysed the mechanism of primary break of the liquid jet in a cross flow using proper orthogonal decomposition to identify the liquid flow structures that are responsible for the breakup. Studies of bag-type breakup of non-turbulent liquid jets in a crossflow were carried out by Ng *et al.* [31] and results showed that the waves on the surface of the liquid column within the bag breakup regime could be explained from Rayleigh – Taylor instability. Rachner *et al.* [32] modeled the penetration and atomization of a plain jet of kerosene fuel in air crossflow and could identify the two main breakup mechanisms, which are known as the surface breakup and the liquid column breakup. Sedarsky *et al.* [33] used Particle Image Velocimetry, high-speed shadowgraphy and ballistic imaging to observe the breakup of a liquid jet in a crossflow of air under a variety of conditions. The experimental configuration consisted of four interchangeable nozzle tips of different exit diameter. Bai *et al.* [34] presented an experimental study on turbulent mixing of spray droplets for different injection angles. The optimum mixing effect can be achieved for an angle of 60° and the most stable of the flow field structure and the greatest sustained distance of the counter rotating-vortex pair can be found when the angle is 90°. A numerical study to model the liquid jet breakup in high speed crossflow was attempted by Balasubramanyam and Chen [35] using an improved drag coefficient correlation, which would capture the spray phenomenon more accurately specifically for application to high speed flow. Phase Doppler Anemometry measurements of the two-phase flow structure and droplet dispersion were performed by Fan *et al.* [36] and confirmed the complex interaction between the liquid jet and crossflow and suggested that the flow field depends primarily on the jet-to-crossflow velocity ratio. Hale *et al.* [37] investigated surface heat transfer in a row of short length nozzles of jets in crossflow and found that horseshoe vortices are weak structures that dissipate as their legs wrap around the jet. The turbulence characteristics of a jet in crossflow were examined by Barata *et al.* [38] using Laser Doppler Anemometry. Their aim was to investigate the effect of the velocity ratio between the jet and the crossflow. The conclusion of Hale *et al.* [37] that the flow appears as a vortex wrapped around the jet with its size increasing with the velocity ratio was established by the measurements of [38]. Shedd *et al.* [39] used high-speed

digital imaging to visualize the formation of the liquid film formed on the surface of a channel due to the injection of a liquid jet in crossflow and it was observed that film thickness increased with increasing momentum flux ratio.

The spray structure in the near-injector region of an aerated liquid jet in subsonic crossflow was investigated by Lee *et al.* [40]. Six holograms were recorded and the droplet velocities in the streamwise and the crossflow direction could be measured by observing the displacements of the center of each droplet between the double pulses. Osta *et al.* [41] examined the effect of nozzle length/diameter ratio on the breakup using nozzles with different length-to-diameter ratios. The liquid jets were observed using single- and double-pulsed shadowgraphy and holography. The main conclusion was that the breakup length decreases with increasing length-to-diameter ratio. Kihm *et al.* [42] visualized both under expanded sonic gas jets from a converging nozzle (SN-type) and over expanded supersonic gas jets from a converging-diverging nozzle (CD-type). They found out that the SN-type develops wider spray, which lowers the probability of droplet coalescence and generates finer sprays. Lee *et al.* [43] used pulsed shadowgraph and holography for turbulent round liquid jets injected normal to air crossflow in a shock tube. They used two different nozzles with different injector passages and smooth rounded entrances with length-to-diameter ratios larger than 100 to ensure fully developed turbulent pipe flow at the jet exit for large Re. Sallam *et al.* [44] investigated the breakup at the surface of turbulent round liquid jets in still gases using single- and double- pulse shadowgraphy and holography for nozzle with smooth rounded entrances with length-to-diameter ratio larger than 100 to ensure fully developed turbulent pipe flow at the jet exit for large Reynolds numbers. Three modes of liquid column breakup were observed: (a) a weakly turbulent Rayleigh-like breakup mode at small jet exit We and Re, (b) a turbulent breakup mode at moderate jet exit We and Re and (c) an aerodynamic bag/shear breakup mode at large jet exit We. Finally, Sallam *et al.* [45], for nonturbulent liquid jets, used shadowgraphy to demonstrate three regimes of primary breakup: bag breakup, multimode (or bag/shear) breakup and shear breakup. It is worth noting that round supercavitating nozzles were used that had sharp edged inlets and exits, with length-to-diameter ratios smaller than 3. This arrangement yields uniform non-turbulent round liquid jets in opposition to findings of Reference [44]. Finally, several studies were performed of liquid jets injected in supersonic cross-streams of air [46-51]. Although effects of the supersonic streams are present, the overall structure and development of the liquid jets remain qualitatively the same.

The above review confirms that all the studies of liquid jets injected in cross-stream of air have been performed in geometries that could not consider a swirling component of air stream velocity. As a consequence, an experimental facility was designed which allows the study of liquid jets exposed to a swirling air stream. This is relevant to atomizers that are used in aero-engines and gas turbine combustors.

3.3.2 Considerations for atomizer design

The new atomizer should inject a liquid jet in an air cross-stream, which could have a swirling velocity component. Also, this atomizer should have the capability to operate without swirling air stream and at conditions already studied in planar geometries of jets in crossflows. The first step was to review the literature and determine which factors are important and can influence the operation of the atomizer, which was performed above and established the relevant non-dimensional quantities.

The next step was to perform some calculations and find out how the atomizer will behave for

different air flow conditions without swirl. An important aspect of the design was to establish the trajectory of the liquid jet in a cross-stream of air, since this will determine the width of the air stream of the atomizer. This is a requirement in order to avoid the impingement of the liquid jet on the external wall of the air stream. We used the empirical correlation reported by Lee *et al.* [43] to establish the trajectory of the liquid jet. In addition, the momentum flux ratio, the gas crossflow and the liquid Weber numbers and the liquid jet Reynolds number were calculated for different dimensions and flow conditions of the atomizer. These factors decide the atomization characteristics, the structure of the spray and the distance from the injection location, where the breakup of the liquid core occurs.

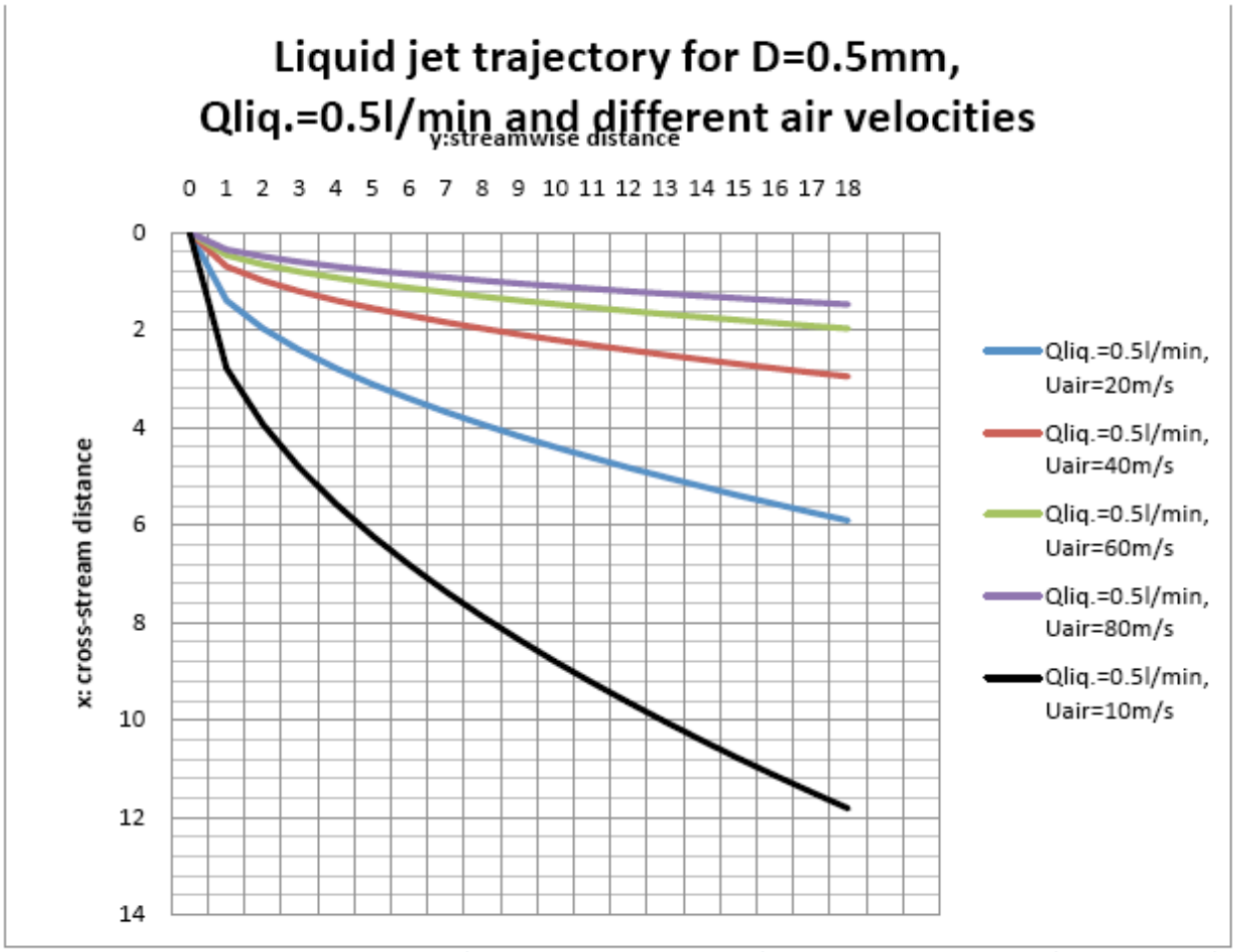

	Crossflow We	Liquid We	Momentum ratios	Jet Re
	8.276566757	122579.3066	14810.40512	18928.07002
	33.10626703	122579.3066	3702.601279	18928.07002
	132.4250681	122579.3066	925.6503197	18928.07002
	297.9564033	122579.3066	411.4001421	18928.07002
	529.7002725	122579.3066	231.4125799	18928.07002

Figure 24(a). Liquid jet trajectory for diameter of liquid jet exit D=0.5mm, liquid flow rate of 0.5l/min and different air velocities

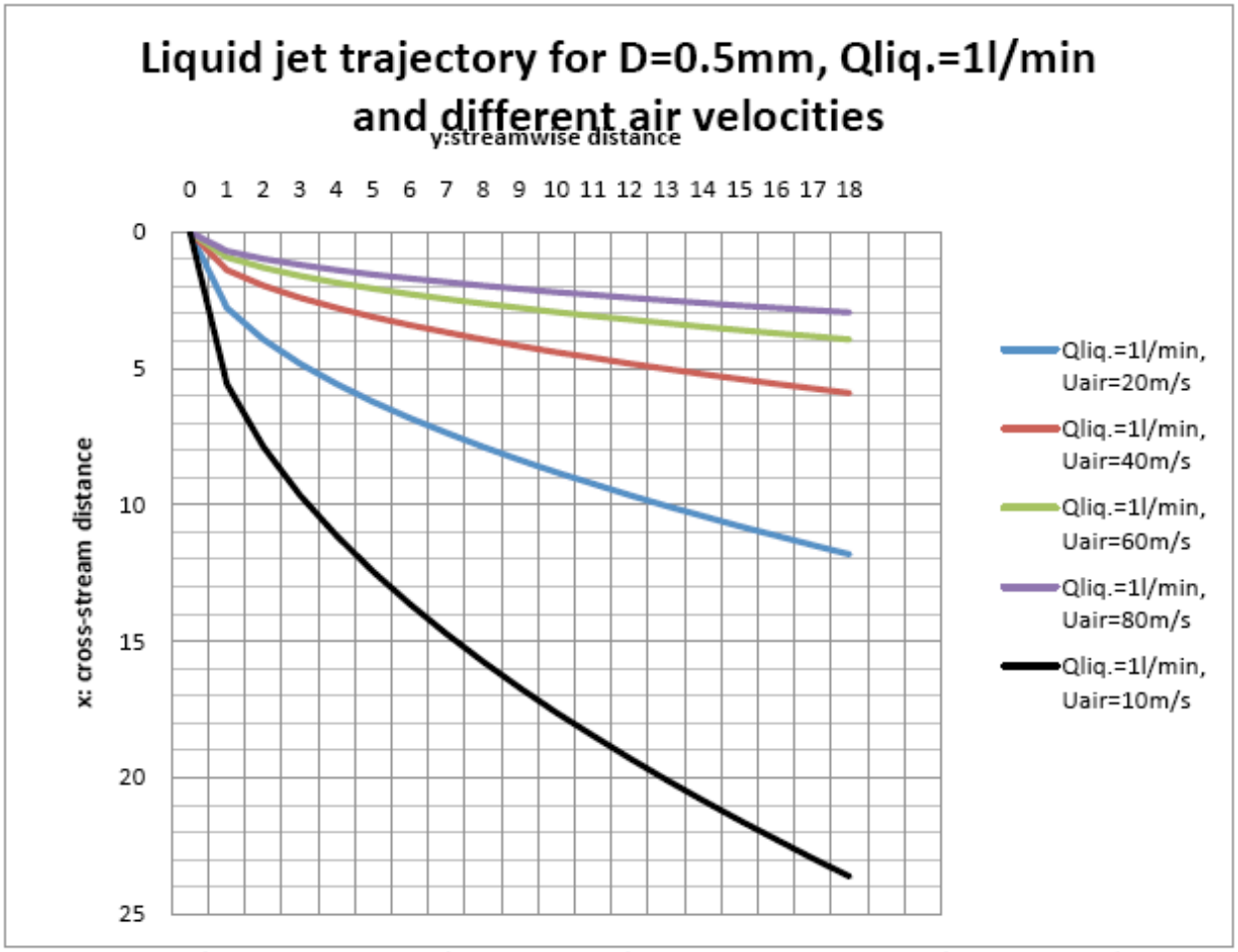

	Crossflow We	Liquid We	Momentum ratios	Jet Re
	8.276566757	490317.2266	59241.62046	37856.14004
	33.10626703	490317.2266	14810.40512	37856.14004
	132.4250681	490317.2266	3702.601279	37856.14004
	297.9564033	490317.2266	1645.600568	37856.14004
	529.7002725	490317.2266	925.6503197	37856.14004

Figure 24(b). Liquid jet trajectory for diameter of liquid jet exit D=0.5mm, liquid flow rate of 1 l/min and different air velocities

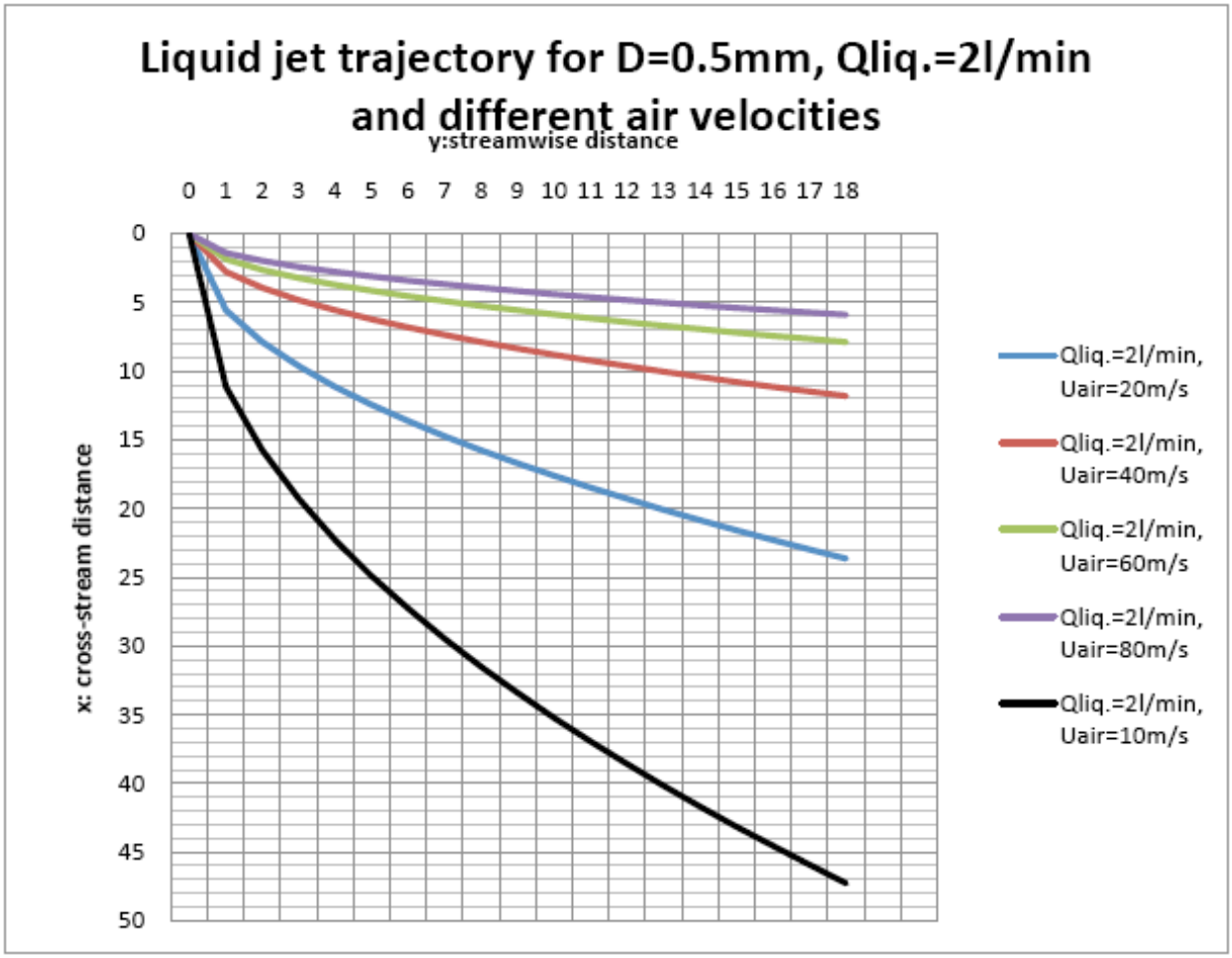

	Crossflow We	Liquid We	Momentum ratios	Jet Re
	8.276566757	1961268.906	236966.4818	75712.28007
	33.10626703	1961268.906	59241.62046	75712.28007
	132.4250681	1961268.906	14810.40512	75712.28007
	297.9564033	1961268.906	6582.402273	75712.28007
	529.7002725	1961268.906	3702.601279	75712.28007

Figure 24(c). Liquid jet trajectory for diameter of liquid jet exit D=0.5mm, liquid flow rate of 2 l/min and different air velocities

Therefore, **Figures 24 and 25** present the predictions of the trajectory of the liquid jet based on the correlation of Lee *et al.* [43]. The vertical axis is the cross-stream distance and the horizontal is the streamwise distance, presented in dimensional form with units of mm. These calculations were performed for two liquid jet exit diameters, namely 0.5mm (**Figure 24(a), (b)** and **(c)**) and 1mm (**Figure 25(a), (b)** and **(c)**) and for different liquid flowrates and cross-stream air velocities. Underneath each figure, a small table is presented, which includes the corresponding momentum flux ratio, the gas crossflow and liquid Weber numbers and the liquid jet Reynolds number for all the examined conditions. These parameters were defined in Equations (13), (14), (15) and (16).

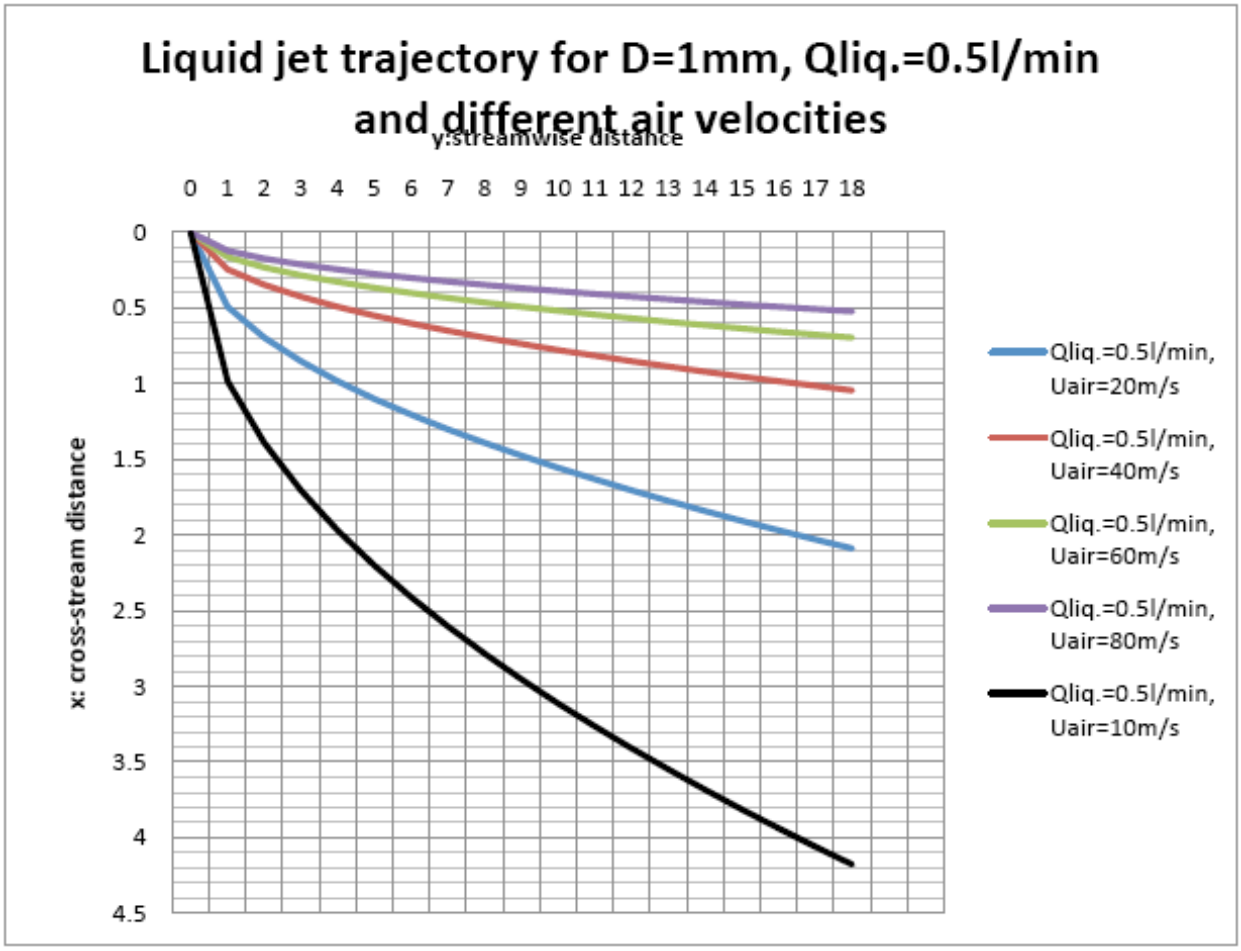

	Crossflow We	Liquid We	Momentum ratios	Jet Re
	16.55313351	15322.41333	925.6503197	9464.035009
	66.21253406	15322.41333	231.4125799	9464.035009
	264.8501362	15322.41333	57.85314498	9464.035009
	595.9128065	15322.41333	25.71250888	9464.035009
	1059.400545	15322.41333	14.46328625	9464.035009

Figure 25(a). Liquid jet trajectory for diameter of liquid jet exit D=1mm, liquid flow rate of 0.5 l/min and different air velocities

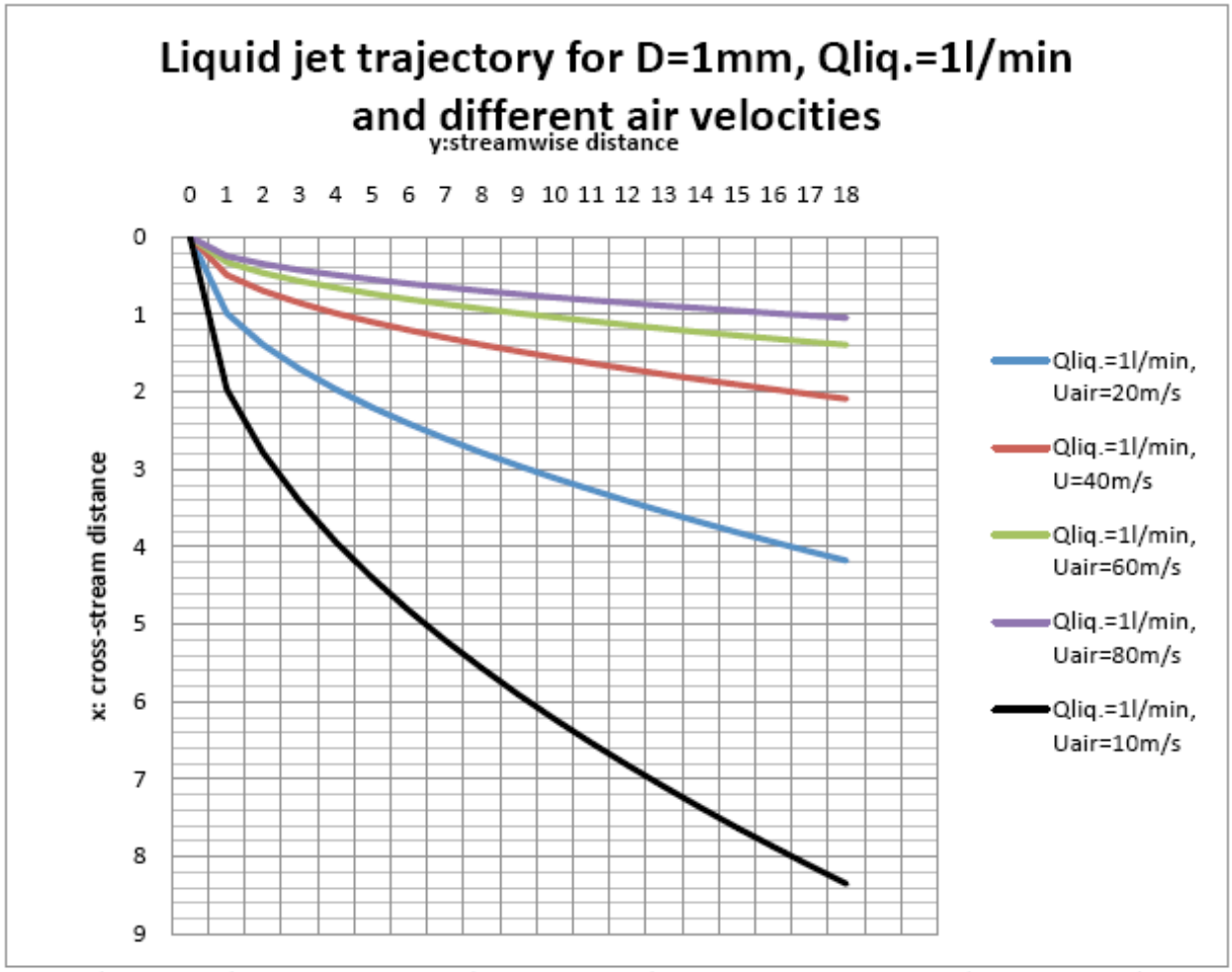

	Crossflow We	Liquid We	Momentum ratios	Jet Re
	16.55313351	61289.65332	3702.601279	18928.07002
	66.21253406	61289.65332	925.6503197	18928.07002
	264.8501362	61289.65332	231.4125799	18928.07002
	595.9128065	61289.65332	102.8500355	18928.07002
	1059.400545	61289.65332	57.85314498	18928.07002

Figure 25(b). Liquid jet trajectory for diameter of liquid jet exit D=1mm, liquid flow rate of 1 l/min and different air velocities

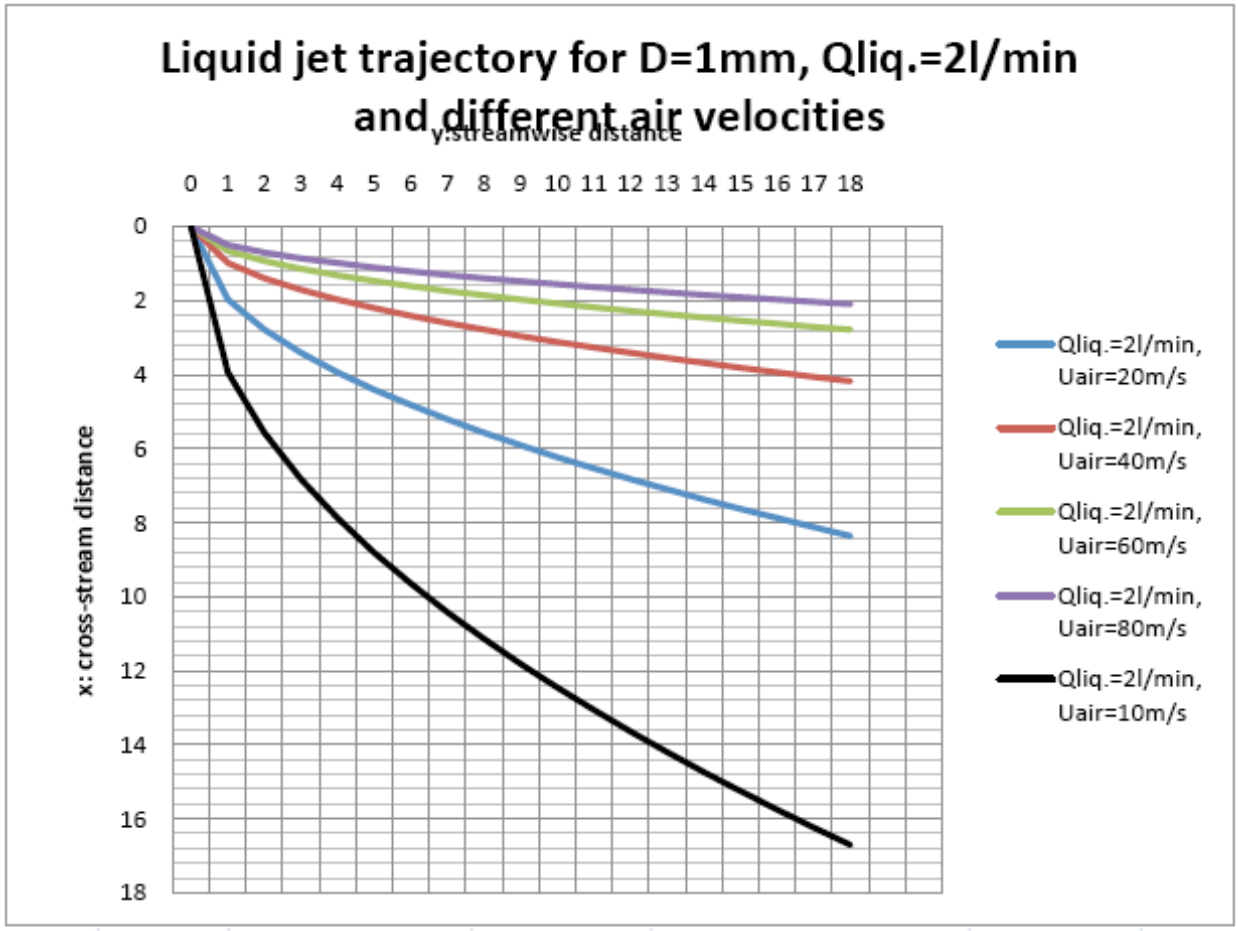

	Crossflow We	Liquid We	Momentum ratios	Jet Re
	16.55313351	245158.6133	14810.40512	37856.14004
	66.21253406	245158.6133	3702.601279	37856.14004
	264.8501362	245158.6133	925.6503197	37856.14004
	595.9128065	245158.6133	411.4001421	37856.14004
	1059.400545	245158.6133	231.4125799	37856.14004

Figure 25(c). Liquid jet trajectory for diameter of liquid jet exit D=1mm, liquid flow rate of 2 l/min and different air velocities

3.3.3 Atomizer Design

Figure 26 presents the atomizer design. The air stream has to be axisymmetric, and not planar as found in the literature, in order to be able to introduce swirl and control the relative magnitude of axial and swirling component of air velocity. The swirling air flow component will be generated by introducing the air flow in the upstream pipe through tangential air inlets.

The above analysis provided estimates of the effects of the dimensions of the liquid jet exit and flow conditions on the diameter of the crossflow air stream. The most suitable liquid jet exit diameter is 1mm, according to the calculations presented above, because the diameter of the air stream can remain smaller for a wider range of flow conditions without the trajectory of the

liquid jet hitting at the outer wall of the airstream. The selected width of the air stream is 15mm. However, the section of the atomizer exit can be exchanged by connecting a new converging section at the flange shown in **Figure 26**. This flexibility is important in order to allow for differences of the behaviour of the liquid jet from what is expected in the literature, especially when swirl is introduced to the air stream.

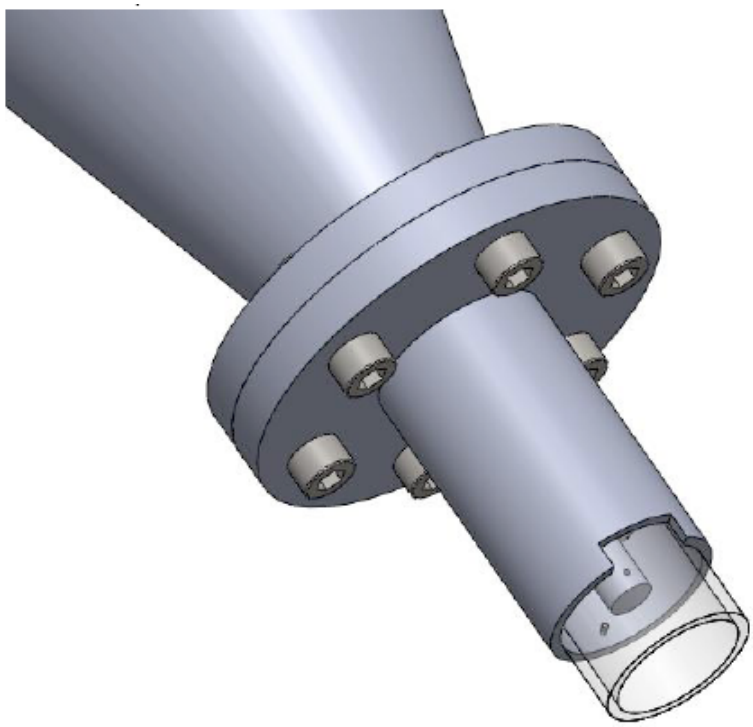

Figure 26. The atomizer design of a liquid jet exposed to a crossflow of air, which can have a swirling velocity component.

An important detail is shown in **Figure 26**. One hole is present at the outer wall of the air stream and at the opposite side of the liquid jet injection nozzle. A second hole, which cannot be observed at the current view of **Figure 26**, exists on the surface of the liquid tube and at the opposite side of the injection nozzle. These two holes have the same diameter as the injection nozzle (1 mm) and are required in order to allow the laser beam to be introduced in the liquid jet. This is an important requirement for the application of the optical connectivity technique to the measurement of the intact length of the liquid jet. These two holes are sealed by appropriate quartz windows. **Figure 27** shows a close up of the liquid jet nozzle exit on the liquid supply tube, which will have rounded edges in order to avoid liquid cavitation due to flow separation through the injection nozzle.

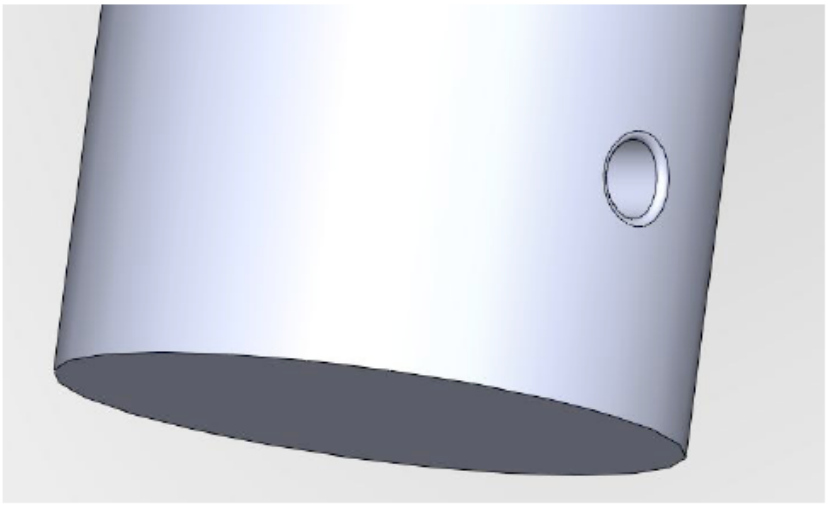

Figure 27. The inner tube of the atomizer, which supplies the liquid to the round-edged nozzle with diameter of 1mm.

In **Figure 28,** the quartz tube that is added at the nozzle exit is presented. The quartz tube, which is 15mm long, is added to confine the air flow and ensure that the flow remains the same while it interacts with the liquid jet. The length of this tube was selected on the basis of the expected longest breakup length for the selected flow conditions of **Figures 24 and 25**. The breakup of the liquid column should be completed inside the quartz tube before the air stream begins to expand. However, this estimate is based on liquid jets exposed to non-swirling air streams. It is clear that the results will change when swirl is introduced but the expectation is that the selected distance will be adequate for liquid jets in swirling air cross stream.

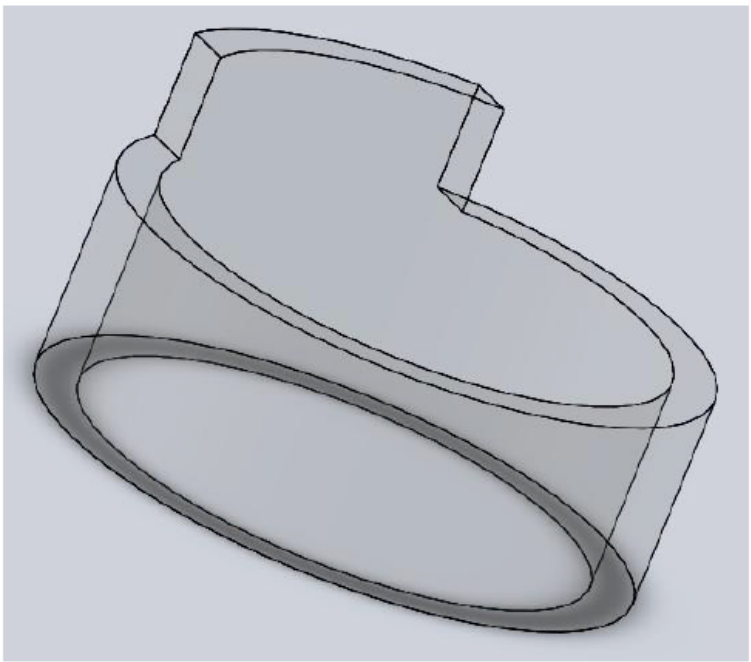

Figure 28. The quartz tube extends the length of the nozzle downstream of the liquid jet injection location in order to maintain the confinement of the air stream and avoid its expansion.

4. Summary

The research during the second year of the project contributed to three areas. (a) The application of time-resolved optical connectivity in a liquid jet of a coaxial airblast atomizer and the assessment of relevant physics for atomization through Proper Orthogonal Decomposition (POD) analysis of optical connectivity and shadowgraphy images. (b) The theoretical assessment of the performance of the optical connectivity technique for measurements in inclined jets, like those exposed to cross-flows of air. (c) Design of a new atomizer for studies of liquid jets exposed to cross-flows of swirling air streams. The findings are summarized below.

(a) The atomization of a liquid jet by a coaxial flow of air was investigated using high speed shadowgraphy and optical connectivity imaging of the liquid jet core. The shadowgraphic approach considered the full spray structure, including the continuous liquid jet core and the products of atomization, while the optical connectivity method probed only the continuous liquid jet core. The processing of the acquired images using POD revealed a multiplicity of modes with spatial characteristics that range in scale of the liquid jet length down to the resolution of the imaging system. Modes with broad spatial features were found to contain more information on the variation of the intensity of the imaged jet than the modes that capture finer features. While many modes are clearly identifiable, in none of the investigated flow conditions did they account for a portion of the intensity variability of the images that would imply dominance of a single or combination of a few modes. However, the first 10 POD modes contributed between 30 and 60% of the total intensity fluctuations identified on the images. This suggests that for the flow conditions examined, the atomization process is complex and cannot be described as a simple process, but needs to be examined as a complex combination of overlapping effects. Further investigation is required to examine the combined effect of the individual modes to the atomization process.

(b) The assessment of the optical connectivity technique for measurement of breakup length of different types of liquid jets continued by considering the effect of inclined liquid jets that occur when they are exposed to a cross-stream of air. The previously developed ray tracing software software was extended for applications to light propagation in inclined liquid columns and it was used for the evaluation of the fluorescent intensity distribution along the length of the column.

The numerical evaluation of the technique identified the following:

(i) For non-diverging beams, the fluorescent intensity profiles maintain high intensity up to a certain distance along the column beyond which the intensity decreases quickly. This distance depends on the degree of inclination of the column, but the fluorescent intensity was maintained over 20% of intensity at the entrance for at least 5 column base widths in all cases.

(ii) For diverging beams, the fluorescent intensity profiles follow an exponential trend and are largely independent of the rate of inclination of the liquid column.

(iii) The characteristics of the waves on the surface of the liquid column were found to have an effect on the degree of propagation of fluorescent intensity along the column length with longer waves enabling the laser beam to remain significant further along the column.

(c) An atomizer design for injection of a liquid jet in a cross-stream of air, which can be swirling or non-swirling, was achieved as follows:

(i) An extensive literature review was performed of atomization studies of liquid jets in a cross-stream of air, which established that no information is available on the breakup of liquid jets that are exposed to a swirling air stream.
(ii) The design parameters were established and calculations were performed using available correlations from the literature for liquid jets in non-swirling air cross-streams in order to establish the trajectory of the liquid jet for different liquid jet diameters, liquid and gas flowrates. In this way, the dimensions of the liquid jet nozzle and the width of the annular air stream in the new atomizer were evaluated.
(iii) An axisymmetric design of the atomizer was established, which allows the introduction of variable level of swirl in the cross-stream, which interacts with the liquid jet. The atomizer has appropriate optical access in order to introduce the laser light within the liquid jet through the injection nozzle. Also, appropriate optical access is provided in order to observe the development and breakup of the liquid jet. The design is flexible so that the dimensions of the air stream can be varied, as required.

5. References

1. Charalampous G., Hardalupas Y. and Taylor A.M.K.P., "A novel technique for measurements of the intact liquid jet core in a coaxial airblast atomizer". Presented at *45th AIAA Aerospace Sciences Meeting and Exhibit,* Reno, USA, 2007, *paper no. AIAA 2007-1337*.

2. Lefebvre A.H., *Atomization and sprays*, Hemisphere Publishing Corporation 1989.

3. Lasheras J.C. and Hopfinger E.J., "Liquid jet instability and atomization in a coaxial gas stream". *Annual Review of Fluid Mechanics*, Vol. 32, 2000, pp. 275-308.

4. Engelbert C., Hardalupas Y. and Whitelaw J.H., "Breakup Phenomena in Coaxial Airblast Atomizers". *Proceedings of the Royal Society of London Series A-Mathematical and Physical Sciences*, Vol. 451, No. 1941, 1995, pp. 189-229.

5. Varga C.M., Lasheras J.C. and Hopfinger E.J., "Initial breakup of a small-diameter liquid jet by a high-speed gas stream". *Journal of Fluid Mechanics*, Vol. 497, 2003, pp. 405-434.

6. Chehroudi B., Chen S.H. and Bracco F.V., "On the intact core of full-cone sprays". *SAE Technical Papers 850126*, 1985.

7. Hiroyasu H., Arai M. and Shimizu M., "Break-up length of a liquid jet and internal flow in a nozzle". ICLASS-91. 1991.

8. Yule A.J. and Salters D.G., "A Conductivity Probe Technique for Investigating the Breakup of Diesel Sprays". *Atomization and Sprays*, Vol. 4, No. 1, 1994, pp. 41-63.

9. Hiroyasu H., Shimizu M. and Arai M., "The breakup of high speed jet in a high pressure gaseous atmosphere". *ICLASS-82*, 1982.

10. Cai W.Y., Powell C.F., Yue Y., Narayanan S., Wang J., Tate M.W., Renzi M.J., Ercan A., Fontes E. and Gruner S.M., "Quantitative analysis of highly transient fuel sprays by time-resolved x-radiography". *Applied Physics Letters*, Vol. 83, No. 8, 2003, pp. 1671-1673.

11. Renzi M.J., Tate M.W., Ercan A., Gruner S.M., Fontes E., Powell C.F., MacPhee A.G., Narayanan S., Wang J., Yue Y. and Cuenca R., "Pixel array detectors for time resolved radiography (invited)". *Review of Scientific Instruments*, Vol. 73, No. 3, 2002, pp. 1621-1624.

12. Yue Y., Powell C.F., Poola R., Wang J. and Schaller J.K., "Quantitative measurements of diesel fuel spray characteristics in the near-nozzle region using X-ray absorption". *Atomization and Sprays*, Vol. 11, No. 4, 2001, pp. 471-490.

13. Linne M., Paciaroni M., Hall T. and Parker T., "Ballistic imaging of the near field in a diesel spray". *Experiments in Fluids*, Vol. 40, No. 6, 2006, pp. 836-846.

14. Linne M.A., Paciaroni M., Gord J.R. and Meyer T.R., "Ballistic imaging of the liquid core for a steady jet in crossflow". *Applied Optics*, Vol. 44, No. 31, 2005, pp. 6627-6634.

15. Paciaroni M., Linne M., Hall T., Delplanque J.P. and Parker T., "Single-shot two-dimensional ballistic imaging of the liquid core in an atomizing spray". *Atomization and Sprays*, Vol. 16, No. 1, 2006, pp. 51-69.

16. Charalampous G., Hardalupas Y. and Taylor A.M.K.P., "Novel Technique for Measurements of Continuous Liquid Jet Core in an Atomizer". *AIAA Journal*, Vol. 47, No. 11, 2009, pp. 2605-2615.

17. Charalampous G., Hardalupas Y. and Taylor A.M.K.P., “3-Dimensional structure of the intact liquid jet core during coaxial air-blast atomisation”. *Intern. Journal of Spray and Combustion Dynamics (IJSCD)*, Vol. 1, 2009, pp. 389-415.

18. Colladon D. "On the reflections of a ray of light inside a parabolic liquid stream". *Comptes Rendus*, Vol. 15, 1842, pp. 800-802.

19. Charalampous G, Hardalupas Y, Taylor A.M.K.P. (2010) “Numerical and experimental evaluation of the optical connectivity technique for measurement of liquid breakup length in atomizers”. Presented at 48th Aerospace Sciences Meeting & Exhibit, AIAA paper 2010-0200, AIAA, Washington, 2010.

20. Charalampous G., Hadjiyiannis C., Hardalupas Y. and Taylor A.M.K.P. (2010) “Measurement of continuous liquid jet length in atomizers with optical connectivity, electrical conductivity and high-speed photography techniques”. In “Proceedings of 23rd Annual Conference on Liquid Atomization and Spray Systems, ILASS – Europe 2010”, paper 152, Brno, Czech Republic, 6-8 September 2010.

21. Marmottant, P. H., and Villermaux, E. "On spray formation," *Journal of Fluid Mechanics* Vol. 498, 2004, pp. 73-111.

22. Berkooz, G., Holmes, P., and Lumley, J. L. "The Proper Orthogonal Decomposition in the Analysis of Turbulent Flows," *Annual Review of Fluid Mechanics* Vol. 25, 1993, pp. 539-575.

23. Fogleman, M., Lumley, J., Rempfer, D., and Haworth, D. "Application of the proper orthogonal decomposition to datasets of internal combustion engine flows," *Journal of Turbulence* Vol. 5, 2004.

24. Arienti, M., and Soteriou, M. C. "Time-resolved proper orthogonal decomposition of liquid jet dynamics," *Physics of Fluids* Vol. 21, No. 11, 2009.

25. Chatterjee, A. "An introduction to the proper orthogonal decomposition," *Current Science* Vol. 78, No. 7, 2000, pp. 808-817.

26. Less D.M. and Schertz J.A., “Transient behavior of liquid jets injected normal to a high-velocity gas stream”, AIAA J., Vol. 24, 1986, pp. 1979-1985.

27. Wu P.K., Kirkendall K.A., Fuller R.P. and Nejad A.S., “Breakup processes of liquid jets in subsonic crossflows”, J. Propul. Power, Vol. 13, 1997, pp. 64-73,.

28. Aavani, K., Taeibi-Rahni, M., Soltani, M. R., Experiments in near-field of turbulent jets into a crossflow, Scientia Iranica, Vol. 13, No. 2, pp. 134-151.

29. Ghosh, S., and Hunt, J. C. R., Spray jets in a cross-flow, J. Fluid Mech., 1998, vol. 365, pp. 109-136.

30. Arienti M. and Soteriou M.C., "Time-resolved proper orthogonal decomposition of liquid jet dynamics", Physics Of Fluids, Vol. 21, 2009, 112104.

31. Ng C.-L., Sankarakrishnan R. and Sallam K.A., “Bag breakup of nonturbulent liquid jets in crossflow”, Int. J. Multiphase Flow, Vol. 34, 2008, 241.

32. Rachner, M., Becker, J., Hassa, C., Doerr, T., Modelling of the atomization of a plain liquid fuel jet in crossflow at gas turbine conditions, Aerospace Science and Technology, Vol. 6, 2002, pp. 495-506.

33. Sedarsky, D., Paciaroni, M., Berrocal, E., Petterson, P., Zelina, J., Gord, J., Linne, M., "Model validation image data for breakup of a liquid jet in crossflow: part I", Experiments in Fluids, Vol. 49, 2010, pp. 391-408.

34. Bai, B. F., Zhang, H. B., Liu, L., Sun, H. J., "Experimental study on turbulent mixing of spray droplets in crossflow", Experimental Thermal and Fluid Science, Vol. 33, 2009, pp. 1012-1020.

35. Balasubramanyam, M. S. and Chen, C. P., "Modeling liquid jet breakup in high speed cross-flow with finite-conductivity evaporation", International Journal of Heat and Mass Transfer, Vol. 51, 2008, pp. 3896-3905.

36. Fan, J. Y., Xu, S. L. and Wang, D. Z., “PDA measurements of two-phase flow structure and particle dispersion for a particle-laden jet in crossflow”, Journal of Hydrodynamics, Vol. 22, No. 1, 2010, pp. 9-18.

37. Hale, C. A., Plesniak, M. W. and Ramadhyani, S., “Structural features and surface heat transfer associated with a row of short-hole jets in crossflow”, International Journal of Heat and Fluid Flow, Vol. 21, 2000, pp. 542-553.

38. Barata, J. M. M., Durao, D. F. G., Heitor, M. V. and McGuirk, J. J., "The turbulence characteristics of a single impinging jet through a crossflow", Experimental Thermal and Fluid Science, Vol. 5, 1992, pp. 487-498.

39. Shedd, T. A., Corn, M. L., Cohen, J. M., Arienti, M. and Soteriou, M. C., "Liquid film formation by an impinging jet in a high-velocity air stream", 47th AIAA Aerospace Sciences Meeting Including the New Horizons Forum and Aerospace Exposition, AIAA 2009-0998, 2009.

40. Lee, J., Sallam, K. A., Lin, K.-C. and Carter, C. D., "Spray structure in near-injector region of aerated jet in subsonic crossflow", 46th AIAA Aerospace Sciences Meeting and Exhibit, AIAA 2008-1043, 2008.

41. Osta, A. and Sallam, K. A., "Effect of nozzle length/diameter ratio on the breakup of liquid jets in crossflow", 46th AIAA Aerospace Sciences Meeting and Exhibit AIAA 2008-1040, 2008.

42. Kihm, K. D., Kim, T. K. and Son, S. Y., "Visualization of high-speed gas jets and their airblast sprays of cross-injected liquid", Experiments in Fluids Vol. 27, 1999, pp. 102-106.

43. Lee, K., Aalburg, C., Diez, F. J. and Faeth, G. M., Sallam, K. A., “Primary breakup of turbulent round liquid jets in uniform crossflows”, AIAA Journal, Vol. 45, No. 8, 2007.

44. Sallam, K. A., Dai, Z. and Faeth, G. M., "Liquid breakup at the surface of turbulent round liquid jets in still gases", International Journal of Multiphase Flow, Vol. 28, 2002, pp. 427-449.

45. Sallam, K. A., Aalburg, C. and Faeth, G. M., Breakup of round nonturbulent liquid jets in gaseous crossflows, 41st Aerospace Sciences Meeting and Exhibit, AIAA 2003-1326, 2003.

46. Geary E.L. and Margettes M.J., “Penetration of a High Velocity Gas Stream by a Water Jet”, *Journal of Spacecraft*, Vol. 6, No. 1, 1969, pp. 79-81.

47. Reichenbach P.R. and Horn K.P., “Investigation of Injectant Properties in Jet Penetration in a Supersonic Stream”, *AIAA Journal*, Vol. 9, No. 3, 1971, pp. 469-471.

48. Kush E.A. and Schetz J.A., “Liquid Jet Injection into a Supersonic Flow”, *AIAA Journal*, Vol. 11, No. 9, 1979, pp. 1223-1224.

49. Schetz J.A., Kush E.A. and Joshi P.B., “Wave Phenomena in Liquid Jet Breakup in a Supersonic Crossflow,” *AIAA Journal*, Vol. 15, 1979, pp. 774-778.

50. Nejad A.S. and Schetz J.A., “Effects of Properties and Location in the Plume on Droplet Diameter for Injection in a Supersonic Stream”, *AIAA Journal*, Vol. 21, No. 7, 1983, pp. 956-961.

51. Nejad A.S. and Schetz J.A., “Effects of Viscosity and Surface Tension on a Jet Plume in Supersonic Cross-Flow”, *AIAA Journal*, Vol. 22, No. 4, 1984, pp. 458-459.

List of Symbols, Abbreviations and Acronyms

D_L = inner diameter of the liquid jet nozzle
G = Amplitude of wave on jet surface
L = Wavelength of wave on jet surface
MFR = Liquid-to-Gas Momentum Flux ratio
Re_L = Reynolds number of liquid jet
We_L = Weber number based on liquid jet velocity
We_G = Weber number based on gas velocity
n_1 = Index of refraction of liquid
n_2 = Index of refraction of gas
U_G = Average gaseous velocity of the cross stream
U_L = Average liquid velocity at the nozzle exit
γ = Absorption coefficient
μ = Kinematic viscosity of the liquid
ν_L = Dynamic Viscosity of the liquid
ρ_G or ρ_L = Density of gas or liquid
ϕ = Phase of sinus surface wave
ω = Laser beam divergence
σ = Surface tension

PROGRESS REPORT

AWARD N°: FA8655-09-1-3036 1

TITLE: Novel laser-based technique for measurements of primary atomization characteristics of liquid jets

INVESTIGATOR: Professor Y. Hardalupas

ORGANISATION: Imperial College of Science, Technology and Medicine

REPORTING PERIOD: From: 20 July 2011 To: 19 January 2012

PROJECT START DATE: 20 July 2009

DATE OF ISSUE OF THIS REPORT: 1 February 2012

ADMINISTRATIVE OFFICE: European Office of Aerospace Research and Development (EOARD)

GOVERNMENT PROGRAM MANAGER: Dr. Gregg Abate

Table of Contents

List of Figures

Summary

During the first stages of atomization of an airblast atomizer, the liquid stream is destabilized under the influence of a stream of air, until its continuity is broken. The geometry of the injector affects the way that the liquid jet breaks up and understanding the physics of the primary atomization process is important for the control of the spatial and temporal spray characteristics downstream of the nozzle. A novel technique (Charalampous *et al.* 2007 [1]) has been proposed to measure the length of the continuous liquid jet, quantify the spatial and temporal characteristics of the instabilities along the liquid-gas interface and examine the way that the liquid breaks up to form droplets. This technique relies on the optical connectivity of a liquid jet when it is internally illuminated through the spray nozzle. The liquid jet acts as a light guide, which allows light to propagate along the length of the jet in the same way as light travels along an optical fiber. The laser light excites a fluorescent dye that is dissolved in the liquid jet, making the volume of the liquid jet luminous. Then, the connectivity of the liquid jet is linked to the optical connectivity of the fluorescent jet. However, since the optical characteristics of the liquid jet are not the same as those of an optical fiber, there are losses of light intensity due to refraction through the liquid-gas interface and absorption by the fluorescence dye, as it propagates along the liquid jet. Therefore, the applicability of the technique requires evaluation in different geometries of liquid jets.

During the current reporting period, two areas were addressed:

(a) Design and manufacturing of a cross flow atomizer, which allows a liquid jet to be injected in an airstream that can operate with or without swirling motion and is capable of implementing the optical connectivity technique for studies of the primary breakup of the liquid jet.

(b) Testing of the cross flow atomizer and initial experimental evaluation of the applicability of the optical connectivity technique in liquid jets exposed to a cross stream of air.

This experimental facility is unique, because it allows swirling air flow to interact with the injected liquid jet. No measurements have been reported in the literature of the behavior of liquid jets exposed to a swirling air cross-stream. The facility provides appropriate optical access to the liquid jet in order to illuminate it with laser light through its injection nozzle and allow measurements of the liquid jet development and breakup using the optical connectivity technique.

The evaluation of the optical connectivity in swirling cross flow is also novel. Successful implementation of optical connectivity in swirling cross flow is however challenging due to the complex evolution of the liquid jet which may cause excessive intensity losses of the laser beam along the jet length. For this reason the evaluation process proceeds in stages to allow proper evaluation.

1. Introduction

During the first stages of atomization of a liquid jet, the jet is progressively destabilized under the influence of the forces that result from the interaction of the liquid stream with the surrounding air (2; 3). During this process the jet geometry changes as liquid is removed from its surface and waves develop on the surface until their amplitude becomes large enough to lead to breakup of the liquid jet. The distance from the nozzle exit to the point downstream the nozzle where the liquid jet breaks up defines what is known as the “primary atomization region”. The length of the continuous core of the liquid jet, known as the “breakup length”, determines the extent of the primary atomization region and the performance of atomizing nozzles.

A number of techniques have been proposed for the measurement of the length of the continuous jet. These include photography [4, 5], electrical conductivity [6-9], X-ray absorption [10-12] and ballistic imaging [13-15]. A recently proposed method is the optical connectivity technique [1]. It has been shown that, in dense sprays, the optical connectivity technique can measure the breakup length of the liquid jet at conditions where the continuous length of the jet is difficult to measure with photography, as the atomization products that surround the jet hinder the view to the continuous jet.

Photography (usually shadowgraphy) is the most commonly used method, as it is straightforward to apply and places only moderate demands on equipment. In this method, the atomizing jet is imaged directly by a camera. A light source illuminates the liquid jet and is usually placed on the opposite side of the camera to allow the light to propagate through the liquid jet. In this way, the shadow of the jet is imaged and its contour is well defined in the acquired images. The break-up length is estimated from the geometry of the recorded contour. While this method is easy to implement, when atomization becomes more intense, the droplets around the jet core might obstruct parts of the jet and the break-up length may be measured longer than its real value.

The electrical conductivity technique is based on the conduction of electricity along the length of a continuous liquid jet downstream the nozzle exit. A potential is applied between the atomizer nozzle and a probe downstream. If there is continuity of the liquid phase between the nozzle and the probe, a closed electrical circuit will ensue. The probe can be moved across different positions to determine the continuity of the liquid jet as a function of downstream distance. If the detected potential is low it is verified that there is electrical connectivity up to a specific point indicating continuity of the liquid jet core. On the contrary, the discontinuity of the liquid jet can be located where the conductivity is negligible. In earlier work, many researchers developed a conductivity probe technique to enable the investigation of the breakup zone in a variety of applications. Yule and Salters [8] investigated the breakup zone of a transient diesel spray as a function of time and position employing a wire probe. Hiroyasu et al [7, 9] studied the breakup length of a high-speed liquid jet by measuring an electrical resistance between the nozzle and a fine wire screen detector located in a spray jet. Chehroudi et al. [6] tried to determine the shape and length of the intact liquid core by applying a voltage between the nozzle unit and fine needles, rods and screens. The results show that current is carried not only by intact liquid cores but also by atomized unconnected sprays.

The novel optical connectivity technique [16, 17] relies on illuminating a liquid jet from within the nozzle by a laser beam, which propagates downstream, while reflecting at the gas-liquid interface. Due to the higher index of refraction of the liquid jet to that of the surrounding gas, a

laser light ray that interacts with the gas-liquid interface at a sufficiently large incident angle undergoes total internal reflection. As a consequence, the laser beam is reflected completely back into the liquid stream and propagates downstream for a long distance in the same way that light propagates along optical fibers. Collandon [18] demonstrated this phenomenon as early as 1842. The addition of a fluorescent dye, *e.g.* Rhodamine WT, in the liquid jet causes some of the intensity of the laser beam to be absorbed and re-emitted at a longer wavelength as fluorescence. This causes the volume of the continuous jet to become luminous, which allows the evaluation of the break-up length. Beyond the point of liquid discontinuity, the laser beam is diffused and its intensity is significantly reduced. The optical connectivity technique has limitations. Since the technique is based on the propagation of light within an atomizing liquid jet, there will unavoidably be scattering losses at the gas-liquid interface that will reduce the intensity of the propagating light. Therefore, for long liquid jets, the technique will not operate due to complete attenuation of the propagating light along the liquid before the break up point. Therefore, a numerical model of light propagation along a liquid jet was developed to determine how the laser light that is seeded at the base of the jet propagates along its length and what are the effects of its geometry on the losses of the intensity of the laser light [19].

During the first year of the project, measurements of break-up length of a liquid jet in an airblast coaxial atomizer were obtained with the optical connectivity technique, the electrical connectivity and high-speed photography. The results from the three measurement techniques were compared and advantages and limitations of the optical connectivity technique were identified [19, 20].

In the second year, the emphasis was directed in two directions: (a) the development of time-dependent optical connectivity technique and its application to the measurement of the temporal and spatial characteristics of the gas-liquid interface and the breakup length of a liquid jet in a coaxial airblast atomizer; (b) the applicability of the optical connectivity technique in liquid jets exposed to a cross stream flow of gas.

In the current reporting period the experimental investigation of cross flow atomization was initiated. First the cross flow atomizer was manufactured and installed. The operation of the new experimental arrangement was tested to ensure its functionality. Then, the suitability of the optical connectivity technique was examined for jets in a cross flow.

The next section presents the fundamentals of the optical connectivity technique for coaxial flow atomization. The third section presents and discusses the design of an atomizer that allows the study of a liquid jet exposed to a cross-stream of air. This describes a unique facility that allows the air flow to acquire variable levels of swirl and, as a consequence, study the primary breakup of a liquid jet in a cross-stream of swirling air flow. This section provides an initial literature review, which verifies the lack of studies of liquid jets exposed to swirling cross flow of air, presents the design criteria and describes the final design and implementation of the cross flow atomizer. The fourth section presents the first results of the implementation of the optical connectivity technique in the newly manufactured cross flow atomiser. The technique is initially applied in relatively slow cross flows in order to evaluate the effect of the inclination of the liquid stream in the propagation of light across its length. This will form the basis on which further testing will be conducted during the next reporting period. The report ends with a summary of the main achievements.

2. Principle of Optical Connectivity Technique

An optical connectivity technique has been developed for the measurement of the continuous length of liquid jets during the atomization process in atomizers. The technique works by introducing a laser beam within the flow of the liquid upstream of the nozzle that exits with the liquid through the nozzle in the direction parallel to the nozzle axis. In this way the laser beam is largely contained within the liquid jet by reflecting on the liquid interface propagating downstream and illuminating the liquid jet volume. A ray of laser light is guided along the length of the liquid jet by reflecting on the gas-liquid interface at the jet surface. As long as the angle of incidence between the surface of the jet and the laser light rays is greater then the angle of total internal reflection, the rays are completely reflected back inside the liquid without intensity losses from refraction. This principle is similar to the way that a laser beam propagates within an optical fiber. However, if the angle of incidence of a laser light ray on the liquid jet interface becomes smaller than that for total internal reflection then there will be some intensity losses due to refraction.

The laser beam continues to propagate along the liquid jet until it meets its breaking point, where it can no longer be contained within the jet and is diffused randomly in different directions. The introduction of a fluorescing dye into the liquid makes part of the laser beam to be absorbed along the length of the liquid jet, and subsequently be re-emitted as fluorescence. In this way the atomizing jet becomes luminous and can be imaged (**Figure 1**).

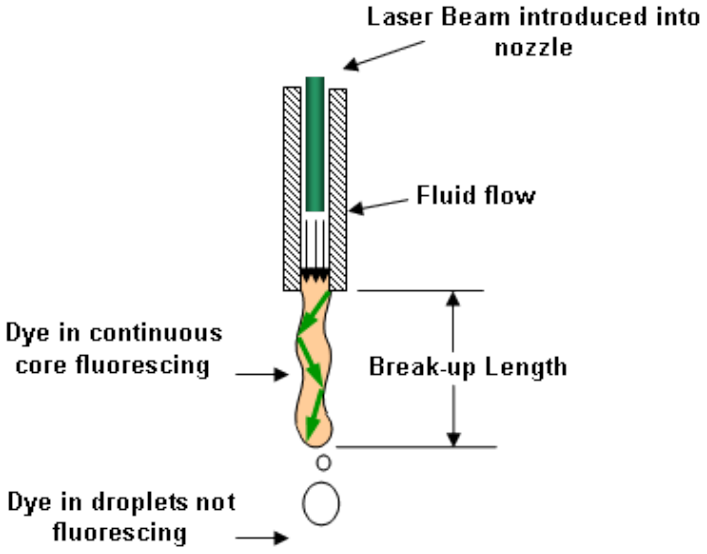

Figure 1 Principle of the optical connectivity technique

An example of the instantaneous image of a highly magnified liquid jet, illuminated by a laser beam according to the principle of the optical connectivity technique, is presented in **Figure 2**. The ability to detect the instabilities along the surface of the interface of liquid jet can be identified.

(a) (b)

Figure 2 (a) Example instantaneous image of a liquid jet obtained from the optical connectivity technique. (b) The image of (a) after image processing, which indicates the intact length of the liquid jet and the instabilities along the gas-liquid interface of the liquid jet.

3. Design of experimental facility for the study of a liquid jet in a cross stream of swirling air flow

This section describes the design of an experimental facility for the study of liquid jets exposed to a cross stream of air flow which can operate without or with swirling motion. A summary of the literature is presented first to establish that there is no available study for such atomizer geometry, which is important to many aero engine and gas turbine applications. An evaluation of the design criteria follows and the section ends with the reporting of the design of the experimental facility.

3.1 Literature review

The atomization of liquid jets in a cross stream air flow is relevant to many aero engines, gas turbine combustors and combustors for hypersonic vehicles. The atomization of a liquid jet in a cross-stream of air is characterized by two main regions:

(i) Primary breakup of liquid jet

In this region, the liquid jet penetrates into the air cross stream and becomes inclined in the direction of the air flow, while its shape changes. During this process, ligaments are formed from the liquid jet surface, which eventually become droplets.

(ii) The spray region

In this region, some surviving ligaments break up further and form stable droplets, which, together with the other existing droplets from the upstream region, determine the downstream spray characteristics.

In all the available studies, which are reviewed below, a planar air flow geometry has been

used. As a consequence, the air stream is mainly flowing in one direction and it is not possible to introduce additional velocity components to the air stream (*i.e.* swirling motion). However, in atomizers of aero-engines and gas turbine combustors, the liquid jet is injected in an axisymmetric annular flow of air, which tends to have a swirling component. Therefore, the emphasis here is to design an injector of a liquid jet in a cross stream of air, which can have variable levels of swirling component, and provides appropriate optical access for studies of the development of the liquid jet. However, information available from the literature must be considered in order to obtain some guidelines for the dimensions of the new atomizer design.

Some earlier studies, which also provide a review, are those of Less and Schertz [21] and Wu *et al.* [22]. These studies establish that the Momentum Flux Ratio (MFR) of the liquid jet to the air cross-flow of Equ. (1) is a relevant parameter that characterizes the behaviour of the liquid jet.

$$MFR = \frac{\rho_L U_L^2}{\rho_G U_G^2} \tag{1}$$

Increase of MFR leads to increase of jet penetration, which delays the breakup of the liquid column into large fragments and enhances the stripping-off of fine droplets from the liquid jet surface. However, both breakup mechanisms of the liquid jet are present at variable degree at the same time depending on the value of the MFR. Some additional relevant parameters for the characterization of the behaviour of the liquid jet are:

Weber number, based on the gas velocity $$We_G = \frac{\rho_G U_G^2 D_L}{\sigma} \tag{2}$$

Weber number, based on the liquid velocity $$We_L = \frac{\rho_L U_L^2 D_L}{\sigma} \tag{3}$$

Reynolds number of liquid jet $$\mathrm{Re}_L = \frac{U_L D_L}{\nu_L} \tag{4}$$

All these parameters will be used in the atomizer design analysis below.

The available studies in the literature and their main findings are summarized below. Low-speed wind tunnel experiments were conducted by Aavani *et al.* [23] to examine the effect of jet exit behaviour on the near-field characteristics of jets in cross-flow. Ghosh and Hunt [24] focused on the interaction between an external air cross-flow and the spray jet. Arienti and Soteriou [25] analysed the mechanism of primary break of the liquid jet in a cross flow using proper orthogonal decomposition to identify the liquid flow structures that are responsible for the breakup. Studies of bag-type breakup of non-turbulent liquid jets in a crossflow were carried out by Ng *et al.* [26] and results showed that the waves on the surface of the liquid column within the bag breakup regime could be explained from Rayleigh – Taylor instability. Rachner *et al.* [27] modeled the penetration and atomization of a plain jet of kerosene fuel in air crossflow and could identify the two main breakup mechanisms, which are known as the surface breakup and the liquid column breakup. Sedarsky *et al.* [28] used Particle Image Velocimetry, high-speed shadowgraphy and ballistic imaging to observe the breakup of a liquid jet in a crossflow of air under a variety of conditions. The experimental configuration consisted of four interchangeable nozzle tips of different exit diameter. Bai *et al.* [29] presented an experimental study on turbulent mixing of spray droplets for different injection angles. The optimum mixing effect can be

achieved for an angle of 60° and the most stable of the flow field structure and the greatest sustained distance of the counter rotating-vortex pair can be found when the angle is 90°. A numerical study to model the liquid jet breakup in high speed crossflow was attempted by Balasubramanyam and Chen [30] using an improved drag coefficient correlation, which would capture the spray phenomenon more accurately specifically for application to high speed flow. Phase Doppler Anemometry measurements of the two-phase flow structure and droplet dispersion were performed by Fan *et al.* [31] and confirmed the complex interaction between the liquid jet and crossflow and suggested that the flow field depends primarily on the jet-to-crossflow velocity ratio. Hale *et al.* [32] investigated surface heat transfer in a row of short length nozzles of jets in crossflow and found that horseshoe vortices are weak structures that dissipate as their legs wrap around the jet. The turbulence characteristics of a jet in crossflow were examined by Barata *et al.* [33] using Laser Doppler Anemometry. Their aim was to investigate the effect of the velocity ratio between the jet and the crossflow. The conclusion of Hale *et al.* [32] that the flow appears as a vortex wrapped around the jet with its size increasing with the velocity ratio was established by the measurements of [33]. Shedd *et al.* [34] used high-speed digital imaging to visualize the formation of the liquid film formed on the surface of a channel due to the injection of a liquid jet in crossflow and it was observed that film thickness increased with increasing momentum flux ratio.

The spray structure in the near-injector region of an aerated liquid jet in subsonic crossflow was investigated by Lee *et al.* [35]. Six holograms were recorded and the droplet velocities in the streamwise and the crossflow direction could be measured by observing the displacements of the center of each droplet between the double pulses. Osta *et al.* [36] examined the effect of nozzle length/diameter ratio on the breakup using nozzles with different length-to-diameter ratios. The liquid jets were observed using single- and double-pulsed shadowgraphy and holography. The main conclusion was that the breakup length decreases with increasing length-to-diameter ratio. Kihm *et al.* [37] visualized both under expanded sonic gas jets from a converging nozzle (SN-type) and over expanded supersonic gas jets from a converging-diverging nozzle (CD-type). They found out that the SN-type develops wider spray, which lowers the probability of droplet coalescence and generates finer sprays. Lee *et al.* [38] used pulsed shadowgraph and holography for turbulent round liquid jets injected normal to air crossflow in a shock tube. They used two different nozzles with different injector passages and smooth rounded entrances with length-to-diameter ratios larger than 100 to ensure fully developed turbulent pipe flow at the jet exit for large Re. Sallam *et al.* [39] investigated the breakup at the surface of turbulent round liquid jets in still gases using single- and double- pulse shadowgraphy and holography for nozzle with smooth rounded entrances with length-to-diameter ratio larger than 100 to ensure fully developed turbulent pipe flow at the jet exit for large Reynolds numbers. Three modes of liquid column breakup were observed: (a) a weakly turbulent Rayleigh-like breakup mode at small jet exit We and Re, (b) a turbulent breakup mode at moderate jet exit We and Re and (c) an aerodynamic bag/shear breakup mode at large jet exit We. Finally, Sallam *et al.* [40], for nonturbulent liquid jets, used shadowgraphy to demonstrate three regimes of primary breakup: bag breakup, multimode (or bag/shear) breakup and shear breakup. It is worth noting that round supercavitating nozzles were used that had sharp edged inlets and exits, with length-to-diameter ratios smaller than 3. This arrangement yields uniform non-turbulent round liquid jets in opposition to findings of Reference [39]. Finally, several studies were performed of liquid jets injected in supersonic cross-streams of air [41-46]. Although effects of the supersonic streams are present, the overall structure and development of the liquid jets remain qualitatively the same.

The above review confirms that all the studies of liquid jets injected in cross-stream of air have been performed in geometries that could not impart a swirling component to the air stream

velocity. As a consequence, an experimental facility was designed which allows the study of liquid jets exposed to an air stream with variable swirling component. This is relevant to atomizers that are used in aero-engines and gas turbine combustors.

3.2 Considerations for atomizer design

The new atomizer should inject a liquid jet in an air cross-stream, which could have a swirling velocity component. Also, this atomizer should have the capability to operate without swirling air stream and at conditions already studied in planar geometries of jets in crossflows. The first step was to review the literature and determine which factors are important and can influence the operation of the atomizer, which was performed above and established the relevant non-dimensional quantities.

The next step was to perform some calculations and find out how the atomizer will behave for different air flow conditions without swirl. An important aspect of the design was to establish the trajectory of the liquid jet in a cross-stream of air, since this will determine the width of the air stream of the atomizer. This is a requirement in order to avoid the impingement of the liquid jet on the external wall of the air stream. We used the empirical correlation reported by Lee *et al.* [38] to establish the trajectory of the liquid jet. In addition, the momentum flux ratio, the gas crossflow and the liquid Weber numbers and the liquid jet Reynolds number (Eqs. (1-4)) were calculated for different dimensions and flow conditions of the atomizer. These factors decide the atomization characteristics, the structure of the spray and the distance from the injection location, where the breakup of the liquid core occurs.

Therefore, **Figure 3** through **Figure 8** present the predictions of the trajectory of the liquid jet based on the correlation of Lee *et al.* [38]. The vertical axis is the cross-stream distance and the horizontal is the streamwise distance, presented in dimensional form with units of mm. These calculations were performed for two liquid jet exit diameters, namely 0.5mm (**Figure 3** through **Figure 5**) and 1mm (**Figure 6** through **Figure 8**) and for different liquid flowrates and cross-stream air velocities. Underneath each figure, a small table is presented, which includes the corresponding momentum flux ratio, the gas cross flow and liquid Weber numbers and the liquid jet Reynolds number for all the examined conditions. These parameters were defined in Equations (1), (2), (3) and (4) respectively.

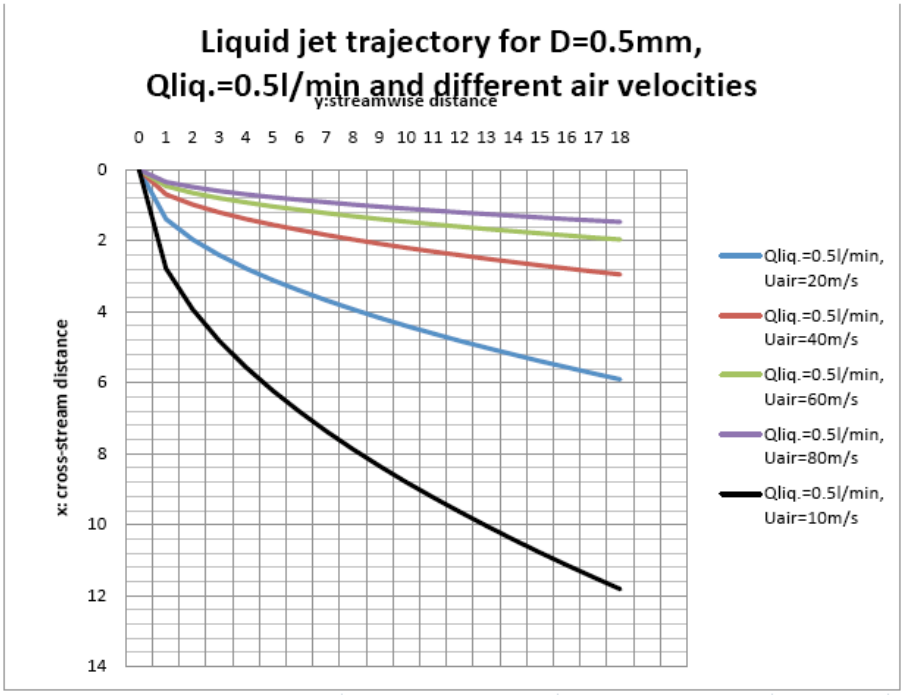

Crossflow We	Liquid We	Momentum ratios	Jet Re
8.276566757	122579.3066	14810.40512	18928.07002
33.10626703	122579.3066	3702.601279	18928.07002
132.4250681	122579.3066	925.6503197	18928.07002
297.9564033	122579.3066	411.4001421	18928.07002
529.7002725	122579.3066	231.4125799	18928.07002

Figure 3 Liquid jet trajectory for diameter of liquid jet exit D=0.5mm, liquid flow rate of 0.5l/min and different air velocities.

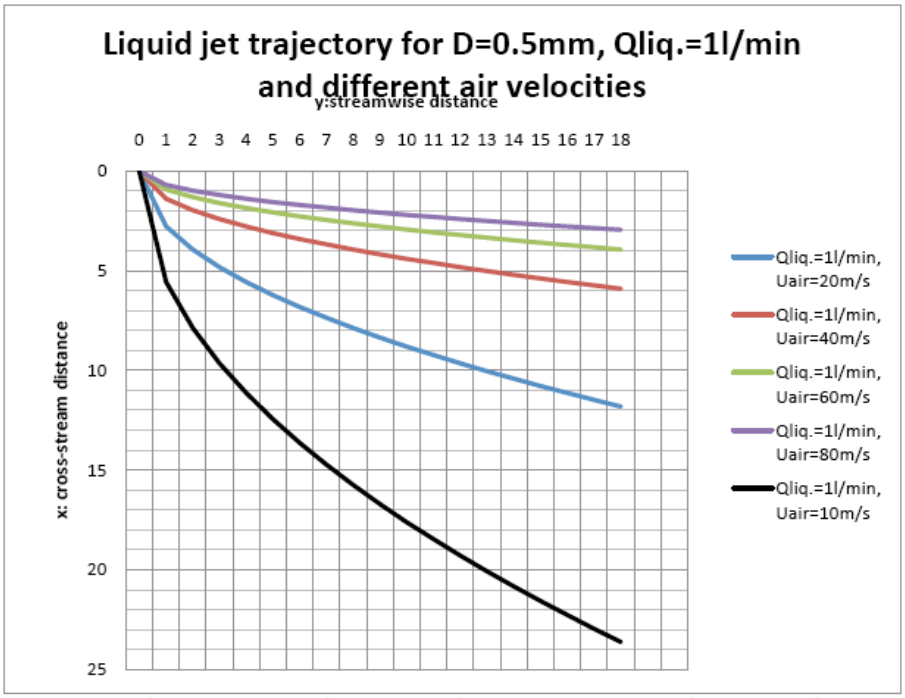

	Crossflow We	Liquid We	Momentum ratios	Jet Re
	8.276566757	490317.2266	59241.62046	37856.14004
	33.10626703	490317.2266	14810.40512	37856.14004
	132.4250681	490317.2266	3702.601279	37856.14004
	297.9564033	490317.2266	1645.600568	37856.14004
	529.7002725	490317.2266	925.6503197	37856.14004

Figure 4 Liquid jet trajectory for diameter of liquid jet exit D=0.5mm, liquid flow rate of 1 l/min and different air velocities.

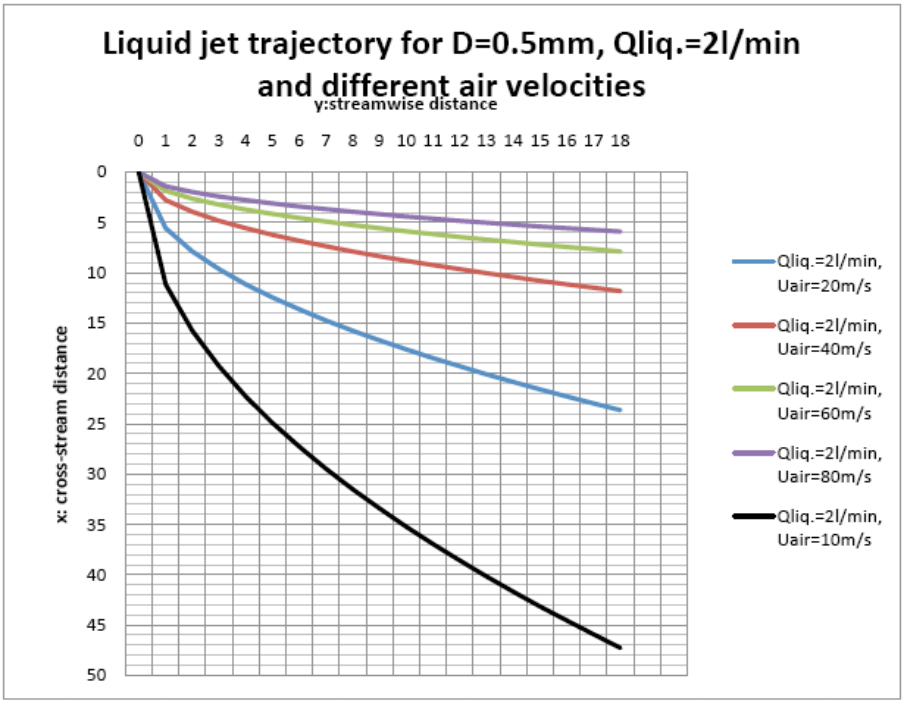

	Crossflow We	Liquid We	Momentum ratios	Jet Re
	8.276566757	1961268.906	236966.4818	75712.28007
	33.10626703	1961268.906	59241.62046	75712.28007
	132.4250681	1961268.906	14810.40512	75712.28007
	297.9564033	1961268.906	6582.402273	75712.28007
	529.7002725	1961268.906	3702.601279	75712.28007

Figure 5 Liquid jet trajectory for diameter of liquid jet exit D=0.5mm, liquid flow rate of 2 l/min and different air velocities.

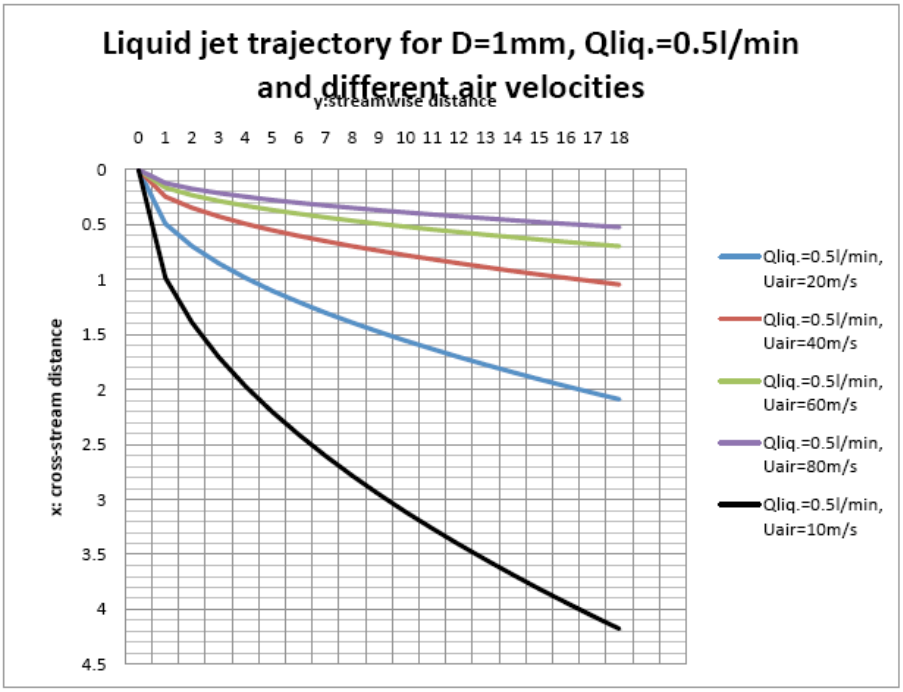

	Crossflow We	Liquid We	Momentum ratios	Jet Re
	16.55313351	15322.41333	925.6503197	9464.035009
	66.21253406	15322.41333	231.4125799	9464.035009
	264.8501362	15322.41333	57.85314498	9464.035009
	595.9128065	15322.41333	25.71250888	9464.035009
	1059.400545	15322.41333	14.46328625	9464.035009

Figure 6 Liquid jet trajectory for diameter of liquid jet exit D=1mm, liquid flow rate of 0.5 l/min and different air velocities.

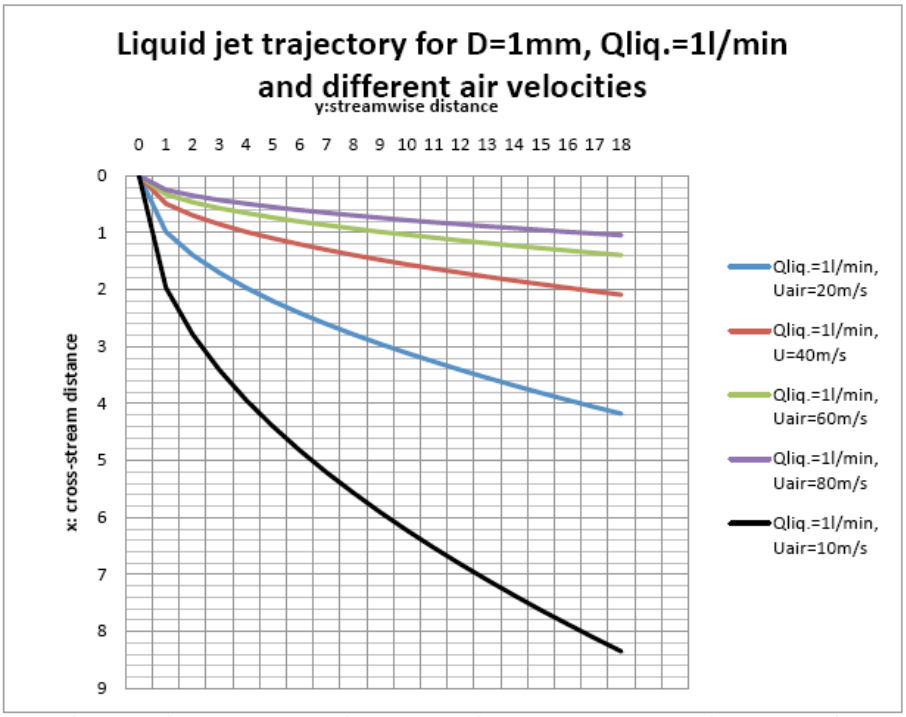

	Crossflow We	Liquid We	Momentum ratios	Jet Re
	16.55313351	61289.65332	3702.601279	18928.07002
	66.21253406	61289.65332	925.6503197	18928.07002
	264.8501362	61289.65332	231.4125799	18928.07002
	595.9128065	61289.65332	102.8500355	18928.07002
	1059.400545	61289.65332	57.85314498	18928.07002

Figure 7 Liquid jet trajectory for diameter of liquid jet exit D=1mm, liquid flow rate of 1 l/min and different air velocities.

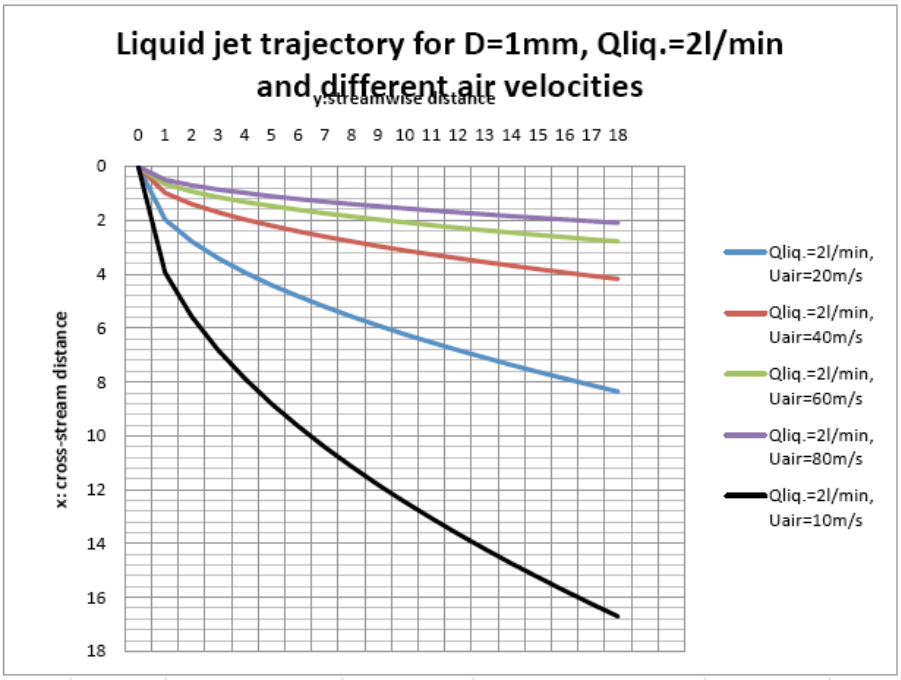

	Crossflow We	Liquid We	Momentum ratios	Jet Re
	16.55313351	245158.6133	14810.40512	37856.14004
	66.21253406	245158.6133	3702.601279	37856.14004
	264.8501362	245158.6133	925.6503197	37856.14004
	595.9128065	245158.6133	411.4001421	37856.14004
	1059.400545	245158.6133	231.4125799	37856.14004

Figure 8 Liquid jet trajectory for diameter of liquid jet exit D=1mm, liquid flow rate of 2 l/min and different air velocities.

3.3 Atomizer Design

The design of the atomizer is presented in **Figure 9** and the design details can be seen in the rendered image in **Figure 10**. The air stream has to be axisymmetric, and not planar as in all studies available in the literature, in order to be able to introduce swirl and control the relative magnitude of axial and swirling component of air velocity. The swirling air flow component will be generated by introducing the air flow in the upstream pipe through tangential air inlets.

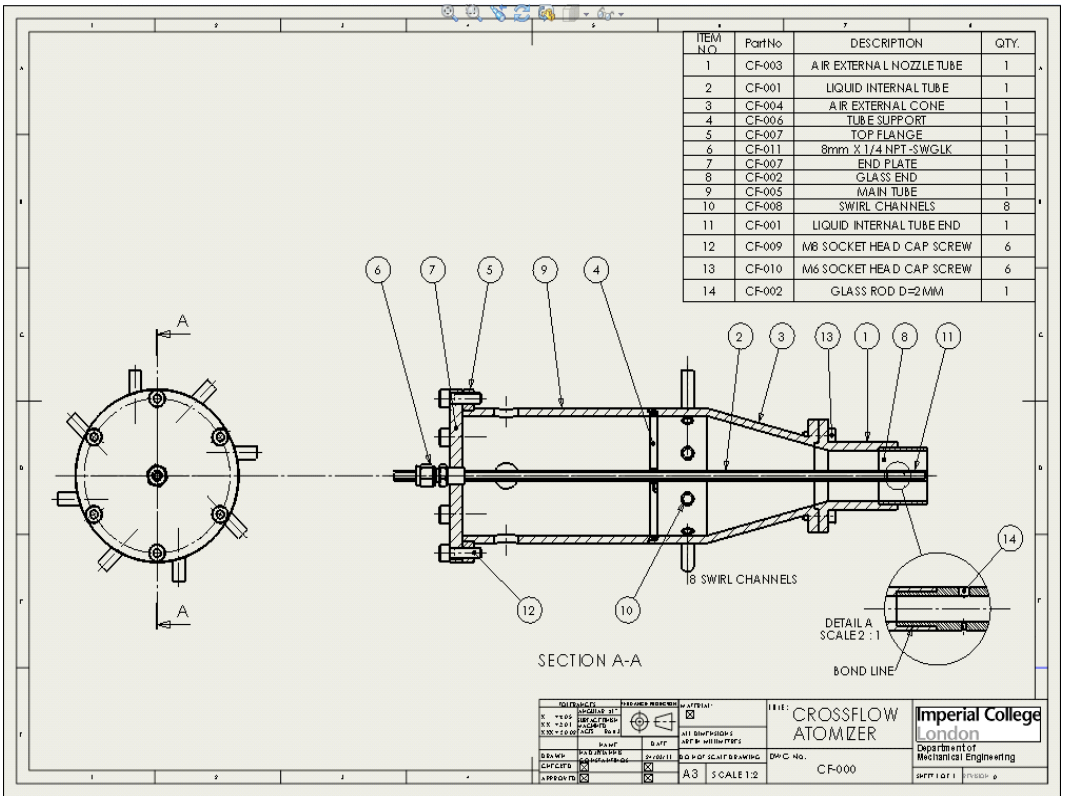

Figure 9 The atomizer design of a liquid jet exposed to a cross flow of air, which can have a swirling velocity component.

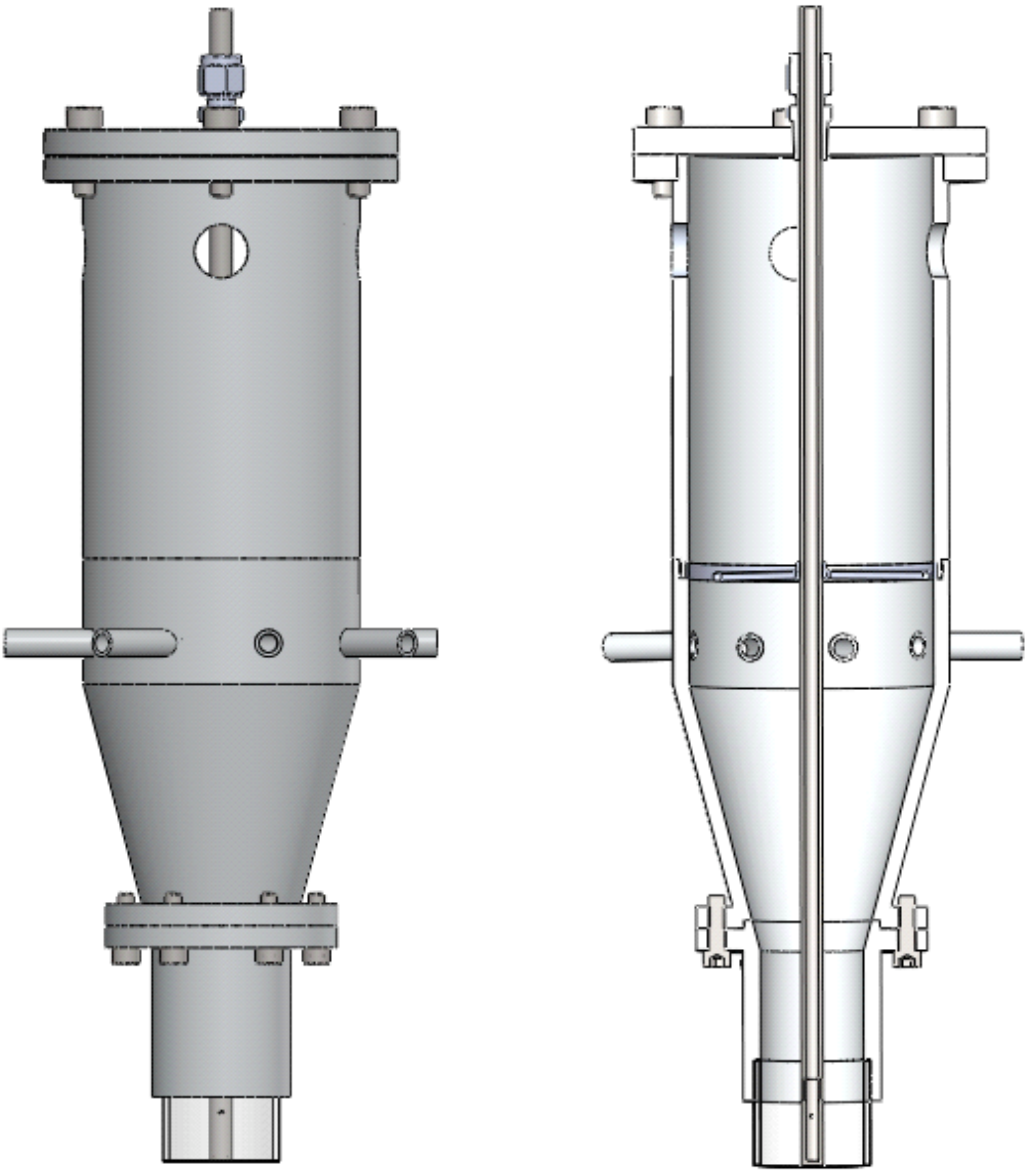

Figure 10 Rendered external and cross sectional views of the cross flow atomiser.

The analysis of section 3.2 provided estimates of the effects of the dimensions of the liquid jet exit and flow conditions on the diameter of the crossflow air stream. The most suitable liquid jet exit diameter is 1mm, according to the calculations presented above, because the diameter of the annular air stream can remain smaller for a wider range of flow conditions without the trajectory of the liquid jet hitting at the outer wall of the airstream. The selected width of the air stream is 15mm. However, the section of the atomizer exit can be exchanged by connecting a new converging section at the flange shown in

Figure 11. This flexibility is important in order to allow for differences of the behavior of the liquid jet from what is expected in the literature, especially when swirl is introduced to the air stream.

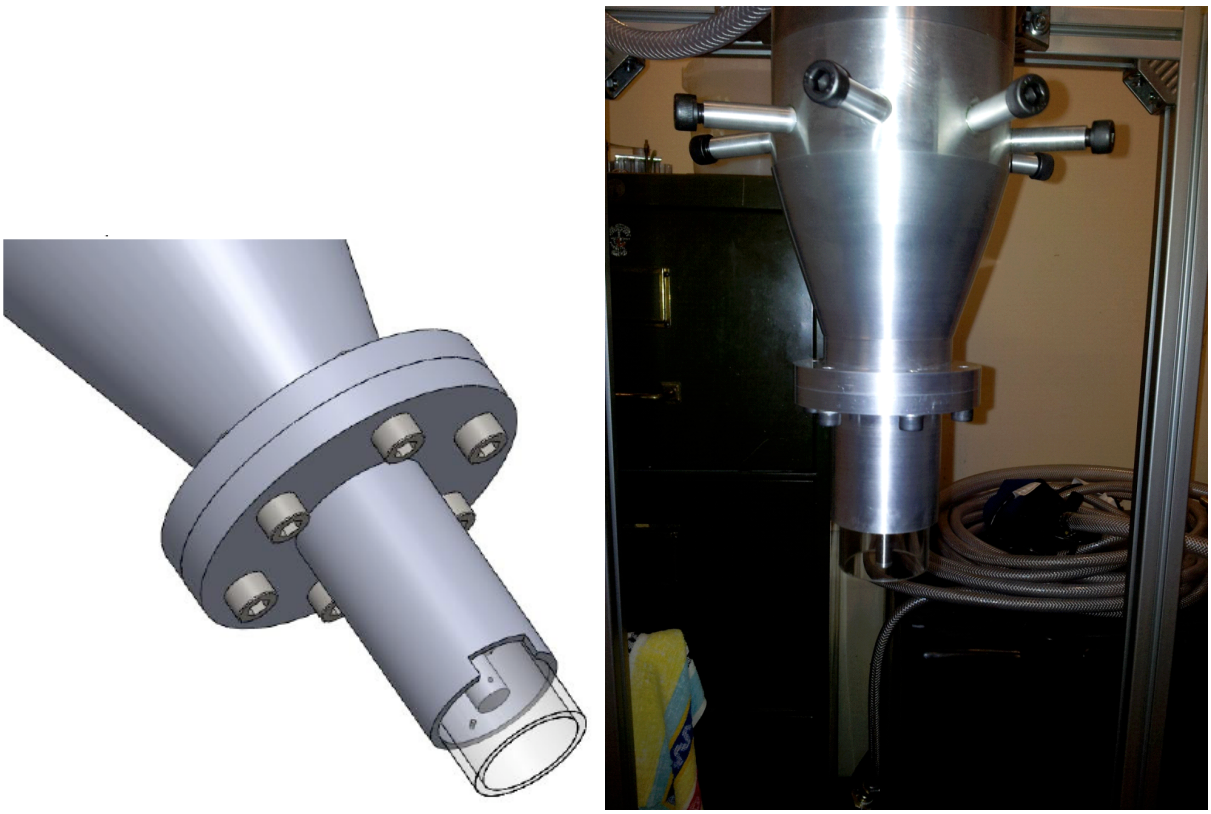

Figure 11 Interchangeable gas nozzle that provides flexibility to modify the dimensions of the geometry of the air stream in order to account for differences to the breakup process of the liquid jet from what is expected from literature, when swirling air stream is introduced.

An important detail is shown in **Figure 13**. One hole exists on the surface of the liquid tube and at the opposite side of the injection nozzle. The diameter of this hole is 2mm, which is larger than the diameter of the liquid jet injection nozzle (1 mm) and is required in order to allow the laser beam to be introduced in the liquid jet. This is an important requirement for the application of the optical connectivity technique to the measurement of the intact length of the liquid jet. This hole is sealed by an appropriate quartz window. **Figure 14** shows a close up of the manufactured and installed liquid jet nozzle. Excellent alignment of the window and the injection nozzle can be observed as light propagates through both of them.

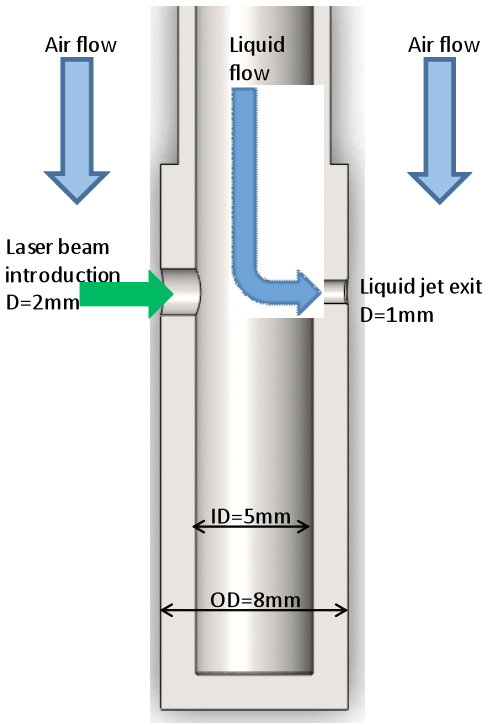

Figure 13 The design of the inner tube of the atomizer, which supplies the liquid to a round-edged nozzle with diameter of 1mm. The cross section is also showing the illuminating laser beam optical access behind the liquid nozzle.

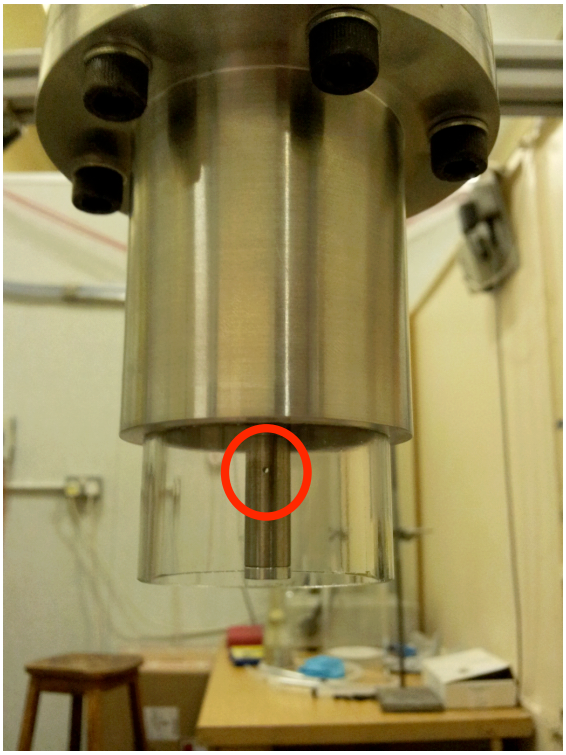

Figure 14 Detail of injection nozzle orifice. The window at the back of the nozzle enables unobstructed illumination of the liquid stream with a laser beam through the back of the orifice.

In **Figure 15,** the geometry of the quartz tube that is added at the nozzle exit is presented. The quartz tube, which is 15mm long, is added to confine the air flow stream and ensure that the flow remains the same while it interacts with the liquid jet. The length of this tube was selected on the basis of the expected longest breakup length for the selected flow conditions of **Figure 3** through **Figure 8**. The breakup of the liquid column should be completed inside the quartz tube before the air stream begins to expand. However, this estimate is based on liquid jets exposed to non-swirling air streams. It is clear that the results will change when swirl is introduced but the expectation is that the selected distance will be adequate for liquid jets in swirling air cross stream. The installed quartz tube on the injection nozzle can be seen in **Figure 14.** The good optical quality of the quartz tube is verified by the sharp image of the liquid nozzle in **Figure 13**. Therefore, the visualization of the fluorescent liquid jet core can be achieved without uncertainties due to optical distortion.

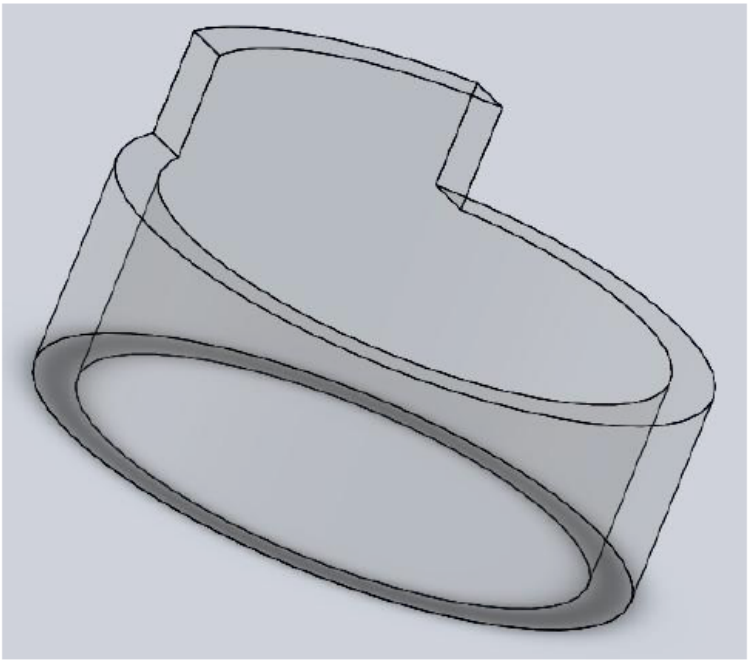

Figure 15 The quartz tube allows the extension of the length of the nozzle downstream of the liquid jet injection location in order to maintain the confinement of the air stream and avoid its expansion.

Figure 16 Photograph of the full body of the manufactured cross flow atomiser, as installed on the test rig.

The cross flow air-blast atomizer was set up vertically and exhausted downwards as seen in **Figure 16**. In this way, it is easy to collect the atomized liquid and prevent atomized water from accumulating inside the atomizer, which will happen if the atomizer was injected the liquid upwards and against gravity. The atomizer was connected to a flow circuit illustrated in **Figure 17**. Water is delivered from the water tank (A) to pump (B). The flow rate was controlled by adjusting valves (C), (D) and (L). The water flow rate was measured by rotameter (E) on a scale of 0-2 l/min with a 0.1 l/min resolution. The atomized liquid was collected in tank (I) and then was returned to the main tank (A) using a water pump (J). The air flow rate was adjusted from vane valve (F) and the flowrate was measured by rotameter (G) on a scale of 0-2000 l/min with a resolution of 50 l/min. Air flow rate measurements were corrected for atmospheric temperature and pressure conditions by monitoring the pressure at the exit of the rotameter.

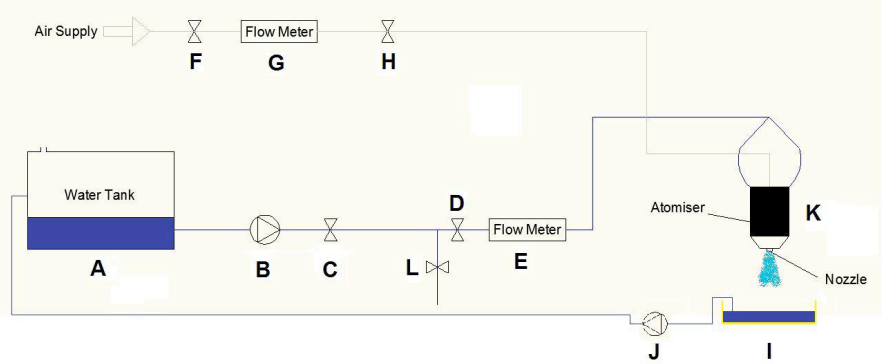

Figure 17 Air and water supply circuit to the cross flow air-blast atomizer.

In order to prevent asymmetries in the radial velocity profile of the gas stream, the gas supply was initially supplied to a plenum shown in **Figure 18**. Then, it was split to 4 hoses of equal length. In this way, the pressure drop between the plenum and each inlet of the atomizer was the same and differences between the gas flowrate supplied to each of the 4 inlets are expected to be minimal, ensuring an even gas distribution in the annular gas stream and around the nozzle exit. The atomizer was tested for water and gas leaks, which allowed the initiation of the implementation and testing of measurements with the optical connectivity technique.

Figure 18 Cross flow atomiser with plenum for the even distribution of the gas flow across all inlets.

4. Experimental evaluation of application of optical connectivity technique to a liquid jet exposed to a cross flow airstream

The first experimental evaluation of the operation of the newly manufactured cross-flow atomiser and the implementation of the optical connectivity technique to study the breakup of the liquid jet exposed to a cross flow airstream are presented in this section.

The atomized liquid was water, doped with Rhodamine WT dye. The use of this dye has shown good results with optical connectivity measurements under coaxial atomisation, so it was

preferred. Fluorescence from the dye in the liquid jet was excited by an Nd:YAG laser beam at 532nm from a continuous wave frequency doubled SSDP laser. The beam was focused on the optical window behind the liquid nozzle exit. In this way, some of the laser light was transmitted through the nozzle and into the liquid jet. The concentration of the dye in the injected liquid was adjusted so that the absorption within the measured length of the jet was adequately high for the resulting fluorescent light intensity to be sufficient for the visualisation of the liquid jet, but not excessively high that would absorb the laser beam before it travelled the full length of the liquid jet. For the imaging of the emitted fluorescent intensity from the liquid jet, an Andor classic iCCD camera was used. The camera lens was fitted with an OG590 optical filter, which does not transmit the scattered light at 532nm, but allows the transmission in the fluorescence spectrum of the dye. In this way, only the emitted intensity from the liquid jet core was recorded.

Since this is the first implementation of the optical connectivity in the cross flow atomiser it was decided that the atomiser would be operated initially without swirl. In this way, two goals are achieved. First, the investigation of the optical connectivity is extended in inclined liquid jets, which are expected to be more difficult to characterize due to the increased scattering losses predicted by the numerical calculations. Secondly, the complexities of visualisation of a liquid jet core that develops in three dimensions, which might require the use of two cameras, are removed. When the optical connectivity technique is thoroughly investigated with simple cross flow and the atomisation process is characterised the investigation can continue with the addition of swirl and both the applicability of the optical connectivity technique and the atomisation of a liquid stream with swirl can be examined.

The flow characteristics of the tested cases are presented in the table below. The initial investigation was performed under mild atomisation conditions, so that the laser light losses to scattered light through the liquid jet interface are minimised.

Table 1: Flow conditions for cross flow atomisation

U_{gas} (m/s)	U_{liquid} (m/s)	Re	We
0.0	1.0	1061	0
10.8	1.0	1061	1.9
12.3	1.0	1061	2.5
13.8	1.3	1273	3.2
13.8	1.5	1485	3.2

Initially atomisation without any gas coflowing stream was tested. In this way, the curvature of the liquid jet obtained a well-defined parabolic profile that is attained due to the gravitational acceleration and the surface of the jet is smooth across its length. Since the curvature of the jet was small, there was impingement on the jet on the glass wall of the flow channel, as shown in **Figure 20**. The fluorescent intensity emitted from the liquid jet was found to be strong for a small inclination of the liquid jet. In addition, while the impingement of the liquid jet on the glass wall caused splattering and the formation of a liquid film on the wall of the confinement quartz tube, there was no interference in the acquired images due to these potential sources of light, which demonstrates that the technique can detect only the continuous liquid jet.

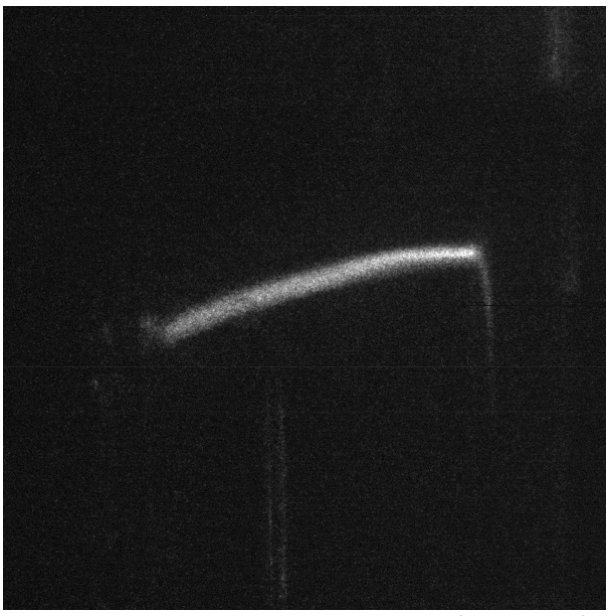

Figure 20 Example of optical connectivity implementation for a jet of Re=1061 and cross flow We of 0 (no cross flow).

When the gas flow was introduced, there was significantly more inclination of the liquid jet trajectory which deflected about 45° from its original direction. In addition the jet developed waves on its surface. Nevertheless the beam was able to travel for the whole length of the liquid jet and full visualisation was obtained. An example can be seen in **Figure 21**. This demonstrates that the optical connectivity technique is applicable to inclined liquid jets even with significant deflection.

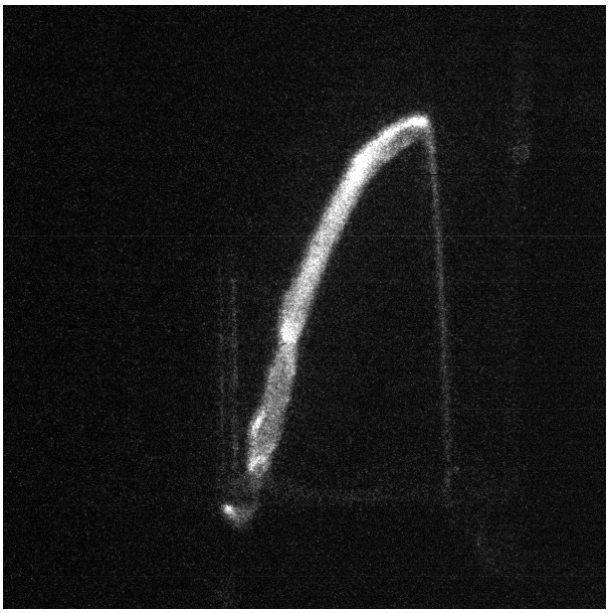

Figure 21 Example of optical connectivity implementation for a jet of Re=1061 and cross flow We of 1.9.

Finally, flow conditions were investigated for which the liquid jet was deflected by 90° from its initial direction. For these conditions, the liquid stream aligned with the gas stream direction before complete breakup for an extended length. It is clear from the examples of **Figure 22**

through **Figure 24** that the fluorescent intensity of the liquid jet decreases significantly along the jet length. This is more pronounced, when the liquid jet interface becomes increasingly more disturbed by propagating waves. Nevertheless, a large part of the liquid jet close to the nozzle exit is clearly visualised even after the jet has inclined by 90° and aligned with the gas flow direction. As the optical connectivity technique is designed to visualise the liquid jet when there is intense atomisation, where the liquid jet length becomes shorter than for the current conditions, it is demonstrated here that the optical connectivity can be applicable to visualise liquid jets that are inclined by 90° for lengths that are of practical interest. The details of the application of optical connectivity for intensely atomised liquid jets exposed to the cross stream of air is the next step of the investigation.

Figure 22 Example of optical connectivity implementation for a jet of Re=1061 and cross flow We of 1.9.

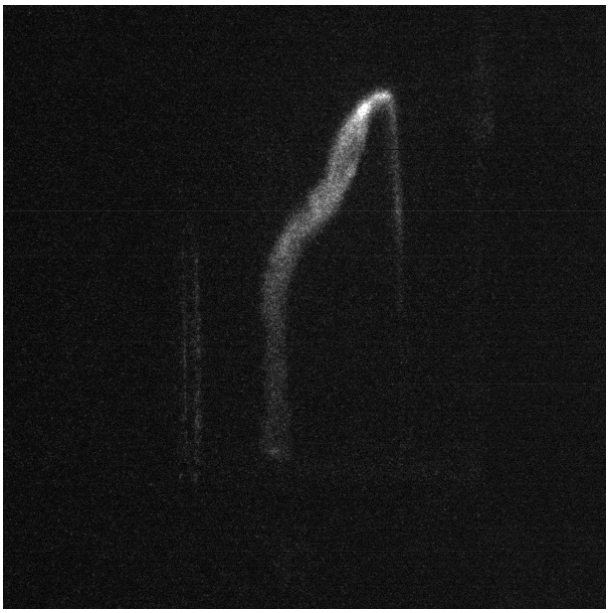

Figure 21 Example of optical connectivity implementation for a jet of Re=1273 and cross flow We of 3.2.

Figure 24 Example of optical connectivity implementation for a jet of Re=1485 and cross flow We of 3.2.

5. Summary

The research during the current reporting period of the project contributed to two areas.

(a) The final design, manufacturing and installation of a new atomizer for studies of liquid jets exposed to cross-streams of air without and with a swirling component.

(b) The implementation and experimental assessment of the optical connectivity technique for jets in cross flow.

The findings are summarized below.

(a) An atomizer design for injection of a liquid jet in a cross-stream of air without and with a swirling component was achieved, as follows:

(i) An extensive literature review was performed of atomization studies of liquid jets in a cross-stream of air, which established that no information is available on the breakup of liquid jets that are exposed to cross flow of a swirling air stream.
(ii) The design parameters were established and calculations were performed using available correlations from the literature for liquid jets in non-swirling air cross-streams in order to establish the trajectory of the liquid jet for different liquid jet diameters, liquid and gas flowrates. In this way, the dimensions of the liquid jet nozzle and the width of the annular air stream in the new atomizer were evaluated.
(iii) An axisymmetric design of the atomizer was established, which allows the introduction of variable level of swirl in the air cross-stream, which interacts with the liquid jet.
(iv) The atomizer was manufactured and installed. Testing of the atomizer showed that its operation is problem free. No leaks were detected, the alignment of the optical window

with the liquid nozzle exit is excellent and the optical quality of the annular quartz tube at the gas nozzle exit allows the clear imaging of the breakup process.

(b) The implementation of the optical connectivity technique for liquid jets in a non-swirling cross flow demonstrated the following:

(i) The optical connectivity technique is applicable to liquid jets in a cross flow and the laser beam can propagate along a liquid jet even if the liquid jet is inclined by 90° relative to its original direction and aligned with the gas flow.
(ii) In cases where the length of the liquid jet is long there is significant attenuation of the laser beam at downstream locations of the jet. In such cases, the applicability of the optical connectivity technique is limited. However, as the optical connectivity technique is designed for liquid jets with shorter break length and dense droplet clouds around the liquid core, this limitation is not detrimental. Therefore, the optical connectivity technique is expected to perform well in liquid jets exposed to cross-flow air streams of practical interest. This will form the emphasis of the work during the next reporting period.

6. References

1. Charalampous, G., Hardalupas, Y., and Taylor, A. M. K. P., "A novel technique for measurements of the intact liquid jet core in a coaxial airblast atomizer," Presented at *45th AIAA Aerospace Sciences Meeting and Exhibit, AIAA 2007-1337*, 2007, Reno, USA.
2. Lefebvre A.H., Atomization and sprays, Hemisphere Publishing Corporation 1989.
3. Lasheras J.C. and Hopfinger E.J., "Liquid jet instability and atomization in a coaxial gas stream". Annual Review of Fluid Mechanics, Vol. 32, 2000, pp. 275-308.
4. Engelbert C., Hardalupas Y. and Whitelaw J.H., "Breakup Phenomena in Coaxial Airblast Atomizers". Proceedings of the Royal Society of London Series A-Mathematical and Physical Sciences, Vol. 451, No. 1941, 1995, pp. 189-229.
5. Varga C.M., Lasheras J.C. and Hopfinger E.J., "Initial breakup of a small-diameter liquid jet by a high-speed gas stream". Journal of Fluid Mechanics, Vol. 497, 2003, pp. 405-434.
6. Chehroudi B., Chen S.H. and Bracco F.V., "On the intact core of full-cone sprays". SAE Technical Papers 850126, 1985.
7. Hiroyasu H., Arai M. and Shimizu M., "Break-up length of a liquid jet and internal flow in a nozzle". ICLASS-91. 1991.
8. Yule A.J. and Salters D.G., "A Conductivity Probe Technique for Investigating the Breakup of Diesel Sprays". Atomization and Sprays, Vol. 4, No. 1, 1994, pp. 41-63.
9. Hiroyasu H., Shimizu M. and Arai M., "The breakup of high speed jet in a high pressure gaseous atmosphere". ICLASS-82, 1982.
10. Cai W.Y., Powell C.F., Yue Y., Narayanan S., Wang J., Tate M.W., Renzi M.J., Ercan A., Fontes E. and Gruner S.M., "Quantitative analysis of highly transient fuel sprays by time-resolved x-radiography". Applied Physics Letters, Vol. 83, No. 8, 2003, pp. 1671-1673.

11. Renzi M.J., Tate M.W., Ercan A., Gruner S.M., Fontes E., Powell C.F., MacPhee A.G., Narayanan S., Wang J., Yue Y. and Cuenca R., "Pixel array detectors for time resolved radiography (invited)". Review of Scientific Instruments, Vol. 73, No. 3, 2002, pp. 1621-1624.
12. Yue Y., Powell C.F., Poola R., Wang J. and Schaller J.K., "Quantitative measurements of diesel fuel spray characteristics in the near-nozzle region using X-ray absorption". Atomization and Sprays, Vol. 11, No. 4, 2001, pp. 471-490.
13. Linne M., Paciaroni M., Hall T. and Parker T., "Ballistic imaging of the near field in a diesel spray". Experiments in Fluids, Vol. 40, No. 6, 2006, pp. 836-846.
14. Linne M.A., Paciaroni M., Gord J.R. and Meyer T.R., "Ballistic imaging of the liquid core for a steady jet in crossflow". Applied Optics, Vol. 44, No. 31, 2005, pp. 6627-6634.
15. Paciaroni M., Linne M., Hall T., Delplanque J.P. and Parker T., "Single-shot two-dimensional ballistic imaging of the liquid core in an atomizing spray". Atomization and Sprays, Vol. 16, No. 1, 2006, pp. 51-69.
16. Charalampous G., Hardalupas Y. and Taylor A.M.K.P., "Novel Technique for Measurements of Continuous Liquid Jet Core in an Atomizer". AIAA Journal, Vol. 47, No. 11, 2009, pp. 2605-2615.
17. Charalampous G., Hardalupas Y. and Taylor A.M.K.P., “3-Dimensional structure of the intact liquid jet core during coaxial air-blast atomisation”. Intern. Journal of Spray and Combustion Dynamics (IJSCD), Vol. 1, 2009, pp. 389-415.
18. Colladon D. "On the reflections of a ray of light inside a parabolic liquid stream". Comptes Rendus, Vol. 15, 1842, pp. 800-802.
19. Charalampous G, Hardalupas Y, Taylor A.M.K.P. “Numerical and experimental evaluation of the optical connectivity technique for measurement of liquid breakup length in atomizers”. Presented at 48th Aerospace Sciences Meeting & Exhibit, AIAA paper 2010-0200, 2010, Orlando, USA.
20. Charalampous G., Hadjiyiannis C., Hardalupas Y. and Taylor A.M.K.P. “Measurement of continuous liquid jet length in atomizers with optical connectivity, electrical conductivity and high-speed photography techniques”. In “Proceedings of 23rd Annual Conference on Liquid Atomization and Spray Systems, ILASS – Europe 2010”, paper 152, Brno, Czech Republic, 6-8 September 2010.
21. Less D.M. and Schertz J.A., “Transient behavior of liquid jets injected normal to a high-velocity gas stream”, AIAA J., Vol. 24, 1986, pp. 1979-1985.
22. Wu P.K., Kirkendall K.A., Fuller R.P. and Nejad A.S., “Breakup processes of liquid jets in subsonic crossflows”, J. Propul. Power, Vol. 13, 1997, pp. 64-73.
23. Aavani, K., Taeibi-Rahni, M., Soltani, M. R., Experiments in near-field of turbulent jets into a crossflow, Scientia Iranica, Vol. 13, No. 2, pp. 134-151.
24. Ghosh, S., and Hunt, J. C. R., Spray jets in a cross-flow, J. Fluid Mech., 1998, vol. 365, pp. 109-136.
25. Arienti M. and Soteriou M.C., "Time-resolved proper orthogonal decomposition of liquid jet dynamics", Physics Of Fluids, Vol. 21, 2009, 112104.
26. Ng C.-L., Sankarakrishnan R. and Sallam K.A., “Bag breakup of nonturbulent liquid jets in crossflow”, Int. J. Multiphase Flow, Vol. 34, 2008, 241.

27. Rachner, M., Becker, J., Hassa, C., Doerr, T., Modelling of the atomization of a plain liquid fuel jet in crossflow at gas turbine conditions, Aerospace Science and Technology, Vol. 6, 2002, pp. 495-506.

28. Sedarsky, D., Paciaroni, M., Berrocal, E., Petterson, P., Zelina, J., Gord, J., Linne, M., "Model validation image data for breakup of a liquid jet in crossflow: part I", Experiments in Fluids, Vol. 49, 2010, pp. 391-408.

29. Bai, B. F., Zhang, H. B., Liu, L., Sun, H. J., "Experimental study on turbulent mixing of spray droplets in crossflow", Experimental Thermal and Fluid Science, Vol. 33, 2009, pp. 1012-1020.

30. Balasubramanyam, M. S. and Chen, C. P., "Modeling liquid jet breakup in high speed cross-flow with finite-conductivity evaporation", International Journal of Heat and Mass Transfer, Vol. 51, 2008, pp. 3896-3905.

31. Fan, J. Y., Xu, S. L. and Wang, D. Z., “PDA measurements of two-phase flow structure and particle dispersion for a particle-laden jet in crossflow”, Journal of Hydrodynamics, Vol. 22, No. 1, 2010, pp. 9-18.

32. Hale, C. A., Plesniak, M. W. and Ramadhyani, S., “Structural features and surface heat transfer associated with a row of short-hole jets in crossflow”, International Journal of Heat and Fluid Flow, Vol. 21, 2000, pp. 542-553.

33. Barata, J. M. M., Durao, D. F. G., Heitor, M. V. and McGuirk, J. J., "The turbulence characteristics of a single impinging jet through a crossflow", Experimental Thermal and Fluid Science, Vol. 5, 1992, pp. 487-498.

34. Shedd, T. A., Corn, M. L., Cohen, J. M., Arienti, M. and Soteriou, M. C., "Liquid film formation by an impinging jet in a high-velocity air stream", Presented at 47th AIAA Aerospace Sciences Meeting Including the New Horizons Forum and Aerospace Exposition, AIAA 2009-0998, 2009, Orlando, USA.

35. Lee, J., Sallam, K. A., Lin, K.-C. and Carter, C. D., "Spray structure in near-injector region of aerated jet in subsonic crossflow", Presented at 46th AIAA Aerospace Sciences Meeting and Exhibit, AIAA 2008-1043, 2008.

36. Osta, A. and Sallam, K. A., "Effect of nozzle length/diameter ratio on the breakup of liquid jets in crossflow", Presented at 46th AIAA Aerospace Sciences Meeting and Exhibit AIAA 2008-1040, 2008.

37. Kihm, K. D., Kim, T. K. and Son, S. Y., "Visualization of high-speed gas jets and their airblast sprays of cross-injected liquid", Experiments in Fluids Vol. 27, 1999, pp. 102-106.

38. Lee, K., Aalburg, C., Diez, F. J. and Faeth, G. M., Sallam, K. A., “Primary breakup of turbulent round liquid jets in uniform crossflows”, AIAA Journal, Vol. 45, 2007, No. 8.

39. Sallam, K. A., Dai, Z. and Faeth, G. M., "Liquid breakup at the surface of turbulent round liquid jets in still gases", International Journal of Multiphase Flow, Vol. 28, 2002, pp. 427-449.

40. Sallam, K. A., Aalburg, C. and Faeth, G. M., Breakup of round nonturbulent liquid jets in gaseous crossflows, Presented at 41st Aerospace Sciences Meeting and Exhibit, AIAA 2003-1326, 2003, Reno, USA.

41. Geary E.L. and Margettes M.J., “Penetration of a High Velocity Gas Stream by a Water Jet”, Journal of Spacecraft, Vol. 6, No. 1, 1969, pp. 79-81.

42. Reichenbach P.R. and Horn K.P., “Investigation of Injectant Properties in Jet Penetration in a Supersonic Stream”, AIAA Journal, Vol. 9, No. 3, 1971, pp. 469-471.

43. Kush E.A. and Schetz J.A., “Liquid Jet Injection into a Supersonic Flow”, AIAA Journal, Vol. 11, No. 9, 1979, pp. 1223-1224.

44. Schetz J.A., Kush E.A. and Joshi P.B., “Wave Phenomena in Liquid Jet Breakup in a Supersonic Crossflow,” AIAA Journal, Vol. 15, 1979, pp. 774-778.

45. Nejad A.S. and Schetz J.A., “Effects of Properties and Location in the Plume on Droplet Diameter for Injection in a Supersonic Stream”, AIAA Journal, Vol. 21, No. 7, 1983, pp. 956-961.

46. Nejad A.S. and Schetz J.A., “Effects of Viscosity and Surface Tension on a Jet Plume in Supersonic Cross-Flow”, AIAA Journal, Vol. 22, No. 4, 1984, pp. 458-459.

List of Symbols, Abbreviations and Acronyms

D_L = inner diameter of the liquid jet nozzle
MFR = Liquid-to-Gas Momentum Flux ratio
Re_L = Reynolds number of liquid jet
We_L = Weber number based on liquid jet velocity
We_G = Weber number based on gas velocity
U_G = Average gaseous velocity of the cross stream
U_L = Average liquid velocity at the nozzle exit
μ = Kinematic viscosity of the liquid
ν_L = Dynamic Viscosity of the liquid
ρ_G or ρ_L = Density of gas or liquid
σ = Surface tension

PROGRESS REPORT

AWARD N°: FA8655-09-1-3036 1

TITLE: Novel laser-based technique for measurements of primary atomization characteristics of liquid jets

INVESTIGATOR: Professor Y. Hardalupas

ORGANISATION: Imperial College of Science, Technology and Medicine

REPORTING PERIOD: From: 20 January 2012 To: 19 July 2012

PROJECT START DATE: 20 July 2009

DATE OF ISSUE OF THIS REPORT: 21 July 2012

ADMINISTRATIVE OFFICE: European Office of Aerospace Research and Development (EOARD)

GOVERNMENT PROGRAM MANAGER: Dr. Gregg Abate

Table of Contents

List of Figures

Summary

During the first stages of atomization of an airblast atomizer, the liquid stream is destabilized under the influence of a stream of air, until its continuity is broken. The geometry of the injector affects the way that the liquid jet breaks up and understanding the physics of the primary atomization process is important for the control of the spatial and temporal spray characteristics downstream of the nozzle. A novel technique (Charalampous *et al.* 2007 (1)) has been proposed to measure the length of the continuous liquid jet, quantify the spatial and temporal characteristics of the instabilities along the liquid-gas interface and examine the way that the liquid breaks up to form droplets. This technique relies on the optical connectivity of a liquid jet when it is internally illuminated through the spray nozzle. The liquid jet acts as a light guide, which allows light to propagate along the length of the jet in the same way as light travels along an optical fiber. The laser light excites a fluorescent dye that is dissolved in the liquid jet, making the volume of the liquid jet luminous. Then, the connectivity of the liquid jet is linked to the optical connectivity of the fluorescent jet. However, since the optical characteristics of the liquid jet are not the same as those of an optical fiber, there are losses of light intensity due to refraction through the liquid-gas interface and absorption by the fluorescence dye, as it propagates along the liquid jet. Therefore, the applicability of the technique requires evaluation in different geometries of liquid jets.

During the current reporting period, three areas were addressed:

(a) Numerical evaluation of the optical connectivity technique for a jet in cross flow similar to the one studied experimentally.

(b) Testing of the cross flow atomizer, manufactured during the previous reporting period, and experimental evaluation of the applicability of the optical connectivity technique in liquid jets exposed to a cross stream of air.

(c) Comparison between numerical and experimental findings on the behaviour of liquid fluorescence intensity when applying the optical connectivity technique in liquid jets in cross-flow.

It should also be noted that a paper entitled “Numerical and experimental investigation of the optical connectivity technique in cross flow atomization” authored by G. Charalampous, C. Hadjiyiannis and Y. Hardalupas will be presented at the ICLASS 2012, 12th Triennial International Conference on Liquid Atomization and Spray Systems, Heidelberg, Germany, September 2-6, 2012. In addition, a paper related to the numerical evaluation of the technique has been submitted for journal publication and is under review.

1. Introduction

During the first stages of atomization of a liquid jet, the jet is progressively destabilized under the influence of the forces that result from the interaction of the liquid stream with the surrounding air [2; 3]. During this process the jet geometry changes as liquid is removed from its surface and waves develop on the surface until their amplitude becomes large enough to lead to breakup of the liquid jet. The distance from the nozzle exit to the point downstream the nozzle, where the liquid jet breaks up defines what is known as the “primary atomization region”. The length of the continuous core of the liquid jet, known as the “breakup length”, determines the extent of the primary atomization region and the performance of atomizing nozzles.

A number of techniques have been proposed for the measurement of the length of the continuous jet. These include photography [4; 5], electrical conductivity (6-9), X-ray absorption [10-12] and ballistic imaging [13-15]. A recently proposed method is the optical connectivity technique [1]. It has been shown that, in dense sprays, the optical connectivity technique can measure the breakup length of the liquid jet at conditions where the continuous length of the jet is difficult to measure with photography, as the atomization products that surround the jet hinder the view to the continuous jet.

Photography (usually shadowgraphy) is the most commonly used method, as it is straightforward to apply and places only moderate demands on equipment. In this method, the atomizing jet is imaged directly by a camera. A light source illuminates the liquid jet and is usually placed on the opposite side of the camera to allow the light to propagate through the liquid jet. In this way, the shadow of the jet is imaged and its contour is well defined in the acquired images. The break-up length is estimated from the geometry of the recorded contour. While this method is easy to implement, when atomization becomes more intense, the droplets around the jet core might obstruct parts of the jet and the break-up length may be measured longer than its real value.

The electrical conductivity technique is based on the conduction of electricity along the length of a continuous liquid jet downstream the nozzle exit. A potential is applied between the atomizer nozzle and a probe downstream. If there is continuity of the liquid phase between the nozzle and the probe, a closed electrical circuit will ensue. The probe can be moved across different positions to determine the continuity of the liquid jet as a function of downstream distance. If the detected potential is low it is verified that there is electrical connectivity up to a specific point indicating continuity of the liquid jet core. On the contrary, the discontinuity of the liquid jet can be located where the conductivity is negligible. In earlier work, many researchers developed a conductivity probe technique to enable the investigation of the breakup zone in a variety of applications. Yule and Salters [8] investigated the breakup zone of a transient diesel spray as a function of time and position employing a wire probe. Hiroyasu et al [7, 9] studied the breakup length of a high-speed liquid jet by measuring an electrical resistance between the nozzle and a fine wire screen detector located in a spray jet. Chehroudi et al. [6] tried to determine the shape and length of the intact liquid core by applying a voltage between the nozzle unit and fine needles, rods and screens. The results show that current is carried not only by intact liquid cores but also by atomized unconnected sprays.

The novel optical connectivity technique [16, 17] relies on illuminating a liquid jet from within the nozzle by a laser beam, which propagates downstream, while reflecting at the gas-liquid interface. Due to the higher index of refraction of the liquid jet to that of the surrounding gas, a

laser light ray that interacts with the gas-liquid interface at a sufficiently large incident angle undergoes total internal reflection. As a consequence, the laser beam is reflected completely back into the liquid stream and propagates downstream for a long distance in the same way that light propagates along optical fibers. Collandon [18] demonstrated this phenomenon as early as 1842. The addition of a fluorescent dye, such a Rhodamine WT in the liquid jet, causes some of the intensity of the laser beam to be absorbed and re-emitted at a longer wavelength as fluorescence. This causes the volume of the continuous jet to become luminous, which allows the evaluation of the break-up length. Beyond the point of liquid discontinuity, the laser beam is diffused and its intensity is significantly reduced. The optical connectivity technique is not without limitations. As the technique is based on the propagation of light within an atomizing liquid jet, there will unavoidably be some scattering losses at the gas-liquid interface that will reduce the intensity of the propagating light. Therefore, for long liquid jets, the technique will not be possible to operate due to complete attenuation of the propagating light along the liquid before the break up point. Therefore, a numerical model of light propagation along a liquid jet was developed to determine how the laser light that is seeded at the base of the jet propagates along its length and what are the effects of its geometry on the losses of the intensity of the laser light.

During the first year of the current project, measurements of break-up length of a liquid jet in an airblast coaxial atomizer were obtained with the optical connectivity technique, the electrical connectivity and high-speed photography. The results from the three measurement techniques were compared and advantages and limitations of the optical connectivity technique were identified [19, 20].

In the second year, the emphasis was directed in two directions: (a) the development of time-dependent optical connectivity technique and its application to the measurement of the temporal and spatial characteristics of the gas-liquid interface and the breakup length of a liquid jet in a coaxial airblast atomizer; (b) the applicability of the optical connectivity technique in liquid jets exposed to a cross stream flow of gas.

In the last reporting period the experimental investigation of cross flow atomization was initiated. First the cross flow atomizer was manufactured and installed. The operation of the new experimental arrangement was tested to ensure its functionality. Next the suitability of the optical connectivity technique was examined for jets in a cross flow.

In the current reporting period a systematic examination of the optical connectivity technique is performed (a) numerically so that a systematic evaluation of the atomizing jet geometry on the performance of optical connectivity is performed and (b) a systematic experimental evaluation of optical connectivity for jets in cross flow is performed.

The next section presents the numerical evaluation of optical connectivity in cross flow. The third section presents and discusses the experimental application of optical connectivity in cross flow. The report ends with a summary of the main achievements.

2. Principle of Optical Connectivity Technique

An optical connectivity technique has been developed for the measurement of the continuous length of liquid jets during the atomization process in atomizers. The technique works by introducing a laser beam within the flow of the liquid upstream of the nozzle that exits with the liquid through the nozzle in the direction parallel to the nozzle axis. In this way the laser beam is largely contained within the liquid jet by reflecting on the liquid interface propagating downstream and illuminating the liquid jet volume. A ray of laser light is guided along the length of the liquid jet by reflecting on the gas-liquid interface at the jet surface. As long as the angle of incidence between the surface of the jet and the laser light rays is greater then the angle of total internal reflection, the rays are completely reflected back inside the liquid without intensity losses from refraction. This principle is similar to the way that a laser beam propagates within an optical fiber. However, if the angle of incidence of a laser light ray on the liquid jet interface becomes smaller than that for total internal reflection then there will be some intensity losses due to refraction.

The laser beam continues to propagate downstream the jet until it meets the breaking point of liquid jet, where it can no longer be contained within the jet and is diffused randomly in different directions. The introduction of a fluorescing dye into the liquid makes part of the laser beam to be absorbed along the length of the liquid jet, and subsequently be re-emitted as fluorescence. In this way the atomizing jet becomes luminous and can be imaged (**Figure 1**).

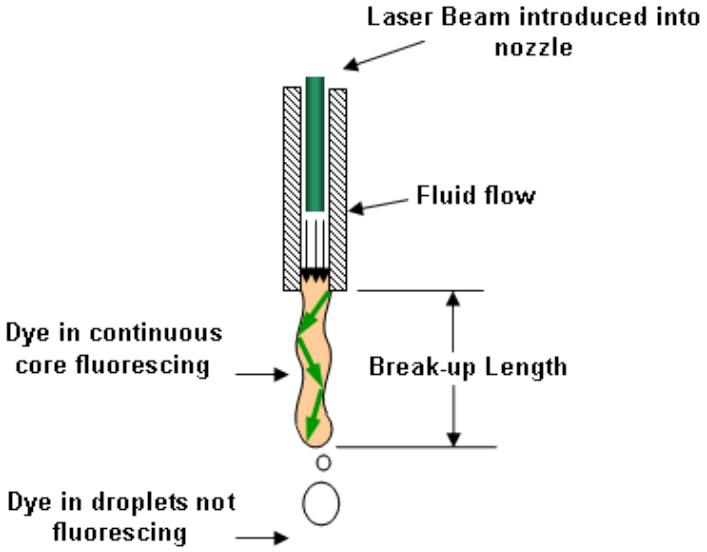

Figure 1 Principle of the optical connectivity technique

An example of the instantaneous image of a highly magnified liquid jet, illuminated by a laser beam according to the principle of the optical connectivity technique, is presented in **Figure 2**. The ability to detect the instabilities along the surface of the interface of liquid jet can be identified.

(a) (b)

Figure 2 (a) Example instantaneous image of a liquid jet obtained from the optical connectivity technique. (b) The image of (a) after image processing, which indicates the intact length of the liquid jet and the instabilities along the gas-liquid interface of the liquid jet.

3 Numerical evaluation of the performance of optical connectivity in liquid jet in cross flow of air.

A numerical simulation of the laser beam propagation within the liquid jet can evaluate the effect of influencing parameters independently on the performance of the optical connectivity technique. Such experimental investigation is difficult to realise.

3.1 Numerical method

The liquid column interface is described by a sinusoidal function along the X-axis of a Cartesian coordinate system:

$$Y = G \cdot \sin\left(\frac{2\pi X}{\lambda}\right) + a \cdot \left(\frac{X}{50}\right)^2 + y_0 \qquad (1)$$

where G is the amplitude of the wave on the interface and λ is the wavelength of the wave on the surface of the column. The offset in the equation is the distance that the liquid interface is displaced from the central axis coordinate system at the base of the column. By considering an offset of 0.5 and -0.5 for the top and bottom boundaries respectively, the base of the liquid column is unity. The inclination of the jet relative to the X-axis is controlled by parameter α. When α is zero the liquid is a 'straight' column. For $\alpha \neq 0$, a quadratic deflection is introduced on the column centreline, which increases with increasing α.

The laser beam that propagates inside the liquid column is simulated using a large number of rays that start at the base of the jet and propagate downstream the nozzle exit. The rays are not always parallel to the X-axis but can diverge to account for the divergence of the laser beam. The rays interacting with the interface are reflected back at an angle that is equal to the angle of incidence (**Figure 4**). An example of the path of the rays inside 'straight' and 'inclined' columns with similar geometrical characteristics is presented in **Figure 3**, which demonstrates the influence of the inclination of the liquid jet.

a)

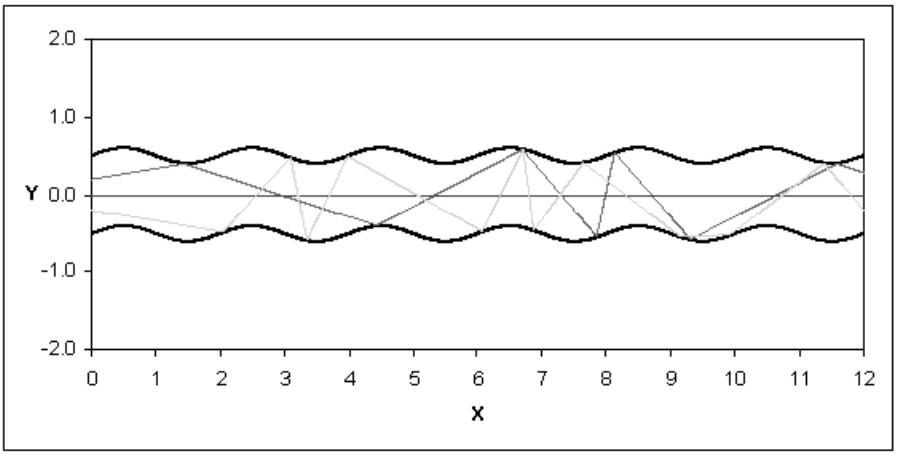

b)

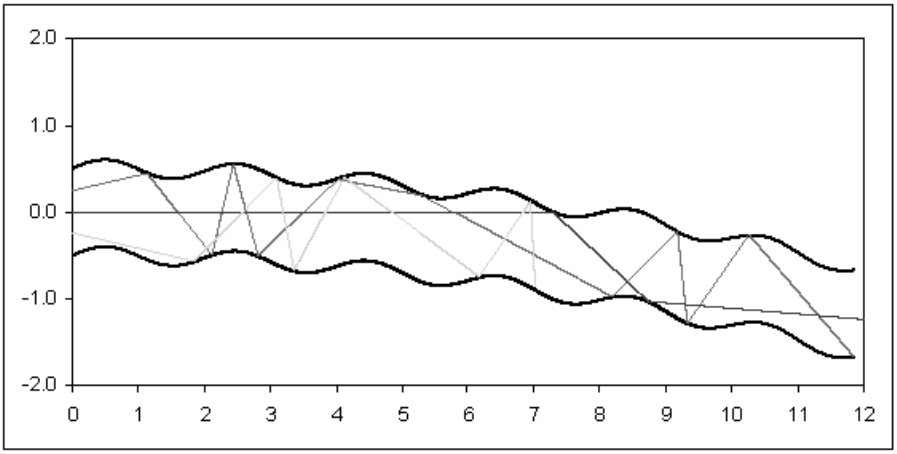

Figure 3: Example of propagation of light rays within a) 'straight' and b) 'inclined' liquid column, as determined by ray tracing.

When the angle of incidence is greater than the angle of total internal reflection:

$$\theta_{crit} = \sin^{-1}\left(\frac{n_2}{n_1}\right) \tag{2}$$

where n_1, n_2 the refractive indices of the liquid and the gas phases, the beam is completely reflected back inside the liquid at an angle that is equal to the angle of incidence. However, if the angle of incidence becomes smaller than that for total internal reflection, some of the laser light escapes through refraction at an angle determined by Snell's law:

$$\frac{\sin\theta_1}{\sin\theta_2} = \frac{n_2}{n_1} \tag{3}$$

where θ_1 is the angle of incidence on the surface and θ_2 is the angle of refraction (**Figure 4**). In this case the intensity of the laser beam within the liquid jet decreases.

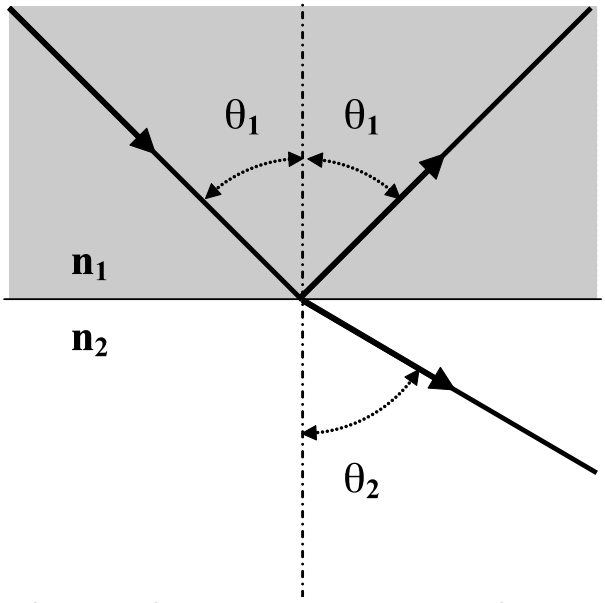

Figure 4: Reflection and refraction of a ray incident on the interface at an angle θ_1.

As the rays propagate inside the liquid column, the initial intensity of each beam I_0 is reduced due to absorption of light by the fluorescent dye in the liquid and refraction of light at the liquid interface when the angle of incidence of the rays on the surface of the column is smaller than the critical angle for total internal reflection. The reduction of the intensity of the rays due to the absorption caused by the medium through which the ray is travelling is estimated by the Beer-Lambert law:

$$I = I_0 e^{-\gamma z} \tag{4}$$

where γ is the absorption coefficient, z the distance travelled by the ray, I_0 is the initial intensity of the ray and I the intensity of the ray after it has travelled a distance z in the absorbing medium.

The Fresnel equations are used to calculate the fraction of the incident ray intensity R that is reflected back into the liquid. The Fresnel coefficients depend on the polarisation of the incident ray. If the electric field of light is perpendicular to the plane of incidence, the reflection coefficient is:

$$R_s = \left[\frac{\sin\left(\theta_1 - \theta_2\right)}{\sin\left(\theta_1 + \theta_2\right)}\right]^2 \tag{5}$$

If the electric field of light is parallel to the plane of incidence, the reflection coefficient R is:

$$R_p = \left[\frac{\tan\left(\theta_1 - \theta_2\right)}{\tan\left(\theta_1 + \theta_2\right)}\right]^2 \tag{6}$$

and the overall reflectance R is equal to the mean of R_s and R_p.

$$R = \frac{R_p + R_s}{2} \tag{7}$$

The conditions under which the numerical simulations were performed are summarised in the table below. The absorption cross section of the liquid was deliberately chosen to be small, in order to avoid considerable decrease of the fluorescent intensity close to the base of the column due to absorption.

Table 1: Numerical simulation parameters	
n_1	1.33
n_2	1.0
λ	0.5, 1.0, 2.0
G	0.1
α	0, 10, 20, 30
Divergence	0°, 10°
γ	0.0001

3.2 Numerical results

From the numerical calculations of the ray propagation and absorption within the liquid column, the fluorescent intensity along the length of the column was calculated by integrating the amount of absorbed light intensity across the transverse (Y-axis) cross-section of the column. The fluorescent intensity was considered to be directly proportional to the absorbed light.

From the fluorescent intensity profiles presented in **Figure 5**, a number of significant differences in the evolution of fluorescent intensity can be observed that depend on the column geometry and the divergence of the laser beam. The most profound effects on the distribution of fluorescent intensity along the column length are a consequence of the divergence of the laser beam. When the beam is collimated (**Figure 5**a-c), the fluorescent intensity along the liquid column is initially exhibiting an exponential decrease. After some distance from the column base, the decrease of the fluorescent intensity follows a parabolic function. This pattern persists until the fluorescent intensity of the column becomes minimal. From this point on, the fluorescent intensity decrease follows an exponential function. Also, there is significant differentiation of the fluorescent intensity profiles with respect to the amount of deflection from the centreline, as greater amounts of deflection cause the fluorescent intensity emitted from the liquid column to decrease more rapidly with distance from the column base.

In contrast to the case of the collimated beam, when the light rays are diverging, the fluorescent intensity along the length of the liquid column decreases according to an exponential fashion (**Figure 5**d-f) for the entire length of the column. In addition, in the presence of laser beam divergence, the differences between the fluorescent intensity profiles of jets become largely independent of the amount of inclination of the column.

The development of the fluorescent intensity profile can be interpreted in terms of the propagation of the light rays in the column. In the case of a collimated beam in a straight column, only a few of the rays impinge on the interfacial waves close to the base of the column. Some of them impinge at angles that are smaller than the angle for total internal reflection and immediately scatter outside the column, resulting in some immediate losses of laser light while the rest propagate further along the liquid column and scatter gradually. This is the mechanism that is responsible for the initial exponential decay of fluorescent intensity. The wavelength of the surface instability plays a significant role here. Shorter waves cause the exponential decay to develop within a short distance from the column base as the rougher interface makes it more likely that the rays will impinge of the column surface at an angle that is smaller than the angle of total internal reflection and scatter. Longer wavelengths of surface instabilities make it more likely that the non-diverging rays will interact with the smoother surface at an angle that is greater than the angle for total internal reflection and continue to propagate along a greater distance of the initial length of the column. In the case of the non-deflected column, past the initial fluorescent intensity decrease there are no more significant losses since the absorption due to the fluorescent dye is small and the rays do not further interact with the interface. In this case, the fluorescent intensity along the remaining column length is uniform. This is also the case for instability wavelength λ=2.0, although the initial decrease of the fluorescent intensity is not complete within the examined length and cannot be seen in **Figure 5**. When the column is deflected, there is a transition from the initially exponential fluorescent intensity decay to a parabolic intensity decay. The decrease becomes more profound as the deflection of the column increases. This is because a significant number of parallel rays, which impinge on the liquid interface at angles of incidence smaller than the angle for total internal reflection and, therefore, there is a rapid loss of intensity due to refraction.

The observations change considerably when the rays at the base of the column are diverging. Because of the divergence of the rays, many of them interact with the liquid interface at angles that are less than the angle for total internal reflection. This causes rapid fluorescent intensity losses close to the base of the column, which persist along the rest of its length. Even for straight columns, there is a continuous decrease of the fluorescent intensity along the column length. However, the variance in the direction of the ray causes the fluorescent intensity along the column length to become largely insensitive to the instability wavelength and the deflection of the column. In fact, for this reason, the fluorescent intensity at the end of the column is greater for the more deflected columns when the rays are divergent than collimated.

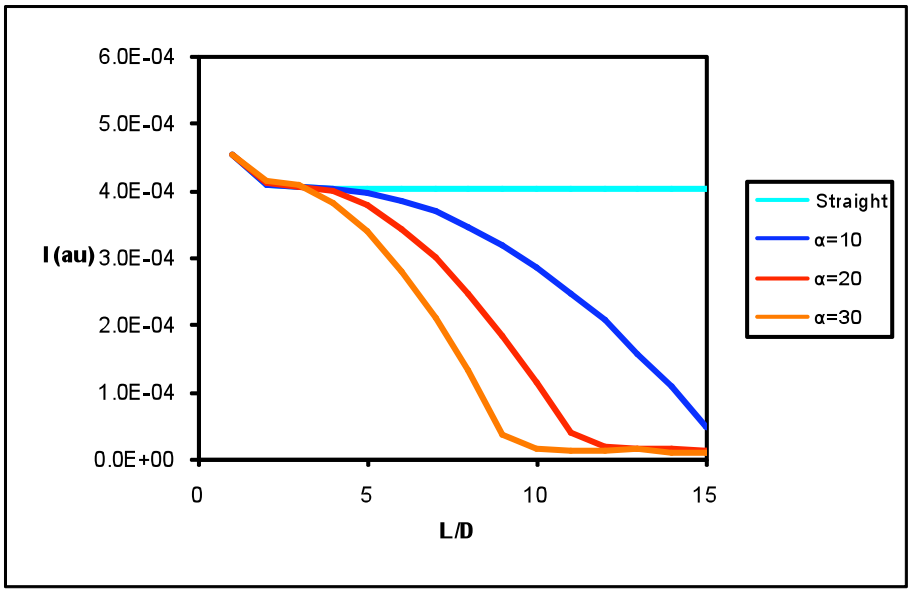

a) G=0.1, λ=0.5, γ=0.0001, no laser beam divergence

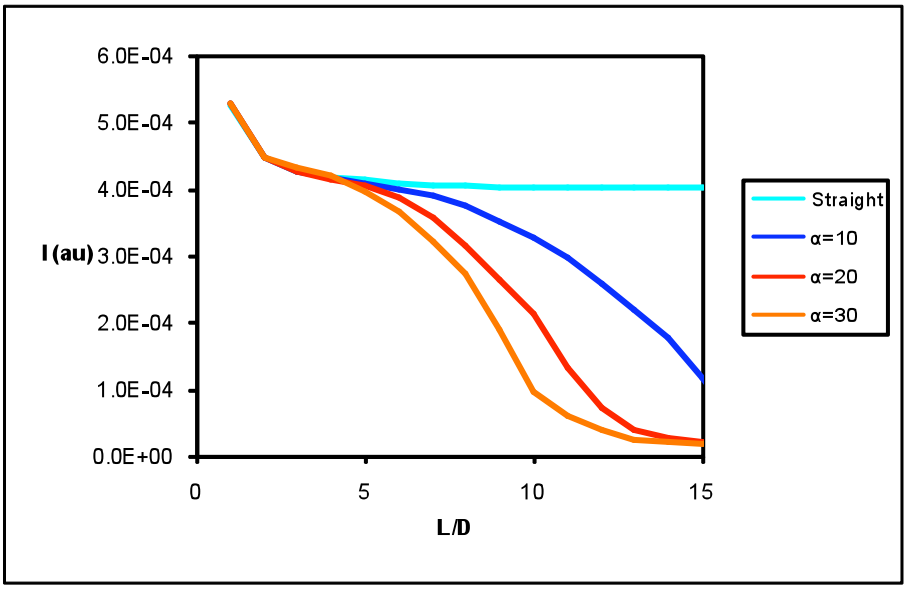

b) G=0.1, λ=1.0, γ=0.0001, no laser beam divergence

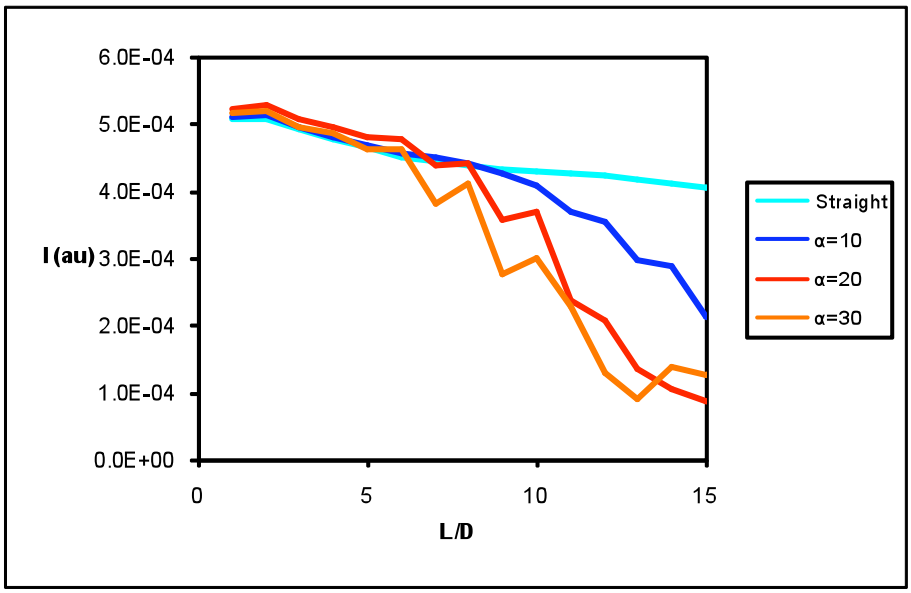

c) G=0.1, λ=2.0, γ=0.0001, no laser beam divergence

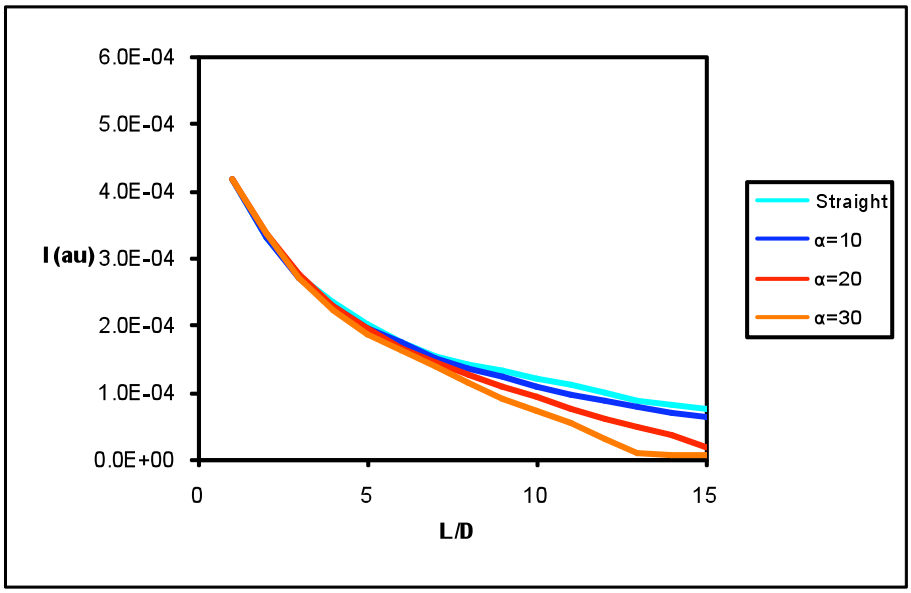

d) G=0.1, λ=0.5, γ=0.0001, 10° laser beam divergence

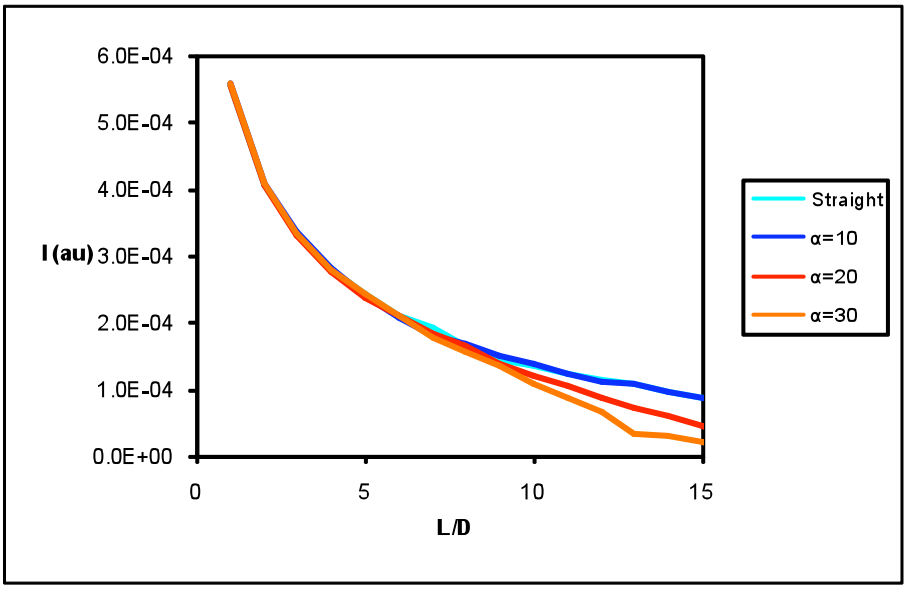

e) G=0.1, λ=1.0, γ=0.0001, 10° laser beam divergence

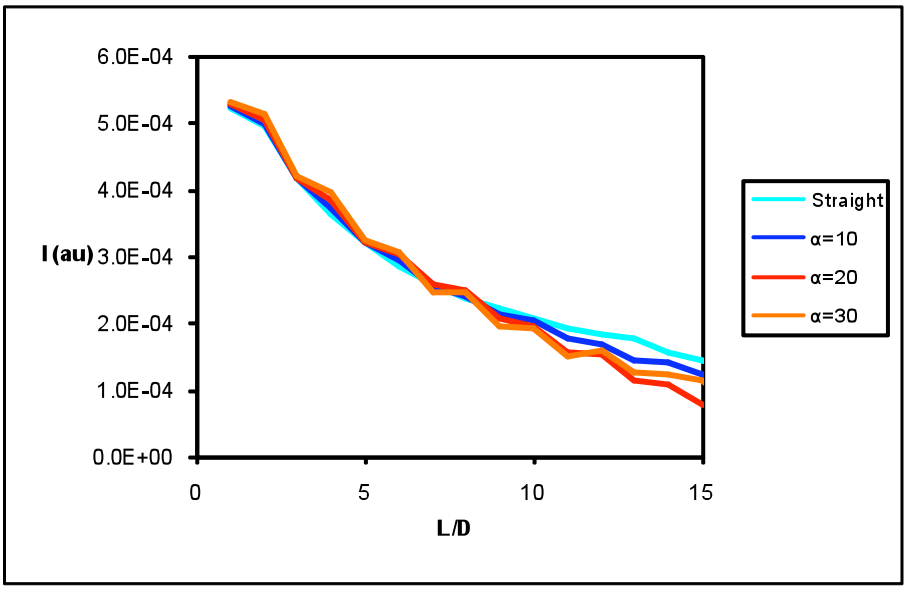

f) G=0.1, λ=2.0, γ=0.0001, 10° laser beam divergence

Figure 5: Numerically calculated profiles of fluorescent intensity along the length of straight and inclined liquid columns. The length L from the nozzle exit is normalised by the initial dimension D of the liquid jet.

4 Experimental study of a liquid jet in a cross stream of air

4.1 Experimental arrangement

For the experimental investigation, a cross-flow air-blast atomizer was used that was specifically designed to accommodate optical connectivity. The design of the cross flow atomiser was discussed in detail in the report of the previous reporting period. A summary is provided here.

The schematic of the cross section of the atomiser is presented in **Figure 6**. The air flow was supplied by four inlets at the far end of a cylindrical plenum chamber (9). The chamber was closed at the far end by a plate (7) and, at the other side, it was connected to a contraction (3) of 38mm exit diameter that accelerated the air flow. The contraction ended in a straight nozzle (1), which was extended by a straight quartz tube (8). The quartz tube contained the air flow stream and, in addition, allowed optical access to the flow. It is within the length of the quartz tube that the atomization of the liquid jet takes place and can be studied, while the surrounding air flow velocity remains constant. The assembly of the above components comprised the main body of the atomiser.

The atomizing liquid was delivered by a long straight steel tube of circular cross-section (2) with 8mm external diameter. The tube was supported along the centreline of the atomiser main body. One end (6) of the tube was connected to the liquid supply, while the other end was closed. A circular hole was drilled at the side of the tube normal to the tube centreline at the start of the transparent nozzle (**Figure 6**, detail). In this way, a liquid jet could be injected normal to the air flow within the bounds of the transparent nozzle. The annular gap between the central tube and the quartz tube was 15mm. For the implementation of the optical connectivity technique, an optical window (14) was placed on the liquid delivery tube immediately opposite to the liquid exit, as shown in the detail at bottom right of **Figure 6**. In combination with the transparent straight nozzle of the air flow, direct optical access was obtained at the back of the liquid injection orifice, so that a laser beam can be directed into the liquid jet and the optical connectivity technique applied.

The atomized liquid was water, doped with Rhodamine WT fluorescing dye. The fluorescent dye was excited by the second harmonic of a Nd:YAG laser beam at 532nm. The laser beam was focused on the optical window behind the liquid nozzle exit, so that some of the laser light was transmitted through the nozzle and into the liquid jet. The fluorescent intensity images emitted by the liquid jet were recorded by a 12-bit PCO sensicam QE CCD camera. The camera lens was fitted with an OG590 optical filter, which suppresses the scattered light at 532nm but allows transmission of the red-shifted fluorescence spectrum of the dye.

The considered flow conditions are summarized in **Table 2** below. The relevant parameter that characterizes the behaviour of the liquid jet is the momentum flux ratio

$$MFR = \frac{\rho_L U_L^2}{\rho_G U_G^2} \tag{13}$$

Increase of MFR leads to increase of jet penetration, which delays the breakup of the liquid column into large fragments and enhances the stripping-off of fine droplets from the liquid jet surface. However, both breakup mechanism of the liquid jet are present at variable degree at

the same time depending on the value of the MFR. Some additional relevant parameters for the characterization of the behaviour of the liquid jet are:

Weber number, based on the gas velocity

$$We_G = \frac{\rho_G U_G^2 D_L}{\sigma} \tag{14}$$

Reynolds number of liquid jet

$$\mathrm{Re}_L = \frac{U_L D_L}{\nu_L} \tag{16}$$

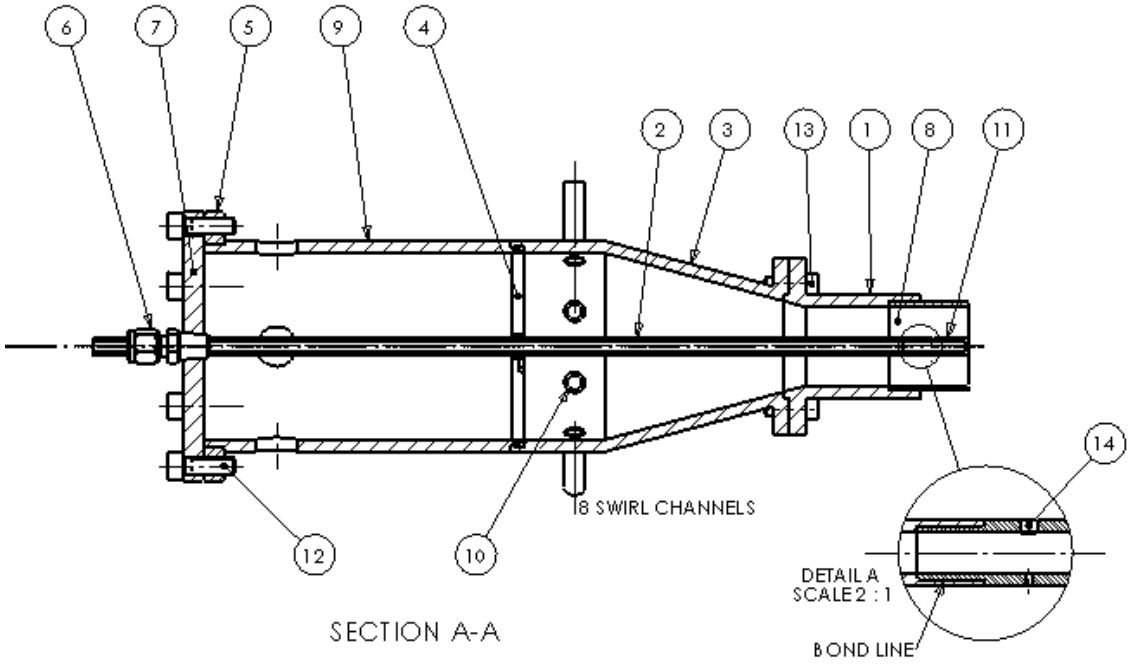

Figure 6: Schematic of atomizer of liquid jet exposed to a cross stream of air. Detail at bottom right shows design of liquid nozzle exit and optical window.

The chosen air and liquid velocities were a compromise between introducing sufficient deflection on the liquid jet to avoid impingement of the jet on the quartz tube wall and simultaneously preventing filming along the length of the liquid delivery tube. In total 10 flow conditions were considered and for all flow conditions 500 image samples were acquired.

Table 2: Flow conditions

U_{Liquid}	U_{Gas}	Re	We	U_{Liquid}	U_{Gas}	Re	We
m/s	m/s			m/s	m/s		
2.1	21.5	1895	7.7	3.2	27.7	2842	12.8
2.1	24.6	1895	10.1	3.2	30.8	2842	15.8
2.1	27.7	1895	12.8	3.2	33.8	2842	19.1
2.1	30.8	1895	15.8	3.2	36.9	2842	22.7
2.1	33.8	1895	19.1	3.2	40.0	2842	26.7

4.2 Experimental results

The results focus on the development of the mean fluorescent intensity across the liquid jet length as it can be compared with the numerical results. Despite the difference between the infinite length jet that was considered in the numerical investigation and the finite length jet of the experimental investigation which is limited by both the height of the annular gap in which the jet develops, which is 15 jet diameters here, and the breakup of the jet due to atomisation the general conclusions of the former investigation can be applied to the latter.

The images of the mean fluorescent intensities along the jet core in **Figure 7** and **Figure 8** show that the deflected jets can be visualised for a considerable length even in cases where the deflection of the jet reaches almost 90°. However, the inclination of the jet imposes some limitations on the propagation of the illuminating laser light through the jet volume. The most apparent effect of inclination is that the fluorescent intensity of the jet is not uniform throughout the jet volume. Close to the point of maximum inflection of the jet, the fluorescent intensity is always increased along an oblique line through the jet. This is significant since the images shown in the figures represent the mean intensity of 500 samples. Therefore, this intensity distribution is not a coincidental occurrence but a temporally persistent characteristic of the jet visualisation that prevails over the particular details of the individual image samples. It can be explained by considering that the illuminating beam is deflected on the curved interface at certain angles that depend on the inclination of the jet. In this case, much of the reflected light is concentrated along a narrow strip of the jet increasing the local fluorescent intensity.

From the mean intensity images of the jet, the mean fluorescent intensity profiles are calculated by evaluating the mean fluorescent intensity along the jet cross-section and presented in **Figure 10**. Comparison with the profiles of **Figure 5** shows that there are some differences, which can be attributed to the more complex geometry of real jets. Nevertheless, the experimental observations can be explained in the same way as the results of the numerical simulation.

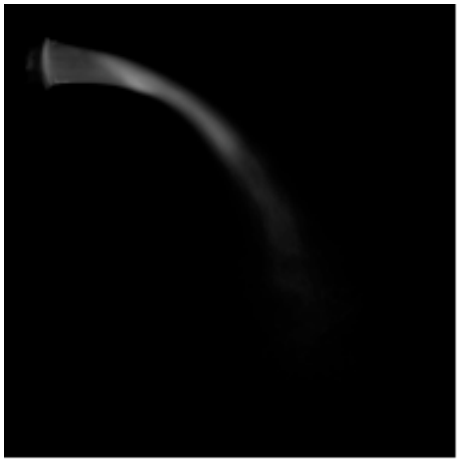

a) Re=1895, We=7.7

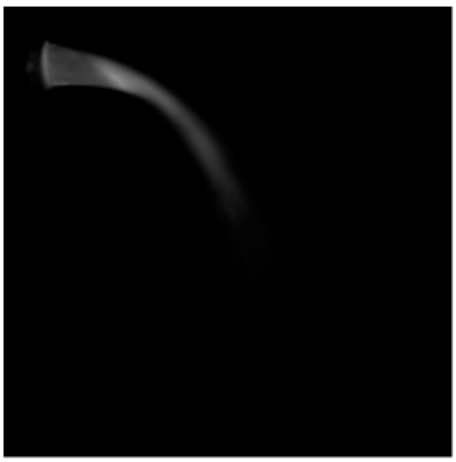

b) Re=1895, We=10.1

c) Re=1895, We=12.8

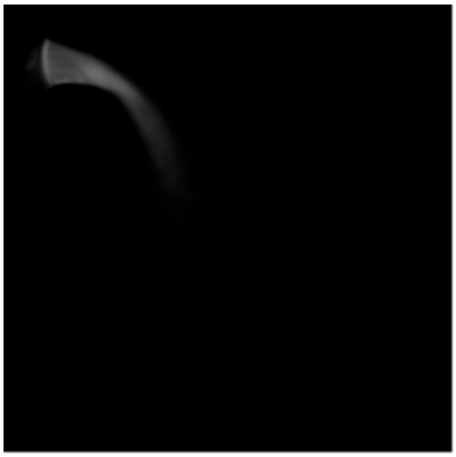

d) Re=1895, We=15.8

e) Re=1895, We=19.1

Figure 7: Experimentally measured mean fluorescent intensity emitted by the liquid jet for Re=1895.

a) Re=2842, We=12.8

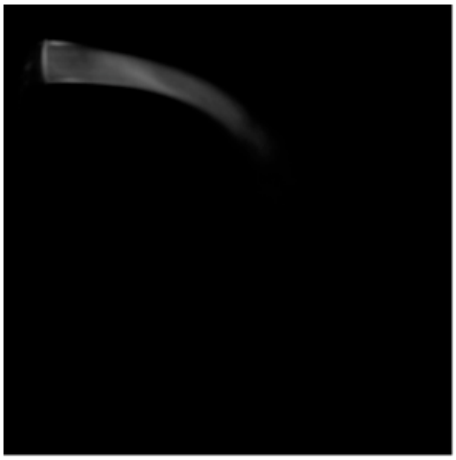

b) Re=2842, We=15.8

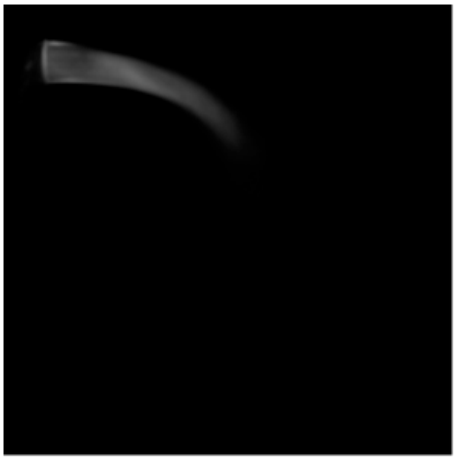

c) Re=2842, We=19.1

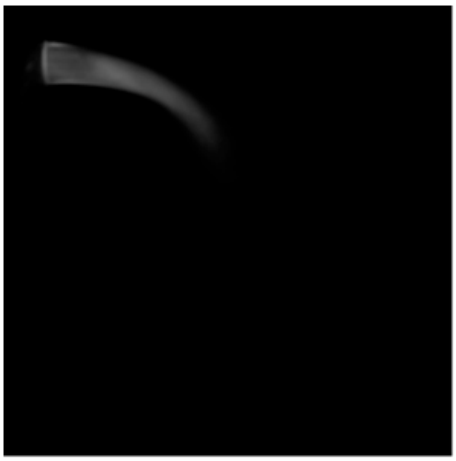

d) Re=2842, We=22.7

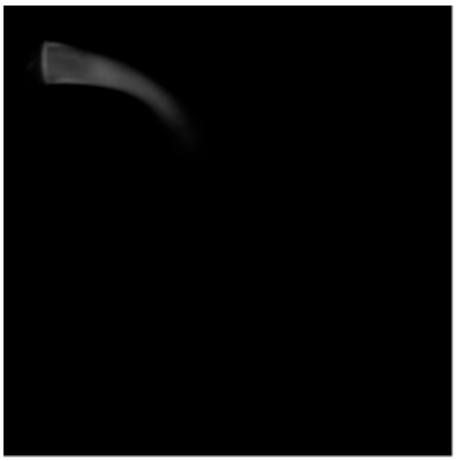

e) Re=2842, We=26.7

Figure 8: Experimentally measured mean fluorescent intensity emitted by the liquid jet for Re=2842.

The initial development of the fluorescent intensity profile shows an increase of the fluorescent intensity, which peaks at the point of maximum jet inflection. After this point an exponential decrease of the fluorescent intensity follows for the remaining length of the jet. While the fluorescent intensity profiles do not overlap with each other, it can be observed that with the exemption of Re=1896, We=7.7 in all other cases the rate of decrease of the fluorescent intensity is almost identical. This suggests that the laser light losses of the illuminating laser beam become independent of the details of the jet geometry. As before, this can be explained by a considerable number of rays from the illuminating beam interacting with the interface at angles that are less than the angle for total internal reflection, which is in agreement with the numerical simulations as it is unlikely that the illuminating beam in our experimental implementation is collimated at the base of the jet.

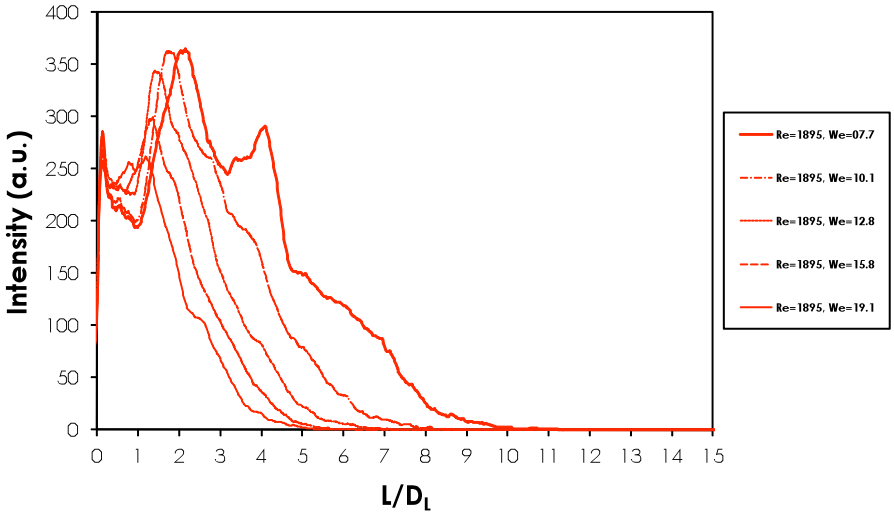

a)

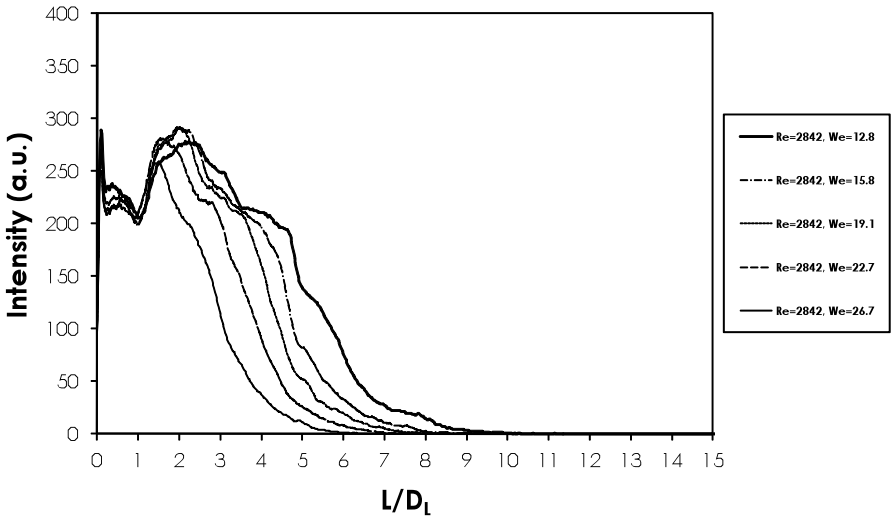

b)

Figure 10: Cross-section averaged fluorescent intensity profiles of the liquid jet for a) Re=1895 and b) Re=2842

It should be noted that the visualized liquid jets of **Figures 7 and 8** all become thinner as they approach at the breakup point. This occurs because the shape of the liquid jet becomes more like a liquid sheet, as it gets deflected by the air stream.

5. Summary

The research during the current period of the project contributed to two areas.

(a) The numerical investigation of the application of the optical connectivity to study the atomization of liquid jets exposed to cross flow of air.

(b) The experimental investigation of the application of the optical connectivity to study the primary atomization exposed to a cross flow of air in the experimental facility that was designed and manufactured at the previous reporting period of the project.

The findings are summarized below.

(a) The numerical investigation revealed that:

1. The fluorescent intensity profiles along the liquid column length are highly sensitive to the divergence of the illuminating laser beam.
2. The wavelength and deflection of the jet had a significant effect on the fluorescent intensity profiles only for a collimated illuminating laser beam.

(b) From the experimental investigation, it was found that:

1. The fluorescent intensity is not uniformly emitted throughout the volume of the jet but a fluorescent intensity maximum exists at the point of maximum jet inflection.
2. The rate of decay of the fluorescent intensity along the length of the jet is similar among the jets regardless of the length of the jet, which suggests that, after the jet maximum inflection, there are considerable losses of the illuminating beam due to refraction through the liquid-air interface.

6. References

1. Charalampous, G., Hardalupas, Y., and Taylor, A. M. K. P., "A novel technique for measurements of the intact liquid jet core in a coaxial airblast atomizer," *45th AIAA Aerospace Sciences Meeting and Exhibit, AIAA 2007-1337*, Reno, USA 2007.
2. Lefebvre A.H., Atomization and sprays, Hemisphere Publishing Corporation 1989.
3. Lasheras J.C. and Hopfinger E.J., "Liquid jet instability and atomization in a coaxial gas stream". Annual Review of Fluid Mechanics, Vol. 32, 2000, pp. 275-308.
4. Engelbert C., Hardalupas Y. and Whitelaw J.H., "Breakup Phenomena in Coaxial Airblast Atomizers". Proceedings of the Royal Society of London Series A-Mathematical and Physical Sciences, Vol. 451, No. 1941, 1995, pp. 189-229.
5. Varga C.M., Lasheras J.C. and Hopfinger E.J., "Initial breakup of a small-diameter liquid jet by a high-speed gas stream". Journal of Fluid Mechanics, Vol. 497, 2003, pp. 405-434.
6. Chehroudi B., Chen S.H. and Bracco F.V., "On the intact core of full-cone sprays". SAE Technical Papers 850126, 1985.

7. Hiroyasu H., Arai M. and Shimizu M., "Break-up length of a liquid jet and internal flow in a nozzle". ICLASS-91. 1991.

8. Yule A.J. and Salters D.G., "A Conductivity Probe Technique for Investigating the Breakup of Diesel Sprays". Atomization and Sprays, Vol. 4, No. 1, 1994, pp. 41-63.

9. Hiroyasu H., Shimizu M. and Arai M., "The breakup of high speed jet in a high pressure gaseous atmosphere". ICLASS-82, 1982.

10. Cai W.Y., Powell C.F., Yue Y., Narayanan S., Wang J., Tate M.W., Renzi M.J., Ercan A., Fontes E. and Gruner S.M., "Quantitative analysis of highly transient fuel sprays by time-resolved x-radiography". Applied Physics Letters, Vol. 83, No. 8, 2003, pp. 1671-1673.

11. Renzi M.J., Tate M.W., Ercan A., Gruner S.M., Fontes E., Powell C.F., MacPhee A.G., Narayanan S., Wang J., Yue Y. and Cuenca R., "Pixel array detectors for time resolved radiography (invited)". Review of Scientific Instruments, Vol. 73, No. 3, 2002, pp. 1621-1624.

12. Yue Y., Powell C.F., Poola R., Wang J. and Schaller J.K., "Quantitative measurements of diesel fuel spray characteristics in the near-nozzle region using X-ray absorption". Atomization and Sprays, Vol. 11, No. 4, 2001, pp. 471-490.

13. Linne M., Paciaroni M., Hall T. and Parker T., "Ballistic imaging of the near field in a diesel spray". Experiments in Fluids, Vol. 40, No. 6, 2006, pp. 836-846.

14. Linne M.A., Paciaroni M., Gord J.R. and Meyer T.R., "Ballistic imaging of the liquid core for a steady jet in crossflow". Applied Optics, Vol. 44, No. 31, 2005, pp. 6627-6634.

15. Paciaroni M., Linne M., Hall T., Delplanque J.P. and Parker T., "Single-shot two-dimensional ballistic imaging of the liquid core in an atomizing spray". Atomization and Sprays, Vol. 16, No. 1, 2006, pp. 51-69.

16. Charalampous G., Hardalupas Y. and Taylor A.M.K.P., "Novel Technique for Measurements of Continuous Liquid Jet Core in an Atomizer". AIAA Journal, Vol. 47, No. 11, 2009, pp. 2605-2615.

17. Charalampous G., Hardalupas Y. and Taylor A.M.K.P., “3-Dimensional structure of the intact liquid jet core during coaxial air-blast atomisation”. Intern. Journal of Spray and Combustion Dynamics (IJSCD), Vol. 1, 2009, pp. 389-415.

18. Colladon D. "On the reflections of a ray of light inside a parabolic liquid stream". Comptes Rendus, Vol. 15, 1842, pp. 800-802.

19. Charalampous G, Hardalupas Y, Taylor A.M.K.P. (2010) “Numerical and experimental evaluation of the optical connectivity technique for measurement of liquid breakup length in atomizers”. Presented at 48th Aerospace Sciences Meeting & Exhibit, AIAA paper 2010-0200, AIAA, Washington, 2010.

20. Charalampous G., Hadjiyiannis C., Hardalupas Y. and Taylor A.M.K.P. (2010) “Measurement of continuous liquid jet length in atomizers with optical connectivity, electrical conductivity and high-speed photography techniques”. In “Proceedings of 23rd Annual Conference on Liquid Atomization and Spray Systems, ILASS – Europe 2010”, paper 152, Brno, Czech Republic, 6-8 September 2010.

List of Symbols, Abbreviations and Acronyms

D_L = inner diameter of the liquid jet nozzle
MFR = Liquid-to-Gas Momentum Flux ratio
Re_L = Reynolds number of liquid jet
We_L = Weber number based on liquid jet velocity
We_G = Weber number based on gas velocity
U_G = Average gaseous velocity of the cross stream
U_L = Average liquid velocity at the nozzle exit
μ = Kinematic viscosity of the liquid
ν_L = Dynamic Viscosity of the liquid
ρ_G or ρ_L = Density of gas or liquid
σ = Surface tension